Ion source operation at GSI

R. Hollinger, K. Tinschert*, A. Adonin*, D. Agahi, R. Berezov, M. Brühl, B. Gutermuth, F. Heymach, V. Ivanova, R. Lang, J. Mäder, F. Maimone, K. Ochs, P. T. Patchakui, J. Roßbach, P. Schäffer, S. Schäffer, C. Vierheller, A. Wesp, S. Zulauf*

GSI, Darmstadt, Germany

High Current Ion Sources

In 2014 ion sources from Terminal North (MUCIS, CHORDIS and VARIS) and Terminal South (PIG ion sources) were supplying the GSI accelerator with various types of ions. The following Table 1 gives an overview of the ion species, which were delivered for physics and accelerator development experiments. A good representative value for delivered intensity to the linear accelerator UNILAC is the analysed current in the transfer section *UH1* in front of the RFQ.

Table 1: Ion beams generated with high current ion sources in 2014. Filament driven volume type ion sources: MUCIS and CHORDIS; Vacuum arc ion sources: VARIS; Penning type ion sources PIG

Ion species	Duration (days)	Ion source	Beam for experiment	Analyzed intensity (emA)
$^{3}H_3^+$	8	CHORDIS	SIS	0.9
$^{6}D_3^+$	7	CHORDIS	UNI	2.4
$^{15}CH_3^+$	33	CHORDIS	UNI/SIS/ESR	3
$^{28}N_2^+$	52	CHORDIS	SIS/ESR	5
$^{20}Ne^+$	5	PIG	UNI/SIS/ESR	0.1
$^{56}Fe^{3+}$	3	PIG	UNI	0.15
$^{58}Ni^{2+}$	32	VARIS	SIS	5.8
$^{86}Kr^{2+}$	16	MUCIS	SIS	9.5
$^{132}Xe^{3+}$	19	PIG	UNI/ESR	0.05
$^{152}Sm^{3+}$	15	PIG	UNI/SIS/ESR	0.03
$^{197}Au^{4+}$	11	PIG	UNI/SIS/ESR	0.3
$^{197}Au^{8+}$	45	PIG	UNI	0.07
$^{209}Bi^{4+}$	16	PIG	UNI/SIS/ESR	0.07
$^{238}U^{4+}$	53	VARIS	UNI/SIS/ESR	15

From Table 1 it can be deducted that the most requested ion beams in 2014 were gold, uranium and nitrogen. It is also shown that most of the time both terminals were operated at the same time with mostly different ion species.

One of the main highlights of 2014 was the development of CH_3^+ molecular ion beam operation from MUCIS ion source for production of intense proton beam behind the gas stripper [1,2]. This approach allowed reaching up to 25% of the FAIR design proton beam intensity with the existing UNILAC [2].

Another notable highlight is an upgrade of MUCIS new (design 2010) ion source for better performance with heavy gases (Kr, Xe). Stronger Nd-Fe-B permanent magnets (1.4 T instead of 1 T) have been used for generation of multi-cusp field in the plasma chamber. The geometry of filament holder was improved. External magnetic coil was installed around the plasma chamber to focus the plasma bunch and to increase the emission current density in the extraction region. Due to these improvements new record intensities in front of the RFQ of 9.5 mA for Kr^{2+} and of 6.5 mA for Xe^{3+} ion beams have been established. That beats the previous intensity record more than 30% for Kr-case and more than 150% for Xe-case.

Notable performance improvement of VARIS source for $^{238}U^{4+}$ beam was successfully demonstrated in Oct.-Nov. 2014 [3]. Implementation of a new multi aperture (7-holes, ø4 mm) extraction system in the ion source allowed to reduce the horizontal beam emittance (measured in UH1) by 15%, while the vertical beam emittance remained comparable (less than 2% difference) with standard extraction system. Also the source performance with various duty cycles: 1 Hz, 2 Hz and 3 Hz have been tested, showing the principle possibility of high duty cycle operation with existing uranium ion sources.

To fulfil the requirements of future FAIR-experimental programs the tests with Fe^{2+} (required by BIOMAT) and Ag^{2+} (required by CBM) ion beams from high current VARIS ion source have been performed. As the result, stable operation with new intensity records in front of the RFQ of 9 mA and 12 mA for Fe^{2+} and Ag^{2+}, respectively, has been achieved.

Renewing and development of the PIG sources is in process. Two sources are successfully putted into the operation after the complete renewing. For further investigations and development of PIG sources the construction of the new test bench is in process. The investigations will be focused on compactification of the source as well as increasing the beam current and the life time. For these purpose the compact PIG source will be tested on the new test bench.

High Charge State Injector HLI

For the operation of the GSI accelerator the CAPRICE ECR ion source (ECRIS) at the High Charge State Injector (HLI) delivered the ion species listed in Table 1 for various physics experiments in the regular beam time schedule as well as for dedicated ion beam development.

* Corresponding authors

DOI:10.15120/GR-2015-1-FG-UNILAC-01

Table 1: Ion beam operation of the HLI-ECRIS in 2014; additional time for tests and beam development in brackets.

Ion species	Auxiliary gas	Duration (days)	Analyzed intensity (eμA)
$^{12}C^{2+}$	O_2	24	100
$^{12}C^{5+}$	He	13(17)	50
$^{14}N^{3+}$	He	16	210
$^{22}Ne^{4+}$	He	8	250
$^{40}Ar^{8+}$	He	23	200
$^{48}Ca^{10+}$	He	26(7)	120(170)
$^{50}Ti^{8+}$	He	21	70

After the long shut down period in 2013 an $^{40}Ar^{8+}$ ion beam was used for machine commissioning at the HLI.

Two beam time periods in 2014 dedicated to biophysics experiments at the SIS under therapy conditions and to biophysics experiments at the UNILAC were provided with $^{12}C^{2+}$ ion beams.

Due to a special constellation of parallel ion beam operation with protons from the high current injector and C ion beam from the ECRIS for experiments of biophysics and material research at the UNILAC $^{12}C^{2+}$ could not be accelerated in the Alvarez section of the UNILAC. The charge state had to be increased to $^{12}C^{5+}$. Such a hydrogen-like C ion beam had not been operated with the ECRIS before. Therefore extensive investigations were necessary for optimization of the operating conditions of the ECRIS before the dedicated beam time. As the ECRIS test facility was not available due to upgrade activities an ion beam development period was performed at the HLI during a gap of the beam time [4].

Upon a request from an experiment at the PHELIX LASER facility a $^{14}N^{3+}$ ion beam had to be established for the first time and could be delivered from the ECRIS in a very stable mode.

The major part of the beam time in 2014 was dedicated to various experiments on Super Heavy Element (SHE) research at SHIP, TASCA and SHIPTRAP, respectively. After the dedicated development of a $^{50}Ti^{8+}$ ion beam from highly enriched isotope material during the past years this beam was delivered to experiments for the first time. Figure 1 shows a mass/charge spectrum taken during this run. An average material consumption of 3.6 mg/h was determined for the whole run.

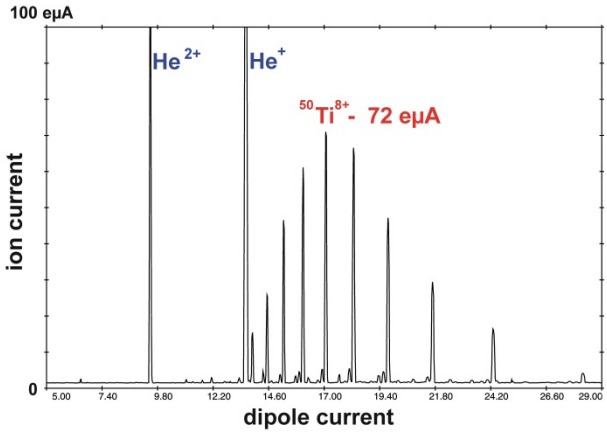

Figure 1: Mass/charge spectrum of ^{50}Ti.

Finally in 2014 a long run with $^{48}Ca^{10+}$ was dedicated to experiments of the Super Heavy Element (SHE) program at TASCA and at SHIPTRAP. This run was characterized by very stable long time behaviour of the ion beam at high intensity with the typical low average material consumption of less than 200 μg/h. For a thermal load test of the target during the final stage of the experiment the intensity of the analyzed $^{48}Ca^{10+}$ in beam could be increased to 170 eμA, a value as high as it could never be obtained before.

During the long shut down period in 2013/14 a major upgrade of the ECRIS facility at the HLI had been performed including the implementation of new TWTA-based microwave transmitters and a new high precision gas injection system for the working gas and for the auxiliary gas, respectively. All components of the new equipment could prove its reliable long term operation.

References

[1] A. Adonin, R. Hollinger, this report.
[2] M. Heilmann et al., this report.
[3] W. Barth et al., U^{28+}-intensity record applying a H_2-gas stripper cell at GSI-UNILAC, to be published.
[4] K. Tinschert et al., Development and Upgrade of the ECRIS Facility, this report.

DOI:10.15120/GR-2015-1-FG-UNILAC-01

UNILAC status report

P. Gerhard[1], *W. Barth*[1], *L. Groening*[1], *M. Maier*[1], *S. Mickat*[1], *U. Scheeler*[1], *H. Vormann*[1], *and C. Xiao*[1]

[1]GSI, Darmstadt, Germany

Operation

After 13 months of shutdown, the UNILAC commissioning began in early January with the start up of all devices and systems. The first beam accelerated to full UNILAC energy ($^{40}Ar^{10+}$ from the PIG) was recorded on 29 January 2014. On 9 February the first beam ($^{40}Ar^{8+}$) was available in the transfer channel and was subsequently delivered for the commissioning of the synchrotron. The busy, but — having the long shutdown in mind — quite successful commissioning ended on 13 February 2014. Still, operation was affected by numerous and frequent interruptions and breakdowns, though. The major drawback was, that some rf cavities needed additional conditioning in order to accelerate $^{238}U^{28+}$, which was requested for the SIS18 commissioning already. $^{238}U^{29+}$ with less intensity had to be chosen several times throughout the year.

The UNILAC was in operation for nearly 250 days, restricted to two ion species in parallel in order to compensate for the tight beam time schedule in 2014. Delivering high current beams of ^{14}N (CHORDIS), ^{58}Ni (VARIS), ^{1}H and ^{86}Kr (both MUCIS) to the synchrotron for physics experiments and machine development dominated the operation. At UNILAC energies material sciences, biology and SHE experiments (TASCA, SHIPTRAP) were the main recipients for ^{197}Au, ^{209}Bi (both PIG), ^{48}Ca and ^{50}Ti (both ECR). ^{238}U (MeVVA), ^{124}Xe (MUCIS) and ^{132}Xe (PIG) were accelerated for physics experiments and machine development both at the UNILAC and SIS18. Shorter beam times with ^{56}Fe and ^{153}Sm (both PIG) have been conducted mainly for physics experiments, while $^{2}H_3^+$ (MUCIS) was accelerated for EMTEX (see below), and ^{20}Ne (PIG) for HITRAP. The HLI also provided four weeks of ^{12}C, mainly for therapy development, and ^{22}Ne for TASCA.

For the first time a high current proton beam was accelerated for the synchrotron by cracking $^{15}CH_3^+$ (CHORDIS) in the gas stripper, thereby delivering 2 mA ($7{\cdot}10^{11}/100\mu$s) of protons with very good beam quality [1, 2].

Shutdown Activities

Due to the short shutdown periods in 2014, no major activities had been carried out. The second buncher cavity in the Alvarez section (BB6) could not be operated at high power levels due to a blocked cooling channel of the spiral. After several rinsing attempts it was finally removed from the beamline, repaired in the workshop during the second beamtime period, and placed back in November. Additionally, two inner tank triplets of the first HSI-IH tank had ground fault. They were operated by means of a work around, one of them will be repaired during the shutdown 2014/15. One drift tube in the Alvarez I tank has a vacuum leak, it will be replaced this year.

Machine Experiments

In May and October successful tests were carried out by the source department to reach higher proton beam intensities by accelerating molecules like $^{15}CH_3^+$ and $C_2H_6^+$ from the MUCIS and crack them in the gas stripper [3]. Increasing the intensity, especially for heavy ions, by using a pulsed gas jet with different gases and thereby increasing the stripping efficiency, also was the topic of very successful machine experiments in February and November conducted in close collaboration with TASCA [4, 5]. Three accelerator beamtimes were dedicated to the emittance transfer experiment EMTEX [6, 7]. During several machine experiments new rf working points for all HSI accelerator cavities were identified using $^{181}Ta^{4+}$, and rf breakdowns of the superlens were investigated. Experimental data for advanced DYNAMION simulations of the matching of high current beams to the HSI-RFQ were gathered, and multi charge operation of the poststripper section was studied [8]. In autumn, the amplitude calibration of the bunchers US4BB3 and BB4 was investigated and emittance measurements along the whole UNILAC, especially behind the poststripper section, were conducted [8], besides experiments of the beam diagnostics department related to the longitudinal beam structure. In total, 179 shifts were staffed by the linac department, including assistance for three successful HITRAP beamtimes [9].

References

[1] W. Barth et al., LINAC'14, Geneva, TUPP056

[2] M. Heilmann et al. (this report)

[3] A. Adonin et al. (this report)

[4] W. Barth et al. (this report)

[5] P. Scharrer et al. (this report)

[6] M. Maier et al. (this report)

[7] L. Groening et al., http://dx.doi.org/10.1103/PhysRevLett.113.264802

[8] H. Vormann (ed.), Accelerator Experiments Beamblock 1 & 2 2014, https://www.gsi.de/work/fairgsi/linac_operations/↩ linac/publications/accelerator_experiments/2014.htm

[9] F. Herfurth et al. (this report)

DOI:10.15120/GR-2015-1-FG-UNILAC-02

Development and upgrade of the ECRIS facility

K. Tinschert, R. Lang, J. Mäder, F. Maimone, P. T. Patchakui
GSI, Darmstadt, Germany

Upgrade of the ECR injector setup

A new version of the 1.2 T CAPRICE ECRIS (ECR Ion Source) was assembled and installed at the ECR injector setup (EIS). This version is equipped with a new hexapole construction with improved permanent magnet materials providing increased remanence. Table 1 shows a comparison of the specifications of the magnet materials.

The original 1.2 T hexapoles were assembled in 1999 from 6 cuboids for each pole, which were procured as magnetized single magnet pieces. At present improved technology facilitates the fabrication as one single piece with subsequent magnetization by the manufacturer [1]. As in the original version trapezoidal magnets are filling the space between the pole pieces to provide a closed magnetic flux. The new hexapoles were obtained from the manufacturer as complete items. The improved manufacturing technique should provide a good homogeneity of the magnetic flux density along the pole faces.

Table 1: Comparison of the magnet specifications.

	1,2 T new version		1,2 T original type	
	Pole	Trapezoid	Pole	Trapezoid
Material VACODYM®	745HR	655HR	362HR	383HR
Remanence typ. [T]	1,44	1,28	1,33	1,28
Coercivity [kA/m]	1115	990	1010	980
Temperature max. [°C]	70	150	120	150

In order to check the magnetic field distribution a field mapping was performed by the ENMA (NC Magnets & Alignment) department of GSI. For comparison one of the original hexapoles was included in this series of measurements. Due to the optimized design the magnetic flux density of the new hexapoles could be increased by about 3% with respect to the original design. As the new magnet materials for the poles tolerate lower limits of the operating temperature the cooling technique had to be improved by optimizing the conditions of the cooling water flow.

Ion beam development

Due to special operating conditions of the Alvarez LINAC a $^{12}C^{5+}$ ion beam was requested from the ECRIS. For the generation of hydrogen like C ions all L-shell electrons plus one further K-shell electron have to be ionized in the plasma by successive electron impact ionization. This requires high power operation modes of the ECRIS. In order to optimize for best C^{5+} performance various combinations have been explored. Besides the standard configuration for $^{12}C^{2+}$ ion beam with CO_2 as working gas and O_2 as auxiliary gas, respectively, CH_4 was investigated as alternative working gas, while H_2 or He were used as auxiliary gases. For both working gases the operation at the required high level of microwave power and high magnetic mirror field exhibited strong plasma instabilities inside the quartz gas injection tube at the location of the first electron cyclotron resonance. Therefore the normally used quartz tube was replaced by a pure copper tube of the same dimensions, which led to much better plasma stability. H_2 and He as auxiliary gas turned out to give better performance than O_2. With respect to the fixed frequency operation with the klystron amplifier slightly higher intensity could be obtained by careful frequency tuning of the travelling wave tube amplifier. Formerly CH_4 had been used without additional auxiliary gas for the production of a $^{12}C^{3+}$ beam; however, the absence of auxiliary gas did not facilitate a successful optimization of C^{5+} in the present experiments. Finally the combination of CO_2 with He as auxiliary gas turned out to be the best choice in order to provide stable long term conditions at an intensity level of 60 eμA analyzed C^{5+} beam.

Radiation protection survey

For an improved survey of the X-ray emission from the ECRIS as well as for related studies dedicated X-ray monitors (energy range: 6 keV to 15 MeV) were procured which can be operated continuously under long term conditions with remote data storing for offline analysis.

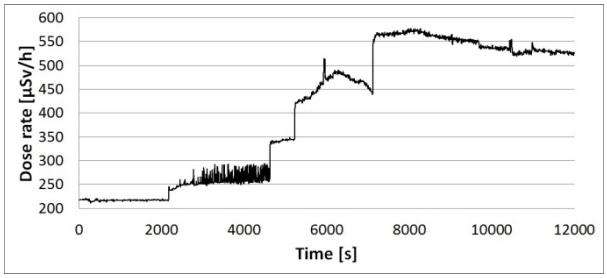

Figure 1: Recorded dose rate during optimization

For a first test one probe was placed next to the extraction of the ECRIS, where a high X-ray level is expected. Figure 1 shows the recorded dose rate during an optimization process of $^{48}Ca^{10+}$ operation in high power mode. The steps in the course of the dose rate are clearly correlated with a stepwise increase of the microwave power from 250 W to 450 W. Phases with plasma instabilities are also identified like around 4000 s in the diagram.

References

[1] VACUUMSCHMELZE GmbH & Co. KG, Grüner Weg 37, D-63450 Hanau, Germany; http://www.vacuumschmelze.de/

DOI:10.15120/GR-2015-1-FG-UNILAC-03

Ion source development of H-rich molecular beam operation for production of high-intensity proton beams at the UNILAC

A. Adonin and R. Hollinger

GSI, Darmstadt, Germany.

The operation of UNILAC high current injector with light ions (M/Q < 8) is strongly limited due to high transmission losses in the LEBT and RFQ. Another limitation is the low extraction voltage applied at the ion source due to the fixed specific ion energy of 2.2 keV/u at the RFQ entrance. These factors make the HSI operation with proton beams extremely inefficient. However the situation can be dramatically improved by production of singly charged heavy (up to M = 50 a.m.u.) molecular ion beams with a high content of hydrogen atoms. These molecular ions can be accelerated in the HSI with much lower transmission losses and when converted into a proton beam at the gas stripper [1].

For the experimental investigations the first two elements from alkane group: methane (CH_4) and ethane (C_2H_6) have been considered because they are non-toxic and could be used in the ion sources under the same safety requirements as a hydrogen gas. The first experiments have been performed with methane gas using high current MUCIS ion source. The mass spectrum of extracted beam is shown on Figure 1. It contains several different molecule species (including higher order alkane chain). However by tuning the operation parameters of the ion source it was possible to optimize the spectrum and get the maximum output of CH_3^+ ions.

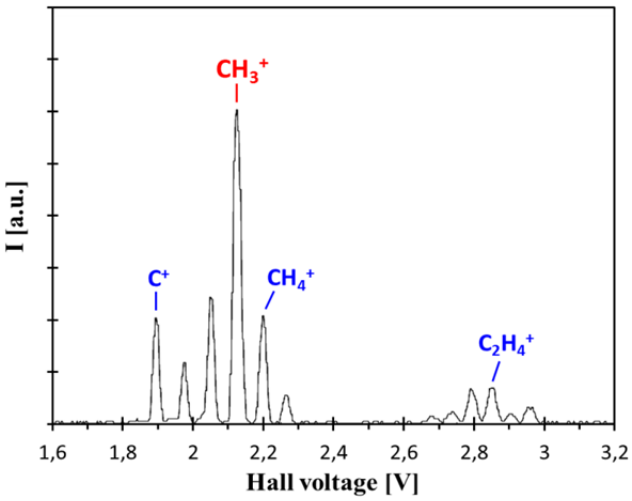

Figure 1: Mass-spectrum of methane gas optimized for CH_3^+ production

The operation was performed with duty cycle of 2 Hz and the pulse length from the ion source of 1 ms. The maximum beam currents achieved in the tests were 11 mA for unanalysed beam and 4 mA for CH_3^+ ions.

Tests with ethane gas have been performed with the same ion source and under the same conditions as with methane. The mass spectrum is more complex than for methane (Fig.2). The production maximum was achieved for $C_2H_4^+$ ions and maximum beam current in front of the RFQ was 2 mA.

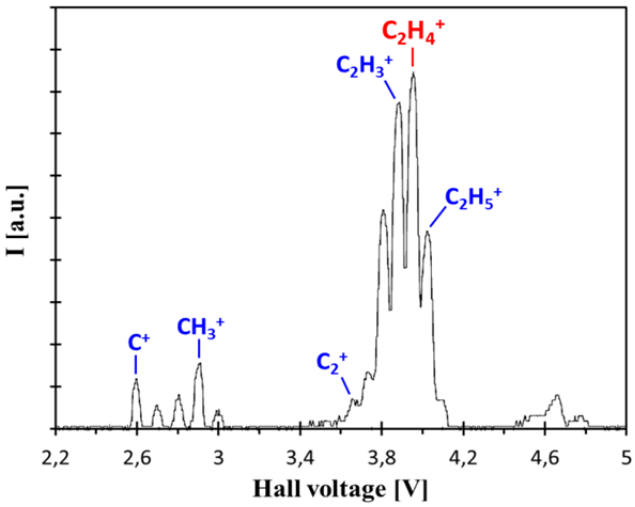

Figure 2: Mass-spectrum of ethane gas optimized for $C_2H_4^+$ production

A notable disadvantage in operation with CH_4 and C_2H_6 gases is strong and relatively fast contamination of the plasma chamber and the extraction system of the ion source with carbon. The carbon ions embedded in the heating filaments make them more fragile and reduce their durability and lifetime. Carbon deposits on the extraction electrodes causes sparking and breakdowns in the extraction system. Thus the operation with alkanes requires a full service of the ion source with cleaning of the plasma chamber once a week. While hydrogen operation requires only a filament service every 7-10 days.

The HSI operation with molecular CH_3^+ ion beam results in proton intensity up to 3 mA behind the gas stripper that is more than 1 order of magnitude higher (at transferline to SIS) than the intensity achieved with hydrogen operation. For further performance improvement of the ion source the optimization of the extraction system for singly-charged molecular beam production and reduction of carbon contamination effect are foreseen. Besides using of more heavy H-rich gases (such as propane, butane, trimethylamine, etc.) could provide better transmission and even higher yield of protons behind the gas stripper for future proton operation.

References

[1] W. Barth et al., LINAC-2014 proceedings.

DOI:10.15120/GR-2015-1-FG-UNILAC-04

Status of the Compact LEBT Project

H. Vormann, A. Adonin, H. Al Omari, W. Barth, L. Dahl, P. Gerhard, L. Groening, R. Hollinger, M. Maier, S. Mickat, A. Orzhekhovskaya, C. Xiao, and S. Yaramyshev

GSI, Darmstadt, Germany

The particle dynamics design of the new high current uranium low energy beam line for FAIR is fixed. Simulations based on uranium beam measurements at the North Terminal 2013 have shown that a straight beam line with quadrupoles as focusing elements allows for best beam quality and transmission [1-3]. The beam line components of this Compact LEBT, to be integrated into the existing High Current Injector (HSI) complex, are now under construction.

Design of the LEBT

Uranium beam measurements at the existing high current ion source North Terminal confirmed the performance of the ion source: From about 50 mA total beam current, 25 mA U^{4+} is provided within an emittance of 280 mm mrad (assumed RFQ acceptance) (Fig. 1).

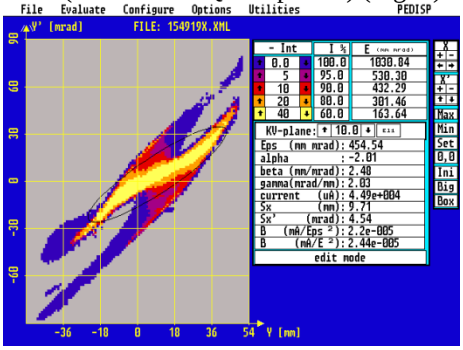

Figure 1: Uranium emittance behind ion source (49 mA tot. beam curr., 32 mA U^{4+}, 15 mA within 280 mm mrad).

Based on these measurements beam dynamics simulations have been performed [2, 3]. Considering a minimum distance of at least 4 meters from the new uranium terminal to the switching magnet (restricted space because of existing branches), two focusing elements must be used in this part of the LEBT. A quadrupole quartet (QQ) and a quadrupole triplet (QT) turned out to be the best solution. With this LEBT a focus 1.5 meter behind the QQ can be achieved, allowing for partly scraping off the undesired U^{3+} partition of the uranium beam with a collimator (see Fig. 2) [3].

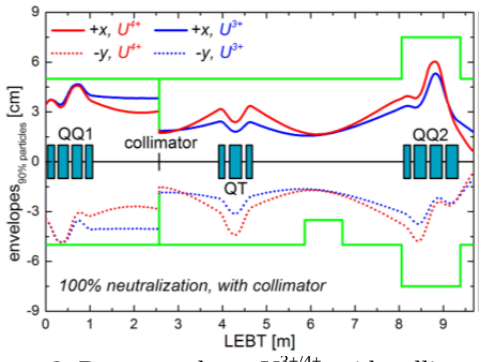

Figure 2: Beam envelopes $U^{3+/4+}$, with collimator.

U^{3+} ions are scraped off in the collimator or will be lost in the following LEBT and RFQ at low energy. Simulations show that more than 15 emA U^{4+} can be transported through the new LEBT [3].

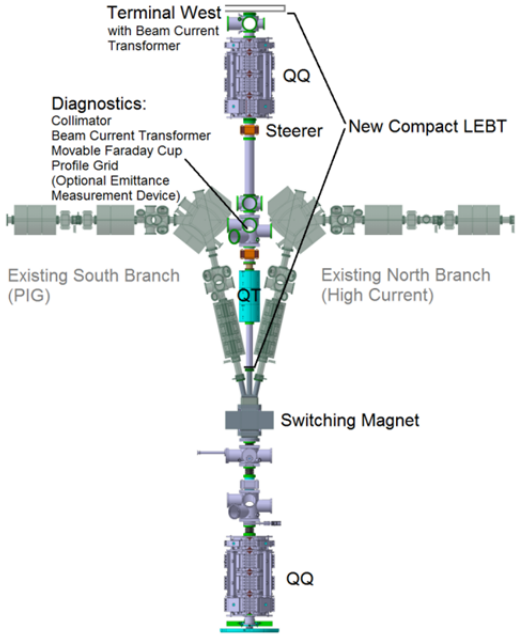

Figure 3: Planned modified HSI-LEBT (Courtesy V. Gettmann).

Besides a beam current transformer with large aperture (115 mm diameter) behind the ion source, a second beam current transformer is foreseen behind the first quadrupole quartet and the collimator, together with a profile grid (width 94 mm) and a movable Faraday cup (diameter 80 mm) as beam diagnostics.

For the commissioning phase, an emittance measurement device is also desirable. To avoid problems from space restrictions, this could be a device measuring only one plane (e.g. only vertically), as the beam shape from the ion source is symmetric.

Status of Components

The tendering for the power supply for the new quadrupole quartet has now started.

Civil construction and stress analysis is starting, magnet design work is going on, and the definition of beam diagnostics components is almost done.

References

[1] L. Dahl, proc. LINAC 2006
[2] S. Yaramyshev et al., proc. IPAC 2014
[3] C. Xiao et al., this report.

DOI:10.15120/GR-2015-1-FG-UNILAC-05

Beam dynamics layout of the compact LEBT*

C. Xiao† [1], *L. Groening*[1], *H. Vormann*[1], *S. Mickat*[1], *M. Maier*[1], *W. Barth*[1], *S. Yaramyshev*[1], *and O.K. Kester*[1,2]

[1]GSI, Darmstadt, Germany; [2]IAP, Frankfurt am Main, Germany

The present high current VARIS ion source [1] delivers about 50 mA of uranium beam and about 8 mA of U^{4+} was measured behind the HSI. In order to increase the beam intensity downstream the HSI, a dedicated straight LEBT for uranium is proposed as a part of the upgrade and further development of the high current heavy ion linac UNILAC for the Facility for Antiproton and Ion Research (FAIR).

A symmetric beam is required at the entrance to the RFQ. The beam Twiss parameters are determined to be α_f=0.6, β_f=13.6 cm/rad and the transverse acceptance of the RFQ is calculated as A_f=280 π mm mrad. 15.4 mA U^{4+} are inside the RFQ-acceptance already at the source. Beam dynamics design has been performed with the TRACE-3D code [2]. It is optimized to maximize the primary component inside the RFQ acceptance and to minimize the secondary component and transport almost all U^{4+} ions which are in the acceptance form source to RFQ. Beam dynamics simulations have been performed using the multi-particle tracking TRACK code [3]. A macro-particle distribution is generated at the entrance of the new LEBT from the measured phase space distribution directly behind the ion source post acceleration gap. Fig. 1 illustrates final particle distributions at the exit of the LEBT.

Simulations show that 60% (10.5 mA) of the undesirable U^{3+} beam is removed by the aperture and collimator and the remaining U^{3+} beam will be lost in the RFQ. About 50% (15.4 mA) of the U^{4+} beam is transported from the source to the RFQ (for the U^{4+} particles within the RFQ-acceptance, 100% transmission is achieved from the ion source to the RFQ) when the space-charge effects are fully compensated. When the space-charge effects are included (for example 95% compensated), 81% (14.2 mA) of the undesirable U^{3+} beam is removed by the aperture and collimator, and about 44% (14.2 mA) of the desired U^{4+} beam is delivered to the RFQ (for the U^{4+} particles within the RFQ-acceptance, 93% transmission is achieved). The FAIR requirements still impose improvement to 25 mA within the RFQ-acceptance. To this end further developments of the source performance are planned.

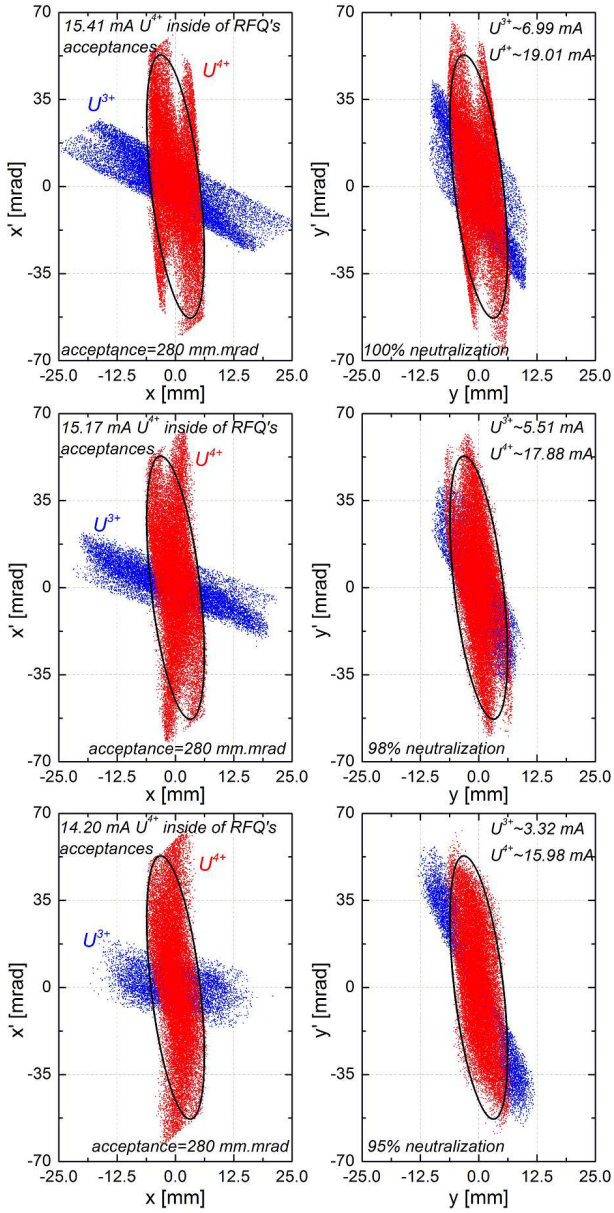

Figure 1: Particle distributions at the exit of the LEBT. Space-charge compensation factor is 100%, 98%, and 95%, respectively. Blue dots indicate the U^{3+} particles, red dots indicate the U^{4+} particles and black ellipses indicate the acceptance of the RFQ.

References

[1] R. Hollinger et al. ReV. Sci. Instrum. **75**, 1595 (2004).

[2] K.R. Crandall et al. LA-UR-97-886 (1997).

[3] P.N. Ostroumov et al. http://www.phy.anl.gov/atlas/TRACK/.

* PSP code: 7.1.2.1.

† c.xiao@gsi.de

DOI:10.15120/GR-2015-1-FG-UNILAC-06

Development of a MEBT Design to replace current UNILAC Superlens*

H. Hähnel† [1], *U. Ratzinger*[1], *R. Tiede*[1], *and S. Mickat*[2]
[1]IAP, Goethe University, Frankfurt, Germany; [2]GSI, Darmstadt, Germany

As part of the UNILAC upgrade, a new MEBT section is proposed [1]. It will provide improved matching to the IH-DTL and therefore a significant reduction in emittance growth and lossless transmission at 20.75 mA U^{4+}. This way the FAIR requirement of 18 mA U^{4+} behind the IH-DTL can easily be reached with the new MEBT. The design comprises of two quadrupole triplet lenses and a two-gap buncher cavity (see Figure 1), providing more flexibility than the existing "Superlens" MEBT [2]. This layout allows to reuse the existing XY-steerer, the vacuum valve and the diagnostics box. It also provides some spare room for additional/redesigned components.

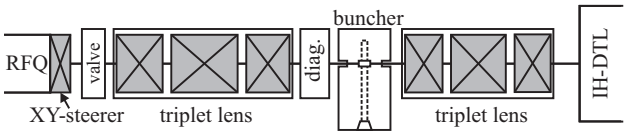

Figure 1: Layout of the proposed MEBT section.

The overall length of the new MEBT is 1.82 m which is 0.4 m longer than the existing MEBT section. The posibility of providing the extra length by moving the IH-DTL is currently being investigated.

At 20.75 mA the simulated losses in the Superlens using the RFQ output distribution after the 2008 upgrade amount to 12 % [1][3]. Losses are caused by insufficient transversal focusing and the limiting aperture of the Superlens.

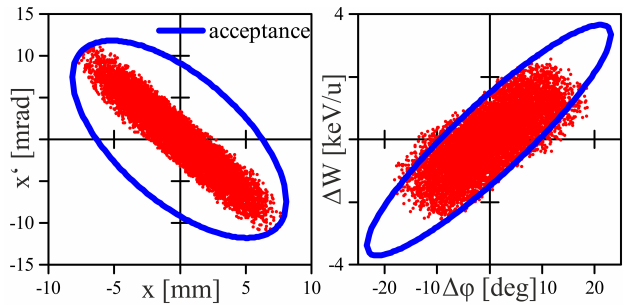

Figure 2: Output distribution of new MEBT with IH-DTL acceptance as reported in [4].

The new MEBT ensures transversal and longitudinal focusing matched to the IH-DTL input acceptance (Figure 2). By using two quadrupole triplet lenses, the design provides some flexibility to compensate changes in the input distribution. The gap voltage of the buncher cavity can also be adjusted if necessary to change longitudinal focusing.

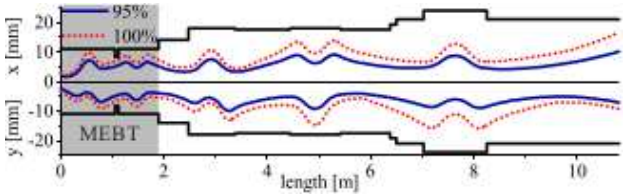

Figure 3: Envelopes of new MEBT and IH1 at 20.75 mA.

Table 1: Prestripper output parameter comparison.

	SL MEBT	**New MEBT**
Total length	1.4 m	1.82 m
Design current	16.5 mA	20.75 mA
Design A/q	65	59.5 (U^{4+})
MEBT-out	for 20.75 mA U^{4+}	
Transmission	87.94 %	100 %
ϵ_{rms} [mm mrad]	x:0.108 y:0.09	x:0.072 y:0.073
ϵ_{rms} [$\frac{keV}{u}$ ns]	0.389	0.358
IH-out		
Transmission	85.7 %	100 %
ϵ_{rms} [mm mrad]	x:0.162 y:0.158	x:0.117 y:0.138
ϵ_{rms} [$\frac{keV}{u}$ ns]	1.279	0.517

A comparison of output parameters of the prestripper section is made in Table 1 showing a reduction of rms emittance growth of 27.8 %, 12.7 % for x-x',y-y' and 59.6 % for the longitudinal plane behind the IH-DTL. Simulations with currents from 10 to 20.75 mA U^{4+} show lossless transmission for the MEBT+IH and even low losses at 35 mA U^{4+}. Upgrading the MEBT section would significantly improve the overall UNILAC efficiency and provide flexibility for high current operation which is required for FAIR.

References

[1] H. Hähnel, U. Ratzinger, R. Tiede, MOPP062, Proc. LINAC2014

[2] U. Ratzinger, R. Tiede, MOP31, Proc. LINAC96

[3] All simulations were performed with LORASR.

[4] R. Tiede, "HSI IH-DTL Acceptance Studies", Talk at IAP-GSI UNILAC-Upgrade meeting, Frankfurt, January 16th, 2014

* Work supported by BMBF 05P12RFRB9
† haehnel@iap.uni-frankfurt.de

DOI:10.15120/GR-2015-1-FG-UNILAC-07

Application of the Savitzky-Golay-Filter to analyze the energy-loss of a heavy ion beam in an X-ray-heated CHO-foam

R. Maeder[2] ; T. Rienecker[2]; S. Hagmann[1] ; L. Borisenko[3] ; M. Schächinger[2]; A. Schönlein[2]; S. Zaehter[2]; O. Rosmej[1,2], J. Jacoby[2]

[1]GSI, Darmstadt, Germany; [2]University Frankfurt am Main, Germany; [3] Moscow State University, Russia

Measurements of the ion beam energy loss in low density CHO-foams in solid and plasma states have been carried out at the Z6-experimental area using a combination of the UNILAC ion beam and PHELIX laser pulses.
The Savitzky-Golay-Filter was applied to increase the accuracy of the measured data.
The Ti $^{+12}$ ions, accelerated up to 4.77MeV/u energy, pass the low density 1 mm thick CHO foam layer a Triacetate-Cellulose with the chemical structure $C_{12}H_{16}O_{8.}$ The energy loss in cold foam layer was measured by means of a time-of-flight method. Interaction of a 100-180J PHELIX nanosecond laser pulse with a gold-layered hohlraum, placed above the foam target, gave rise to soft X-ray emission with close to Planckian spectral distribution. Supersonic X-ray waves heat the foam and transfer it from a solid into a hydrodynamically stable plasma layer with homogeneous distributions of density, temperature and ionization degree.
The energy loss in the cold and converted to plasma target was registered by means of the diamond stop-detector, placed 12,126m far away from the interaction region, and evaluated using the data-analysis program Origin9. [1]
The received data is influenced by a low signal-to-noise-ratio, which disturbs the data-sets and reduces the data accuracy. In order to remove these errors and improve the accuracy of the measured data, the Savitzky-Golay-Filter-Method (SGF-Method) was applied.

The Savitzky-Golay-Filter is a digital filter, used to smooth digital data-sets, thus increasing their signal-to-noise ratio without distortion of the data. It is based on the standard method of least squares. Therefore a convolution process, combining the method of least squares with a k-degree polynomial, is used. This process fits every data-point x_i of the data-set I, in an area of k successive adjacent data points. Thus a sum of 2k+1 data points is included in the process. [2]

$$f(x_i) = \sum_{j=-k}^{k} c_n x_{i+j}$$

Variation of the filter-coefficient c_n provides the smoothed data points $f(x_i)$. The efficiency of the smoothing process can be seen in the following graphic, presented in fig.1.

The smoothed data-sets are evaluated and the energy-loss ΔEi of Ti-Ions in solid- and plasma-foams is recorded.

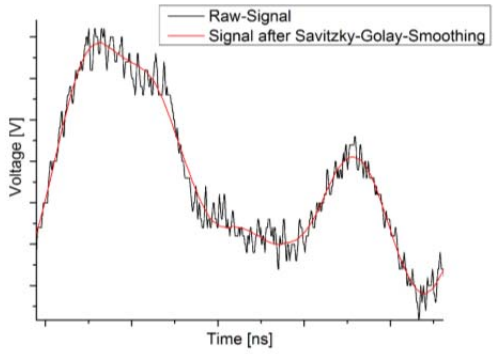

Figure 1: Raw and smoothed data-signals.

The average energy-loss in TAC-foams with 2mg/cc density is compared to theoretical expectation-values and results of former experiments: [3]

	ΔE_S [MeV/mm]	ΔE_P [MeV/mm]
Smoothed data	5,94 ± 1,19	9,01 ± 1,80
Theoretical values	5,61	7,48
Former data	5,56 ± 1,11	9,30 ± 1,19

The application of the Savitzky-Golay-Filter-Method was successful and delivered reliable results. Through increase of the signal-to-noise-ratio, the amount of data, which can be used for analysis, is raised. Additionally the boundaries of the SGF-Method could be established for a signal-to-noise ratio of the magnitude 1.

References

[1] T. Rienecker, R. Maeder, O. Rosmej, et al., "Measurements of the Heavy Ion Stopping in X-ray heated low-density nanostructured targets." GSI-Report 2013.
[2] D.S.Gilliam, "Mathematical systems theory in biology, communications, computation and finance." Springer (2003), p.301.
[3] R. Maeder, "Messung des Energieverlustes von Titan-Ionen in CHO-Schaum im Fest- und Plasmazustand" Bsc.-Thesis, Goethe-University, Frankfurt a.M. (2013).

DOI:10.15120/GR-2015-1-FG-UNILAC-08

Performance of a modified 1.4 MeV/u gas stripper for $^{238}U^{4+}$

Paul Scharrer[1], Egon Jäger[2], Winfried Barth[1,2], Mario Bevcic[2], Christoph E. Düllmann[1,2,3], Lars Groening[2], Klaus-Peter Horn[2], Khuyagbaatar Jadambaa [1], Jörg Krier[2], Alexander Yakushev[2]
[1]HIM, Mainz, Germany; [2]GSI, Darmstadt, Germany; [3]Johannes Gutenberg-Universität, Mainz, Germany

The GSI UNILAC will serve as an injector system for the FAIR facility. Therefore it has to meet high demands in terms of beam brilliance. A key projectile for FAIR will be ^{238}U [1]. In current routine operation U^{4+}-ions from a MEVVA ion source are accelerated to 1.4 MeV/u by the High Current Injector (HSI). Inside the adjacent gas stripper, the charge state of the ions is increased to raise the efficiency of further acceleration. Behind the stripper, a system of dipole magnets allows the selection of ions with the desired charge state (U^{28+}) [2].

To increase the beam intensity after the gas stripper, an upgrade program has started to increase the stripping efficiency into the desired charge state. The current gas stripper is based on a supersonic N_2-jet, created through a laval nozzle at 0.4 MPa back-pressure. The continuous gas flow limits the usable gas pressure due to the high gas load for the differential pumping system. This also prevents the optimal use of other promising stripper gases, as a saturated charge distribution cannot be reached [3].

To overcome this limit, a modified gas stripper setup was developed [4]. The flange with the laval nozzle on top of the main stripper chamber was replaced by a new flange, featuring a pulsed gas valve designed for a back-pressure of up to 12 MPa and an opening time down to a few microseconds. The new flange is shown in Fig. 1. To prevent the gas from instantaneous removal, an extension was added to the flange with a T-fitting at the end to match the beam line. This creates a high-pressure interaction zone for the stripping process. The valve is located in the extension, facing down towards the beam line. The pulsed gas injection is triggered by a timing signal of the central accelerator control unit. The valve is opened only when a beam pulse passes the stripper and closed immediately afterwards, decreasing the gas load for the pumping system and lowering the gas consumption by a factor of up to 200.

During two measurement campaigns in 2014 the new stripper setup was tested with a U^{4+}-beam (1 Hz, 100 µs pulse length). An opening time of 0.5 ms was used for the pulsed gas valve. The opening time was chosen based on pressure measurements near the gas inlet as well as beam current measurements behind the stripper. Besides N_2, which allowed comparing the setup to the current gas-jet stripper, the charge spectra were measured for various other gases (H_2, He, O_2, Ne, Ar and CO_2).

For all used gases except H_2, a saturation of the charge state distribution was observed with an increase of the back-pressure. The beam emittance and the energy loss were measured using the determined settings for a saturated charge state distribution. Additionally, the stripping efficiency was measured for every populated charge state. A saturation of the charge state distribution with H_2 could not be observed due to the pressure limitations of the pulsed gas valve. Therefore, one can assume that the average charge state will rise, if the pressure is increased further.

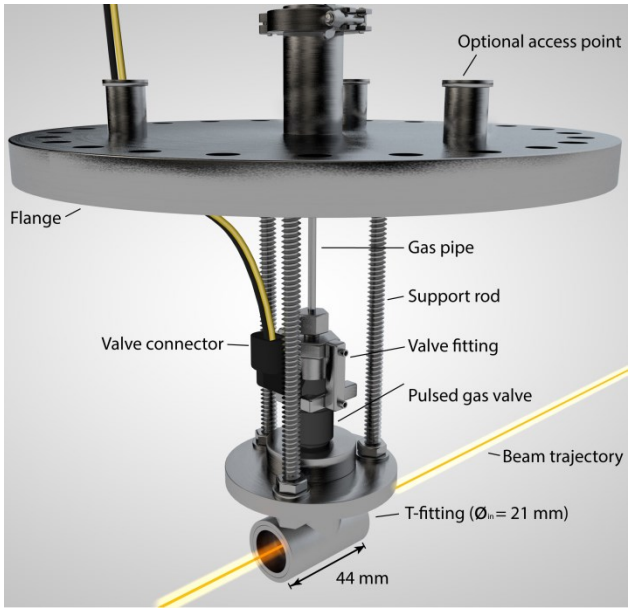

Figure 1: Model of the new stripper flange

Using H_2 with the pulsed gas cell, it was possible to set a new record for the U^{28+} beam intensity behind the gas stripper at the GSI UNILAC [5].

The pulsed gas injection enables various possibilities for the use at the GSI UNILAC, including the simultaneous use of different stripper gases for particular ion beams. Preparing for routine operation, the pulsed gas cell has to be tested and optimized for all to be used types of ion beams.

References

[1] FAIR Baseline Technical Report, Vol. 2, (2006) GSI Darmstadt, p. 355
[2] Barth W. et al., Proceedings of LINAC2000, 21th-25th August 2000, Monterey, California, USA.
[3] Schlitt B. et al., Proceedings of IPAC2013, 13th-17th May 2013, Shanghai, China.
[4] Jäger E. et al., GSI Scientific Report 2013, p. 304.
[5] Barth W. et al., contribution to this GSI Scientific Report.

DOI:10.15120/GR-2015-1-FG-UNILAC-09

High current proton beam operation at GSI UNILAC

M. Heilmann[1], W. Barth[1,2], A. Adonin[1], P. Gerhard[1], R. Hollinger[1], W. Vinzenz[1], H. Vormann[1], S. Yaramyshev[1]
[1]GSI, Darmstadt, Germany; [2]HIM, Mainz, Germany;

A significant part of the experimental program at FAIR is dedicated to pbar physics requiring a high number of cooled pbars per hour [1]. The primary proton beam has to be provided by a 70 MeV proton linac followed by two synchrotrons. The new FAIR proton linac [2] will deliver a 35 mA beam of 36 µs pulse duration. The recent GSI heavy ion linac (UNILAC) is able to deliver world record uranium beam [3] intensities for injection into the synchrotrons, but it was not dedicated to high intensity proton beam operation relevant for FAIR. In an advanced machine investigation program it could be shown, that the UNILAC is able to provide for sufficient CH_3-beam intensities, cracked (and stripped) in a supersonic nitrogen gas jet into protons and carbon ions [4]. This advanced operational approach results in up to 2 mA of proton intensity at a maximum beam energy of 20 MeV, 100 µs pulse duration and a sufficient rep. rate to fill the SIS18 (max. 2.7 Hz). It could be shown, that the UNILAC is able to serve as a proton FAIR injector for the first time, while the performance is limited to 17% of the FAIR requirements.

MACHINE DEVELOPMENT

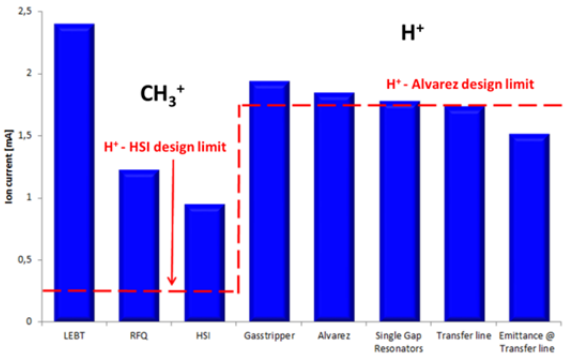

Figure 1: Measured beam current along UNILAC and transfer line to the SIS18; the proton design limit (to fill the SIS18 up to the space charge limit) was reached in the post stripper section.

The MUCIS source [5] was operated with methane (CH_4) gas while a high-current CH_3^+-beam (2.3 emA) is delivered to the HSI. Due to the huge emittance in the LEBT only 50% of the CH_3-beam could be accepted by the HSI-RFQ, minor additional particle losses in the matching section to the HSI-IH-DTL limits the overall HSI-transmission to 40%. Anyway, due to the increased HSI design limitations for the CH_3^+-beam, the improved beam transmission compared to a pure proton beam is evident. Furthermore a triple particle output (for protons) from each CH_3^+ molecule behind the stripping section allows for proton beam operation at the design limit of the poststripper linac (Fig. 1). Strong efforts were launched to push the high current proton beam transmission through the entire poststripper and transfer line to a value of up to 80%.

20 MeV proton beam

The single-gap resonators (SGR) provide intermediate energies between 3.6 and 13.0 MeV/u for all ion species. During the high current experiment protons were preaccelerated in the UNILAC to a beam energy of 11.4 MeV/u. Inside the following eight single gap resonators, each providing for an energy increase of more than 1 MV, a final energy of 20 MeV could be reached (Fig. 2). This final energy corresponds to 28.5% of the required beam energy of the FAIR p-linac. Besides optimizing the high current proton beam performance for the ongoing GSI experiment program, the UNILAC is able to serve as a high performance proton injector for FAIR-commissioning and for first pbar experiments as a redundant option for the FAIR proton linac injector.

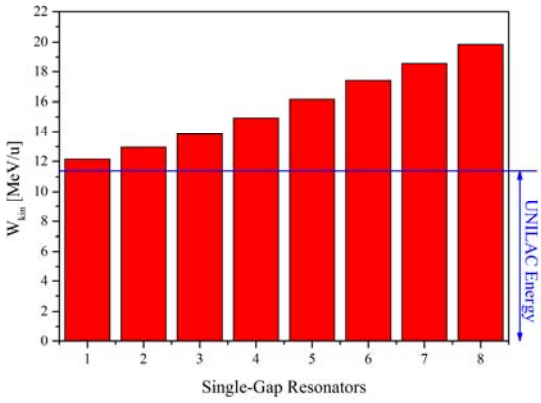

Figure 2: UNILAC operation with eight SGR for maximum proton beam energy of 20 MeV

References

[1] O. Kester, et al., Status of FAIR Accelerator Facility, Proc. of IPAC, Dresden, Germany, p. 2084. (2014)
[2] R. Brodhage et al., First Coupled CH Power Cavity for the FAIR Proton Injector, Proceedings of IPAC, Dresden, Germany, p. 3232 (2014)
[3] W. Barth, et al., GSI Scientific Report 2014
[4] W. Barth, et al., High Current Proton Beam Operation at GSI UNILAC, Proceedings of LINAC, Geneva, Switzerland (2014)
[5] R. Keller, Multi charged Ion Production with MUCIS, GSI Scientific. Rep. 1987, p. 385. (1987)

DOI:10.15120/GR-2015-1-FG-UNILAC-10

Simulation of charge state distributions in stripper applications*

O. S. Haas† [1,2] *and O. Boine-Frankenheim*[1]
[1]TEMF TU-Darmstadt, Darmstadt, Germany; [2]GSI, Darmstadt, Germany

Abstract

The presented work focuses on theoretical studies of the interaction of an heavy ion beam with possible future charge stripping media. The main interest in the presented studies is the final charge state distribution of the ion beam in the context of charge stripping. Different models for solving the corresponding rate equations were devoloped, taking into account ionization, recombination and energy loss processes. In this report one example case relevant for GSI is presented.

Results

The model used for calculations in this section are mainly based on Ref. [1]. The presented example case relevant for GSI is uranium with $1.4\,\mathrm{MeV/u}$ and a desired charge state of $q_0 = 28$. The rates for low atomic densities $n < 10^{23}\,\mathrm{m}^{-3}$ in different media are given in Fig. 1. All gas media do not achieve the desired equilibrium charge state, while in case of a hydrogen plasma the equilibrium charge state is actually higher than the desired charge state. Increasing the atomic density to larger than $10^{23}\,\mathrm{m}^{-3}$ leads

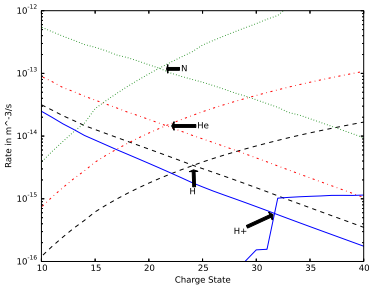

Figure 1: Rates of uranium with $1.4\,\mathrm{MeV/u}$ in different gases and a plasma without density effect. Rising and falling curves are the sum of recombination and ionization rates respectively.

to the onset of the density effect (see Ref. [1]), increasing the equilibrium charge state.

To compare the charge state distribution widths of the different media the density was increased such that the charge state $q_0 = 28$ is achieved, as depicted in Fig. 2. For the hydrogen plasma the charge state distribution is not in equilibrium, as the desired charge state is smaller than the

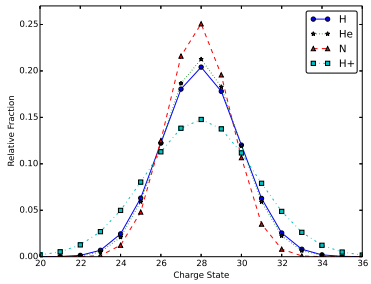

Figure 2: Widths of the charge state distribution for different media. Required atomic density of the gases are $4.65 \cdot 10^{26}\,\mathrm{m}^{-3}$, $1.6 \cdot 10^{27}\,\mathrm{m}^{-3}$ and $3.7 \cdot 10^{27}\,\mathrm{m}^{-3}$ for hydrogen, helium and nitrogen respectively. The density of the hydrogen plasma was assumed to be $10^{23}\,\mathrm{m}^{-3}$ for both electrons and protons.

equilibrium one. This explains the larger charge state distribution width of the plasma stripping medium. In experiments a much broader charge state distribution for nitrogen gas is observed. This however can not easilybe explained by the current model. The charge state distribution width can be approximated as

$$\sigma^2 = \left(\frac{\alpha'_{\mathrm{ion}}(q_0)}{\alpha_{\mathrm{ion}}(q_0)} - \frac{\alpha'_{\mathrm{rec}}(q_0)}{\alpha_{\mathrm{rec}}(q_0)} \right)^{-1} . \qquad (1)$$

This implies that either the shape or value of the rates has to be significantly different for nitrogen, or further effects broaden the distribution specifically for heavier gases. The influence of the mean energy loss in the charge stripping process is of minor importance for typical projectile and target paramters.

Outlook

Future studies intend to improve the calculation methods of the necessary cross section, and include detailed models for the gas and plasma conditions (e.g. inhomogenities, multiple electron capture or loss, and ionization degree of the target). Furthermore comparisons are planned with charge state distributions achieved in the different plasma pinch and gas stripper experiments at GSI.

References

[1] T. Peter, J. Meyer-ter-Vehn, “Energy loss of heavy ions in dense plasma. II. Nonequilibrium charge states and stopping powers”, Phys. Rev. A 43, 1991, p. 2015

* Work supported by HGShire.
† ohaas@gsi.de

DOI:10.15120/GR-2015-1-FG-UNILAC-11

Status of the HE-Linac project at GSI

S. Mickat[1], M. Droba[2], X. Du[1], L. Groening[1], H. Hähnel[2], A. Orzhekovskaya[1], U. Ratzinger[2], A. Seibel[2], R. Tiede[2], H. Vormann[1], C. Xiao[1]

[1]GSI, Darmstadt, Germany; [2]IAP, Goethe University Frankfurt, Germany

UNILAC Upgrade

The High-Energy (HE) Linac project is defined by the substitution of the existing post-stripper (Alvarez) section of the UNILAC. The substition of the existing Alvarez section is one of the major steps towards an adequate FAIR injector linac. Nevertheless the whole accelerator chain has to be taken into account. Starting from the ion sources to the SIS18 transfer channel every section is re-investigated for improvements in beam quality and intensity. Workpackages are defined together with the Institute of Applied Physics (IAP) at Frankfurt University [1]:

- 3rd ion source terminal and Compact-LEBT [2]
- HSI RFQ
- alternative MEBT design
  for an improved beam matching to the HSI IH [3]
- pulsed gas stripper [4] and Emtex [5]

Alvarez DTL and IH DTL

Concerning the post-stripper section itself, two concepts are discussed: On the one hand the substitution of the existing Alvarez structure by six IH cavities [6], on the other hand the substitution by redesigned and new Alvarez tanks. Regarding the design comprising six IH cavities efforts were made to develop a recipe for finding an optimum parameter setting in daily operation. Such a recipe was not found per se, but the design was optimized, which results in an improvement of transmission through the post-stripper section from 88% to 92%. The beam brilliance behind the post-stripper increased by a factor of 1.5 simultaneously [7]. The transmission is limited by the assumed longitudinal beam particle input distribution. It was set to 20 keV/u·ns for comparison reasons. Activities at GSI focus on the substitution of the post-stripper by an Alvarez section. Nevertheless within the IAP-GSI-collaboration the substitution of the post-stripper by six IH-tanks is followed. At the end of the designing phase both concepts are planned to be presented to an external review committee for receiving a qualified recommendation. Both concepts are compatible to the modernisation of the 108 MHz RF systems of the UNILAC post stripper section [8].

Designing phase

Concerning the Alvarez DTL option investigations about optimizing the rf design have started aiming at improvement of the accelerating field properties and increase of the shunt impedance. First results are promising. Optimising the driftube geometry, especially smoothening the drifttube's cap, lower the surface peak fields. The shunt impedance could be increased by 10 percent. Another task is initiated through discussions with the colleagues, who designed the LINAC4 at CERN. At LINAC4 post-couplers are applied to reduce field instabilities. The function of post-couplers are covered by the two stem suspension of the drifttubes, which is applied at GSI. The angle between the stems as well as the stem configuration of group of drifttubes is playing a key role [9]. All this rf design studies will be complemented by measurements. For that purpose an aluminium rf model (scale 1:3) is ordered. In a start version a ten gap model is planned. It is designed for testing different drifttube shapes and confirming the calculated predictions w.r.t. the stem configuration [10]. Focusing on the optimization of the rf-properties the installation space of the quadrupole, which is usually integrated in the drifttube, is an important issue. Theoretical studies and corresponding measurements at the GSI UNILAC provide evidence of space charge driven resonant emittance coupling in high current operation [11]. The operation at these resonances, which leads to an emittance growth, could be avoided by setting an adequate transverse phase advance. An adequate phase advance can be set if the quadrupoles for the new design are specified to reach 20% higher gradients than the existing. First studies for high gradients quadrupoles, which fit into the smaller installation space of the new drifttube geometry, are done [12].

References

[1] S. Mickat et al., "The status of the HE-Linac project at GSI", GSI Scientific Report 2013
[2] H. Vormann et al., The status of the Compact LEBT project", this report
[3] H Hähnel et al., "Development of a MEBT Design to replace current UNILAC Superlens", this report
[4] P. Scharrer et al., "Performance of a modified 1.4 MeV/u gas stripper for $^{238}U^{4+}$ ", this report
[5] M. Maier et al., "Results of the experiments on emittance transfer EMTEX", this report
[6] G. Clemente et al., Proceedings IPAC2011, WEPS032, San Sebastián, Spain
[7] A. Orzhekovskaya et al., "Optimization of the KONUS beam dynamics for the HE-Linac", this report
[8] B. Schlitt et al., "Modernisation of the 108 MHz RF systems of the UNILAC post stripper section", this report
[9] X. Du et al., "Activities on the HE-Linac DTL cavity rf-design", this report
[10] A. Seibel et al., "Status of the cold model for the HE-Linac cavities", this report.
[11] L. Groening et al., , Phys. Rev. Lett.103, 224801 (2009)
[12] D. Daehn, internal note (2014)

DOI:10.15120/GR-2015-1-FG-UNILAC-12

Development of a KONUS based High Energy Linac for the UNILAC*

H. Hähnel†[1], *U. Ratzinger*[1], *R. Tiede*[1], *and S. Mickat*[2]
[1]IAP, Goethe University, Frankfurt, Germany; [2]GSI, Darmstadt, Germany

To meet the requirements of 15 mA U^{28+} at 11.4 AMeV for injection into the SIS18, the GSI UNILAC has to be upgraded. The Alvarez linac in the poststripper U^{28+} section of the UNILAC is nearing 40 years of operation and therefore has to be replaced to ensure reliable and efficient operation for FAIR. We propose an IH-DTL linac as replacement for the current GSI UNILAC Alvarez. The new design is based on the KONUS beam dynamics concept and delivers high beam quality well within FAIR requirements. It will drastically reduce the fabrication costs and will leave about 30 m within the UNILAC (Fig. 1) for later linac energy upgrades by e.g. 325 MHz CH-DTL cavities as in [1].

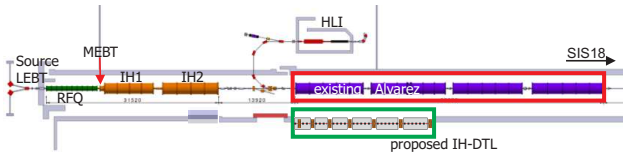

Figure 1: Sketch of the UNILAC accelerator (adapted [2]).

The proposed linac consists of six 108 MHz IH-tanks and seven quadrupole triplet lenses (Fig. 2). It is designed to accelerate 15 mA U^{28+} from 1.4 MeV/u to 11.4 MeV/u. The beam dynamics simulation includes realistic estimations of necessary drift lengths for tank walls, lens housing and phase probes for all lenses. The drift tube aperture is 25 mm and the lens aperture 40 mm with a maximum pole tip field of 1.05 T for the highest gradient of 50.1 T/m. The maximum on axis field is 11 MV/m.

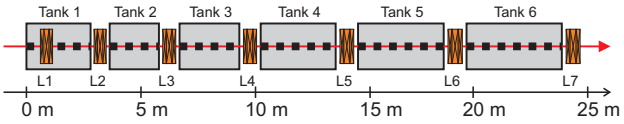

Figure 2: Sketch of the proposed IH-DTL.

Beam Dynamics (preliminary)

Beam dynamics simulations (LORASR) for the proposed high energy linac already show very promising results. The used input emittances are a pessimistic estimation based on the prestripper output emittances using the MEBT upgrade as proposed by the authors in [3]. The transversal input emittances are 0.8 mm mrad (90 %) and the longitudinal input emittance is 6.3 keV/u ns (90 %). A matching section with buncher will be necessary in front of the proposed design.

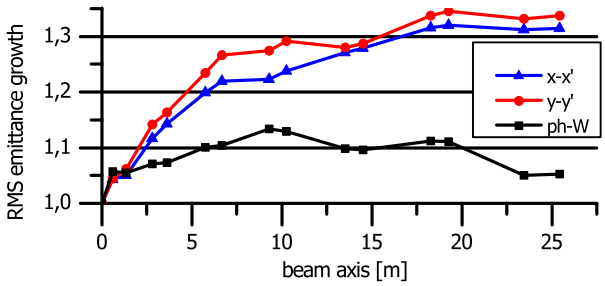

Figure 3: RMS emittance growth of the proposed high energy linac section.

The rms emittance growth along the proposed linac is shown in Fig. 3, indicating only 5.3 % in the longitudinal plane and about 30 % in the transversal planes. Further improvement in the transversal planes is expected to be achieved by adjusting the focusing scheme (Fig. 4).

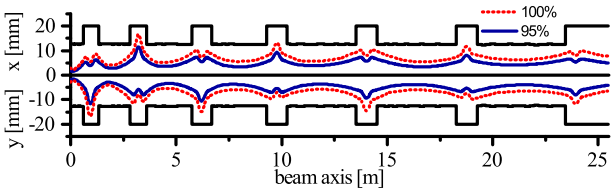

Figure 4: Transversal beam envelopes of the proposed high energy linac section.

In conclusion the proposed concept provides a modern alternative to the Alvarez concept. With a higher RF efficiency and lower production cost it can provide good beam quality. Further optimizations regarding beam quality as well as first CST model studies are currently ongoing at IAP. Final judgment on beam quality relies on the availability of beam dynamics simulations for the proposed new Alvarez.

References

[1] A. Almomani, U. Ratzinger, THPME010, Proc. IPAC2014
[2] S. Mickat et al., MOPP060, Proc. LINAC2014
[3] H. Hähnel, U. Ratzinger, R. Tiede, MOPP062, Proc. LINAC2014

* Work supported by BMBF 05P12RFRB9
† haehnel@iap.uni-frankfurt.de

DOI:10.15120/GR-2015-1-FG-UNILAC-13

Optimization of the KONUS beam dynamics for the HE-Linac

A. Orzhekhovskaya[1], *G. Clemente*[1], *L. Groening*[1], *S. Mickat*[1], *and B. Schlitt*[1]
[1]GSI, Darmstadt, Germany

Introduction

A new high energy heavy-ion injector (HE-Linac) for the FAIR project was proposed as replacement for the existing post-stripper linac at the GSI UNILAC [1]. Six 108 MHz IH-type drift-tube linac cavities within a total length of about 17 m accelerate the ions (up to U28+) from 1.4 MeV/u up to 11.4 MeV/u (Fig.1). The previous beam dynamics of the entire HE-Linac is based on the KONUS concept [2], with an external magnetic quadrupole triplet lens behind each cavity. Particle tracking was performed with the LORASR code, developed at the IAP, Frankfurt [3]. The optimization of the particle tracking through the HE-Linac [4] with respect to the emittance growth reduction is investigated.

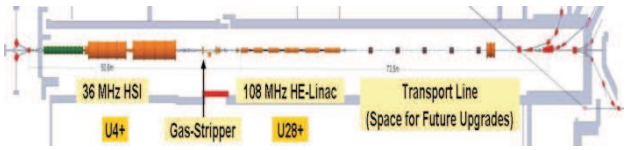

Figure 1: The scheme of the HE-Linac concept.

The Improved Design of HE-Linac

As the first step the influence of the input Twiss parameters on the emittance growth was investigated separately for each of the six cavities. The transverse emittances before the IH1 are 14 mm·mrad and 21 mm·mrad. The assumed longitudinal distribution was generated using the results of measurements for the HIPPI project [5]. The beam current is 20 mA.

The optimum $\alpha_{x,y}$(n) at the beginning of n-th cavity are found in the interval [2.0, 4.0]. The correspondent $\beta_{x,y}$(n) (in mm/mrad) depends on $\alpha_{x,y}$(n) by following rules:

β(1)=0.5α(1), β(2)=0.7α(2), β(3)=0.9α(3),
β(4)=1.3α(4), β(5)=1.6α(5), β(6)=1.9α(6).

These values can be changed by 20%. Then the additional emittance growth is less than 1% for each IH-cavity. For the beam current of 15mA the emittance growth is by 1-2% lower for each tank than for the current of 20mA.

The improved design of the HE-Linac (Fig.2) aims at defined Twiss parameters before each cavity, keeping the KONUS beam dynamics. The triplet gradients and the position of triplets are varied for this matching. The total length of the HE-Linac is increased by 1.4 m. The larger distance between the cavities allows integration of diagnostics devices.

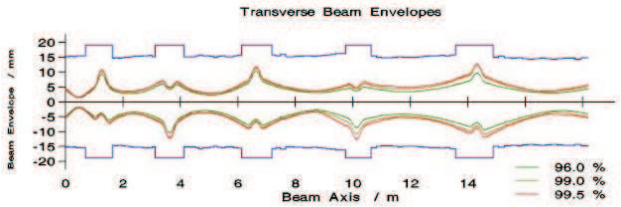

Figure 2: The transverse envelopes through the HE-Linac for the improved design.

The improved design increases transmission from 88% to 92%. By artificial decrease of the longitudinal input emittance from 20 keV/u·ns to 15 keV/u·ns the transmission can be increased up to 100% . The transversal emittance growth along the line is about 35% (instead of 50%). The beam brilliance behind the HE-Linac is about 1.5 times higher for the improved design.

Periodic Solution

The solution is called periodic, if α_x, α_y are the same at the beginning of each period (entrance to the IH-tank) and β_x, β_y change correspondently to the energy growth: (β(n)/ β(n-1))^2 = $\beta\gamma$(n) /$\beta\gamma$(n-1). Any α from the interval [2.0, 4.0] satisfy the conditions for the smallest emittance growth in each period and can be fixed for the periodic solution. The energy growth is known from the cavities design. Taking into account, that β defined above can be changed by 20% without significant emittance growth, the periodic solution, corresponding to the energy changes and being inside this 20% corridor, is found as:

β(1)=0.57α(1), β(2)=0.72α(2), β(3)=0.93α(3),
β(4)=1.15α(4), β(5)=1.35α(5), β(6)=1.53α(6).

References

[1] W. Barth, The injector systems for the FAIR project, in: Proc. LINAC08, Victoria, Canada, 2008. p. 31.

[2] R. Tiede et al., KONUS beam dynamics designs using H mode cavities, in: Proc. Hadron Beams 2008, Nashville, USA, 2008, p. 223.

[3] R. Tiede et al., LORASR code development, in: Proc. EPAC2006, Edinburgh, Scotland, 2006, p. 2194.

[4] B. Schlitt et al., Status of the High-Energy Linac Project at GSI, GSI Scientific report 2012, Darmstadt, Germany, p.270

[5] L. Groening et al., Benchmarking of measurement and simulation of transverse rms-emittance growth, PRST-AB 11 (2008), 094201

DOI:10.15120/GR-2015-1-FG-UNILAC-14

Status of the cold model for the HE-Linac cavities

A. Seibel, X. Du, L. Groening, O. Kester, S. Mickat
GSI, Darmstadt, Germany

Design of a ten gap model

In order to meet the challenges of the FAIR project requiring highest beam intensities an upgrade of the existing Universal Linear Accelerator (UNILAC) is planned. The 108.408 MHz post-stripper section is recommended to be replaced after almost 40 years in operation. All activities are focused on substitution of this UNILAC section by an improved Alvarez DTL [1]. Simulations are done to improve the rf-properties. The geometry of the drift tubes is to be changed to improve the ratio of shunt impedance to maximum surface field [2]. This geometry allows a more homogeneous surface current distribution as well.

A test bench for low power rf measurements with a 10 gap aluminum model (scale 1:3) is under construction (Fig. 1). The frequency scales correspondingly to three times 108.408 MHz (= 325.224 MHz). In the simulations the frequency is 324.694 MHz. It is chosen a bit lower than the reference frequency to have some freedom to reach the right frequency after the fabrication and shift it up with tuners. There could be some small unexpected errors in fabrication which influence the frequency. If the frequency is too high it is hard to tune it to lower frequency.

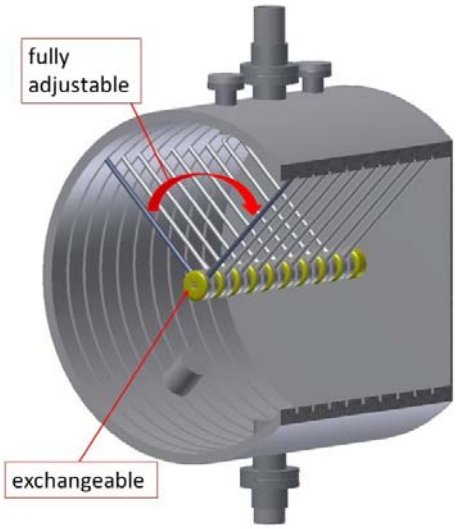

Figure 1: Design of the ten gap Alvarez model for a test bench for low power rf measurements.

The ten gap model with nine full and two half drift tubes at the tank cabs allows to vary the angle between the stems. The stem configuration of each drift tube has an influence on the field stability. In addition the drift tube cabs are dismountable to compare different drift tube geometries as mentioned above.

The goal is to optimize the rf-design geometry with respect to the field distribution stability. The calculated electric field profile along the beam axis shows a flatness better than 3 % (Fig. 2).

With the bead pull method the electrical field distribution will be confirmed as well as the field stability with respect to parasitic modes.

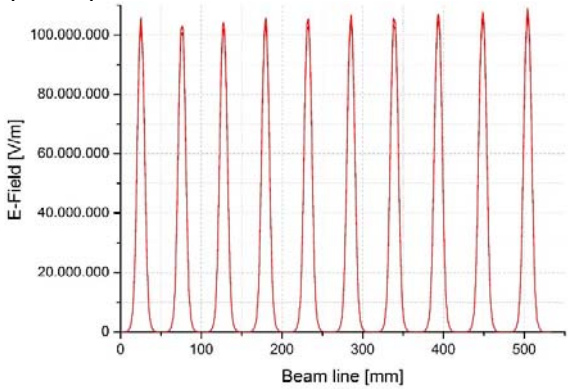

Figure 2: The calculated accelerating electrical field is very flat a βλ-type structure.

Tuning

To match the operation frequency tuners are needed. Three different positions for the tuners along the tank are investigated. The inductively coupling tuners are cylindrical with a diameter of 60 mm. The frequency deviation is 0.4 MHz per Tuner per 100 mm plug-in depth (Fig. 3). The field distribution is independent of the tuner position for all three tuners. The frequency shift of each tuner is the same.

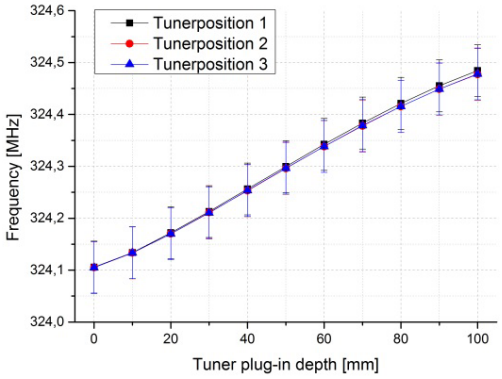

Figure 3: Simulated frequency deviation for the three possible tuner positions to test different fix and dynamic tuners.

Outlook

The fabrication of the 10 gap model is already started. The delivery of the model is expected in summer 2015. Tests are planned at the p-linac test bench.

References

[1] S. Mickat et al., internal report 2014
[2] X. Du et al. (this report)

DOI:10.15120/GR-2015-1-FG-UNILAC-15

Activities on the HE-Linac DTL cavity RF-design

X. Du[1], L. Groening[1], S. Mickat[1], A. Seibel[1,2], A. Orzhekhovskaya[1]
[1]GSI, Darmstadt, Germany; [2]Goethe-University, Frankfurt, Germany

Abstract

The new 108 MHz Drift Tube Linac (DTL) of the UNILAC upgrade program at GSI is in the stage of designing and RF simulations. The DTL accelerates heavy ions with a maximum A/q of 8.5 from 1.4 MeV/u to 11.4 MeV/u. The planned accelerator consists of 5 tanks [1]. Several new features have been studied in the design for better performance regarding the peak surface field (E_{surf}), the shunt impedance (ZTT), and the electric field distribution.

Tube optimization

The optimizations started from existing Alvarez cavities at the UNILAC of GSI, with tank1 that has 3.6 MeV/u as output energy. The new tube shape, which is generated by smooth spline function, is used to replace the traditional shape that is based on blend and chamfer as shown in figure 1. With this new tube shape, the surface field is uniformly distributed on the surface of the drift tube keeping the shunt impedance constant, while the maximum E_{surf} is reduced by about 20%. The tube shape is the same for all cells in one cavity.

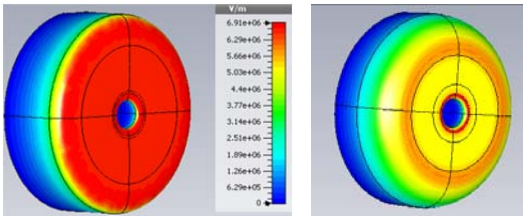

(a) (b)

Figure 1: The surface field distribution on new tube shape (a) and on the original tube shape (b).

Beta profile design

The tube sequence design is based on an optimized 3D tube model, predefined input energy, and maximum E_{surf}. The effective voltage is calculated from a single cell 3D model simulation, which provides the information of power loss, the transient time factor (TTF), maximum allowed E_{surf}, and the shunt impedance. The cell length is defined by the output energy of the former cell. The gap length is defined by the limit of maximum E_{surf} and the operational local frequency. The Visual Basic code in CST-MWS is used to perform continuous cell by cell design. Several different versions for DTL tank1 with different maximum E_{surf} and ZTT are weighted with respect to other considerations such as length of the tunnel and ability of RF power. We prefer a constant average electric field (E_0) with 1.0 Kilpatrick limit for maximum E_{surf}.

Field flatness

The designed electric field distribution may be disturbed in the real cavity due to perturbation, which is caused by mechanical errors. This effect may be decreased by post couplers. The simulation shows that by rotating specific stems in the cavity as shown in figure 2, the TM modes which are close to the operational mode, will be pushed away, and the sensitivity of field flatness to the local frequency uncertainty could be reduced significantly. The improvement is shown in figure 3.

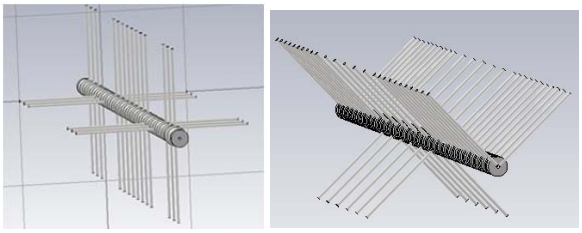

Figure 2: Stem arrangement for better field stability.

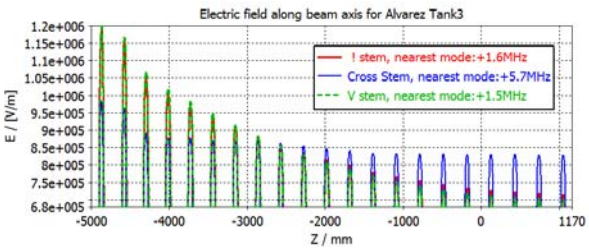

Figure 3: Electric field distribution with perturbation at the first cell of cavity.

The RF design of Alvarez cavities for UNILAC upgrade is in process, magnet design for Tank 1 has started, and the beta profile of other tanks will be designed with the same principle as tank1. A corresponding aluminium 1:3 Alvarez RF model is ordered for mechanical studies and RF measurement [2].

References

[1] S. Mickat et al., this report.
[2] A. Seibel et al., this report.

DOI:10.15120/GR-2015-1-FG-UNILAC-16

Bunch tomography for longitudinal diagnostics at FAIR

O. Chorniy, H.Bräuning, P.Miedzik, A.Reiter
GSI, Darmstadt, Germany

The longitudinal diagnostics is an important tool to observe the beam behaviour under various RF gymnastic processes in FAIR rings. After installation of a dedicated FESA based data acquisition (DAQ) system for bunch measurements [1] the software and hardware parts were expanded providing the ability to perform the on-line bunch tomography. Presently, the system is under further developments which includes fine tuning of the GUI, debugging of the FESA class and final assembling of the electronics.

On-line bunch tomography

Tomographic reconstruction of longitudinal phase space is a reliable instrument in bunched beam diagnostic [2]. At GSI, the first simple on-line tool was realized [1] using Mathematica software and the tomography code. Measurements in the SIS18 were done using the sum signal of a single BPM. The Lecroy oscilloscope was used as DAQ. It was required to preview signal in a form of a waterfall plot and to choose different important parameters for tomography. For this purposes a test GUI in Mathematica was written. The tomographic reconstruction itself was done using a FORTRAN based code written at CERN [2].

After installation of the broadband FCT, the aim was to implement the tomography tool into the new FCT DAQ described below. First tests were performed in a "quasi on-line" regime which means the signal source was signal generator, the timing source was in-house developed timing simulator. A snapshot of the GUI is shown in Figure 1.

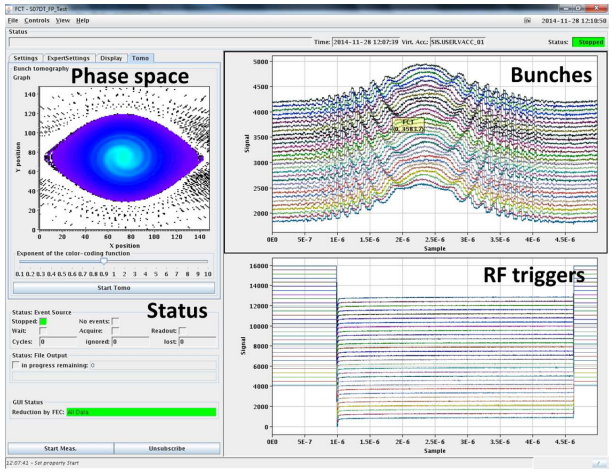

Figure 1: GUI with reconstructed phase space.

Temporarily, the tomography code resides on the PC where the GUI runs. It is planned to use a dedicated PC with a multi-core CPU in order to accelerate the reconstruction process. A more advanced option is to consider a GPU based tomography, while a speedup of 10-100 times can be achieved in comparison to a CPU. In addition, this option will require the development of a new tomography code.

DAQ system for bunch diagnostics

In parallel to the feasibility study of tomography the on-line system for the diagnostics using FCT was developed. This system consists of the FAIR specified VME based DAQ with FESA framework based software and Java GUI. The system was successfully tested in 2012 [3].

The length of the synchrotron cycle can ranges up to several seconds. At high sampling rates it will lead to a large amount of raw data. Data reduction can be achieved by triggering the DAQ system on a rate divider output to which the RF master oscillator is connected.

Previously the data reduction was realized using NIM modules. A new FPGA based single board electronics card covering multiple-event functionality including the timing receiver was designed, tested and will be assembled. The board is shown in Fig.2.

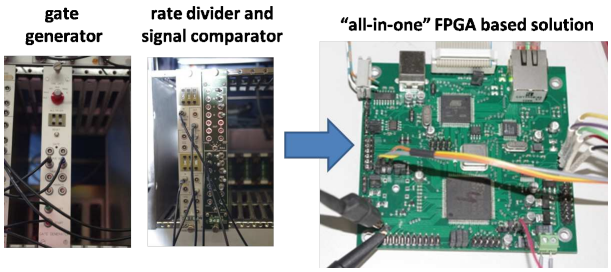

Figure 2: FPGA based single board electronics (right) for multiple-events triggering to replace NIM based solution (left).

References

[1] O. Chorniy, H. Bräuning, T. Hoffmann, H. Reeg, A. Reiter, "A FESA DAQ for Fast Current Transformer in SIS 18", IBIC2013, Oxford, September 2013

[2] S. Hancock, P. Knaus, M. Lindroos, Tomographic measurements of longitudinal phase space density, EPAC98.

[3] O. Chorniy, H. Bräuning, T. Hoffmann, H. Reeg, A. Reiter, M. Witthaus, "New Data Acquisition for Beam Transformers in SIS18 and Transfer Lines", GSI Scientific Report 2013

DOI:10.15120/GR-2015-1-FG-UNILAC-17

Modernisation of the 108 MHz RF systems of the UNILAC post stripper section

B. Schlitt, G. Eichler, S. Hermann, M. Hörr, A. Schnase, G. Schreiber, W. Vinzenz
GSI, Darmstadt, Germany

For the FAIR facility, all ion beams heavier than protons will be provided by the existing UNILAC for injection into the SIS18 synchrotron. Since the UNILAC is in operation successfully since about 40 years, an extensive modernisation of the post stripper RF systems and a replacement of the Alvarez DTL are planned to assure reliable operation for FAIR as well as the required beam quality [1,2]. To match the FAIR conditions, the UNILAC will be converted into a short-pulse accelerator, the RF beam pulse length and duty cycle being reduced from up to 6 ms / 30 % to ≤ 2 ms / ≤ 2 %. Long duty cycle beams will not be provided anymore.

Modernisation of the existing RF systems

Substantial modernisations of the existing post stripper RF systems are planned:

- The old control components of the existing 1.7 MW high power amplifier (HPA) stages equipped with RS 2074HF tubes to feed the five Alvarez tanks will be substituted by state-of-the-art PLCs. Modern fast measurement and interlock systems and commercial control grid power supplies will replace the old equipment.
- 120 – 150 kW solid state driver amplifiers will replace the existing tube drivers. A call for tenders for a prototype was started recently.
- The original relay based control of the 1 MVA anode power supplies for the HPAs will be substituted by modern PLC systems.
- Substitution of the resonance tuning circuits and of the LLRF systems by new developments.

Extensive preparations and developments of these tasks as well as the procurement of various components were performed in 2014. A stepwise realisation of major measures is planned during longer shutdown periods of the GSI accelerators during 2015 to 2017.

New 1.8 MW cavity amplifier prototype

On a long-term schedule, a replacement of the existing high power amplifiers is considered. The development and manufacturing of a 1.8 MW cavity amplifier prototype was ordered to Thales Electron Devices, based on a Thales TH 558SC tetrode, which is widely used worldwide for broadcast transmitters as well as for scientific applications. Thus, there is no known risk concerning the long-term availability of this tube for the coming decades. The design of the cavity amplifier was almost finished by Thales in 2014 (Fig. 1). Manufacturing, RF tests, and delivery of the amplifier are scheduled for 2015. A test bench will be prepared at the UNILAC RF gallery allowing operation of the new amplifier either on a water dummy load or on one of the Alvarez cavities.

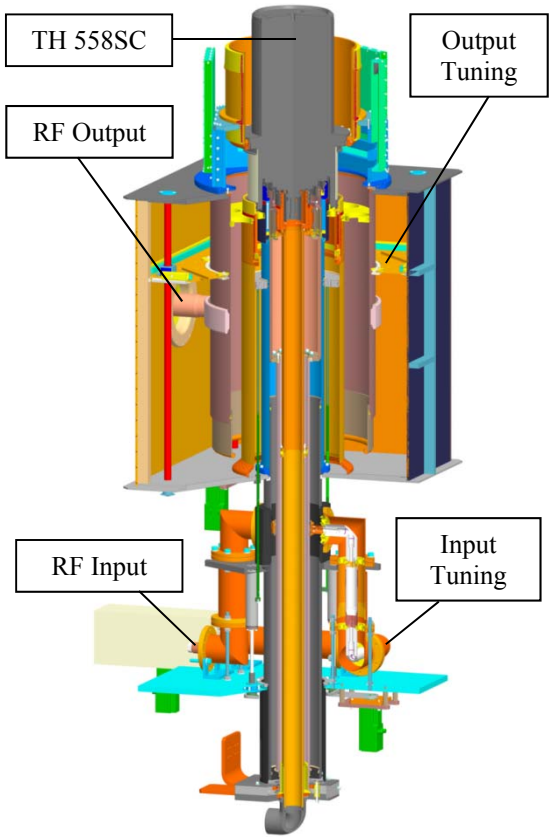

Figure 1: Sketch of the 1.8 MW high power amplifier cavity prototype designed by Thales (by courtesy of Thales Electron Devices, Thonon, France).

D-LLRF system tests

A digital low-level RF (d-LLRF) system designed by industry for 216 MHz linac RF systems for particle therapy facilities [3] was adapted by the supplier to an operating frequency of 108 MHz and was integrated into an existing 160 kW amplifier at GSI [1]. It was tested for RF amplitude and phase control of a single-gap resonator at the UNILAC including ion beam tests using 1.3 mA $^{181}Ta^{24+}$ beams. Stable operation was achieved within a limited amplitude range and beam loading could be partly compensated by the digital control unit [1]. Further improvements and tests of the system are planned.

References

[1] B. Schlitt, M. Hoerr, A. Schnase, G. Schreiber, and W. Vinzenz, RF system development for the new 108 MHz heavy ion high-energy linac at GSI, LINAC2014, Geneva, Switzerland, TUPP058 (2014).
[2] S. Mickat et al., this report.
[3] Ampegon AG, Turgi, Switzerland.

DOI:10.15120/GR-2015-1-FG-UNILAC-18

Results of the experiments on emittance transfer EMTEX

M. Maier, S. Appel, Y. El Hayek, P. Gerhard, L. Groening, S. Mickat, A. Seibel, H. Vormann, M. Vossberg, C. Xiao

GSI, Darmstadt, Germany

Introduction

EMTEX is an experimental setup to proof the principle of transverse emittance partitioning on an ion beam. According to simulations it is possible to transfer emittance by changing only the magnetic field of a solenoid with a charge state changing stripper inside. The change of charge state in the solenoid changes the set of eigen-emittances and the skew quadrupoles serve to remove inter-plane correlations. The field strength of the solenoid determines the amount of transfer between the eigen-emittances. A detailed description of the concept and the beam line itself is given in [1].

Experimental setup

Besides some matching quadrupoles, the setup shown in Figure 1 consists of a stripping foil inside a magnetic solenoid field to couple the transverse planes and for the emittance transfer. Behind the solenoid a skew quadrupole triplet rotated by 45° is used to remove the coupling.

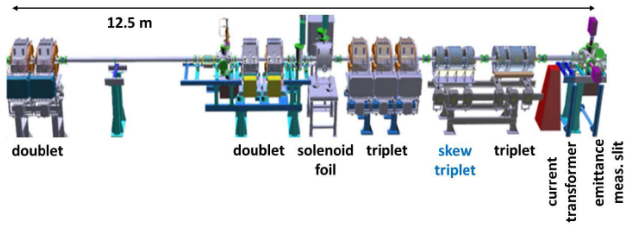

Figure 1: Beam line of EMTEX (Emittance Transfer Experiment) in the transfer channel of GSI.

Results

For the experiment a low intensity beam of $^{14}N^{3+}$ at 11.4 MeV/u was fully stripped to $^{14}N^{7+}$ in a 200µg C-foil placed at the centre of the solenoid. For each solenoid setting full transmission was preserved and the emittances were measured for both planes.

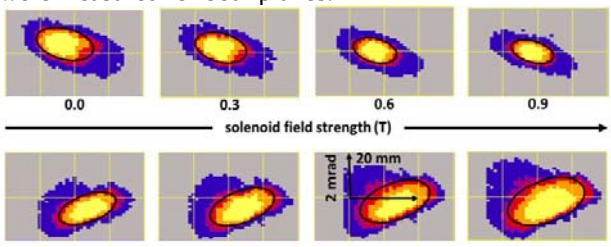

Figure 2: Vertical (upper) and horizontal (lower) phase space distribution measured behind EMTEX for varied solenoid field strength. The black ellipses represent the 4*rms emittances.

*Work supported by: BMBF-Projekt 05E12CD1
*m.maier@gsi.de

Figure 2 shows the measured emittances behind EMTEX for different solenoid field strengths. All other magnet settings were kept constant and the Twiss parameters remained constant. Yet for these solenoid field settings the emittance partitioning changes and, as shown in Figure 3, matches the simulation results [2] very well. For this reason the multi turn injection efficiency into SIS18 has been investigated using this technique [3]. As expected, the reduced horizontal emittance directly translates into increased multi turn injection efficiency shown in Figure 4.

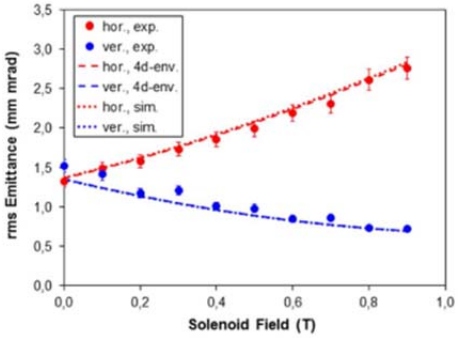

Figure 3: Measured transverse emittances behind EMTEX for different solenoid field strength compared to the simulations.

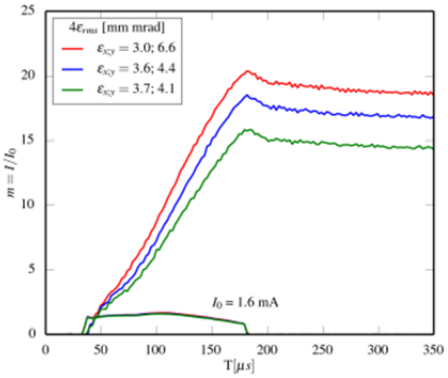

Figure 4: Improved multi turn injection efficiency using EMTEX.

Outlook

To quantify the possible gain factor of this technique the limits should be investigated. This could be achieved by increasing the macro pulse length and thus the injection time above the regularly used 150µs.

References

[1] C. Xiao, et al. PRSTAB **16**, 044201 (2013).
[2] L. Groening et al., PRL **113**, 264802 (2014).
[3] S. Appel, GSI Report 2013-03 (2013).

DOI:10.15120/GR-2015-1-FG-UNILAC-19

Status of the High Gradient CH – Cavity*

Ali Almomani[#] *and Ulrich Ratzinger*
IAP – Goethe Universität, Frankfurt am Main, Germany

This pulsed linac activity aims on compact designs and on a considerable increase of the voltage gain per meter. A high gradient CH – cavity operated at 325 MHz was developed at IAP – Frankfurt. The mean effective accelerating field for this cavity is expected well above 10 MV/m at β = 0.164. This cavity is developed within a funded project. The results might influence the rebuilt and a later energy upgrade of the UNILAC – Alvarez section. Another motivation is the development of an efficient pulsed ion accelerator for significantly higher energies like 60 AMeV. The new GSI 3 MW Thales klystron test stand will be used for the cavity RF power tests. Detailed studies on two different types of copper plating will be performed with this cavity. The first measurement results for this cavity will be presented.

Introduction

Conventional DTL's are seriously limited in maximum field gain by thick walled drift tubes for housing focusing elements. This geometry causes extended parallel surfaces around the gaps loaded by high electric fields. The multipacting probabilities as well as the stored field energies are rather high at these cavities resulting in a reduced field gain. Additionally, maximum achievable electric fields are reduced by the presence of magnetic fields [1].

This paper is focusing on the development of CH – cavities with a high field gradient. One main goal of this work is to prepare for a possible later energy upgrade of GSI – Unilac, which will in future serve as heavy ion injector for the FAIR project.

CH – Cavity Design

At IAP – Frankfurt, a 7 gap CH – cavity (Figure 1) operated at 325 MHz with constant β=0.164 has been developed and expected to have a field gradient of about 13.3 MV/m [2-4]. This cavity was built in NTG GmbH and was delivered to IAP in December 2014. The main parameters of this cavity are given in table 1.

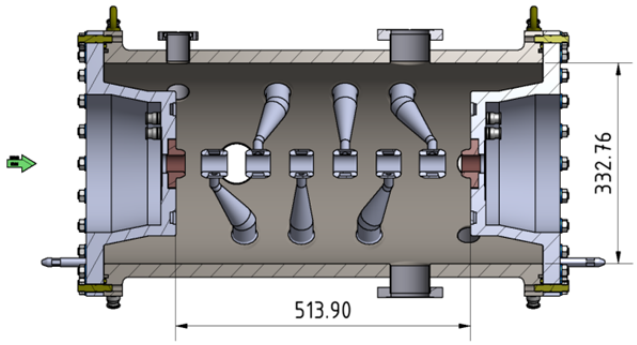

Figure 1: A 3D schematic view of the CH – cavity.

The geometry was optimized for modest surface peak fields – reaching up to 97 MV/m at very small spots on the drift tube edges.

The CH–cavity was built from stainless steel (Figure 2) and will be galvanically copper plated on its inner surface. This will be a challenge for such geometry. The cavity cylinder will contain no screwed connections and the end flanges are sealed by metal joints. Only the end half tubes are from massive copper.

Special care will be taken for the galvanic copper plating of the cavity. Two processes with different bath ingredients will be tested against each other at high rf power levels. Currently, the cavity was sent to Galvano-T for a first copper plating and is expected to be resent by end of March 2015.

Table 1: Main Parameters of the High Field CH – Cavity	
Number of Gaps	7
Frequency (MHz)	325.2
Voltage Gain (MV)	6
Eff. Accel. Length (mm)	513.9
Eff. Accel. Field (MV/m)	13.3
Power Loss (MW)	1.76
Eff. Shunt Impedance (MΩ/m)	52.15
Q_0 – value	12500
Drift Tube Aperture (mm)	27

Figure 2: The 325 MHz high-field cavity before the copper plating.

Conclusion

CH- type cavities may allow for a significant cost and size reduction of future ion linacs in the energy range up to about 100 AMeV.

Detailed investigations on the two different types of copper plating can be performed on this cavity and by using the GSI high power 325 MHz test stand driven by a 3 MW klystron.

References

[1] D. Stratakis et al., NIM A 620, 147–154 (2010).
[2] A. Almomani et al., PRST– AB **15**, 051302 (2012).
[3] A. Almomani et al., IPAC 14, THPWO012 (2014).
[4] A. Almomani et al., LINAC 14, THPB006 (2014).

* Work supported by BMBF, contract No. 05P12RFRB9.
[#]a.almomani@iap.uni-frankfurt.de

4 K and 2 K measurements on the 325 MHz CH-cavity *

M. Busch† [1], *F. Dziuba*[1], *H. Podlech*[1], *U. Ratzinger*[1], *W. Barth*[2,3], *and M. Amberg*[1,3]
[1]Institut für Angewandte Physik, Goethe Universität, Frankfurt; [2]GSI, Darmstadt; [3]HIM, Mainz

At the Institute for Applied Physics (IAP), Frankfurt University, a superconducting 325 MHz CH-Cavity has been designed and built. The 7-cell cavity features a geometrical β of 0.16, corresponding to a beam energy of 11.4 AMeV. The design gradient is 5 MV/m. Main novel features of this resonator are a compact design, low peak fields, easy surface processing and power coupling. Furthermore a new tuning system based on bellow tuners inside the resonator will control the frequency during operation [1]. After the final preparation steps rf measurements at 4 K and 2 K have been performed at the cryo-lab of the Institute for Applied Physics with promising results.

Setup at IAP Cryo-Lab

In April the 325 MHz CH-Cavity returned to IAP after final BCP and HPR at Research Instruments. Then the fully equipped cavity with 40 TLD and four thermal probes has been lowered down the 3 m deep vertical cryostat for power tests (s. Figure 1). After initial pressure issues due to a potential virtual leakage a final pressure of $8 \cdot 10^{-10}$mbar could be achieved. Multipacting conditioning proceeded smoothly.

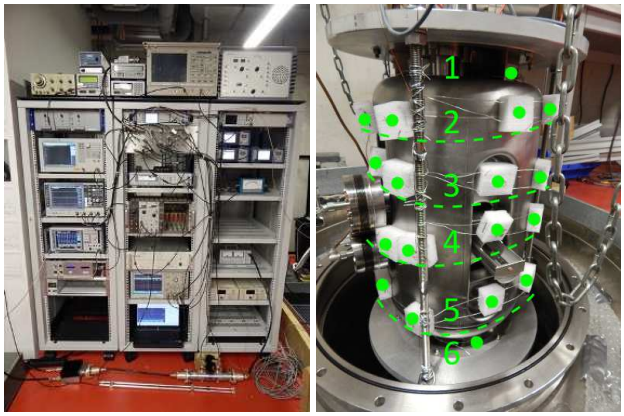

Figure 1: Measurement setup at the cryo-lab. *Left*: Fully equipped racks. *Right*: Array of the TLD on the cavity surface.

Results

The evaluation of the TLD showed only weak radiation events due to field emission after 10 hours of cumulated heavy operation. A small field emitting site is suspected at the bottom of the cavity tank (s. Figure 2). Further surface processing should decrease emission activity continuously. The measured Q vs E curve showed a maximum achievable gradient of 8.5 MV/m at 4 K. After cooling down to 2 K the max field level reached up to 14.1 MV/m limited by thermal quench due to a possible local defect (s. Figure 3) [2].

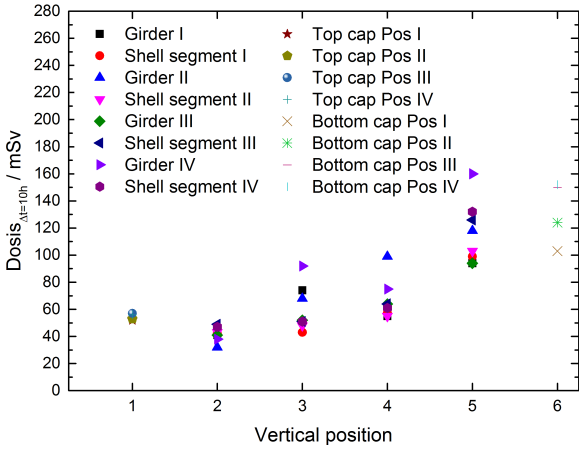

Figure 2: Evaluation of the TLD dosis for the 40 modules.

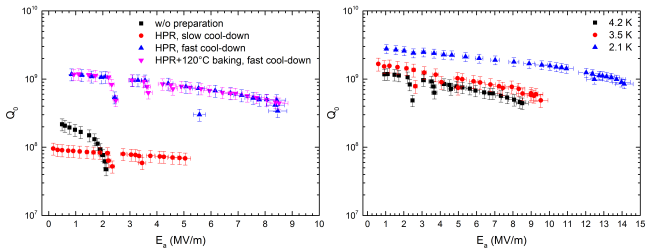

Figure 3: *Left*: Q vs E curve for 4 K measurements and different processed surface qualities. *Right*: Measurements performed at 2 K.

References

[1] M. Amberg, K. Aulenbacher, W.A. Barth, S. Mickat, M. Busch, F.D. Dziuba, H. Podlech, U. Ratzinger, "Structural Mechanical Analysis of Superconducting CH-Cavities", SRF 2011, Chicago, USA.

[2] M. Busch, F. Dziuba, H. Podlech, U. Ratzinger, M.Amberg, "Cold Power Tests of the sc 325 MHz CH Cavity", LINAC 2014, Geneva, Switzerland.

* Work supported by GSI, BMBF Contr. No. 06FY7102
† busch@iap.uni-frankfurt.de

DOI:10.15120/GR-2015-1-FG-UNILAC-21

Accelerator operation report

S.Reimann[1], *P.Schütt*[1]
[1]GSI, Darmstadt, Germany

This report describes the operation statistics of the GSI accelerator facility of the year 2014. The information is based on the data of the GSI electronic operation logbook OLOG [1] which allows a detailed evaluation of operation statistics especially for the time-sharing operation mode of the accelerators.

General Overview

After a long (14 months) shutdown period, which already began in 2012, the re-commissioning started in January. From January till November, two major beam time blocks were scheduled, which resulted in an operating time in the same order of magnitude as in 2012. In total, the SIS has been operated for 5832 hours and the UNILAC for 6432 hours (1032 hours are included for the commissioning of the accelerators after shutdown).

The intermediary shutdown period lasted from May 19th till June 24th. Because of performance issues and the obvious misalignment of the ring, the SIS shutdown was brought forward to May 2nd. The break was used to completely realign the SIS. In addition an aperture limiting piece of aluminium foil could be localized and removed from the vacuum chamber.

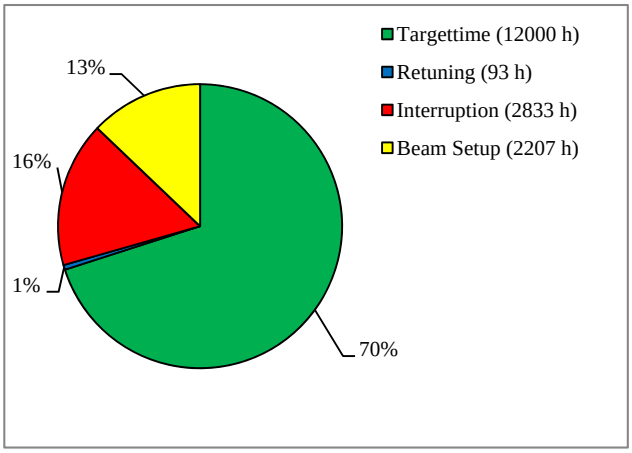

Figure 1: Distribution of overall beam time for all experiments

Figure 1 shows the overall beam time of the whole facility. In total 12000 hours of beam-on-target-time were successfully delivered to the different experiments, which is 70% of total beam time (76% in 2012).

The percentage of interruption time increased by 14%, you find the absolute numbers for 2012 and 2014 in Table 1. Similarly the percentage of the time needed for beam setup increased by 30%. Main reason for this gain was the complicated beam time schedule and the higher percentage of accelerator experiments (22%). At the UNILAC 1575 hours of beam time have been used for accelerator experiments, at the SIS there were 1798 hours and at the ESR 390 hours for accelerator experiments, which is in total an increase by a factor of 6 compared to 2012. At the UNILAC it is even a factor of 8.

Table 1: Overall beam time of the accelerator facility

	2014	2012
Integral target time for all experiments	**12000 h**	12105 h
Beam Setup	**2207 h**	1656 h
Time for retuning	**93 h**	102 h
Time of interruption	**2833 h**	2323 h
Total beam time	**17133 h**	16220 h

Operation for Experiments

Figure 2 gives an overview of target time for different experimental areas. The fraction of the beam branches of the UNILAC are marked in blue, the ESR in green and the different experimental caves behind the SIS are displayed as orange slices. Details corresponding to the different experimental programs are given in [2].

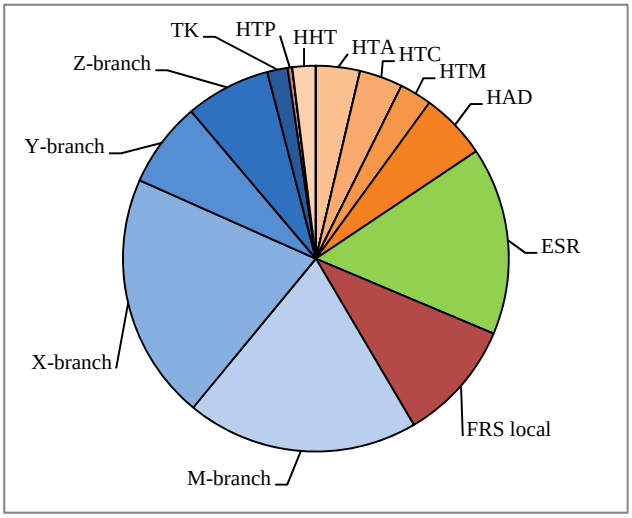

Figure 2: Distribution of target time to the different experimental areas

UNILAC Experiments

Details of the beam time for UNILAC experiments are shown in Table 2. Over the year 23 different experiments have been performed at the UNILAC. In total 6782 hours of target time have been achieved. The main user was the Material Science (2097 hours). The fraction of target time remained almost constant compared to 2012 but an increase of time for accelerator setup was observed.

DOI:10.15120/GR-2015-1-FG-GENERAL-01

Table 2: Beam delivery to UNILAC experiments

	Time	Ratio
Target time for experiments	6782 h	75,2%
Time for retuning	48 h	0,5%
Accelerator setup	1008 h	11,2%
Ion source service	407 h	4,5%
Unscheduled down time	774 h	8,6%
Total beam time	**9018 h**	**100%**

SIS/ESR Experiments

The SIS delivered beams to 19 fixed target experiments and to 7 experiments at the ESR. In total 5219 hours of target time have been achieved. The fraction of target time decreased by more than 10% compared to 2012, which was mainly caused by the increased unscheduled downtime. A more detailed overview is given in Table 3.

Table 3: Beam delivery to SIS/ESR experiments

	Time	Ratio
Target time for experiments	5219 h	64,3%
Time for retuning	45 h	0,6%
Accelerator setup	1199 h	14,8%
Ion source service	114 h	1,4%
Unscheduled down time	1538 h	19,0%
Total beam time	**8115 h**	**100%**

In 2014 the target time for the ESR (direct beam and beam via FRS) increased to 2106 hours. For about 1359 hours the beam was delivered to the local experiments of the FRS. 747 hours of beam time were scheduled for HAD, another main user at the SIS.

Accelerator Operation

Table 4 shows more detailed all unscheduled down time events. In comparison to 2012 the downtime increased by 47%. In addition to the previously described SIS problems, which are excluded from these statistics, a water leak of the newly installed MA-cavity stopped the SIS operation for several days.

The total downtime of power supplies and controls were increased by more than a factor of two, compared to 2012. The main reason for control problems was the high maintenance requirement for old hardware and legacy software during the beam time. The time spent for operation failures increased slightly, which was to be expected in the face of the complex operating mode (switching experiments several times per day) and the special settings for the accelerator experiments.

Table 4: Statistics of all unscheduled down time events

	Down time	No. of events
Power supplies	580 h	412
Vacuum and structures	438 h	119
Beam diagnostics	31 h	19
Operation	38 h	38
Safety-/ Interlock system	38 h	36
Ion Sources	143 h	53
RF system	328 h	434
Controls	164 h	70
Infrastructure	40 h	16
Others / ambiguous	186 h	89
Total of unscheduled down time	**1986 h**	**1286**

During 2014, 19 different isotopes have been accelerated. Figure 3 shows the operation time for each isotope. Besides nitrogen, the heavy elements beyond samarium were dominating the ion source statistics.

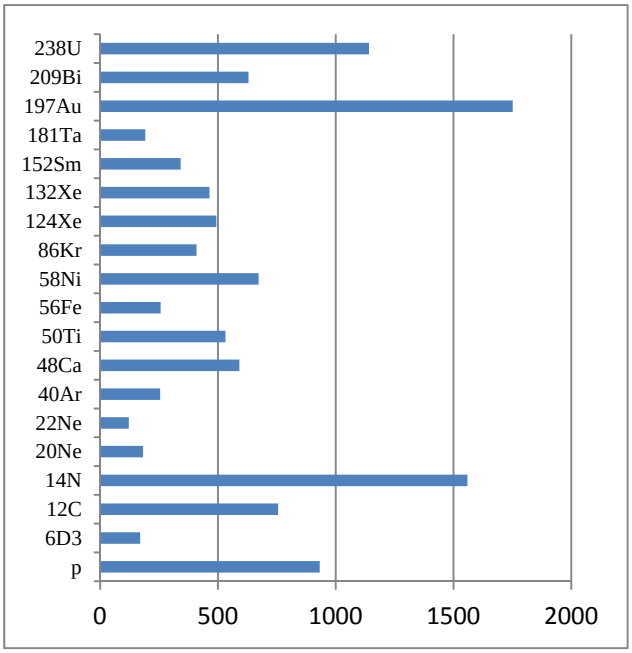

Figure 3: Total beam time for different ion species

References

[1] P.Schuett, the GSI Operation Logbook OLog, WAO2010 (http://wao10.komac.re.kr/PDF/O-17.pdf)
[2] Report of beam time coordinator, this report

DOI:10.15120/GR-2015-1-FG-GENERAL-01

Status of the cw-LINAC demonstrator project

V.Gettmann[2], W.Barth[1, 2], S.Mickat[1, 2], M.Amberg[1], H.Podlech[3], U.Ratzinger[3], F.Dziuba[3], and K. Aulenbacher[1, 4]

[1]GSI, Darmstadt, Germany; [2]HIM, Institute Mainz, Germany; [3]IAP, Frankfurt, Germany; [4]IKP, Mainz, Germany.

Cryostat and cavity

The Demonstrator is the first section of the proposed cw-LINAC [1]. The fabrication of the Demonstrator is still in progress. The complete system is expected to be at GSI in 2015.

Meanwhile the inner structure of the cavity is fabricated (Fig. 1). The operation frequency was checked at Research Instruments (RI) site during the whole fabrication process dependent on mechanical stress from vacuum, and from cooling down. Frequency shifts are not allowed and has to be compensated by an adequate setting of the static tuners length [2]. Also the change in volume after three times buffered chemical polishing (BCP) has to be taken into account during the tuning process. The chemical treatments etch in total 75 µm of the cavity's surface. After the chemical treatments the cavity is high pressure rinsed and sealed under cleanroom conditions for shipment to the IAP. Here RF performance tests in a cold environment are planned. After successful tests the cavity is sent back to RI for the final step in fabrication. The helium jacked out of titanium as well as the suspending blocks will be welded to the cavity.

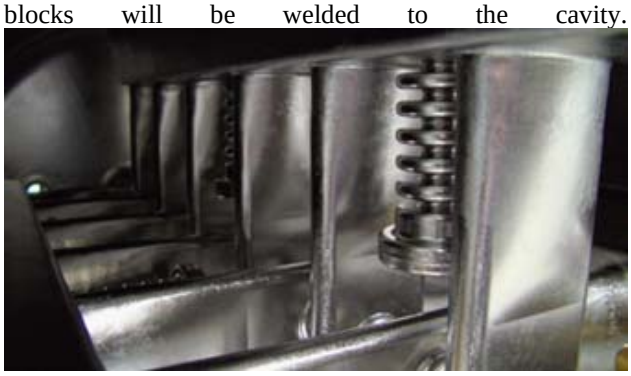

Figure 1: The inner structure of the CH-cavity.

The cryostat itself is ready for assembling at Cryogenic Ltd. Site. Most of the parts are on site (Fig.2). The delay in delivery is mainly caused by finding an adequate provider for the µ-metal shield. According to an updated schedule the overall system including the two solenoids and dummy is expected to be completed until May 2015.

Setup at GSI-HLI

The test environment at GSI-HLI is prepared almost. Recently the control room is arranged for the 5kW-RF-Amplifier for the CH-cavity and the 12kW-RF-Amplifier for the cw Buncher. The additional cw buncher cavity is under development an expected in June 2015. Only the RF-piping is outstanding. The liquid helium supply is rearranged and detailed. The 3000 litre tank will be located near the x-ray radiation protection shelter of the demonstrator, and connected via flexible pipe to the cryostat. The exhaust helium gas will be heated, counted via gas meter, and as planned collected in a 25³m recovery balloon.

Figure 2: The cryostat and the two sc solenoids are ready for assembling at Cryogenic Ltd, London.

References

[1] V. Gettmann et al. STATUS OF THE SC CW-LINAC DEMONSTRATOR INSTALLATION, Proceedings annual report 2013, GSI, Darmstadt, Germany.

[2] F. Dziuba et al. A Superconducting 217 MHz CH Cavity for the CW Demonstrator at GSI, Proceedings of SRF 2013 Paris, France.

DOI:10.15120/GR-2015-1-FG-GENERAL-02

Status of the superconducting 217 MHz CH-cavity*

M. Basten[#,1], M. Amberg[1,3], K. Aulenbacher[3,4], W. Barth[2,3], M. Busch[1], F. Dziuba[1], M. Heilmann[2], D. Mäder[1], S. Mickat[2,3], H. Podlech[1]

[1]Frankfurt Universtiy, 60438 Frankfurt, Germany; [2]GSI Helmholtzzentrum, 64291 Darmstadt, Germany; [3]Helmholtz-Institut Mainz (HIM), 55099 Mainz, Germany; [4]KPH Mainz University, 55128 Mainz, Germany

Presently the demonstrator for the sc cw-LINAC at GSI is under construction and its successful beam operation will be the first milestone realizing the new sc cw-LINAC at GSI [1]. The construction of an advanced demonstrator will be the second milestone towards the sc cw-LINAC at GSI. The presently design of the sc cw-LINAC consists of the demonstrator as first cavity and 4 to 5 additional cryomodules with 2 CH-cavities per cryomodule [2,3]. The design of the advanced demonstrator will be used for all cavities in the sc cw-LINAC after the demonstrator. The cavity is designed and optimized for high power applications, consisting of 8 accelerating cells. The design gradient is 5 MV/m. Its frequency is the second harmonic of the High Charge Injector (HLI) at GSI, Darmstadt. Table 1 shows the main parameters of the sc 217 MHz CH-cavity. In Figure 1 the layout of the sc 217 MHz CH-cavity is depicted.

Cavity Design

The design of the cavity is based on 8 equidistant gaps without girders and with stiffening brackets at the front and end cap to reduce pressure sensitivity. The new design avoids girders because they lead to high fabrication costs and extended fabrication duration. Additionally the girders reduce the mechanical stability of the cavity caused by a break of the cylindrical symmetry. The design of the advanced demonstrator without girders is cylindrically symmetrical which leads to significantly higher stability. Additionally the stiffening brackets at both ends of the cavity increase the mechanical stability of the cavity so that the pressure sensitivity is below 5 Hz/mbar.

Parameter	Unit	
β		0.069
Frequency	MHz	215.5
Accelerating cells		8
Length (βλ-definition)	mm	381.6
Cavity diameter	mm	412
Cell length	mm	47.7
Aperture diameter	mm	30
Static tuner		3
Dynamic bellow tuner		2
Wall thickness	mm	3-4
Accelerating gradient	MV/m	5
E_p/E_a		5.2
B_p/E_a	mT/(MV/m)	8.5
G	Ω	51
R_a/Q_0		1045

Table 1: Specifications of the 217 MHz CH-cavity

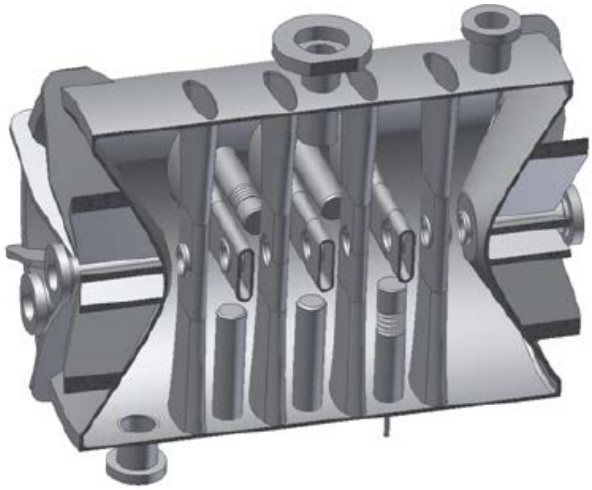

Figure 1: Layout of the sc 217 MHz CH-cavity.

Status

The basic design of the 217 MHz CH-cavity was finished in 2014. Several simulations with CST-Microwave-Studio have been performed to determine parameters as the optimum drift tube length, optimum stem width and cavity diameter [4]. The missing girders in the 217 MHz-cavity require a new design for the dynamic and static tuners. Because of that many simulations concerning the layout and performance of the bellow tuners have been performed to find the optimum geometry. The call for tender started in december 2014 and will end on february 2015. So the communication with the company will start in february 2015 and will be followed by the production start.

References

[1] F. Dziuba, M. Amberg, K. Aulenbacher, W. Barth, M. Busch, H. Podlech, U. Ratzinger, S. Mickat, Superconducting CH Cavities for Heavy Ion Acceleration, in Proc. of IPAC'13, Shanghai, China, p. 3794-3796 (2013)

[2] W. Barth, K. Aulenbacher, F. Dziuba, M. Amberg, V. Gettmann, S. Mickat, H. Podlech, U. Ratzinger, Further R&D for a New Superconducting cw Heavy Ion Linac@GSI, in Proc. of IPAC'14, Dresden, Germany, p. 3211-3213 (2014)

[3] H. Podlech, Proposal for a Superconducting 217 MHz CH-Cavity, institute report: IAP-ACCC-01122013 (2013)

[4] CST Microwave Studio, http://www.cst.com

* Work supported by HIM, GSI

#Basten@iap.uni-frankfurt.de

DOI:10.15120/GR-2015-1-FG-GENERAL-03

Performance demonstration of the non-intercepting Bunch Shape Monitor at UNILAC *

B. Zwicker[1,2], *C. Dorn*[1], *P. Forck*[1,2], *O. Kester*[1,2], *and T. Sieber*[1]
[1]GSI, Darmstadt, Germany; [2]IAP, Frankfurt, Germany

A non-invasive Bunch Shape Monitor (BSM) is foreseen to determine the longitudinal bunch structure with a phase resolution of 1.0°, with respect to the 325 MHz acceleration frequency of the FAIR p-LINAC [1]. It is intended to ensure proper longitudinal matching of the accelerating structures. The presented device is based on the creation of secondary electrons by the ion beam passing a section of high local nitrogen pressure. The secondary electrons are accelerated by an external driving potential towards a time-resolved imaging system [2].

Beam-based Measurements

The non-invasive Bunch Shape Monitor (BSM) has been tested at the UNILAC with several ion beams at 11.4 MeV/u and beam currents in the range from 0.08 to 1 mA. Extensive parameter studies have been executed in 2014. Various parts of the hardware were modified in 2013 and the improved functionality of the device has been clearly demonstrated [3]. For the applied beam settings the BSM is able to obtain profiles down to 250 ps rms with a resolution of 34 ps [4]. As expected, non-Gaussian profiles have been obtained.

By using a single gap resonator (SGR) as a rebuncher longitudinal profile changes have been investigated. This matching is confirmed with a phase probe, while the applied power to the SGR is varied. For the beam tests the ER10 has been used, which implies a distance of 55 m to the location of the BSM (TK5 DK1). The focal length of the ER10 has been varied over several tens of meters to ensure the transmission of the focal point through the location of BSM.

In dependence of the focal length the obtained profile rms widths are depicted in Figure 1. The applied voltage has been varied from 0.53 MV to a feasible maximum of 1.0 MV. The focal length f depends on the applied electric gap voltage U_0 to $U_0 \propto 1$ / f. The BSM is able to detect differences even with a small step size of 0.012 MV. For a value of 0.87 MV the minimum is obtained. From linear beam optics a parabolic dependence of the square of the rms width is expected. For better visualization the rms width is depicted, which should match the square root of this parabola fit. Besides width variation, the bunch shape itself changes and reveals a rather complex composition. This is a hint, as expected, of a distorted phase space distribution of the beam due to the IH-structure's KONUS dynamics. It is foreseen to determine an approximated longitudinal emittance with this measurement by using the parabolic fit parameters for σ^2 over 1/f.

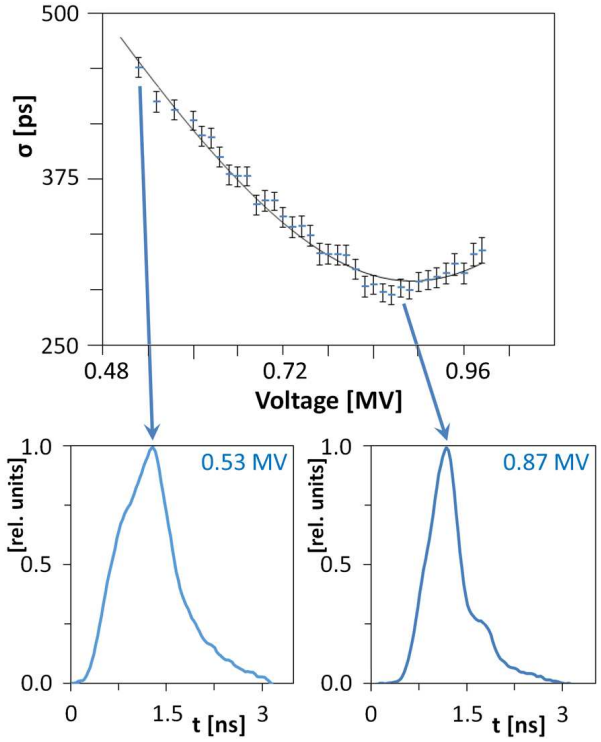

Figure 1: Longitudinal profile widths (rms width of a single Gaussian fit) in dependence of the focal length of single gap resonator ER10. Below are two bunch shapes depicted for different focal length. A non-Gaussian shape is visible. Setting: U^{28+} at 11.4 MeV / u, I = 0.5 mA , τ = 95 μs, p = $5 \cdot 10^{-6}$ mbar, P = 25 W, 16 averages.

References

[1] L. Groening et al., LINAC'12, Tel-Aviv, THPB034, p. 927

[2] P. Forck et al., DIPAC'05, Lyon, p. 48

[3] B. Zwicker et al., IBIC'13, Oxford, MOPC36

[4] B. Zwicker et al., IBIC'14, Monterey, TUDP07

* Supported by EU-Project CRISP, WP3 T1 Non-intercepting Bunch Shape Monitors

Uranium high current development at UNILAC

Winfried Barth[1,2], Aleksey Adonin[2], Christoph E. Düllmann[1,2,3], Peter Gerhard[2], Manuel Heilmann[2], Ralph Hollinger[2], Egon Jäger[2], Jadambaa Khuyagbaatar[1,2], Joerg Krier[2], Paul Scharrer[1], H. Vormann[2], Alexander Yakushev[2], Stepan Yaramyshev[2]

[1] Helmholtz Institute Mainz, Germany
[2] GSI Helmholtzzentrum für Schwerionenforschung, Darmstadt, Germany
[3] Johannes Gutenberg-Universität Mainz, Mainz, Germany

Previously a peak record had been achieved in 2007 (Fig.1), while 30% of the FAIR- U^{28+} beam current was accomplished at the end of the transfer line. Caused by a strong High Current Injector (HSI) performance degradation, up to October 2014 the available beam current dropped down to 13% of the design value only. After re-optimization of the complete front end system the HSI is again able to deliver a high uranium beam current. In a short run applying the new fast pulsed high density H_2-gas cell more than a factor of three higher U^{28+} beam current is now available at 1.4 MeV/u. The stripper performance could be optimized applying significantly higher target densities. The new U^{28+} intensity record exceeds the latest peak record by 56% (Fig. 1).

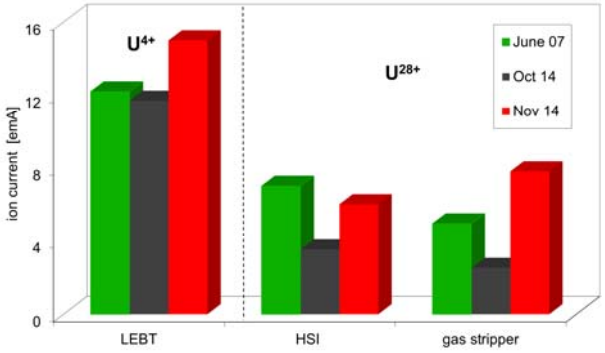

Fig. 1: Achievement of a new uranium beam (28+) intensity record at GSI-HSI and gas stripper section. The former U^{28+}-peak value (2007) was exceeded by 56%.

A new fast pulsed high density gas cell [1] was successfully commissioned with uranium beam from the GSI HSI. Besides, the entire Injector system was optimized for high beam intensity operation. A 25% higher U^{4+} beam current extracted by a newly developed multi aperture beam extraction system (VARIS ion source [2,3]) were used to optimize the Low Energy Beam Transport system and matching line to the RFQ. A beam current of 15.3 emA (Fig. 2) was available for injection into the RFQ. In particular the most sensitive Medium Energy Beam Transport section was optimized for high current high transmission beam transport applying a slightly different set of rf-parameters. With this the HSI was allowed for stable and reliable high current uranium operation. A careful matching of the high power (0.5 MW pulse power) U^{4+} beam to the gas stripper cell was accomplished resulting in a U^{28+} beam current of 7.7 emA (Fig. 2) after stripping and charge separation at 1.4 MeV/u.

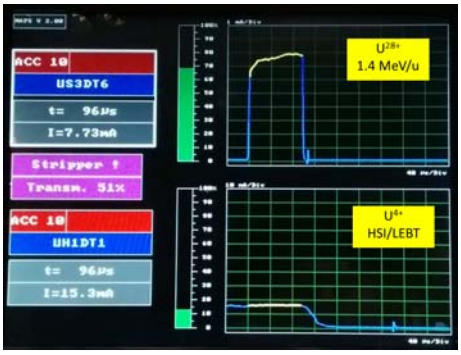

Fig. 2: Beam transformer measurement after careful optimization of a VARIS-uranium beam.

The world intensity record for U^{28+} pulse operation could be reached after less than three days of beam time, including 15 hours beam time spent for commissioning of the H_2-gas cell-stripper. More than 50% of U^{28+}- FAIR intensity requirements (and 65% of beam brilliance) was achieved at 1.4 MeV/u. Increased beam currents for all heavy ions are expected - stripper tests are envisaged using Pb-, Au-, Ta-, Xe-, Kr-, CH_3-beams. An upgrade of the HSI [4-6] is potentially sufficient to meet the FAIR performance at the GSI-UNILAC. Further optimization of stripper performance should be started in an advanced machine experiment program. Beam acceleration up to 11.4 MeV/u and transport to SIS18 is the next step to confirm high intensity operation in the SIS18.

References

[1] Scharrer P., et al., Performance of a modified 1.4 MeV/u gas stripper for $^{238}U^{4+}$, GSI scientific report 2014.

[2] Hollinger R., et al., Status of Vacuum Arc Ion Source Development for Injection of High Current Uranium Ion Beams into the GSI Accelerator Facility, Nucl. Instrum. Meth., B 239 (2005) 227.

[3] Hollinger R., et al., Development of a Vacuum Arc Ion Source For Injection of High Current Uranium Ion Beam into the UNILAC at GSI, Rev. Sci. Instrum., Volume II, 2004.

[4] Kolomiets A., et al., Upgrade of the UNILAC High Current Injector RFQ, LINAC08, Victoria, BC, Canada, p. 136-138 (2008).

[5] Vormann H., et al., Straight injection of an intense uranium beam into the GSI high current RFQ, IPAC2014, Dresden, Germany, p. 3217-3219 (2014)

[6] Yaramyshev S. et.al., Advanced Beam Matching to a High Current RFQ, LINAC2014, Geneva, Suisse, to be published (2014).

DOI:10.15120/GR-2015-1-FG-GENERAL-05

Radiation-hard camera tests near the SIS18 extraction

B. Walasek-Höhne[1], *H. Bräuning*[1], *C. Dorn*[1], *R. Fischer*[1], *P. Forck*[1], *H. Graf*[1], *F. Hagenbuck*[1], *K. Höhne*[2], *T. Radon*[1], *U. Scheeler*[3], *C. Schmidt*[1], *M. Schwickert*[1], *K. Steiner*[1], *and J. Wohlers*[1]

[1]GSI, Darmstadt, Germany; [2]FAIR, Darmstadt, Germany; [3]MIT, Marburg, Germany

For imaging applications in the high radiation environment of heavy ion synchrotrons radiation-hard cameras are required. One possible candidate for such cameras at FAIR is the CCIR MegaRAD3 from Thermo Fischer Scientific. First measurements with this camera, which has been installed at the SIS18 extraction point, have been performed.

Technological advances in solid state camera design provide a wider choice of equipment for beam instrumentation. However, our previous experience with CCD based cameras has shown that their performance degrades during operation due to the background radiation (γ, neutrons, etc.) produced by the heavy ion beam (see Figure 1 left). Any semiconductor device operating in a radiation field suffers from degradation due to radiation damages. Energetic particles incident on the semiconductor bulk lose their energy due to ionizing and non-ionising processes as they travel through a given material. The ionising processes involve electron-hole pair production and subsequent energy deposition (dose) effects. The non-ionizing processes result in displacement damage effects, i.e. defects in the semiconductor lattice like vacancies and interstitials [1].

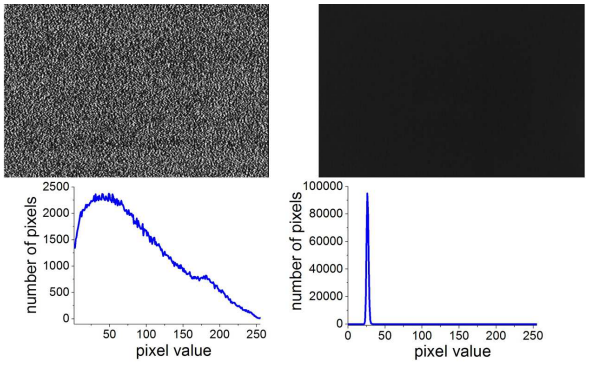

Figure 1: Dark images of the standard CCD camera Sony XC-ES30 (upper left) and the new radiation-hardened solid-state CID camera MegaRad3 (upper right) after a few weeks of irradiation with the corresponding histograms of pixel brightness below (bottom right, bottom left, respectively).

At the GSI SIS18 extraction point a great variety of particles with energy of up to few GeV/u is generated. At this location, where a high radiation level is observed, the CCIR MegaRad3 (8726DX7) radiation-hard solid-state CID (Charge Injection Device)-based camera was installed. According to the manufacturer [2] this device is tolerant to gammas, neutrons, high energy electrons and proton radiation to at least 3 MRad. Only in tests up to 14 MRad a noticeable degradation in the image quality has been reported by the manufacturer.

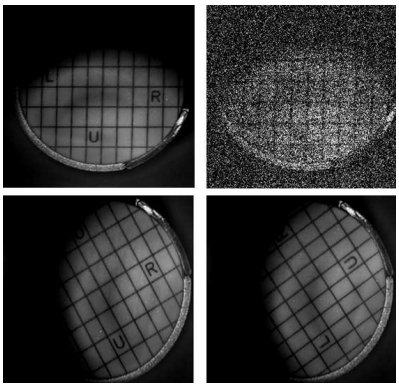

Figure 2: Original pictures of scintillating screen target with progressive level of accumulated dose. Upper left: standard CCD camera before test, upper right: standard CCD camera after few weeks of beam operation. Lower left: Rad-hard camera before test, lower right: standard Rad-hard camera after 8 months beam operation at SIS18.

In our tests, the camera has been placed near the SIS18 extraction. The camera is continuously running since November 2013. The accumulated dose impinging on the camera has been monitored by thermoluminescent dosimeters placed next to the camera. During this test, we found the image quality to be nearly the same after fifteen months of exposure to neutron (accumulated dose: 130 Sv) and γ (accumulated dose: 82 Sv) radiation. As shown in Figure 1 and Figure 2, no significant change in camera performance like loss of contrast and resolution was observed. A standard CCD camera at the same position was out of order due to irradiation within two weeks of operation.

Our first test with this radiation-hard solid-state CID-based camera is very promising. This device exhibits a significant improvement for operation in a radiative area environment as compared to the CCD and CMOS-based cameras. The performed tests show that the camera is not sensitive to radiation damage on the level observed at GSI. This makes this camera suitable for use in precise and reliable profile monitors of high energy heavy ion beams in the vicinity of beam extraction points, targets or beam dumps as well as other higher radiation environments expected at FAIR.

References

[1] S. Hutchins et al., "Radiation tests on solid state cameras for instrumentation" DIPAC 2005 `http://www.JACoW.org/`

[2] S. Bhaskaran, "Research and development efforts at CIDTEC cameras and imagers" 3rd DITANET School 2011 `http://indico.cern.ch/event/112220/contributions/`

DOI:10.15120/GR-2015-1-FG-GENERAL-06

Light output of inorganic scintillating screens induced by fast and slow extracted beams from SIS18*

A. Lieberwirth[1,2,#], P.Forck[2,3], S. Lederer[1], W. Ensinger[1]
[1]TU Darmstadt, Germany, [2]GSI, Darmstadt, Germany; [3]Goethe-Universität Frankfurt, Germany

Scintillating Screens are favoured devices to visualize the transverse beam profile during alignment and are foreseen for the HEBT at FAIR. For high energy ion beams extracted from SIS18 tests on the reproducibility of the scintillation process for different materials were performed to enable a proper choice for FAIR. Moreover, emission spectra were investigated as reported in [1].

Radiation hardness tests were carried out as well. The results concerning ceramic targets in comparison to measurements at UNILAC are summarized in [2].

Experimental Conditions

The investigations were performed with beams of protons, Nitrogen, Nickel, Xenon and Uranium as extracted from SIS18 with 300 MeV/u beam energy and intensities between 10^6 and 10^{10} particles per pulse. At the target location HTP seven different scintillating screens were irradiated in air (P43, P46, YAG:Ce, Chromium-doped and pure Aluminium Oxide). The measurements were performed in slow (300-400 ms) and fast extraction (1 µs) mode to analyze supposed saturation effects.

The scintillation light was recorded by a monochrome camera equipped with a remote-controlled iris and an optical grey filter (transmission ~5 %) to increase the measurement range.

Images with beam induced scintillation profile as well as background images were analyzed by a dedicated Python script to calculate light output (in particular sum of luminescent area) and beam profile characteristics as given by statistical moments. Moreover, a relative light yield was calculated as the light output per ion normalized to the deposited energy. This factor is used to compare the light emission from the targets with respect to the irradiation by different ion species.

Results

For all investigated ions, linearity between the light output with respect to the number of particles per pulse was observed for fast as well as for slow extraction, see Figure 1 exemplary for P43. Statistical moments were analysed in order to investigate changes of the beam reproduction during irradiation. Also the projected beam sizes were found to be independent from the amount of irradiating particles per pulse for each material, apart from variations by operative re-alignment.

The light yields of P43 phosphor for various projectiles relative to the protons light yield are shown in Table 1. A decrease as function of atomic number is clearly observable and the results show a different reaction on the impact of slow and fast extracted beam on the P43 screen. Generally, the light yield varies only by a factor 3 between light and heavy ions. The analysis for other targets is ongoing.

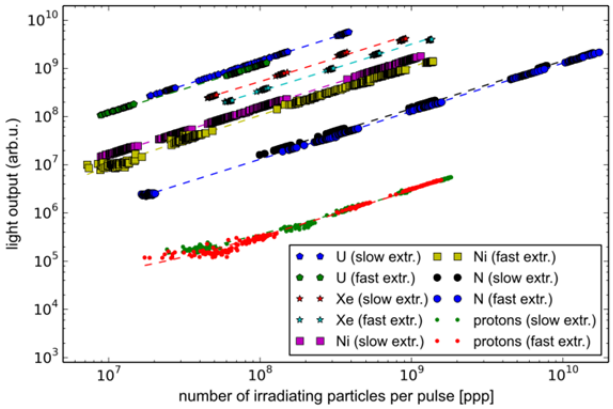

Figure 1: Light output of P43 phosphor screen induced by different ions. All projectiles were accelerated to 300 MeV/u and extracted in fast (1 µs) and slow mode (300-400 ms).

Table 1: Relative light yield of P43 phosphor screen for different projectiles. Proton induced light yield serves as reference. The beam energy at the target is given in brackets. In general ions were fully stripped at the target.

Projectile	Relative Light Yield (slow extr.)	Relative Light Yield (fast extr.)
p	1.00 (299 MeV/u)	1.00 (299 MeV/u)
N	0.97 (297 MeV/u)	0.85 (299 MeV/u)
Ni	0.66 (289 MeV/u)	0.44 (297 MeV/u)
Xe	0.56 (281 MeV/u)	0.34 (294 MeV/u)

Acknowledgements

The authors want to thank the GSI operation team for great support during beam time.

References

[1] A. Lieberwirth, et al., "Luminescence Spectra of Inorganic Scintillating Screens induced by Fast and Slow extracted Beams from SIS18", GSI Scientific Report 2014.

[2] S. Lederer, et al., "Luminescence degradation behaviour of alumina irradiated with heavy ions of high fluences" GSI Scientific Report 2014.

* Work supported by BMBF, contract No. 05P12RDBJ.
#a.lieberwirth@gsi.de

DOI:10.15120/GR-2015-1-FG-GENERAL-07

Lumineschence spectra of inorganic scintillating screens induced by fast and slow extracted beams from SIS18*

A. Lieberwirth[1,2,#], P.Forck[2,3], S. Lederer[1], W. Ensinger[1]
[1]TU Darmstadt, Germany, [2]GSI, Darmstadt, Germany; [3]Goethe-Universität Frankfurt, Germany

The scintillation process of inorganic material is a subject of high interest for material science. To answer questions of material damage processes the analysis of emission spectra is a common tool to compare possible influence of different ionizing particles.

Results on the spectral emission of inorganic scintillators induced by high energy impact of heavy ions were obtained. The emission spectra show no significant variation within the investigated ranges of ion species and beam intensities.

Setup

At the high-energy experimental test bench HTP investigations on the luminescence spectra of inorganic scintillators were performed in the frame of machine experiments preparing for FAIR project. Altogether seven inorganic scintillating screens (P43, P46, YAG:Ce, Chromium-doped and pure Aluminium Oxide) were mounted behind a beam exit window in air and irradiated with different projectiles from proton to Uranium. All projectiles, i.e. protons, nitrogen, nickel, xenon and uranium ions, were extracted from SIS18 with a beam energy of 300 MeV/u and intensities between 10^6 and 10^{10} particles per pulse (ppp). The measurements were performed in slow (300-400 ms) and fast extraction (1 µs) mode to analyze supposed saturation effects.

Beam-induced scintillation of the target material was explored using an optical spectrometer setup (Horiba CP140-202 and appropriate lens) and recorded by a monochrome CCD camera (15.2 mm diagonal chip size). Simultaneously, the complete scintillation light output was measured with a different camera system, see [1].

Experimental Results

The analysis shows no significant variation in the structure of the emission spectra. Examples of YAG:Ce and P43 phosphor emission spectra are presented in Figure 1.

Despite the fact that the emission intensity increases with increasing number of irradiating particles per pulse, no change in the emission spectra could be observed over the complete irradiation period. Moreover, the light emission of the investigated target seems to be independent of ion species. Within the total irradiation of up to $5 \cdot 10^{13}$ accumulated particles of all investigated projectiles, the formation of defects within the material does not seem to be dominant in this high energy region (see also [2]). These findings are comparable to studies on the light emission induced by other projectiles, like X-ray [3] or photons [4].

Acknowledgements

The authors want to thank the GSI operation team for great support during beam time.

References

[1] A. Lieberwirth et. al., “Light Output of Inorganic Scintillating Screens induced by Fast and Slow extracted Beams from SIS18” GSI Scientific Report 2014.
[2] S. Lederer et. al., “High-temperature scintillation of alumina under 32 MeV $^{63}Cu^{5+}$ heavy-ion irradiation” submitted to NIM-B (2015).
[3] E. I. Gorokhova et al., "Luminescence and scintillation properties of Gd_2O_2S: Tb Ce ceramics." IEEE Transactions on Nuclear Science 52.6 (2005): 3129-3132.
[4] Yanagida, Takayuki, et al., "Evaluation of properties of YAG:Ce ceramic scintillators.", IEEE Transactions on Nuclear Science 52.5 (2005): 1836-1841.

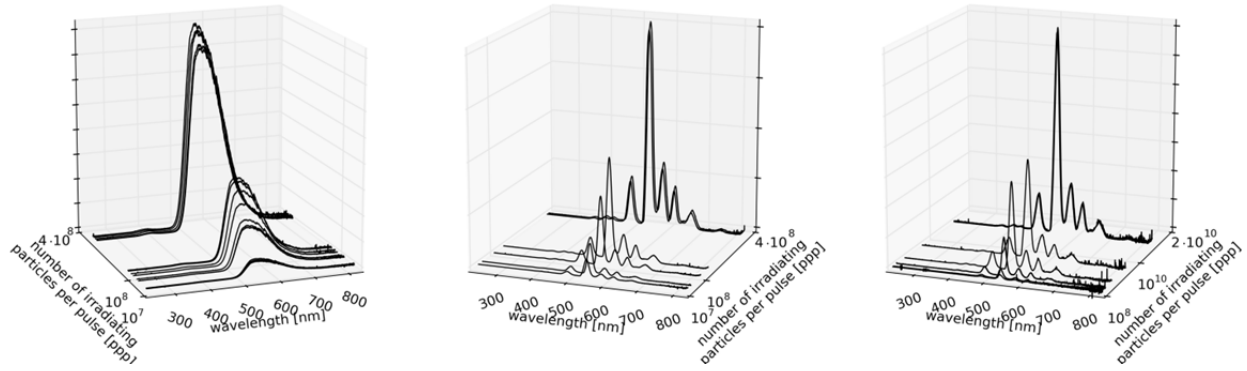

Figure 1: Emission spectra of single crystal YAG:Ce (left) and P43 phosphor (right) screens during irradiation with slow extracted Uranium beam (271 MeV/u, 300 ms extraction) at 10^7 up to $4 \cdot 10^8$ ppp. For comparison P43 spectra during slowly extracted Nitrogen beam (297 MeV/u, 400 ms extraction, 10^7 till $2 \cdot 10^{10}$ ppp) is shown on right side.

* Work supported by BMBF, contract No. 05P12RDBJ.
#a.lieberwirth@gsi.de

DOI:10.15120/GR-2015-1-FG-GENERAL-08

ESR operation and development

C. Dimopoulou, M. Kelnhofer, C.M. Kleffner, S. Litvinov, F. Nolden, C. Peschke, N. Petridis, U. Popp, J. Roßbach, S. Sanjari, M. Steck, D. Winters
GSI, Darmstadt, Germany

The ESR storage ring operation extended in 2014 over a rather long total period of 21 weeks due to the fact that many experiments as well as machine and detector development were scheduled before the complete shutdown foreseen for the years 2015 and 2016. A variety of physics experiments were performed using the different operational modes of the ESR.

An experiment to perform precision laser spectroscopy of the hyperfine transition in the hydrogen-like bismuth ion aimed at an improved accuracy in the measurement of the beam energy by monitoring the accelerating voltage of the electrons applied for electron cooling of the stored beam. A high precision high voltage divider provided by Physikalisch-Technische Bundesanstalt (PTB) was installed. It was found that the output voltage of the power supply showed significant variations with time. By continuous measurement of the voltage with the divider the variations of the high voltage could be tracked and corrected in the offline analysis. Despite the problem of the power supply, an improved determination of the beam energy was achieved and a correspondingly improved value of the energy of the hyperfine transition could be measured by laser spectroscopy. After the experiment the supplier of the high voltage generator found a problem with resistors recently installed in the power supply. After replacement of the resistors the usual stable operation was reestablished.

Experiments at the internal target benefitted from recent improvements of the target performance. A target density of 1×10^{13} cm^{-2} is now routinely available with hydrogen gas. In another experiment xenon gas was used with good reliability, however, with a reduced density of some 10^{11} cm^{-2} due to the high beam loss rate of the stored highly charged Xe-ions at the energy of 50 MeV/u.

For various experiments the beam was decelerated in the ESR. For a scheduled experiment with the internal target with hydrogen gas a $^{124}Xe^{54+}$ beam was decelerated from 230 to 7 MeV/u. So far, this is the lowest energy of an experiment using a stored beam in the ESR and the lifetime of the cooled beam of highly charged ions at the low energy in the residual gas was about 20 s. Due to the target operation and the presence of special detectors in the vacuum, the lifetime decreased to 5 s. Systematic measurements with the stored bare xenon beam at various energies in the range 30 to 7 MeV/u showed a decrease of the lifetime in the residual gas very close to the expected E_{kin}^2–dependence on the kinetic energy E_{kin}. The feasibility of such an experiment using a particle detector installed inside the vacuum chamber of the dipole magnet after the internal target could be demonstrated with the presently achievable vacuum conditions. Unfortunately the experiment had to be cancelled after serious damage to several components caused by a thunderstorm.

In two one week periods with decelerated beam, a beam of bare nitrogen was decelerated to 4 MeV/u for HITRAP commissioning and extracted with the fast kicker extraction. In order to have a short cycle time the nitrogen beam was injected at the low energy of 30 MeV/u which reduced the time for cooling and deceleration of the ion beam to 4 MeV/u to about 30 s.

In the future the ESR has to deliver decelerated ions to the CRYRING which is presently being installed in the target hall south of the ESR. There is no dedicated kicker for fast extraction of a beam from the ESR towards the target hall. However, it was found that with a special closed orbit distortion of the stored beam the existing injection kicker can be used to extract the beam to CRYRING [1]. The implementation of the special orbit distortion and the kick extraction towards CRYRING was investigated first with a stored beam at a rigidity of Bρ=3.2 Tm. Subsequently, the rigidity of the stored beam was reduced iteratively to Bρ=0.58 Tm, with a $^{14}N^{7+}$ beam decelerated to 4 MeV/u. This corresponds to the design values for the transfer of beam from ESR to CRYRING. The extraction was successful and the beam could even be transported about 20 m along the transport line. Further beam transport tests suffered from a lack of available test time. It was also found that with the special orbit distortion the beam can be extracted from the same orbit either to HITRAP (northern extraction channel) or CRYRING (southern extraction channel) simply by tuning the angle of the extraction kick. That would even allow a fast change of the destination of the stored decelerated beam by changing the kick strength pulse to pulse. The major disadvantage of this extraction mode with closed orbit distortion is the fact that the large angle of the closed orbit, which has to be applied in the cooling section does not allow electron cooling in the last phase of beam manipulation before extraction.

In October 2014 beam for a channeling experiment in HTA was provided with charge change extracted Li-like U^{89+} ions at 190 MeV/u. This beam was used to recommission the extraction beamline towards the target hall with the help of the new CUPID diagnostics system [2]. An additional vertical steerer and upgraded scintillating screens in the beamline and the experimental cave now allow for a much more precise adjustment of the beam parameters of the extracted ions.

The requirements of minimal transverse divergence of the cooled extracted beam could be fulfilled by widening it to a parallel beam in the target area, that has further been trimmed with slits to a 5×5 mm quadratic beam spot as shown in fig 1.

DOI:10.15120/GR-2015-1-FG-GENERAL-09

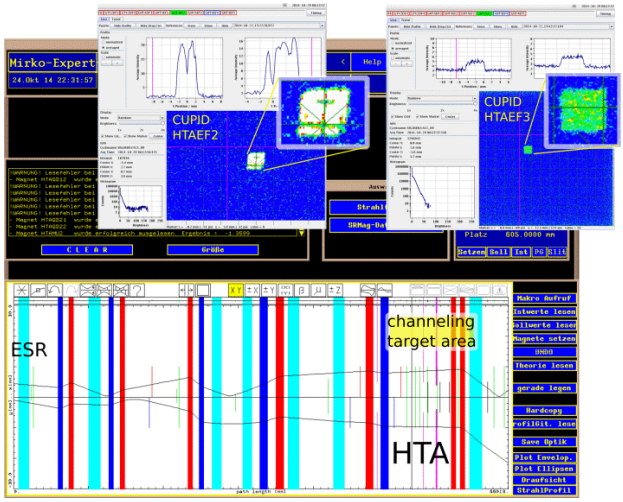

Figure 1: MIRKO envelope of the extracted beam as well as CUPID images of the quadratic beam shape measured with two different scintillating screens in a distance of 2 m installed in the experimental area.

Both transverse emittances could be determined to be smaller than 0.5 π mm mrad (FWHM) with a corresponding divergence of around ±100 µrad in the target area.

The longest experimental period was devoted to a repetition of the measurement of bound-state beta decay of $^{142}Pm^{60+}$ with better statistics. In previous measurements the reliable operation of the injection kicker was doubted. Missing injection kicks were suspected to compromise the determination of the time of decay of the nucleus. During the new measurement all three modules of the injection kicker were monitored individually. Only 1 failure of the injection kicker was found within 10000 injections during the experiment, proving an excellent reliability of the system. The whole experiment including stochastic precooling and final electron cooling of very few secondary ions stored in one injection showed very reliable operation of the ESR and its technical systems.

Over the year various machine experiments were performed. Studies of the isochronous mode were continued aiming at an increased acceptance for isochronous mass measurements and the improvement of the ion optical model. A measurement of the ring dispersion in the isochronous mode and the comparison with lattice calculations is reported in a separate contribution [3].

In another machine development experiment a proton beam was used to test the ability of the ESR cooling systems to prepare a cooled beam of particles with low charge. This was a study in preparation of the potential future use of the ESR in a chain of decelerators for antiprotons at FAIR. It could be demonstrated that both cooling systems, electron cooling and stochastic cooling, can be used. Stochastic cooling with notch filter and time-of-flight (ToF) cooling was performed. The damping time for some 10^8 protons with an initial rms momentum spread of 4×10^{-4} was about 15 s with ToF –cooling and about 8 s with notch filter cooling. With notch filter cooling even for 1×10^9 protons the damping time was as low as 15 s. For electron cooling the damping time for protons at the edge of the initial momentum distribution was 600 s, which is expectedly much longer than for stochastic cooling. The damping time decreased in the course of the cooling process (Fig.2). On the other hand, the final momentum spread with electron cooling was $2\text{-}3\times10^{-5}$ compared to $1\text{-}2\times10^{-4}$ with stochastic cooling.

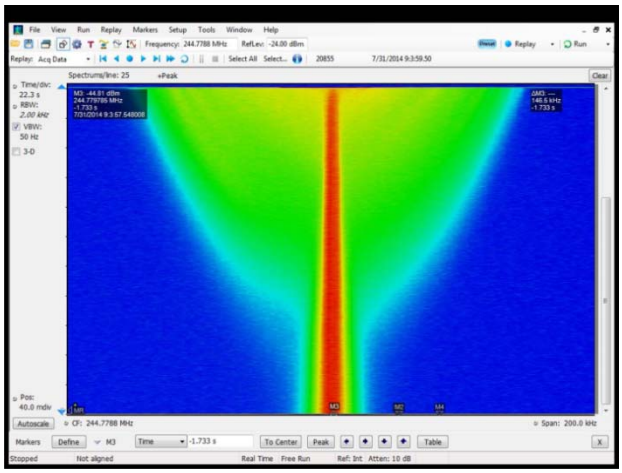

Figure 2: Longitudinal cooling of a proton beam at 400 MeV/u with an electron current of 0.25 A. The total time for the reduction of the momentum spread from 4×10^{-4} to 3×10^{-5} was 7 minutes.

A new controls program for the stochastic cooling system has been developed and is now available for operation of the system. It is a graphical interface which allows control of all components which are needed for operation and tuning of the stochastic cooling system. The new control software is compatible with FAIR standards and will be integrated into the future ESR controls concept.

For an improved understanding of the resonant structure which is used in the ESR for Schottky diagnostics a series of measurements with beam were performed. The main goal was the determination of the sensitivity of the cavity and the dependence of the sensitivity on the beam velocity, which is reflected in the transit time factor of the cavity. Measurements with proton beam at energies between 100 and 400 MeV and more systematic measurements with a $^{58}Ni^{26+}$ beam in the energy range 14 to 376 MeV/u (velocity range β = 0.17 - 0.71) were performed. For a beam velocity below β= 0.17 the Schottky signal vanished due to transit time factor effects.

References

[1] S. Litvinov et al., this annual report.
[2] B. Walasek-Höhne, et al., "CUPID: New System for Scintillating Screen based Diagnostics", GSI scientific report 2013, p. 307.
[3] O. Kovalenko et al., this annual report.

DOI:10.15120/GR-2015-1-FG-GENERAL-09

Optical beam diagnostics at ESR and beyond*

G. Birkl†[1], *M. Bussmann*[2], *Z.K. Huang*[3], *X. Ma*[3], *T. Murböck*[1], *H.B. Wang*[3], *W.Q. Wen*[3], *and D. Winters*[4]

[1]Technische Universität Darmstadt, Germany; [2]Helmholtz-Zentrum Dresden-Rossendorf, Germany; [3]Institute of Modern Physics-CAS, Lanzhou, China; [4]GSI Helmholtzzentrum, Darmstadt, Germany

Laser cooling, applied as a stand-alone cooling technique, or in combination with electron cooling, has high potential to generate relativistic ion beams with high phase-space densities. Even the generation of crystalline ion beams might be accessible. A neccessary prerequisite to reach this goal is the implementation of powerful diagnostics for the characterization of the resulting ion beam parameters. Schottky pick-up techniques [1] will lead a long way in this direction, but might be running short for the highest phase-space densities targeted. Optical diagnostics, making use of the collection of scattered optical photons during resonant excitation of relativistic ions, will open a second window for characterizing the ion beam with improved momentum resolution.

Therefore, we have developed two different detector systems for the UV-range ($\lambda \sim$150 nm): one system uses a photomultiplier tube (PMT) and is mounted in air (on a CaF_2 viewport), the other system is based on a photochanneltron electron multiplier (PEM) and is mounted *in vacuo* (10^{-11} mbar). Figure 1 shows two PEM systems with shielding (cage + mesh), mounted on linear translators with bellows.

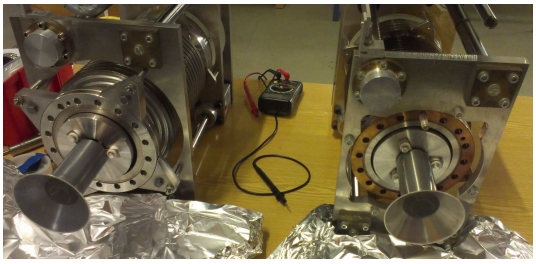

Figure 1: Two moveable PEM detector systems, used for optical diagnostics at the ESR (GSI, Darmstadt). [Now further tested at the CSRe (IMP-CAS, Lanzhou, China).]

During the laser cooling beamtime at the ESR (GSI) in August 2012, these detector systems have been used to detect the fluorescence from laser-cooled carbon ions [2]. At a kinetic energy of 122 MeV/u, or a Lorentz factor $\gamma = 0.47$, the $2s \rightarrow 2p$ cooling transition in $^{12}C^{3+}$ ($\lambda_0 = 155$ nm) is reached by using anti-collinear laser light at a wavelength $\lambda_L = 257$ nm [3]. Figure 2 shows the detected fluorescence signal as a function of time, while the cw-laser system was repetitively scanned over the cooling transition. Therefore, the cw-laser was detuned from the 'red side' (*i.e.* below the transition frequency) to just over the resonance, and back again. During each scan, which took about 30 s, a strong increase in the detected number of fluorescence photons could be recorded at the resonance condition. Strong fluorescence peaks could only be observed when electron cooling was applied in parallel. The overall exponential intensity drop of the signal is due to the limited lifetime of the stored ion beam, caused by charge-changing collisions with the residual gas.

In summer 2013, the detector systems have been shipped to the Institute of Modern Physics (IMP) in Lanzhou, China, for further development and tests at the CSRe. During the experimental run in September 2014, laser cooling of stored, relativistic $^{12}C^{3+}$ ions (@122 MeV/u) was attempted for the first time at the CSRe [4, 5]. Further development of fluorescence diagnostics, especially in the XUV-regime, is required for future laser cooling studies at the HESR ($\gamma \sim 6$) and the SIS100 ($\gamma \sim 12$).

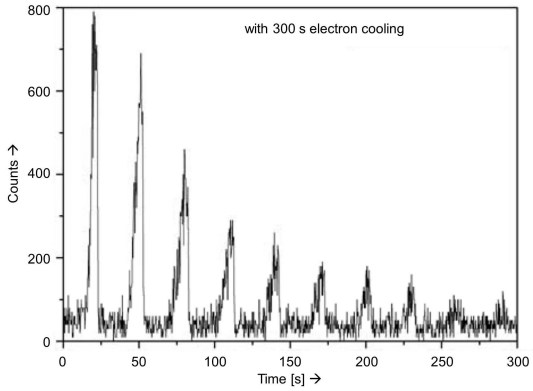

Figure 2: Fluorescence signal ($2p \rightarrow 2s$ transition) from relativistic $^{12}C^{3+}$ ions at the ESR. When the scanning cw-laser is in resonance with the Doppler-shifted cooling transition of the ions, a strong increase in the signal is observed.

References

[1] F. Nolden *et al.*, Nucl. Instr. Meth. Phys. Res. A **659**, 69 (2011).

[2] D. Winters *et al.*, JACOW, COOL 2013 conf. proc., THAM1HA04 166 (2013).

[3] T. Beck *et al.*, GSI Scientific Report (2012).

[4] W.Q. Wen *et al.*, GSI Scientific Report (2014).

[5] M. Löser *et al.*, GSI Scientific Report (2014).

*This work has been supported financially through BMBF contract 05P12RDFA3.

† gerhard.birkl@physik.tu-darmstadt.de

DOI:10.15120/GR-2015-1-FG-GENERAL-10

Performance of the ESR kicker magnet during E082 *

J. Piotrowski[†1,3], *X. Chen*[1,2], *Yu.A. Litvinov*[1,2], *M.S. Sanjari*[1], *and the Two-Body-Weak-Decays collaboration*

[1]GSI, Darmstadt, Germany; [2]University of Heidelberg, Germany; [3]AGH University of Science and Technology, Kraków, Poland

In October 2014 the second run of experiment E082 *"Single-Ion Spectroscopy of Two-Body β-Decays"*[1] took place. After a shortage of time during the 2012 beamtime, this time 12 days were allocated to performing high precision lifetime measurements of ^{142}Pm. The measurements were performed by injecting ions and observing them until they decayed. The data was analyzed online and offline, and the parameter of interest was the exact timing of each decay. In order to get reliable data, one has to assure that injected ions are removed from the *ESR* between injections.

In the first experiment we used the injection kick, considering it powerful enough, to also remove the ions from the ESR stored from a preceding injection. However it was noticed that the *kicker magnet*, that is used to perform injections, had several documented failures and possibly more that went unnoticed. This time the experiment was improved in two ways: there was a dedicated extraction kick at the end of each cycle, and all kicker magnet pulses were monitored and saved using a digital oscilloscope.

The dedicated extraction kick enabled a visual confirmation in the *time resolved Schottky spectra* that all ions had been extracted. Thanks to the monitoring of kicks, it was possible to determine exactly what the failure rate of the kicker magnet is during controlled and repeatable operation for over 10000 accelerator cycles, and get quanititative numbers describing its performance.

Setup

The accelerator was operated using a 70 second cycle. Each cycle began with an injection kick which marked the beginning of data-taking (data acquisition systems were triggered on injection). Injected ions were observed over a 60 second window. After this time an extraction kick was performed, which was followed by a 10 second safety period to finish data acquisition and saving.

The kicker magnet is powered by three power modules. Each module supplies a voltage of up to 80 kV to the magnet and a single module typically suffices to perform a successful extraction of the beam. For the experiment all three modules were used during both extraction and injection phases. The length of the injection kick was set to 500 nanoseconds, and the extraction kicks lasted 1500 nanoseconds. The assumption was that at a revolution frequency of 2 MHz, an extraction pulse lasting 3 full revolutions of the ions would be more than enough to remove all of them with absolute certainty.

* Work supported by Helmholtz-CAS Joint Research Group HGJRG-108, FP7 Marie Curie ITN "oPAC", HGF ARD Program

† j.piotrowski@gsi.de

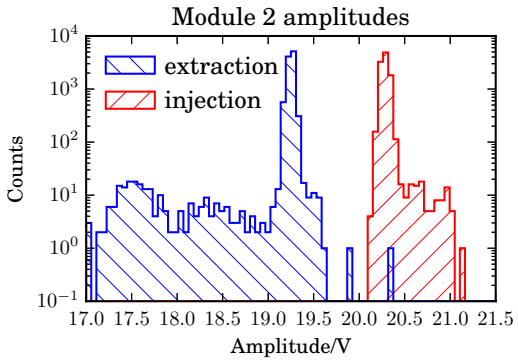

Figure 1: Logarithmic amplitude histogram for module 2. The curves show the extraction (left) and injection (right) amplitudes.

Results

Each power module has a monitoring unit through which a lower-voltage form of the pulse can be observed. We acquired 10359 injection and extraction kicks. We observed that modules 1 and 3 performed reliably throughout the entire experiment. Both delivered a signal with an amplitude of 20 V for injection and 19 V for extraction kicks, both of which are the required values for the monitoring signal. The FWHM of the kicks was around 300 mV. We noticed a single case were the kick was missed by all modules, however as this was a single incident we nonetheless consider the performance to have been extremely stable.

The behaviour of module 2 differed from that of the other modules. A histogram of the amplitudes for module 2 is presented in figure 1. For extraction kicks we counted 242 cases where kicks were weaker than the average amplitude by as much as 2 V. The curves for injections and extractions are visibly different for this one module.

Summary

For the first time in the operation of the *ESR*, the performance of the kicker magnet, crucial to the success of every experiment, has thoroughly been investigated. It was found that 2 out of 3 modules powering the magnet performed without failures in over 10000 accelerator cycles. For module number 2 it was found that the failure rate lies at 0.02%. A value of this magnitude was also confirmed by the Primary Beams High Voltage Pulsed Power group.

Acknowledgments We thank the GSI technical and accelerator groups for invaluable help during the preparation and conduction of the experiment.

References

[1] P. Kienle et al., Phys. Lett. B, 726, 638-645 (2013)

Deceleration of ions in the HITRAP facility

Z. Andelkovic[1], *S. Fedotova*[1], *F. Herfurth*[1], *N. Kotovskiy*[1], *B. Maaß*[2], *D. Neidherr*[1], *J. Steinmann*[3], *G. Vorobyev*[1], *and the HITRAP collaboration*[1]

[1]GSI Darmstadt; [2]Technische Universität Darmstadt; [3]Hochschule Darmstadt

The major challenge for experiments with low-energy highly charged ions (HCI) remains their preparation in sufficient quantities. As the only facility of its kind in the world, HITRAP aims to take advantage of the high intensities of HCI production by in-flight stripping of electrons in an accelerator facility for low-energy experiments. By reducing the energy in several steps from production at 400 down to 4 MeV/u and finally to sub-eV in a trap, a bunch of some 10^5 cold HCI can be forwarded with a chosen transport energy to different experiments.

The first stage of the linear decelerator, an interdigital H-type structure (IH), decelerates ions from 4 to 0.5 MeV/u and was successfully commissioned several years ago with deceleration efficiencies close to the theoretical maximum [1]. The commissioning of the second deceleration stage, the radio-frequency quadrupole (RFQ), has proven to be more challenging because of the very large parameter space combined with a relatively low acceptance of the device. An attempt to improve on this brought a new design of the electrodes [2] and offline tests at MPIK in Heidelberg [3]. The modified RFQ was reinstalled at GSI and commissioned during three beamtimes in 2014. Figure 1 shows the signal of the HCI decelerated from 500 to 6 keV by the RFQ, obtained after systematic scans and optimization of the system parameters during the first two beamtimes. The

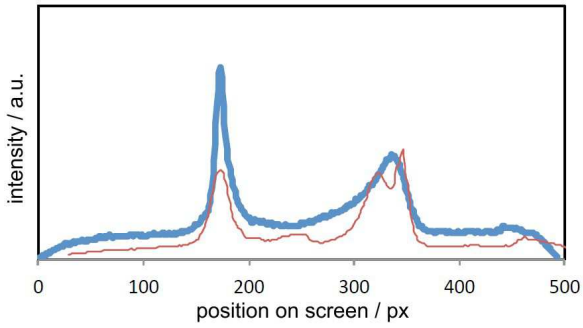

Figure 1: The ion beam from the RFQ after the energy analyser. The thin, red line is the reference signal from the offline tests and the thick, blue line is the online signal from July 2014. The low energy part, i.e. the decelerated ions' signal is the peak to the left. The peak to the right is the undecelerated part of the beam.

ions leaving the RFQ were sent through a magnetic field of a permanent magnet with integrated slits. As a result, the ions with smaller energy get a larger deflection angle (the left peak in Fig. 1) and can be distinguished from the non-decelerated ions. The last HITRAP beamtime of the year was used for systematic tests of deceleration, as well as to transport the decelerated ions through the low energy beamline towards the cooling trap.

The synchrotron cooling of trapped electrons for electron cooling was investigated for the last deceleration stage of HITRAP, the cooling trap. Electrons emitted from a GaAs surface after irradiation with UV light were guided to the trap and stored for extended amounts of time. The cooling effect by synchrotron radiation in the strong magnetic field of the trap was experimentally verified [4]. Further improvements include improvements of the vacuum, the optimization of the ion and electron capture process as well as their mixing and cooling. Detailed simulations of the trapping and the cooling process in the cooling trap have been conducted to that end and show promising results [5].

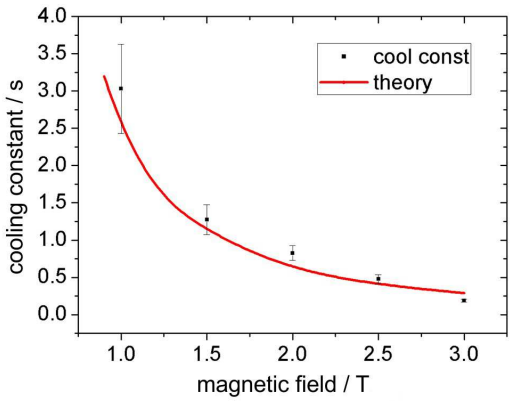

Figure 2: Synchrotron cooling of electrons in the cooling trap. The measured cooling constant of the trapped electrons reduces with the increasing magnetic field. The full, red line shows the value expected from theory.

References

[1] F. Herfurth, et al.: *HITRAP - Heavy, Highly-Charged Ions at Rest - A Status Report*, GSI Scientific Reports 2011

[2] S. Yaramyshev, et al.: *A new Design of the RFQ-Decelerator for HITRAP*, GSI Scientific Reports 2012

[3] M. Maier, at al.: *Offline commissioning of the old and new HITRAP RFQ*, GSI Scientific Reports 2012

[4] B. Maaß: Geladene Teilchen in der Kühlfalle, Master's thesis, TU Darmstadt, 2014

[5] J. Steinmann, PhD Thesis, University Erlangen-Nürnberg, to be submitted, 2015

DOI:10.15120/GR-2015-1-FG-GENERAL-12

The bunch monitoring system of the HITRAP decelerator

A. Reiter, F. Herfurth, W. Kaufmann, C. Krüger, M. Steck
GSI, Darmstadt, Germany

The HITRAP decelerator receives a 3 μs bunch of cooled, highly-charged ions from the experimental storage ring (ESR) and consists of two rebunchers, BB1 and BB2, followed by a drift-tube linac (IH-DTL) and a radio-frequency quadrupole (RFQ). The monitoring system is based on capacitive ring pickups and works for currents above 0.5 μA [1]. In 2014 new purpose-built main amplifiers were installed and extensive tests marked the end of the system development.

Monitoring of Bunched Primary Beam

Rebuncher BB1 generates a longitudinal particle focus at the IH-DTL entrance which decelerates the 4 MeV/u primary beam to ∼500 keV/u. Two pickups monitor the mean bunch energy of each extraction by a time-of-flight (TOF) measurement in front of the IH-DTL [2]. A resolution of σ_E=0.7 keV/u was achieved when the energy was changed during a phase scan of rebuncher BB2 [3]. During regular operation BB2 is switched off because it fails to improve the deceleration efficiency. Due to its simplicity, the TOF measurement has been established as reference and the ESR electron cooler voltage is adjusted to a target energy of 4024 keV/u. The TOF energy is 15 keV/u higher than the more accurate ESR energies based on Schottky (4008±3) keV/u or electron cooler voltage (4013±4) keV/u. Despite the small offset, relative changes are correctly detected.

Monitoring of IH-DTL and Buncher BB3

The ideal secondary IH-DTL beam is characterised by a small bunched fraction of accelerated primary ions and the larger, decelerated 500 keV/u design component. A pickup (DP6) monitors amplitude, i.e. deceleration efficiency, and the relative energy of bunches behind rebuncher BB3, which matches the beam to the RFQ acceptance. Fig. 1A presents bunch signals for three BB3 phases. BB3 affects only the decelerated ions, but its field is too weak to influence the remaining primary beam. Using the zero-crossing point of the decelerated bunch signal as reference, a variation in arrival time at the pickup can be converted to an energy shift. Results are shown for a full phase scan in Fig. 1B (dots) together with the data of the Energy Analyzer EA (triangles), a calibrated dipole spectrometer with position-sensitive optical MCP readout [4]. Both data sets are in excellent agreement and follow the expected sine function. The data have not been corrected for occasional glitches in the trigger which produce spurious offsets, most evident at 30° or 50°.

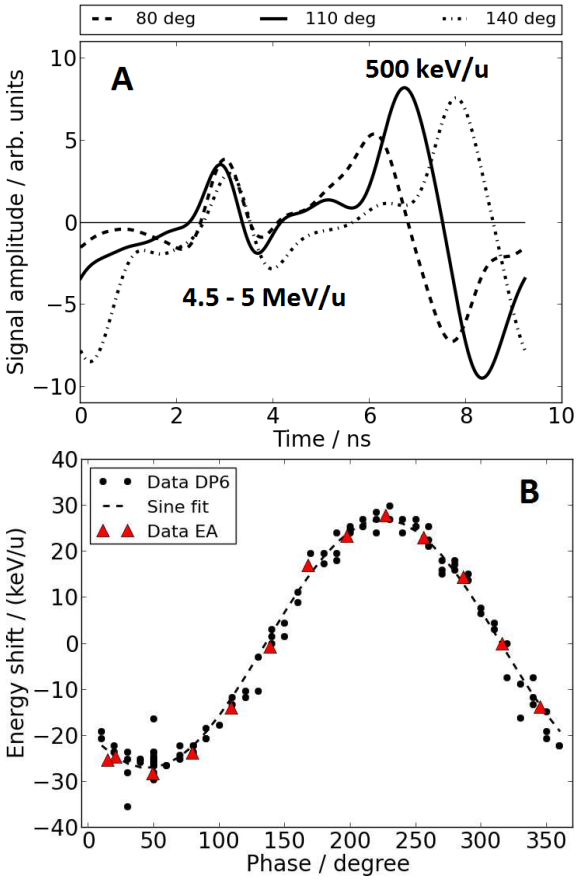

Figure 1: Signals of pickup DP6 for three BB3 phase settings (A). Energy shifts observed by pickup DP6 and Energy Analyzer EA during BB3 phase scan (B).

The HITRAP bunch monitoring system has been completed. Recent tests confirm previous findings and underline the systems' practical potential. The online monitoring system is now part of the standard beam instrumentation.

References

[1] A. Reiter, W. Kaufmann, C. Kleffner, "Novel Analysis for Linac Phase Probes", GSI Scientific Report 2010

[2] A. Reiter et al., MOPD35, DIPAC 2011, Hamburg, Germany

[3] A. Reiter et al., "Improved Monitoring of the HITRAP Double-Drift Buncher", GSI Scientific Report 2011

[4] F. Herfurth et al., THB05, HIAT 2012, Chicago, IL, USA

DOI:10.15120/GR-2015-1-FG-GENERAL-13

The status of the CRYRING@ESR project*

F. Herfurth[†1], *M. Lestinsky*[1], *Z. Andelkovic*[1], *R. Bär*[1], *A. Bräuning-Demian*[1], *S. Litvinov*[1], *O. Dolinskii*[1], *W. Enders*[1], *M. Engström*[1], *S. Fedotova*[1], *B. Franzke*[1], *W. Geithner*[1], *O. Gorda*[1], *A. Källberg*[2], *N. Kotovskiy*[1], *A. Reiter*[1], *A. Simonsson*[2], *T. Sieber*[1], *J. Sjöholm*[2], *M. Steck*[1], *Th. Stöhlker*[1], *and G. Vorobjev*[1]

[1]GSI, Darmstadt, Germany; [2]MSL, Stockholm University, Stockholm, Sweden

The low energy storage ring LSR [1] shall provide highly charged ions and antiprotons at low energy for two collaborations at FAIR, SPARC and FLAIR. Those collaborations intend to perform precision experiments pursuing atomic and nuclear physics questions [3]. The LSR is a Swedish in-kind contribution to the FAIR facility in Darmstadt.

The LSR is the swedisch low energy storage ring CRYRING modernized and adapted to the additional needs for injection and ejection of antiprotons and highly charged ions at about 10 MeV/nucleon. CRYRING has been operated at the Manne Siegbahn Laboratory in Stockholm until 2010, was dismantled in 2012 and transported to GSI in the first months of 2013. At GSI it will be installed behind the ESR, as proposed and described in detail in 2012 by a swedish-german working group [2]. This proposal has been accepted end of 2012 by the relevant committees.

CRYRING can decelerate, cool and store heavy, highly charged ions and anti protons injected at about 10 MeV/nucleon down to a few 100 keV/nucleon. It provides a high performance electron cooler and a straight section for flexible experiment installations as for instance a gas jet target. It is equipped with it's own injector and ion source, to allow for standalone commissioning.

In 2014 the design and installation of infrastructure into the newly constructed Cave B included media supplies like cooling water or compressed air, power cabling, magnet cabling, water cooled cabling, signal cabling. The cable routing and cable tray planning and installation has almost been completed. For electrical supply a new low voltage distribution has been conceived and purchased. The integration into the GSI safety systems is ongoing and well advanced. For this the lock and gate system has been reinstalled to ensure controlled access to the cave.

One prerequisite for the physics part of the CRYRING@ESR project, the transport and injection of heavy, highly charged ions from the ESR, has been advanced. The beam line has been modified and setup in large parts. Furthermore, part of the beam time was used to test the extraction and transport of ESR beam. It has been shown successfully that even close to the lower limit of ESR operation, at 4 MeV/u beam energy, it was possible to extract ions towards CRYRING in Cave B and to transport it beyond the first three dipoles.

* Work supported by GSI/HI Jena/FAIR@GSI PSP code:1.3.4.2./The SPARC collaboration/Uni Krakov/KVI Groningen

† F.Herfurth@gsi.de

Figure 1: Photograph of the situation in the CRYRING cave end of 2014. In the foreground the local injector has been setup and is being aligned. In the background visible is the ring structure with its dipoles and the magnetic sections with quadrupole and sextupole magnets.

The local injector has been mechanically put in place. First pumping down tests of the RFQ were conducted successfully. The required pressure has been reached, showing that the RFQ is ready to be operated after all the refurbishing to update for instance it's cooling circuit.

Setting up of the first components of the ring has begun, i.e. all ring dipoles were installed and the GSI technical divisions are completing inspection and preparation of the subsystems installed in the straight sections.

The Electron cooler has been worked at to repair transport damages and to check primarily the vacuum conditions. A testing stand for cryogenic tests is under preparation.

References

[1] H. Danared, et al. (2011) "LSR - Low-energy Storage Ring, Technical design report", Manne-Siegbahn Laboratory, Stockholm University, version 1.3.

[2] M. Lestinsky, et al. (2012) "CRYRING@ESR: A study group report", Project study, GSI, Darmstadt,

[3] M. Lestinsky, et al. (2014), "CRYRING@ESR: Present Status and Future Research", Proceedings of the STORI 2014, 9th International Conference on Nuclear Physics at Storage Rings, Sankt Goar, Germany.

DOI:10.15120/GR-2015-1-FG-GENERAL-14

A novel scheme for fast extraction of low energy beams from the ESR to the CRYRING

S. Litvinov[1], *C. Kleffner*[1], *F. Nolden*[1], *M. Steck*[1], *and D. Winters*[1]
[1]GSI, Darmstadt, Germany

The CRYRING@ESR facility [1] will provide the unique possibility for studying properties of low energy cooled heavy beams in the field of atomic and nuclear research within the FAIR project [2]. Heavy ion beams will be stored, cooled and decelerated to the energy of about 4 MeV/u in the ESR and then delivered to the CRYRING. Presently, there is no special kicker magnet which could be used for the fast extraction towards the CRYRING. However, a special distorted closed orbit has been suggested, applying it to the stored beam one can perform the fast extraction with the existing injection kicker magnet.

Calculation

The beam from SIS18 is usually injected into the ESR on the orbit of $\Delta p/p \approx +1\%$, and then stored and cooled (solid black curve in Fig. 1). In order to keep the beam parallel to the electron beam in the cooler section, 4 horizontal correctors in 2 neighboring main dipole magnets are used. The ESR is equipped with one injection and two extraction septum magnets. The horizontal width of the beam pipe around the septums is 104 mm and in addition, there is the narrow knife of 17 mm width of each septum (see Fig. 1). The injection kicker magnet is placed after the first dipole downstream. The beam goes after the kick either to the northern extraction septum (towards the HITRAP) or to the wall (dotted black curve in Fig. 1). In order to extract the beam to the CRYRING, it is necessary to change the trajectory of the kicked beam, such that it avoids the knives of the septa but reaches the southern extraction septum. This orbit distortion has been performed with a special bumped closed orbit, which has been calculated using 8 horizontal correctors in 4 main dipoles (dashed black curve in Fig. 1). Applying the kick on the distorted orbit the beam can freely be extracted to the CRYRING (dotted-dashed red curve in Fig. 1).

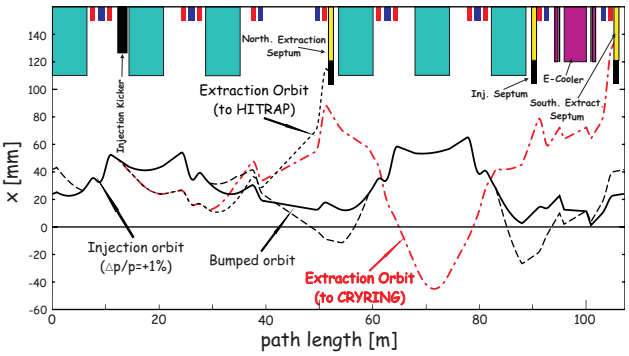

Figure 1: Calculated beam trajectories for one turn in the ESR. The injected stored orbit of $\Delta p/p = +1\%$ is indicated by the solid black curve. Its kicked orbit (extraction to HITRAP) is shown by the black dotted curve. The distorted bumped orbit is marked by the dashed black curve and its kicked orbit (extraction to CRYRING) is shown by the dotted-dashed red curve.

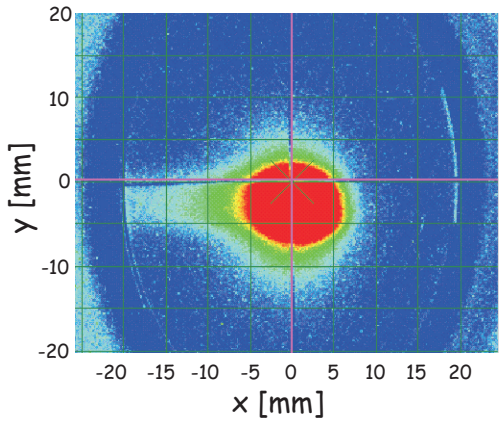

Figure 2: The extracted 100 MeV/u $^{58}Ni^{26+}$ beam directly after the extraction septum.

Experiment

In August 2014, the calculations could be proven by experiments at the ESR. Firstly, the proposed extraction scheme was verified with 100-400 MeV/u proton and $^{58}Ni^{26+}$ beams. The extracted beam was measured directly after the septum using a fluorescent screen (see Fig. 2). Later, a $^{14}N^{7+}$ beam at 30 MeV/u was injected, stored and stepwise decelerated iteratively to the final energy of 4 MeV/u ($B\rho = 0.58$ Tm), the lowest possible magnetic rigidity from the ESR to the CRYRING. At each energy, the beam was successfully extracted, changing only the kick angle of the injection kicker by several tenths of a milliradian. The distortion orbit was unchanged. Despite the lack of experimental time, it could be managed to transport the extracted 4 MeV/u ion beam over a length of 20 m towards the CRYRING for the first time.

References

[1] CRYRING@ESR, A study group report
https://www.gsi.de/fileadmin/SPARC/documents/Cryring/ReportCryring_40ESR.PDF

[2] http://www.fair-center.eu/

DOI:10.15120/GR-2015-1-FG-GENERAL-15

Beam instrumentation for the RFQ injector at CRYRING

A. Reiter, C. Andre, H. Bräuning, C. Dorn, F. Herfurth, O. Gorda, T. Hoffmann, W. Kaufmann, H. Reeg, T. Sieber, G. Vorobjev, B. Walasek-Höhne, M. Witthaus

GSI, Darmstadt, Germany

In 2015 the CRYRING storage ring will resume operation after its installation in Cave B [1]. Commissioning begins with the compact injector, consisting of ion source branch and radio-frequency quadupole (RFQ) linac. It will provide beams of light charged particles for commissioning of the experimental storage ring.
The beam instrumentation of the injector consists of Faraday cups, scintillating screens, and capacitive pickups. All detector systems are compliant to the new FAIR standards and provide a front-end software architecture (FESA) interface to the accelerator control system. CRYRING will be the first machine to be equipped with the new White-Rabbit timing system.

Ion Source and Dipole Spectrometer

Beams of light, singly-charged ions of 10 keV/u, mainly D^+, will be extracted from a MINIS source. Directly behind the ion source and behind the 90° spectrometer dipole, intensity and distribution of the DC beam can be measured with a Faraday cup (FC) or a scintillating screen (SCR). The compact diagnostics chamber with a single motor drive for both detectors was originally designed by KVI Groningen for the HITRAP facility . The driver unit and the controller are a joint FAIR development of GSI and Slovenian in-kind contributor Cosylab.
Expected beam currents along the injector range from 100 μA after the source to 1 μA after the RFQ linac. For the multi-turn injection into CRYRING, the chopper behind the ion source cuts out a $25-100\,\mu$s macropulse from the DC beam. Each FC is equipped with a low-noise amplifier, suited for DC and AC operation, with switchable gains of $10^2 - 10^8$ V/A. The output is sampled by a 100 MSa/s ADC with 16 bit resolution in a VME system. Its embedded controller runs the "CryCup" acquisition software.
The SCRs are composed of 25 mm diameter multi-channel plates and P43 scintillators. Beam images are recorded with triggered 10 bit digital CMOS cameras. They are controlled by an industrial PC which hosts the "CUPID " acquisition software. The application takes care of all data handling (image rotation, region cuts, profile calculation) and acts as server to the control system clients [3].
A special camera system with 75 mm fixed-focus lens and optical x4 extender is mounted on the external 0° port of the dipole chamber and looks approx. 3 m upstream into the ion source. During operation it monitors the plasma around the filament, after ion source service or exchange the fixed camera is used to check the re-alignment. The system resolution was measured to be about 20 pixel/mm.

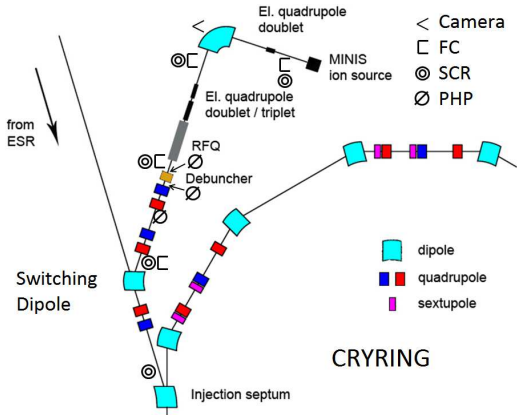

Figure 1: Schematic of RFQ injection for CRYRING; detector positions are indicated with symbols described in the legend. The distance between RFQ and injection is ∼10 m.

RFQ linac and debuncher

The 108.4 MHz RFQ linac accelerates ions of q/A>0.36 from 10 to 300 keV/u. The following debuncher reduces the momentum spread $\Delta p/p$ to $\sim$ 1% and increases the injection efficiency. The new bunch monitoring system analyses pairs of signals selected from 3 pickups (PHP) or RFQ and debuncher tank. The derived information may be the beam energy via time-of-flight, phase relations between beam and rf tank power or the verification of the debuncher operation. Signals are amplified, in the case of PHPs, and routed via a remote-controlled switching matrix to a digital 5 GSa/s oscilloscope. A FESA application integrates amplifiers, switching matrix and data readout. The analysis procedure is identical to the one employed at the HITRAP decelerator and achieves a resolution of ∼10 ps [2].

As in the source branch two FC/SCR pairs, one at the RFQ exit and one after the two quadrupole doublets, measure intensity and distribution of the 300 keV/u beam. In the bakeable area after the switching dipole, a robust, heat-resistant Cromox screen is mounted close to the injection septum on a pneumatic drive. The detectors are part of the readout systems described in the previous section.

References

[1] M. Lestinsky et al., "CRYRING@ESR: A study group report", June 2012

[2] A. Reiter et al., MOPD35, DIPAC 2011, Hamburg, Germany

[3] B. Walasek-Höhne et al., TUPD062, IBIC 2014, Stanford, USA

DOI:10.15120/GR-2015-1-FG-GENERAL-16

Beam test with the Cryogenic Current Comparator*

F. Kurian[1#, 2, 3], R. Geithner[3], P. Huelsmann[2], P. Kowina[1], R.Neubert[4], H. Reeg[1], M. Schwickert[1], R. Singh[1], T. Sieber[1] and T. Stoehlker[1, 3]

[1]GSI, Darmstadt, Germany; [2]Goethe University Frankfurt, Germany; [3] Helmholtz Institute, Jena, Germany;
[4] Friedrich-Schiller-University, Jena, Germany

Cryogenic Current Comparator (CCC) units are foreseen to be installed at various locations of the FAIR facility, for the online measurement of ion beam current down to nA range. In this contribution, successful test measurements of ion beam current using the upgraded CCC at GSI are reported. The CCC data show excellent match of the measured spill structure with the SEM measurements.

For the development of the improved version, the existing CCC system at GSI was refurbished as a prototype for FAIR, to test new sensor components [1]. Based on the studies done on different sensor combinations by R. Geithner *et al*. [2], a new dc-SQUID and new control electronics were selected and installed in the refurbished system. After successful test measurements in lab environment, the CCC was installed in the beam diagnostic test bench HTP at the extraction line of the GSI synchrotron. The signals measured by the CCC were amplified and read out at the equipment room located about 70 m from the beam line.

A built-in single-turn wire loop was used to calibrate the CCC output voltage to equivalent current. Response to known dc currents from a precision source (Keithley 261) in the range of 2 nA to 5 μA was measured. From this, a current sensitivity of 71.5 nA/ϕ_0 was calculated, which is equivalent to 74.2 nA/V output to the oscilloscope.

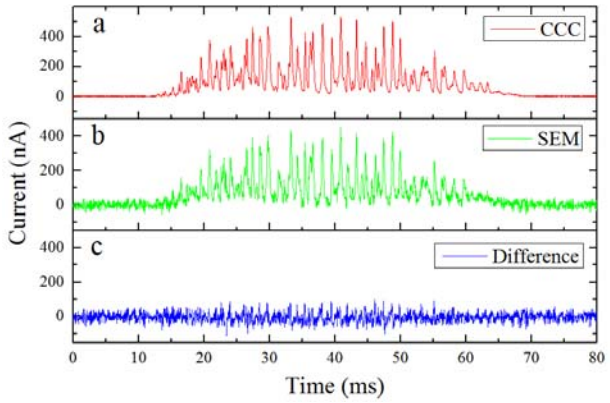

Figure 1: Comparison of the beam current signal measured by (a) CCC, (b) SEM, and the difference between the two signals (c). See text for details.

Slowly extracted Ni^{26+} ion beams at 600MeV/u in the intensity range from 2.8×10^8 particles per spill to 5×10^9 particles per spill were used to test the CCC response to the beam signal. A set of beam signals with the extraction time in the range of 64 ms to 5 seconds at different beam intensities was measured by the CCC. With an anti-aliasing filter (10 kHz cut-off frequency) at the output, the CCC measured the beam current down to 2 nA with a resolution of 1.2 nA rms. To compare the current measured by the CCC with a conventional technique, a Secondary Electron Monitor (SEM) - installed about 1 m downstream the CCC's installation point - was used in parallel. The secondary electron current produced by the SEM was amplified by a trans-impedance amplifier (Femto DHPCA-100).

Figure 1 shows a typical spill structure of an ion beam (about 4×10^9 particles) extracted over 64 ms measured by CCC (a) and SEM (b). The SEM signal was normalized to the CCC signal (normalized to total charge) for comparison. The difference between the spill structures measured by CCC and SEM as plotted in Figure 1 (c) shows excellent agreement. The spikes in the extracted beam, originating from the power converters of the magnets for the resonant extraction, are visible in the CCC measurement as shown in Figure 1. These ripples correspond to 50 Hz and its harmonics in the frequency spectra as expected [3].

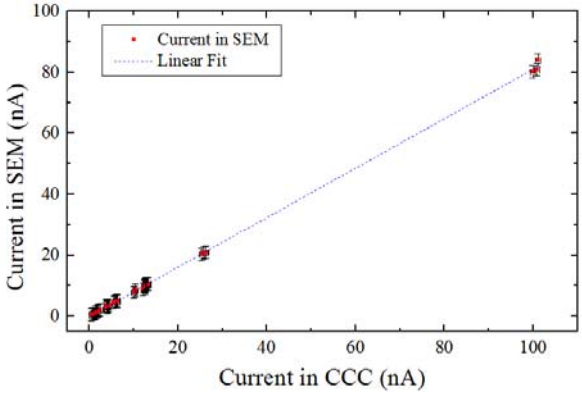

Figure 2: Comparison of the current measurement using CCC and SEM within a bandwidth of 200 Hz.

In Figure 2 the current signals as measured with the CCC are plotted vs. SEM data in the range of 2 nA-105 nA. Whereas the relation is precisely linear (standard error: 0.7%) as expected, the 19% deviation of the measured average current is subject of ongoing examinations.

References

[1] F. Kurian *et al.* "Measurements with the upgraded cryogenic current comparator", IBIC 2013.
[2] R. Geithner *et al.* A Cryogenic Current Comparator for FAIR with Improved Resolution, IBIC 2013.
[3] M. Kirk *et al*. "SIS-18 rf knock-out optimisation studies", IPAC2013, Shanghai, China.

* Work supported by Helmholtz Institute, Jena.
#f.kurian@gsi.de

Pressure and temperature dependence of Cryogenic Current Comparator measurements

F. Kurian[1, 2, 3], P. Huelsmann[1, 2], P. Kowina[1], H. Reeg[1], M. Schwickert[1], T. Sieber[1], R. Singh[1] and T. Stoehlker[1, 3]

[1] GSI, Darmstadt, Germany, [2] Goethe University, Frankfurt, Germany, [3] Helmholtz Institute, Jena, Germany

One of the key features of the Cryogenic Current Comparator (CCC) is its ability to measure extremely small magnetic fields associated with the beam current [1]. However, in a typical accelerator environment, a number of unavoidable noise sources limit its current sensitivity. Main sources of noise are mechanical vibrations, magnetic stray fields including Earth's magnetic field, electromagnetic interferences and temperature fluctuations.

A low T_C dc SQUID (Superconducting Quantum Interference Device) is used in the CCC as magnetic flux detector. It is operated at 4.2 K which is favourable due to low thermal noise. However, as already observed in former measurements [2], the CCC readout is affected by a drift that is correlated with the pressure inside the CCC cryostat (i.e. pressure of the liquid Helium (LHe) vapours above the LHe surface).

The influence of pressure and hence temperature fluctuations were studied for the refurbished CCC system, installed in the beam diagnostics test bench at HTP [1]. A differential pressure sensor connected to an oscilloscope was used to measure the pressure inside the CCC cryostat. The resolution of this measurement was 0.13 mbar with a signal to noise ratio of 2. The absolute calibration of the sensor is 4.86 mV/mbar and was made by means of a mechanical manometer. A needle valve installed at the cryostat exhaust was used to control the pressure of the boiling LHe. The temperature of the superconducting magnetic shield which includes the ring core and pick up coil, was measured by a silicon-diode temperature sensor (Lakeshore, DT-670B) with an accuracy of 1 mK. The temperature of the SQUID was not monitored directly which is a drawback, as mentioned below.

The CCC was operated in its most sensitive range with a current sensitivity of 118.2 nA/Φ_0 and a current resolution of 6 nA, where Φ_0 is the magnetic flux quantum (Φ_0 =h/(2e) = 2.068×10^{-15} Wb). The CCC was calibrated with a known dc current applied to a built-in current loop.

Figure 1 shows the variation of the offset in the CCC measurement and temperature changes with respect to the pressure variation inside the LHe cryostat. The needle valve at the exhaust of the cryostat is closed for about 50 seconds to create an overpressure of 15.3 mbar inside the cryostat by LHe boil-off. This causes a temperature rise of 36.0 mK on the superconducting magnetic shield. The pressure increase of 15.3 mbar result in an instantaneous drift on the CCC output corresponding to an equivalent current of 1.107 µA which is 70% of the full CCC range. The delay of 5 sec in the temperature readout with respect to pressure and CCC readout is due to the bulky magnetic shield that needs more time to reach the same temperature as the SQUID.

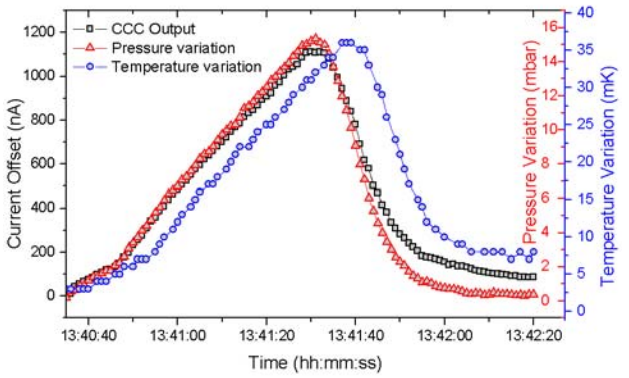

Figure 1: Current offset (black squares) as the result of pressure increase (red triangles) in the LHe cryostat and corresponding temperature variation (blue circles).

The offset of the CCC readout has a linear pressure dependency of 73.7 nA/mbar (0.62 Φ_0/mbar). The corresponding temperature dependence of the CCC offset is 33.5 nA/mK (0.28 Φ_0/mK).

The strong and non-linear temperature dependence of the SQUID drift in presence of an external magnetic field was already observed in other experiments [3], however, only at temperatures lower than 600 mK and explained as an effect of surface defect spins [3 and Refs. therein]. On the contrary, present measurements show by factor of ten stronger and nearly linear drift dependency but at LHe temperature. This may be rather addressed to thermal motion of magnetic flux and/or temperature-dependent critical currents [4].

Since the pressure of the LHe vapour is perfectly correlated with the CCC readout there are two extremely important issues for any future CCC design:

- The pressure of the CCC exhaust must be stabilized (e.g. by means of a pressure regulator) with a precision of better than 1 mbar.
- By simultaneous measurement of the vapour pressure one can calculate and compensate this drift.

References

[1] F. Kurian, et al. *IBIC 2013,* Oxford, UK.
[2] V. Vodel and R. Neubert, private communication.
[3] S. Sendelbach et al., Phys. Rev. Lett. 100, 227006 (2008).
[4] J. Clarke, et al. J. Low Temp. Phys. 25, 99 (1976).

* Work supported by Helmholtz Institute, Jena.
#f.kurian@gsi.de

DOI:10.15120/GR-2015-1-FG-GENERAL-19

Closed orbit correction in CRYRING

O. Gorda, A. Bräuning-Demian, A. Dolinskii, F. Herfurth, C.-M. Kleffner, M. Lestinsky, G. Vorobjev
GSI, Darmstadt, Germany

To avoid acceptance limitations in the CRYRING [1], the close orbit (CO) distortions should not be larger than a few mm. During the multi-turn injection from the local ion source the intensity of the stored beam strongly depends on the ring acceptance and therefore it is important to control the CO. For slow extraction, large CO distortions can change the position and the orientation of the phase space separatrix limiting the extraction efficiency. In this report we describe the CO correction system and discuss the magnet alignment requirements based on ion-optical calculations.

In the present CRYRING layout seven horizontal and seven vertical beam position monitors installed in the sections YR02, YR06, YR07, YR08, YR10, YR11 and YR12 (see Fig. 1) will be used for CO measurements.

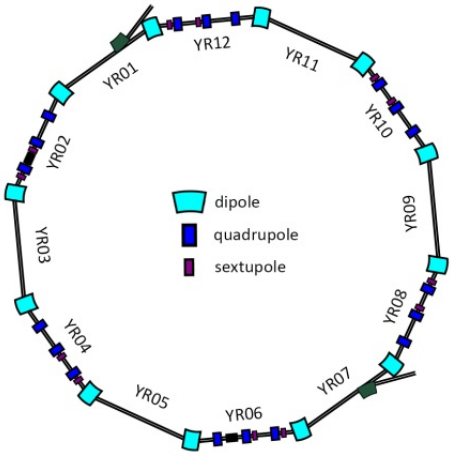

Figure 1: The CRYRING layout.

The CO correction will be provided by six pairs of horizontal and vertical correction magnets. Five pairs are installed in the magnetic sections YR02, YR04, YR08, YR10 and YR12 as described in [2]. In order to leave space for the extraction kicker magnet one horizontal corrector will be installed in section YR06, and a vertical corrector will be moved to section YR07. Additionally, all main dipole magnets have back-leg windings which can be used for corrections of the horizontal CO. According to calculations, a magnet alignment accuracy of 0.1 mm for displacement and 0.3 mrad for roll angle would result in a maximum peak-to-peak CO deviation of a few mm along the ring [3]. In this case, taking into account that the beam position monitors have an absolute measurement uncertainty of 1 mm it is not possible to further reduce the CO deviation. On the other hand, the required alignment accuracy can be slightly relaxed if the available correction magnets are used. Fig. 2 illustrates the calculated distribution of the peak-to-peak CO deviation for magnet displacement and roll accuracy of 0.3 mm and 0.3 mrad, respectively.

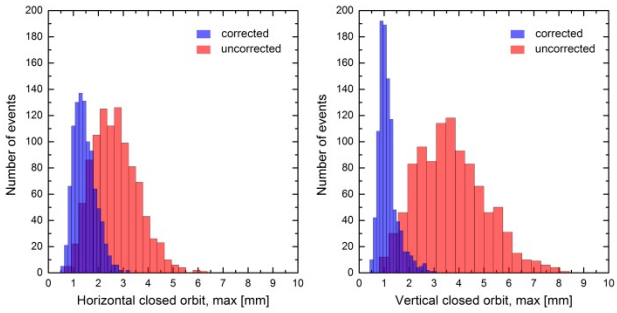

Figure 2: Calculated peak-to-peak deviation of the horizontal (left) and vertical (right) closed orbit.

For these MAD-X calculations 1000 random seeds of alignment errors have been used. The horizontal and vertical CO can be corrected to a RMS value of about 1.5 mm. Kick angles of at most 1.5 mrad, corresponding to a field strength of 0.01 T for a rigidity of 1.44 Tm, are required for correction. This is well within the maximum possible field strength of 0.03 T specified for the correction magnets. As an example, in Fig. 3 calculated CO before and after the correction is shown for several random sets of alignment errors.

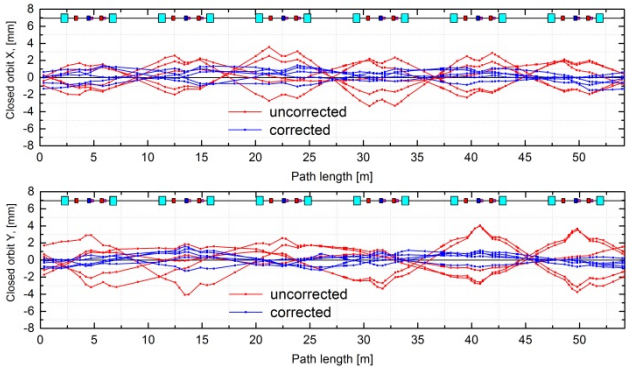

Figure 3: Calculated horizontal (upper) and vertical (lower) closed orbit.

References

[1] Lestinsky M et.al. CRYRING@ESR: A study group report, GSI, 2012.
[2] Danared H et.al. LSR Low-energy Storage Ring, Technical Design Report, MSL, 2011.
[3] Carle P et. al. Magnet alignment and survey in CRYRING, NIM A, v. 366, p.31, 1995

DOI:10.15120/GR-2015-1-FG-GENERAL-20

Status of the proton injector for FAIR

R. Berezov[1], N. Chauvin[2], J. Fils[1], R. Hollinger[1], V. Ivanova[1], C. Ullmann[3]
[1]GSI, Darmstadt, Germany; [2]CEA, Saclay, France; [3]IAP, Frankfurt am Main, Germany

The FAIR proton LINAC, the synchrotrons for heavy ions SIS18 and SIS100 have to provide the primary proton beam for the production of antiprotons [1]. The injector for the proton LINAC has to deliver 100 mA proton beam with an energy of 95 keV and an emittance of 0.3π mm mrad (normalized, rms) at the entrance of the RFQ.

The injector for the p-linac consists of the microwave ion source with "five electrode" extraction system and a low energy beam transport (LEBT) for matching the beam to the RFQ. The Microwave ion source developed and made in CEA/Saclay, will be able to run in pulsed mode by pulsing the RF generator. The ion source operates with a microwave frequency equal to 2.45 GHz based on ECR plasma production with two coils each with 87.5 mT magnetic field [2]. The five electrodes extraction system consists of a plasma electrode (plasma chamber potential), a puller electrode (50 kV), screening electrode (5 kV) and two ground electrodes [3].

The LEBT composes two short solenoids with two H/V integrated magnetic steerers and a diagnostic chamber, which is shown in the Figure 1. The diagnostic chamber is equipped with an iris, as beam diaphragm for transverse beam limitation, an Alison scanner for emittance measurement, a secondary emission grid (SEM) for direct determination of position and angle distribution, a Wien filter for detection of different ion species as a check of beam composition and a beam stopper. It is also planned to install a 4-grid analyser temporally to measure the space charge compensation during the commissioning of the proton injector.

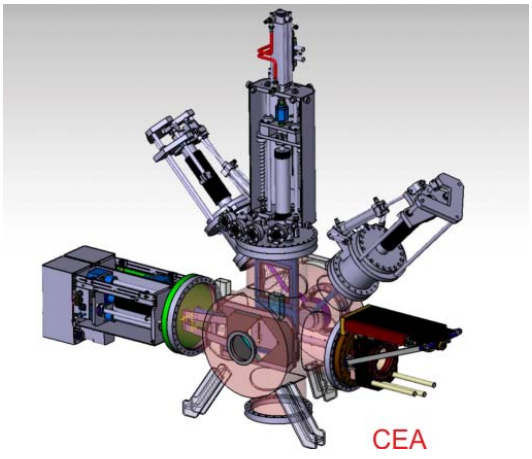

Figure 1. Diagnostic chamber with iris, Alison scanner, Wien filter, SEM grid and beam stopper.

For measuring ion beam intensity two current transformer (ACCT) will be installed behind the pentode extraction system and at the end of the LEBT beam line. The electrostatic chopper will be mounted between the LEBT and the RFQ to cut the beam pulse current to 36 µs. The total length of the compact LEBT is 2.3 m. The length reduced to minimize expected emittance growth along the beam line.

The assembly of the test bench for the commissioning at CEA/Saclay is rather finished. On Figure 2 the 3D model of the test bench is presented. The ion source is located on the platform with a potential of 100 kV inside the Faraday cage. The LEBT is installed outside of the Faraday cage and has ground potential.

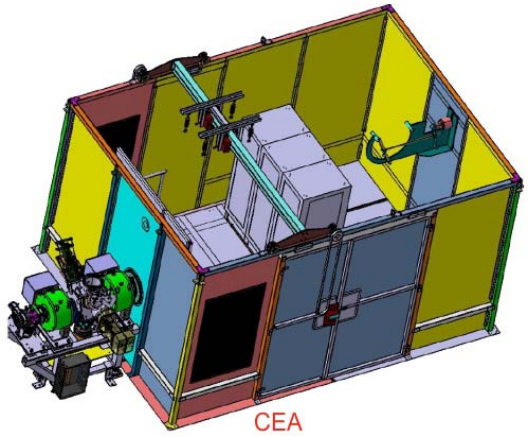

Figure 2: 3D model of the test bench for the commissioning at CEA/Saclay.

The first primary emittance measurement with the Alison scanner directly behind the extraction system is planned in Q2 (2015). After completing the LEBT installation with mini control system and power supplies, planned to start the commissioning in Q4 of 2015. For emittance measurement the mobile slit-grid emittance unit (from GSI) will be installed at the position of the entrance of the RFQ. It is also planned to perform measurements of beam current, stability of the source, space charge compensation and determination of the beam fraction.

References

[1] R. Hollinger, W. Barth et al., "High current proton beam investigations at the SILHI-LEBT at CEA/Saclay", Linac06 (2006) 232.
[2] C. Ullmann, R. Berezov et. al., "The proton injector for the accelerator facility of antiproton and ion research (FAIR)", Rev. Sci. Instrum. 85, 02A952 (2014).
[3] C. Ullmann, R. Berezov et.al., "Status and computer simulations for the front end of the proton injector for FAIR", proceedings of IPAC2014, Dresden, Germany.

DOI:10.15120/GR-2015-1-FG-GENERAL-21

RFQ beam dynamics design for the FAIR Proton Linac*

C. Zhang[#], *W. Vinzenz*
GSI, Darmstadt, Germany

The FAIR (Facility for Antiproton and Ion Research) Proton-Linac (P-LINAC) will be started with a 325.224 MHz, 3 MeV Radio-Frequency Quadrupole (RFQ) accelerator. To ensure that a beam intensity of ≥35 mA can be injected into the downstream synchrotrons, the design beam intensity of this Proton-RFQ (P-RFQ) has been chosen as 70 mA. Based on the so-called NFSP (New Four-Section Procedure) method, two new beam dynamics designs with varying and constant transverse focusing strength, respectively, have been worked out to meet the latest design requirements using a compact structure.

Background

The old reference design (D2009) realized by using the NFSP method [1] and published in 2009 [2] was optimized for 45 mA and can provide good beam performance e.g. ≥95% transmission efficiency for up to 100 mA input beams. This 3.2 m long RFQ is very compact at 95 keV such a relatively high input energy $W_{\text{in, RFQ}}$ (when considering the $W_{\text{in, RFQ}}$ values adopted by other comparable machines e.g. CERN LINAC4, J-PARC RFQ-III, and SNS), as the length of the adiabatic bunching section is proportional to β^3 [3].

The recently updated design requirements for the P-RFQ have two main changes: 1) the design beam intensity I_{in} has been fixed as 70 mA for more safety; 2) the allowed maximum surface electric field $E_{\text{s, max}}$ is lowered to 33 MV/m, corresponding to a Kilpatrick Factor (*KF*) of 1.87 (formerly $KF \leq 2.0$).

An important goal of the new design study is to minimize the output longitudinal emittance for making the matching to the downstream DTL easier and avoiding beam losses in the high-energy range.

Design Method & Results

Due to the success with the old reference design, the NFSP method is still adopted for both new designs. Different than the traditional LANL method, this method is characterized by a soft and symmetric pre-bunching, a fast main bunching, and then a fine bunching with a mixture of bunching and acceleration in the longitudinal plane as well as a varying focusing strength in the transverse plane which is adapted to the changing space-charge situation along the bunching process.

Besides a new NFSP design (D2014a), to meet the possible demands for the 4-vane RFQ version, another new design (D2014b) with a constant mid-cell aperture r_0 has been also developed using a so-called modified NFSP (mNFSP) method [4]: it has a NFSP-style longitudinal bunching but with a constant transverse focusing strength throughout the main RFQ.

For both of the new designs [5], the RFQ structure is even 10 cm shorter than that designed in 2009. As a result of the lowered $E_{\text{s, max}}$, the beam transmission efficiencies T are now slightly lower, but still ≥90%. However, in both cases, the difference in T for transported and accelerated particles is only 0.1%, which means most particles are well bunched and accelerated (see Figure 1). Meanwhile, from D2009 to D2014b and D2014a, the longitudinal output emittance was significantly reduced by 86% (all particles) / 20% (accelerated particles) and 91% (all particles) / 18% (accelerated particles), respectively.

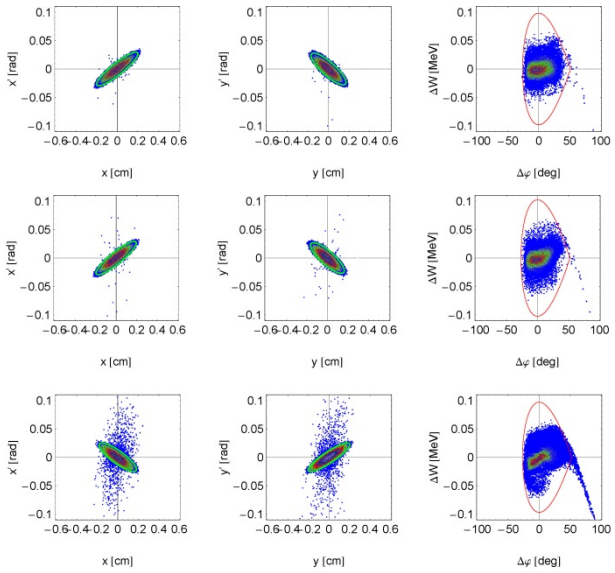

Figure 1: Output Phase Spaces (top: D2014a; middle: D2014b; bottom: D2009).

References

[1] C. Zhang et al., Phys. Rev. ST Accel. Beams 7, 100101 (2004).
[2] C. Zhang, A. Schempp, Nucl. Instrum. Methods Phys. Res., Sect., A, 609 (2009) p. 95-101.
[3] T.P. Wangler, *RF Linear Accelerators*, (Wiley-VCH Verlag GmbH & Co. KG, 2008).
[4] C. Zhang, "RFQ Beam Dynamics Design for Large Science Facilities and Accelerator Driven Systems", HB'12, Beijing, China, September 2012, p. 419, http://www.JACoW.org
[5] C. Zhang, "Beam Dynamics for the FAIR Proton-Linac RFQ", IPAC'14, Dresden, Germany, June 2014, p. 3226, http://www.JACoW.org

[#]c.zhang@gsi.de

Copper-plating of prototype cavities for the Proton Linac Accelerator

K. Dermati[1], J. Boensch[1], N. Boensch[1], R. Brodhage[1], T. Dettinger[1], R. Erlenbach[1], R. Fuchs[1], E. Kammer[1], E. Merz[1], M. Müller[1], N. Norcia [1], R. Reiter[1], M. Romig[1], T. Schiemann[1], T. Schneidler[1], S. Teich[1], D. Volz[1], W. Vinzenz[1]

[1]GSI, Darmstadt, Germany

Introduction

The FAIR anti-proton research program required a dedicated 70 MeV proton injector. The main acceleration of protons in the Proton-Linac will be provided by normal conducting, Crossed-bar, H-mode (CH) cavities according to the requirements and specifications of the accelerator physicists [1], [2]. For a high power RF test at GSI two prototype CH cavities are copper plated in the Galvanic of GSI. The requirement to be achieved was a constant, shiny (mirror finish) copper layer with a thickness of 50 µm all over the inner surface of the stainless steel CH cavities.

There have been two goals to be achieved during the electroplating work. First an exact, high quality copper layer and second the identification and optimisation of the procedure for the copper plating of all the CH cavities of the Drift Tube Linac Structure.

Electroplating / Copper Plating

To comply with the requirements a couple of dummies were produced and copper plated before processing the prototype cavities.

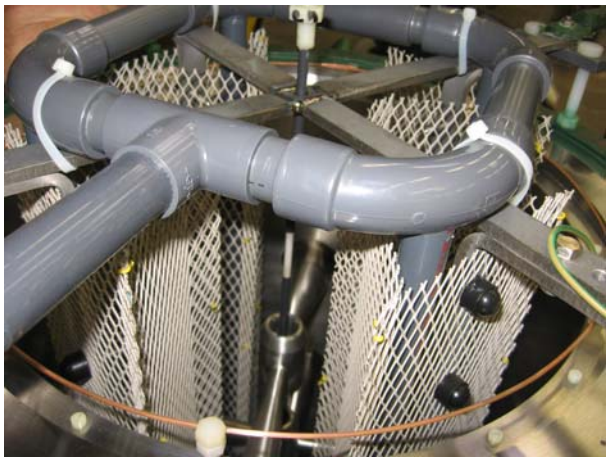

Figure 1: A CH-Cavity prepared for the Electroplating.

Electroplating started after suitable preparation including coating, forming and mounted the expanded metal anode gates. Various parameters should be considered and steered during all process: Shape of the anodes, distance to the surface of the cylindrical wall and stems, deflector plates, amperage, consistence of the baths, agitation during the plating, flow of the electrolyte and action time of each step of the plating.

After a cleaning and strong activation of the surface of the cavities a 15 µm nickel-strike base layer was given. Copper is an active metal and it is difficult directly plating iron-based surfaces. For this reason, such surfaces are first given a nickel-strike base coat, to which the copper can adhere.

The nickel strike bath is based on hydrochloric acid. Its deposition rate was 4,5 A/dm^2. A pulsed current process of 2 minutes current tact and 30 seconds current off was performed to avoid the forming of hydrogen bubbles, “pitting” on the surface. Electrolyte was transferred over the inner surface of the cavity during the current less tact.

The copper bath is based on sulphuric acid with additives which are responsible for the brightness and levelling of the deposited layer. The deposition rate was 3 A/dm^2. According to this ratio and the total inner surface the cavities stayed about two hours in the bath. A final polishing is necessary to get the shiny surface, Figure 2.

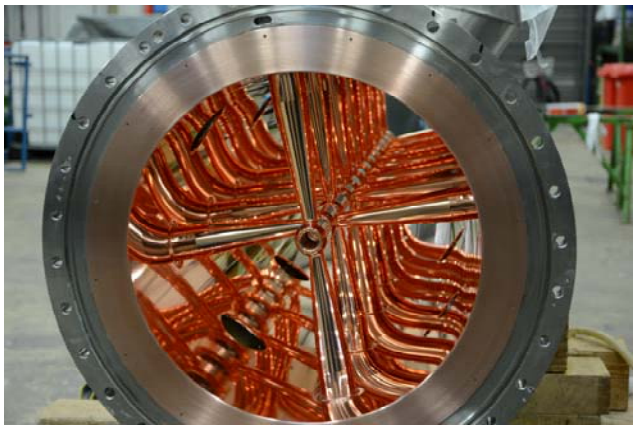

Figure 2: Shiny Copper plated prototype CH-Cavity.

Result

The copper plating of the two prototype CH cavities was commissioned with the expected performance. The required quantity and quality of the copper layer was achieved. The developed procedure and the gained experience might be used for the upcoming accelerator CH structure.

References

[1] Technical Report ”Proton Linac”, https://edms.cern.ch/document/994418/1.

[2] Status of the 70 MeV FAIR Proton Injector, Proceedings of IPAC2013, Shanghai, China, THPWO008.

DOI:10.15120/GR-2015-1-FG-GENERAL-23

Progress of the klystron and cavity test stand for the FAIR proton linac

A. Schnase[1], E. Plechov[1], J. Salvatore[1], G. Schreiber[1], W. Vinzenz[1], C. Joly[2], J. Lesrel[2]
[1]GSI, Darmstadt, Germany; [2]IPN Orsay, CNRS-IN2P3 Université Paris Sud, France

In collaboration between the FAIR project, GSI, and CNRS, the IPNO lab provided the high power RF components at 325.224 MHz for the cavity and klystron test stand [1] in the experimental hall LBH. For initial operation of the 3 MW Thales TH2181 klystron, a high voltage modulator from CERN Linac 4 was received as a loan. The 45 kW amplifiers for the 3 buncher structures of the FAIR proton Linac were carefully checked at the test stand, and prepared for cavity test operation.

Klystron test preparation

The company that originally wanted to provide the high voltage modulator for the klystron faced technical problems and finally abandoned this project. Fortunately the operating voltage and current of the klystrons for the CERN Linac 4 are quite similar to the TH 2181 klystrons foreseen for the FAIR Proton Linac. The Linac 4 repetition rate of 2 Hz is lower, than the 5 Hz rate foreseen for the Proton Linac. The pulse length for the proton Linac is shorter, which provides enough margins for operating the borrowed Linac 4 high voltage modulator. Effort was put into modifying and upgrading the existing infrastructure.

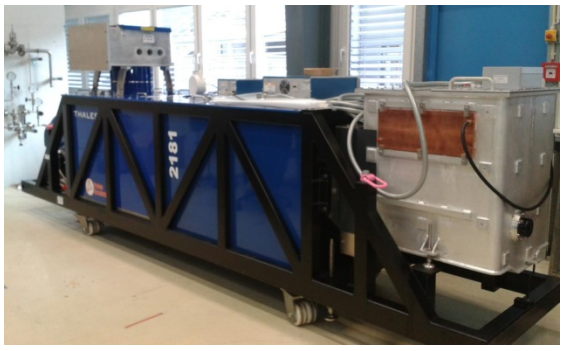

Figure 1: TH2181 Klystron in LBH test area.

The 3 phase electric supply connection was modified to provide sufficient margin for operating high voltage modulator and pulsed transistor amplifiers. At the former setup the auxiliaries were foreseen to be embedded into the modulator. Here we provided an additional rack containing the klystron filament power supply, the 3 solenoid power supplies and the two ion pump power supplies. The company who delivered the circulator for the klystron managed to adapt the cooling temperature range from 30+/-1°C to available 25°C. This allowed simplifying the cooling water distribution, which now can handle testing of klystron and transistor amplifiers.

The heater oil tank was prepared for the CERN modulator, and the filament power supply was tested with the goal to establish the power up and shutdown procedures. In operation of the solenoid power supplies in constant current mode, it was confirmed that they work as expected. The solenoids reach thermal steady state in two hours. The ion pump power supplies and the arc detection require fast acting interlocks. Accordingly the measurement & interlock rack was modified to process the additional signals. Careful checking of the interlock functionality and the signals processed by a PLC will ensure protection of the klystron according to the manufacturer specifications. The fastest response is handled by blanking the low level RF signal within microseconds.

First operation with the klystron will be without applying RF for commissioning and to understand the interaction with the modulator. As next steps, RF power will be send to a dummy load, and then the circulator will be included and measured by calibrated directional couplers. Finally we prepare to exercise the prototype CH cavity in the shielded area.

Transistor amplifier test

In autumn 2014 three 45 kW transistor amplifiers for the 3 (re-)bunchers of the Proton Linac were delivered. The alignment of the amplifiers and the RF output was improved for easier installation and the firmware was adjusted to the expected pulsed operation mode.

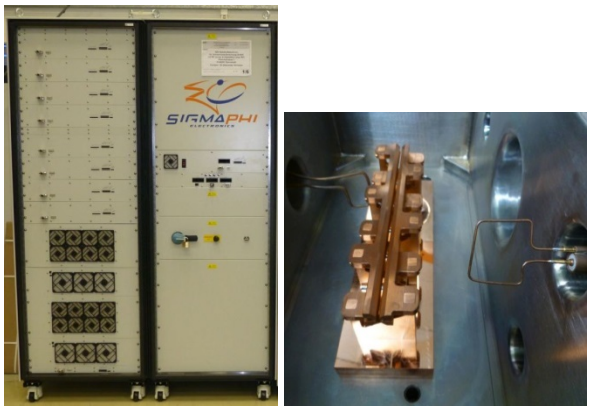

Figure 2: Amplifier (left) and RFQ test cavity structure.

Initial tests were conducted with a 50 Ohm power load at the amplifier output. The required 45 kW pulsed power was confirmed. From University of Frankfurt we received a compact 325 MHz test cavity structure and we prepare a site acceptance test of these amplifiers under pulsed conditions driving a resonant load.

References

[1] J. Lesrel, et. al. “RF Power Systems for the FAIR Proton Linac”, LINAC2014, Geneva, Sept. 2014, MOPP078

DOI:10.15120/GR-2015-1-FG-GENERAL-24

Space charge investigation for low energy ion beams with a 4-grid analyzer

C. Ullmann[1,2], *A. Adonin*[1], *R. Berezov*[1], *R. Hollinger*[1], *V. Ivanova*[1], *and O. Kester*[1,2]
[1]GSI, Darmstadt, Germany; [2]Goethe Universität, Frankfurt

4-grid Analyzer

The 4-grid Analyzer, or Retarding Potential Analyzer (RPA) is dedicated to space charge compensation measurements of ion beams by analyzing the energy distribution of secondary ions accelerated by the beam potential. The RPA consists of four grids, as shown in Figure 1. Grid one is on ground potential to shield the ion beam. Grid two repels electrons coming from the beam tube. The voltage on grid 3 is retarding and can be varied from negative to positive electric potential to filter secondary ions produced during interaction between primary ions and residual gas in the beam. The fourth grid repels electrons produced in the Faraday cup at the end of the RPA. For capturing the signal a current to voltage transformer (I-U transformer) with a high signal acceptance is used.

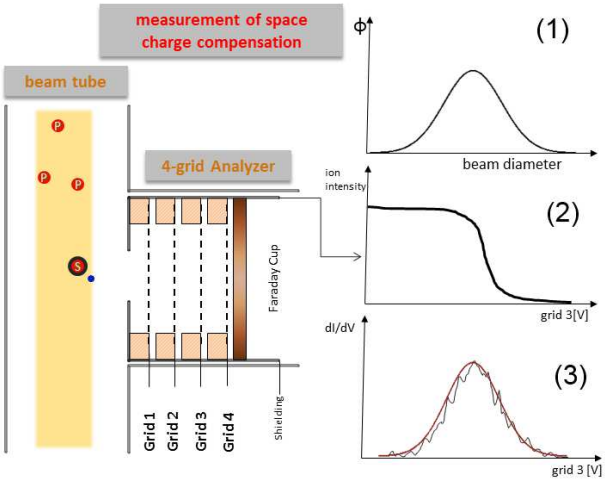

Figure 1: Schematic view of the 4- grid analyzer, data acquisition and analysis.

Secondary ions fully pass the third grid up to a certain potential which leads to a decrease of the Faraday cup signal. (1) shows an example for the ion beam potential as a function of the ion beam diameter. (2) shows the signal captured by the Faraday cup and (3) the estimated ion beam potential received from the measurement by derivation of signal (2). The uncompensated beam potential $\Delta\Phi_{uncomp}$ is calculated using

$$\Delta\Phi_{uncomp} = \frac{I}{4\pi \cdot \epsilon_0 \cdot v_{ion}} \qquad (1)$$

Experimental Results

Measurements are performed at the high current test bench and at the high current test injector under variable conditions. First measurements are performed with a high current ion source (MUCIS), single hole extraction system with He and Ar gas. An example for the results is shown in Figure 2.

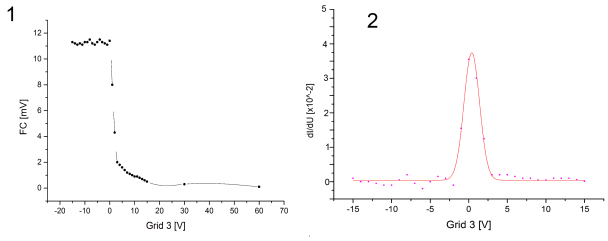

Figure 2: (1) Measurement at high current test bench $U_{Extr} = 20kV$,$I_{FC} = 7mA$; (2) Results via derivation

Above a voltage of $\Delta\Phi_{uncomp} = 122V$. This results in a space charge compensation of the ion beam of apparently 98%.

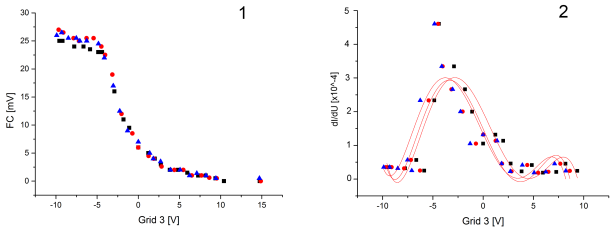

Figure 3: (1)Measurements at HOSTI test injector; $U_{Extr} = 110kV$,$I_{FC} = 10mA$ (2) Results via derivation

At HOSTI the RPA is installed behind a superconducting solenoid to analyze focused ion beams. Potentially inside the solenoid the beam compensation can partly be destroid. In Figure 3 space charge compensation varies round 97% based on $\Delta\Phi_{uncomp} = 23.7V$.

Outlook

It is planned to check on the time dependency of space charge compensation in a pulsed ion beam at HOSTI test bench. Various ion source types with different extraction systems for high current injection will be used to compare light and heavy ion operation as well as metal operation.

DOI:10.15120/GR-2015-1-FG-GENERAL-25

Advanced CST simulations for the FAIR p-LINAC BPMs

M. Almalki[1], *P. Forck*[1], *W. Kaufmann*[1], *T. Sieber*[1], *P. Kowina*[1], *C. Krüger*[1], *O. Kester*[1], *and C. Simon*[2]
[1]GSI, Darmstadt, Germany; [2]CEA-Saclay/DSM/Irfu, Gif-sur Yvette, France

At the planned Proton LINAC of the FAIR facility, four-fold button Beam Position Monitors (BPM) will be installed at 14 locations along the 30 m long FAIR p-LINAC [1,2]. Depending on the location, the BPM design has to be optimized, taking into account an energy range from 3 MeV to 70 MeV, limited insertion length at 30 mm or 50 mm beam pipe aperture. Detailed simulations of the button parameters with the finite element code CST [3] have been executed including pickup capacitance, impedance matching characteristic in time and frequency-domain. Additionally, the signal shape modification with respect to beam parameters, namely beam velocity and bunch length, has been investigated.

Capacitance and Electrical Properties

The pickup capacitance and the electrical properties for different geometries were investigated. The model consists of an inner conductor connected to a button electrode shown in Figure.1.

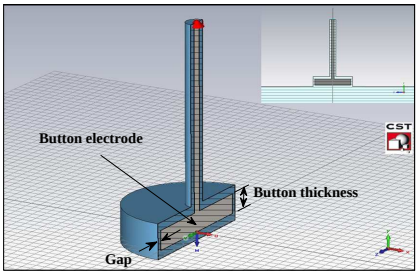

Figure 1: 3D model of the button pickup.

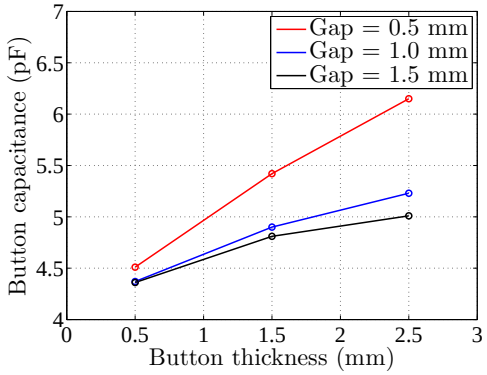

Figure 2: Pickup capacitance as a function of the button thickness calculated by CST Electrostatic Studio solver.

The button geometry has been modified by varying the button thickness and the gap between the button and the housing. The pickup capacitance for different button geometries is shown in Figure.2. A button thickness and gap size of 1 mm each results in a low capacitance, equivalent to high signal, and fits to the commercially available mechanical realization. The influence of further mechanical parameters on signal shape are discussed in [4] using CST Microwave Studio solver.

Bunch Length Investigations

CST Particle Studio was used to characterize the pickup signal width σ_s as a function of Gaussian bunch width σ_b at different beam velocities; β = 0.08, 0.27 and 0.37. The span of simulated bunch width starts from σ_b = 30 up to 960 ps.

The results show a linear relationship between the pickup signal and the bunch width down to a certain limit ($\sigma_b \approx 80$ ps) shown in Figure.3. Below this limit there is no change in the output signal width as the bunch width decreases further. Those limits (for each β value) are used to estimate the pickup signal and the required analogue band width for signal processing.

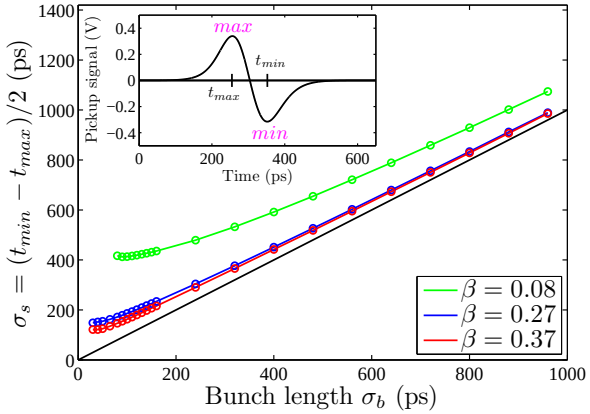

Figure 3: Relationship between bunch width σ_b and pickup signal width σ_s (σ_s calculated from the time difference between min and max values of the pickup signal).

References

[1] L. Groening et al., "Status of the FAIR 70 MeV Proton LINAC", LINAC'12, Tel-Aviv, p. 927 (2012).

[2] P. Forck et al., "Design of the BPM System for the FAIR Proton-LINAC", GSI scientific report 2010.

[3] https://www.cst.com/.

[4] M. Almalki, PhD Thesis, IAP University of Frankfurt, in preparation.

DOI:10.15120/GR-2015-1-FG-GENERAL-26

High power RF coupler for the FAIR p-LINAC cavities

F. Maimone, W. Vinzenz

GSI, Darmstadt, Germany

HISTORY

Since some decades most of the UNILAC cavities are equipped with the same type of RF couplers. Studies in the 80th have shown that a cylindrical ceramic as vacuum seal is nearly ideal. Compared to ceramic disks the real surface area hit by X-rays is much smaller. From fabrication issues much more manufacturing steps, including metallization of both tube ends, have to be passed.
A general composition is shown in [Fig. 1].
For applications at different power levels and different mechanical environments the design has just to be scaled.

APPLICATIONS

Beside the operation at the UNILAC at 36, 108 and 216 MHz the same kind of loop is used at CERN Linac3 (Lead Linac) at 101 MHz, at the therapy Linacs in Heidelberg (HIT) and Padova (CNAO) at 216 MHz [Fig. 1] and at BNL Upton NY at 100 MHz. The coupler is not built for a dedicated kind of cavity. A range of applications goes from RFQ, IH, Alvarez, Spirals to CH cavities covering a power range from 10th of kW up to 2 MW pulse (at 25% duty factor). Therefore a big number of flange-oriented types with respect to the dimensions of the used RF power lines as well are available.

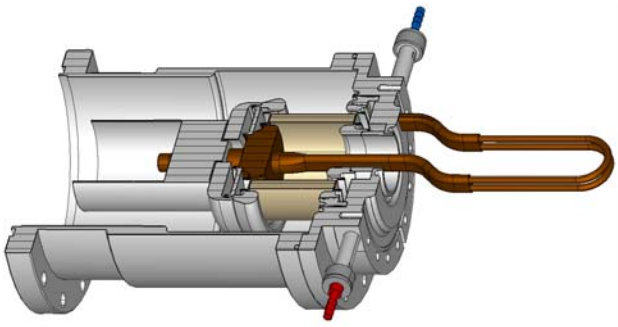

Figure 1: General composition of the GSI RF couplers

HIGH POWER RF COUPLER

The pLINAC providing up to 70 MeV proton beam for the FAIR facility is under construction. The normal conducting DTL of the pLINAC is composed by three Coupled Cross-bar H-mode (CCH) cavities, providing the acceleration up to the energy of 36 MeV, followed by three Cross-bar H-mode (CH) cavities. [1] In order to provide the input power to the CH-cavities a RF inductive coupler has been studied and developed.

The RF power coupler, consisting of a water cooled inductive loop, has to handle up to 3 MW pulsed power at 325 MHz. A dedicated study of the coupling factor and the electromagnetic field for different penetration length of the coupler inside the coupling cell – the intertank unit connecting two neighboured cavities long 2β and hosting the triplet lens - and for different angles with respect to the beam axis has been carried out.

According to the results of the simulations an optimized design of the inductive loop was produced and a prototype of the coupler has been manufactured at the GSI workshop [Fig. 2].
The coupler is vacuum leak tested and low level RF measurements in the build-in condition at the CCH prototype cavity are planned to be performed in March 2015 at the RF test bench.

Figure 2: Prototype of the RF coupler fot the CH-cavities of the pLINAC

References

[1] Technical Report “Proton Linac”, https://edms.cern.ch/document/994418/1.
[2] F. Maimone, G. Clemente, W. Vinzenz, Proc. of LINAC2014, Geneva, 2014

DOI:10.15120/GR-2015-1-FG-GENERAL-27

System Simulation of Bunch-to-Bucket Transfer Between Synchrotrons*

T. Ferrand†[1] *and J. Bai*[2]

[1]TEMF, Technische Universität, Darmstadt, Germany; [2]IAP, Goethe Universität, Frankfurt am Main, Germany

Introduction

A model of the low-level RF (LLRF) synchronization topology at SIS18 and SIS100 under Ptolemy II [1] is currently under development. This model enables to simulate the behavior of the synchronization signals during the synchronization procedure at the transfer flattop within the framework of a deterministic bunch-to-bucket transfer. The Java-based heterogeneous structure of the Ptolemy II software offers an intuitive parallelization procedure by splitting the different sub-models in concurrent threads.

Simulation of the LLRF system

The simulated LLRF system is composed of two independent and non-synchronized entities. The first entity is based on the phase advance measurement between a radio-frequency (RF) signal and a reference (REF) signal. The REF signal is derived from the periodically shared BuTiS synchronization signal $T_0 = 10\ \mu$s:

$$f_{REF} = \frac{N}{T_0} \qquad \text{with} \quad N = floor(f_{RF} T_0) \qquad (1)$$

The REF signal is generated by a DDS. A periodic reset of the DDS phase value consistent with the synchronization signal ensures that the phase advance relation between the REF signal and the synchronization signal remains constant. This REF signal can thus be duplicated to provide a fix phase measurement reference.

The phase advance measurement between the RF and the REF signal relies on a frequency transposition and a direct IQ demodulation [2]. This method benefits from a high phase measurement accuracy and a maximum error value of 0.6^o at 5.4 MHz and delivers its phase measurement asynchronously every $3.22\ \mu$s, i.e. the delay between the most recent phase advance measurement and the next slope of the synchronization signal is not constant.

The second simulated entity corresponds to an additional DDS module, which duplicates an RF signal in real time. This DDS may receive the same frequency value command as the DDS, which generates the original RF signal such, that duplicated and original RF signals have the same frequency but their phase advance relationship remains free. The measured phase advance from the first entity is used to determine the phase offset with respect to a certain time event such as a trigger derived from the synchronization signal. The duplicated DDS resets at this trigger with the calculated offset, which enables the duplicated RF signal to synchronize with the original RF signal.

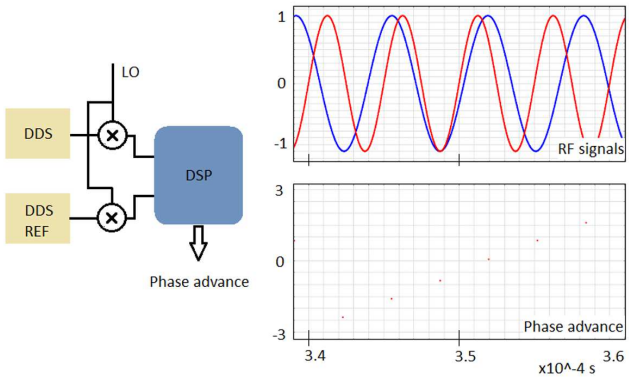

Fig 1, left: representation of the phase measurement entity.
above right: RF signals of 157 and 200 kHz.
below right: relative phase advance measurement.

A conventional synchronization loop may be used to synchronize a DDS RF signal with the locally emulated signal. In the framework of the bunch-to-bucket transfer synchronization between SIS18 and SIS100, a symmetrical implementation of this system may enable duplicating the synchronization RF signals locally, if they are required. The synchronization of such emulated systems needs a data transfer between the two supply rooms only once per acceleration cycle.

Outlook

The implementation of a hardware synchronization system on the basis of this simulation is currently under study and is expected to be implemented in the coming months. This demonstration system may enable to evaluate the reliability and the robustness of the simulation model. A simulation-based optimization for the local resynchronization procedure is foreseen.

References

[1] Claudius Ptolemaeus, editor, “System Design, Modeling, and Simulation using Ptolemy II”, Ptolemy.org, 2014, URL: http://ptolemy.org/books/Systems

[2] H. Klingbeil, “A Fast DSP-Based Phase-Detector for Closed-Loop RF Control in Synchrotrons” IEEE Transactions on Instrumentation and Measurement, Vol. 54, No. 3, June 2005

* Work supported by GSI, cooperation with TU Darmstadt.

Progress in damping of longitudinal beam oscillations during acceleration*

D. Lens† [1], *U. Hartel* [1], *H. Klingbeil* [1,2], *B. Zipfel* [1], *K. Groß* [2], *J. Adamy* [3], *B. Reichardt* [3], *M. Kumm* [4], *K. Möller* [4], *and P. Zipf* [4]

[1]GSI; [2]TU Darmstadt, TEMF; [3]TU Darmstadt, RMR; [4]University of Kassel, Digital Technology Group

Introduction

In the FAIR synchrotrons, coherent longitudinal oscillations of the bunched beam will have to be damped by dedicated feedback systems. While the damping for coasting beam energy has been successfully verified in SIS18 by several experiments (cf. e.g. [1]), the damping of these modes during the acceleration process poses additional challenges. The main technological issues are discussed and a progress status is given. For details on the longitudinal feedback system for FAIR with bunch-by-bunch feedback, we refer to [2].

Status of Main Projects

Group-DDS Phase Calibration

For the low-level RF (LLRF) system, it is essential that reference signals are provided with a phase stability better than 1°, cf. [3]. Such reference signals are generated by DDS modules, which show a frequency-dependent behavior during the acceleration ramp that must be compensated to reach the high accuracy requirements. A compensation strategy using calibration electronics has been employed and verified in beam experiments [3]. In addition, a software tool has been developed which enables a semi-automatic calibration, drastically reducing the effort to perform a calibration of a DDS crate.

Feedback Tuning During Acceleration

A finite impulse response (FIR) filter is used for the damping of longitudinal modes. For this filter, a tuning rule based on the synchrotron frequency was already experimentally verified in the past. In a recent beam experiment [4], the successful damping of coherent quadrupole oscillations during acceleration has now been demonstrated, cf. Fig. 1. The results are currently being used to verify the tuning strategy during acceleration.

FPGA Implementation of Tunable Filter

A dynamically reconfigurable FIR filter has been implemented on an FPGA [5] and will be integrated into the existing framework of the DSP system [1] used for longitudinal feedback. The next step will then include the implementation of the tuning rule for the adaption of the filter coefficients.

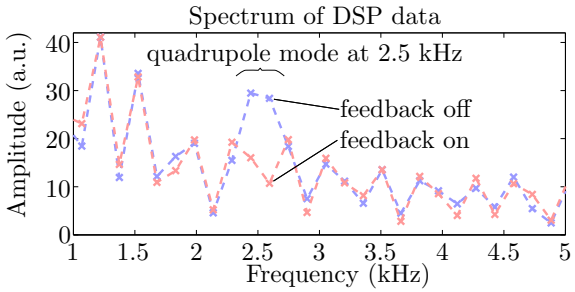

Figure 1: Damping of longitudinal coherent quadrupole modes in SIS18 during acceleration, Sep. 7, 2014.

Optimized Filter Design

The filter implementation [5] in principle allows for more complex filters with a larger number of coefficients than currently used. In a cooperation project with TU Darmstadt (RMR), the potential of these longer filters is currently analyzed. Measurements with beam showed as a proof of principle that the damping of the closed loop may be increased. However, careful investigations are still necessary to study possible implications concerning noise and robustness.

Future Work

The phase response compensation of DDS modules will be automated further to enable periodic calibrations of the reference DDS crate to compensate long-term drifts.

Concerning the damping of longitudinal modes, further steps will be taken towards standard operation as described in [4].

References

[1] H. Klingbeil et al., “A digital beam-phase control system for heavy-ion synchrotrons”, IEEE Trans. Nucl. Sci. 54(6)2604:2610 (2007)

[2] K. Groß et al., “Verification of the Longitudinal Feedback Topology in SIS18”, these proceedings

[3] B. Zipfel et al., “Generation of RF frequency and phase references on the FAIR site”, Proc. IPAC2014, THPRO102 (2014)

[4] D. Lens, “Beam experiment: damping of longitudinal quadrupole oscillations during acceleration in SIS18”, GSI memo (2014)

[5] K. Möller et al., “Dynamically reconfigurable FIR filter architectures with fast reconfiguration”, Proc. ReCoSoC (2013)

* Work supported by GSI.

† d.e.m.lens@gsi.de

DOI:10.15120/GR-2015-1-FG-GENERAL-29

FAIR HEBT System - status report

F. Hagenbuck, L. Bozyk, A. Krämer, B. Merk, C. Mühle, S. Ratschow, B.R. Schlei, P. Spiller, B. Walasek-Höhne, H. Welker, and C. Will
GSI, Darmstadt, Germany

Modifications in the HEBT System Layout

Based on a decision of the project lead FAIR@GSI and FAIR the direct connection from SIS18 to the Collector Ring (CR) via the last part of the Ring Branch of the Super-FRS was included into the planning of the modularized start version.
The concept for the positioning of safety beam plugs in the HEBT system was further worked out in coordination with the radiation protection department. For the beam plugs in four beam line sections detailed FLUKA studies were performed for accidental beam deposition to determine the expected radiation level in neighbouring areas and to optimize length and material of the beam plugs [1].
Pressure profile calculations of the vacuum system were started to determine number, type and location of pumps.

Status of procurement

In July 2014 the CR-like HEBT magnets (2 dipole, 5 quadrupole magnets) were assigned by FAIR Council resolution to the Budker Institute (BINP, Novosibirsk, Russia) whereas the bulk of the HEBT magnets was already assigned in 2011/2012 to the Efremov Institute (NIIEFA, St. Petersburg, Russia; batch1-3). All related vacuum chambers will be built by BINP. The production of the first pre-series dipole magnet (type dip1s_0) of batch1 (51 dipole magnets and vacuum chambers) started in 2014, the coils are produced (see Fig. 1), the laminations punched and the magnet is expected to be finished in May 2015. The vacuum chamber is expected to be ready in June 2015. The preliminary design review for the second pre-series dipole magnet (type dip13_0) was successfully concluded, currently the manufacturing drawings for the final design review are in preparation. The detailed specifications of batch 2 (17 dipole, 102 quadrupole, 80 steering magnets and vacuum chambers) were released in August 2014. The contracts are still under negotiation with NIIEFA and BINP. The detailed specifications of batch3 (5 dipole, 71 quadrupole, 12 steering magnets and vacuum chambers) are supposed to be available in spring 2015.
In May 2014 a first contract between FAIR, the indian shareholder Bose Institute (Kolkata) and the provider ECIL (Electronics Corporation of India Limited) comprising 78 quadrupole power converters was signed. This contract covers all quadrupole power converters needed for the standard quadrupoles (quad2) in the 18 Tm and 13 Tm beamlines of module 0-3. In the meanwhile the conceptual design review for two quadrupole power converter types was successfully concluded (Nov 2014, Jan 2015). With respect to a second contract the detailed specifications of the power converter types for the 18 Tm steering magnets and for further quadrupole magnets were recently given into the EDMS release process.
All technical documents for the HEBT beam diagnostic standard vacuum chambers were handed over to the indian shareholder Bose Institute in 2014. In the tendering process the indian partner was supported in the evaluation of possible providers by GSI experts from the vacuum and quality assurance department. A decision will be taken by an indian selection committee in the beginning of April 2015.
A contract with the slovenian in-kind partner was signed in November 2014, comprising HEBT BPM pre-amplifiers, Data Acquisition (for BPM, Beam-Loss Monitor System and Beam Current Transformer) and Pressurized Air Drives and Control. Furthermore several beam instrumentation developments for applications in the FAIR HEBT system were conducted successfully in 2014 as for example a new system for scintillating screen based diagnostics [2].

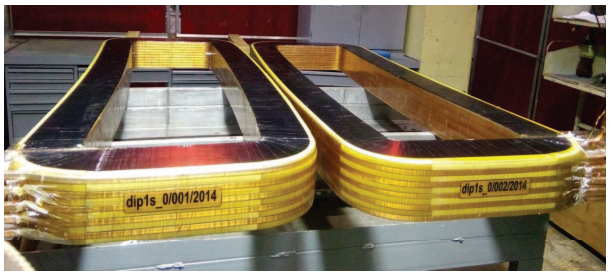

Figure 1: Set of coils for pre-series dipole magnet dip1s_0

Building plannning

The review of the 5th preliminary building shell plan of G0704A and G0702A took place. However 3D collision checks could be done only with the 3D model of the buildings whereas the 3D model of the technical building equipment was not available. Additionally the 4th preliminary building shell plan of H0705A was checked informally.

References

[1] S. Damjanovic et al., “FLUKA Simulations of the FAIR HEBT System: Optimization of the Safety Beam Plugs (Diffusors)”, GSI Scient. Report 2014

[2] B. Walasek-Höhne et al., “CUPID: New System for Scintillating Screens based Diagnostics”, GSI Scient. Report 2014

DOI:10.15120/GR-2015-1-FG-GENERAL-30

FLUKA Simulations of the FAIR HEBT System: Optimization of the Safety Beam Plugs (Diffusors)

S. Damjanovic[1], *F. Hagenbuck*[1], *B. Merk*[1], *T. Radon*[1],
[1]GSI, Darmstadt, Germany

The complex High Energy Beam Transport (HEBT) system of FAIR allows for parallel user operation with different beams. To ensure safe operation the installation of safety beam plugs ('diffusors') is foreseen. These are mobile blocks to be used in case of an emergency situation to intercept an unwanted beam and thereby reduce the radiation level in the neighbouring areas accessible by personnel during normal operation. This provides redundancy to interlock magnets. FLUKA studies have been performed for accidental scenarios with such diffusors (named 'Dnn'), individually for D20, D23, D22 and D14, assessing the resulting radiation level and optimizing the diffusor lengths and material.

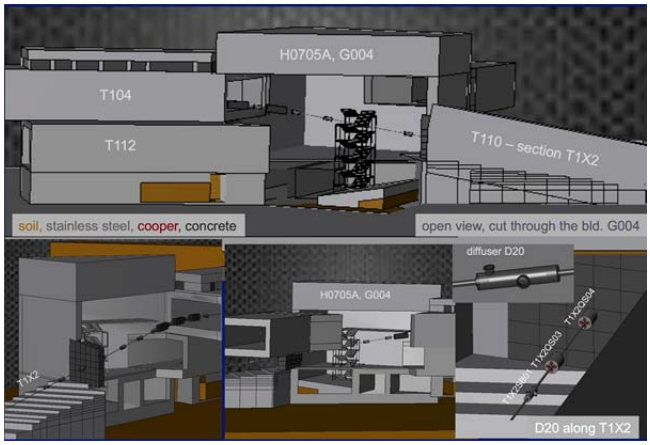

Figure 1: FLUKA geometry of bld. G004 with the diffusor D20 along the sloped beam line T1X2.

To obtain realistic radiation fields, precise modelling of the geometry of the HEBT system over extended regions was required. This includes the complex building G004 with the sloped beam line T1X2 from SIS100 along the tunnel T110 (extraction region) and the complete tunnels T104, T112 (Fig.1), and the tunnel T113 with the beam lines TAP1, TSN1, TAP2, TXL3, TPP1, TPP2 (Fig.2 left). The right part of Fig.2 indicates the two modelled regions with the two shaded areas (upper for Fig.1).

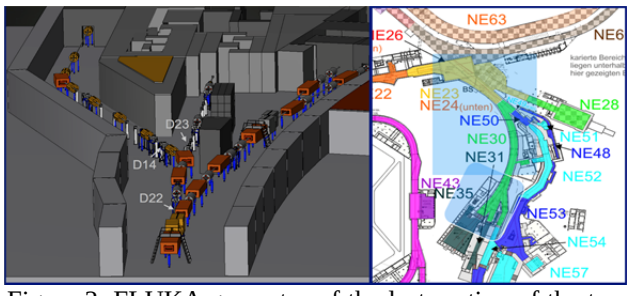

Figure 2: FLUKA geometry of the last section of the tunnel T113 with the diffusors D23, D22 and D14 (left).

The results of the effective dose distribution from a SIS100 proton beam with an intensity of 2.5×10^{13}p at E_k=29 GeV hitting the diffusors D20 and D23 (made of iron) are shown in Figs.3 and 4, resp. It is found that for an accidental scenario with D20 a diffusor length of 20 cm would be optimal. This would lead to effective doses <1μSv at the surface level of bld. G017 (areas NE25 and NE26), allowing for 10 shots per year, and <<1mSv in the areas of NE30 and NE50, allowing for open access to these areas. The length of the diffusors D23, D22 and D14 placed in the last section of the tunnel T113 was optimized to keep the access to the areas NE31, NE35 (antiproton target area and experimental caves) and NE53.

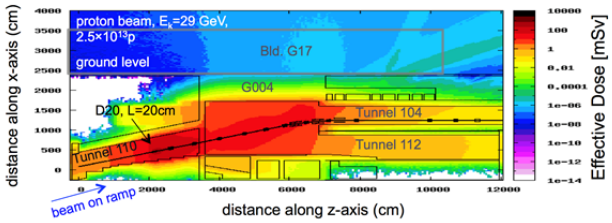

Figure 3: Effective dose for one beam pulse hitting the diffusor D20 placed along the sloped beam line T1X2.

For accidental scenarios with the diffusor D23 where a beam meant to be transported to the APPA cave accidentally was directed to the pbar target area, a minimum length of 40 cm iron would be required to keep the access to all neighbouring areas, while 20 cm would be sufficient for D22 and D14. The replacement of 40cm iron by 20cm

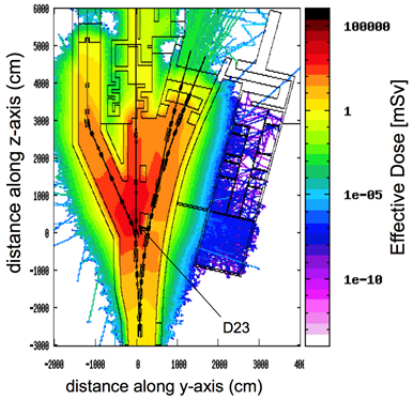

Figure 4: Effective dose for accidental scenario with D23.

tantalum would assure the same length for all diffusors. In the future, two more diffusors, D12 and D13 (intercepting the SIS18 beam) will have to be studied before concluding on the final specification of the material and dimensions of the diffusors and their chambers.

DOI:10.15120/GR-2015-1-FG-GENERAL-31

Pilot study of beam position and profile monitoring for the pBar target

A. Reiter, H. Bräuning, J. Frühauf, H. Graf, S. Löchner, M. Witthaus
GSI, Darmstadt, Germany

At secondary target installations like the FAIR antiproton target, monitoring of the beam-target-overlap is a crucial task for the beam instrumentation. For antiproton production an intense 29 GeV proton beam pulse is extracted within 50 ns from the SIS100 synchrotron. The primary beam is focussed after a 3 m drift section in air on a 3 mm Nickel target rod. Because the target station is surrounded by a 1 m iron shielding, the spot size must be derived from detectors in the short drift section. To this purpose the performance of two detectors operating in air has been studied with 300 MeV/u Nickel beams and fast extraction.

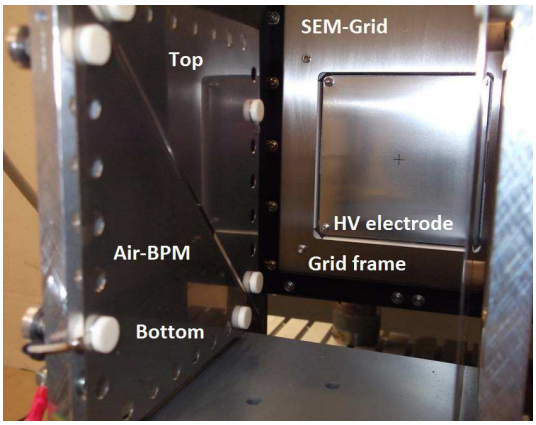

Figure 1: Air-BPM (front) with two electrodes (Bottom and Top) shown on the left; SEM-Grid (at back) with HV electrodes that cover the arrays of Tungsten wires.

Experiment Setup and Results

Two radiation-hard detectors were installed at the end of the HTP beam line next to the dump (see Figure 1):

- ”Air-BPM”: This detector consists of two diagonally-cut 135 mm electrodes, separated by a ground guard, and was placed 50 mm from the beam axis. A vertical motor drive typically moved the device in 1 mm steps.
- SEM-Grid: This detector is an existing GSI design mounted on an external pneumatic drive 20 cm in front of the beam dump. No high voltage was applied.

Both detectors were connected via pulse-stretchers to charge-to-frequency converter POLAND units [1] and read out via FESA, the new FAIR standard for acquisition systems. For each spill offset-corrected data were stored for further analysis. The Air-BPM signals were fed to the POLAND units via 80 m long coaxial cables to emulate the situation in the target hall where 150 m are required.

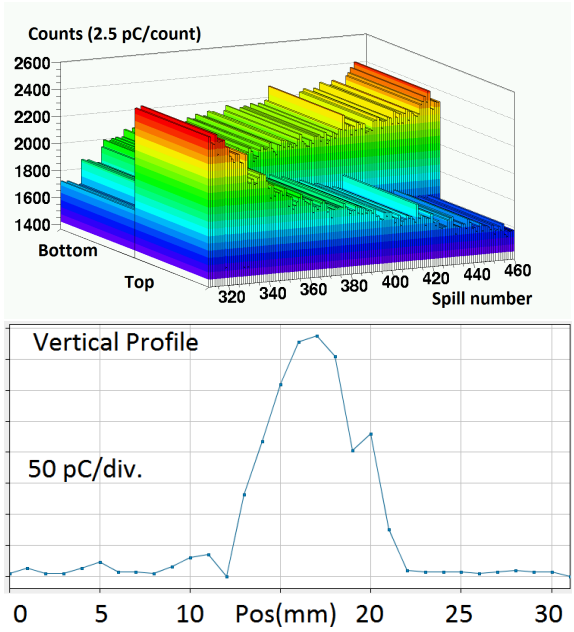

Figure 2: Scan of Air-BPM for 1x10^9 Ni ions (A) and vertical SEM-Grid profile for 2.5x10^9 Ni ions (B).

In Figure 2 detector signals of Air-BPM (A) and SEM-Grid (B) are presented. The Air-BPM was scanned through the beam in 1 mm steps. For each of the 15 positions ten spills were analysed and the normalised ratio ’difference-over-sum’ Δ/Σ calculated. The measured gradient of Δ/Σ=(1.42$\pm$0.02)%/mm is in good agreement with the theoretical value based on the electrode geometry.
The vertical profile shows a smooth distribution with a kink at 19 mm, which might be due to imperfections in the offset subtraction. The full profile width of 10 mm fairly agrees with the data of Cromox screen and SEM-Grid in the upstream diagnostic chamber. The calculated charge integral is only 20% lower than the prediction of Sternglas [2]. Similar ratios have been observed in ref. [3] and by the authors for other data sets of SEM-Grids installed in vacuum. However, the present data are yet too sparce to conclude that the secondary electron yield does not suffer significantly from operation in air. Further data need to back up the present encouraging results.

References

[1] S. Löchner et al., GSI Scientific Report 2013, Darmstadt.
[2] E. J. Sternglas, Phys. Rev. 108 (1957) 1.
[3] C. Nociforo et al., ”Profile Monitors for the Super-FRS”, This Scientific Report.

DOI:10.15120/GR-2015-1-FG-GENERAL-32

Transport concept for highly activated antiproton production targets

M. Helmecke[1], G. Fehrenbacher[1], V. Gostishchev[1], R. Hettinger[1], K. Knie[1], R. Lang[1], J. Fitting[2]
[1]GSI, Darmstadt, Germany; [2]Kraftanlagen Heidelberg GmbH, Heidelberg, Germany.

The antiprotons of the FAIR facility will be produced by a 29 GeV proton beam hitting a nickel target. Then they are focused by a circular magnetic field (magnetic horn) and transferred to the collector ring (CR) [1]. The target and the magnetic horn will become highly activated (up to 10^{11} Bq) during the antiproton production. Dedicated shielding calculations have been performed so far [2].

The target and the magnetic horn have to be exchanged regularly. Their activation leads to several technical challenges: To dismount the target or the magnetic horn these components have to be transported into a hot cell in the building of the Super Fragment Separator (SFRS). It is absolutely mandatory, that during handling and transport target and magnetic horn are surrounded by a sufficient shielding at all times [3]. Additionally, due to the radiation level the access to the target hall is limited (controlled area) and remote handling components have to be used. A target handling concept has been developed that fulfills all of these conditions (see [4]). A study together with Kraftanlagen Heidelberg has been carried out concerning legal aspects of this concept and to develop functional specifications of the necessary handling components in order to obtain the operation permit.

The handling in the pbar building is schematically shown in figure 1: In the first step the target and the magnetic horn are pulled out of the target station by a half-automated transport container via a dedicated rail system (pos. 1). To fix the components a fast coupling system is used. (The target and the magnetic horn are transported separately.) After the transport container is closed it is positioned under a shaft (pos. 2). A shielding flask above the shaft is equipped with a carrying frame that pulls the component through the shaft (pos. 3). Finally the shielding flask is closed (pos. 4) from below and lifted up by a transport trolley to bring it to the SFRS building.

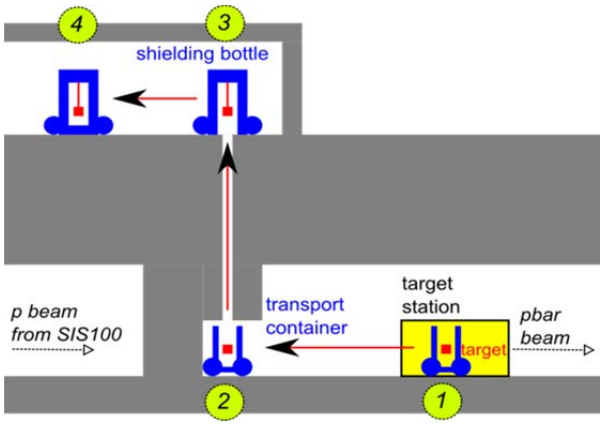

Figure 1: Schematic drawing of the target handling in the pbar building.

Inside of the shielding flask the target or the magnetic horn is fixed vertically, the highest radiation level is at the bottom, the lowest at the top. Figure 2 shows a cut of the flask with the magnetic horn fixed inside at the carrying frame. The wall thickness of the flask is designed in a way that the maximum dose rate at the outer surface is below 100µSv/h. The total weight of the flask is about 24 t.

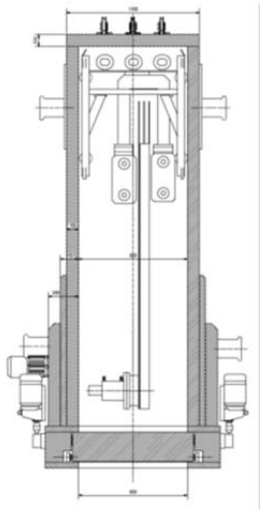

Figure 2: Cut of the shielding flask with magnetic horn and its stripline fixed inside.

Finally inside of the SFRS building the content of the shielding flask is transferred into the hot cell: First a traverse is fixed at the shielding flask that it can be moved by the crane of the building. This crane meets high safety standards, which are already predefined. With this traverse the flask is lowered about 6 m down next to the roof of the hot cell. Then for the final connection with the hot cell an adapter is placed also providing an interlock signal for the shutters of the hot cell and the shielding flask. When both shutters are open the carrying frame of the flask lowers down the component into the hot cell where it is dismounted by a technician of the SFRS group. Then the flask is closed again and is brought back to a parking position in the pbar building. The new target is then brought inside by using the same carrying frame of the shielding flask.

References

[1] Dolinski et al., Nuc. Instr. Meth. A 629 (2011) 16-24.
[2] GSI Scientific report (2011) PNI-ACC-14 483.
[3] 7. Teilerrichtungsgenehmigung, Hessisches Ministerium für Umwelt, Energie, Landwirtschaft und Verbraucherschutz, Wiesbaden (2013).
[4] Technical Design Report on the Antiproton Target and Separator, pbar working group, GSI, Darmstadt (2014).

DOI:10.15120/GR-2015-1-FG-GENERAL-33

Activation of the aluminium target by 200 MeV/u uranium beam *

P. Katrik[1,2,#], D. Hoffmann[1,2], E. Mustafin[2], and I. Strasik[2]
[1]TU Darmstadt, Darmstadt, Germany; [2]GSI, Darmstadt, Germany

Introduction

The paper presents new results of experimental study of the residual activity induced by high-energy heavy ions in common accelerator constructing materials. This study is a part of a broader research activity for validation of Monte Carlo codes and data libraries. There are several publications reporting the activation of different targets by various heavy ions with energies from 500 MeV/u up to 1 GeV/u [1-4].

Experiment and Simulation

The experimental target was designed in the stacked-foil geometry of 70 pieces. The foils were aluminium discs with the thickness of t = 0.1 mm and diameter d = 10 cm. The target was irradiated by 200 MeV/u $^{238}U^{(+73)}$ beam. The total number of projectiles accumulated on the target was 2.8×10^{12} ions. Gamma-ray spectra of each foil were measured individually or in groups of 5 foils together. Two series of measurements were performed: ~6-20 days and ~130-180 days after the end of irradiation. The experimental data were compared with the Monte Carlo simulations by FLUKA 2011.2c.0 code [5]. The residual activities were recalculated to the end of irradiation.

Results and Discussion

Out of all nuclides observed in the spectra we present here only the results for ^{7}Be, ^{22}Na and ^{237}U.

The distribution of ^{237}U (see Table 1) in depth could be used for finding the range of primary ^{238}U ions, because the masses of these nuclei are almost equal [4]. The FLUKA code predicted presence of ^{237}U in only two foils (Nr. 34 and Nr. 35), but we measured activity of this nuclide in the foil Nr. 36 as well. The simulation expects shorter range and about 40% lower production of ^{237}U.

Table 1: Total activity produced by ^{237}U in Al target

Foil Nr.	Depth [mm]	Activity of ^{237}U produced in target [Bq/mm/ion]	
		Simulation	Experiment
34	3.35	$1.262\times10^{-8} \pm 1\times10^{-10}$	$1.546\times10^{-9} \pm 2\times10^{-11}$
35	3.45	$2.710\times10^{-8} \pm 1\times10^{-10}$	$6.276\times10^{-8} \pm 7\times10^{-11}$
36	3.55	0	$3.461\times10^{-9} \pm 2\times10^{-11}$
SUM of Activity:		**$3.973\times10^{-8} \pm 2\times10^{-10}$**	**$6.776\times10^{-8} \pm 8\times10^{-11}$**

The depth profiles of ^{7}Be and ^{22}Na are presented in Figure 1 and Figure 2, respectively. The simulation is in agreement with the 1st and 2nd set of measurement only in the first foils of the target. In the depth of about 1.25 mm (the vertical line 150 MeV/u) differences between simulation and experimental data become evident. The disparities between the 1st and 2nd set of measurement in the range area are caused due to decaying of short-living isotope which was influencing the 1st set of measurement. In the range area the simulation should be compared with the 2nd set of measurement. One may observe an overestimation of the residual activity in the simulation data.

We observed the discrepancy (of the production of the nuclides in the target) between simulation and experimental data starting from the energy of the primary particles slowed down to 150 MeV/u and/or lower. The biggest difference in the case of ^{7}Be is in the depth corresponding to the primary particle energy of 125 MeV/u (see Figure 1). That is exactly the energy of the change between two Nucleus-Nucleus interaction models in FLUKA code (from Relativistic Quantum Molecular Dynamics for higher energies to Boltzmann Master Equation for lower energies) [5].

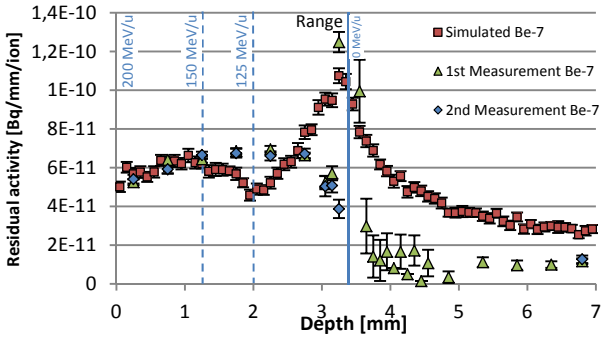

Figure 1: Depth profile of the residual activity of ^{7}Be.

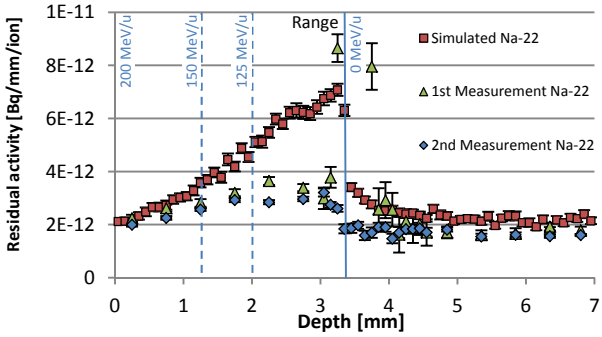

Figure 2: Depth profile of the residual activity of ^{22}Na.

References

[1] I. Strasik at al., Nucl. Instrum. Methods Phys. Res. Sect. B 266 (2008), pp. 3443-3452.
[2] I. Strasik at al., Nucl. Instrum. Methods Phys. Res. Sect. B 268 (2010), pp. 573-580.
[3] V. Chetvertkova at al., Nucl. Instrum. Methods Phys. Res. Sect. B 269 (2011), pp. 1336-1340.
[4] V. Chetvertkova at al., "Activation of Aluminium by Uranium", HB2010, Morschach, Switzerland, 2010, p. 250-253.
[5] A. Ferrari at al., Reports No. CERN-2005-10, INFT/TC_05/11, and SLAC-R-773.

* Work supported by HGS-HIRe.
#p.katrik@gsi.de

Developments of the Palmer pickup tank for stochastic cooling in the CR

D. J. Barker[1], *R. Böhm*[1], *L. Thorndahl*[2], *and C. Dimopoulou*[1]
[1]GSI, Darmstadt, Germany; [2]CERN, Geneva, Switzerland

Introduction

This report details the design and construction progress made on the Palmer pickup tank for the stochastic cooling system of the collector ring (CR) during 2014 at GSI. The CR is designed for the stochastic cooling of antiprotons and RIBs. For details of the complete stochastic cooling system including particle beam parameters see [1]. For the stochastic pre-cooling of RIBs, we use the Palmer method in combination with pickups of large acceptance to cool injected hot ion beams with large momentum spread. For this purpose Faltin type pickups have been designed and published previously [2]. The Faltin rail is a travelling wave pickup in the form of a rectangular coaxial structure with slots in the top which couple to the beam.

Drawing and Construction

Drawing work on the full tank began and finished 2014 as shown in figure 1, although work on the Faltin rails itself continues. To test the pickup designs prototypes were made. During 2014 drawing work on three different prototypes was completed. Construction and procurement of the prototypes was finished in December. The prototypes are shown in figure 2. The robustness of the assembly method was tested. Microwave measurements made on the prototypes which showed good agreement with simulations and are shown in figure 3.

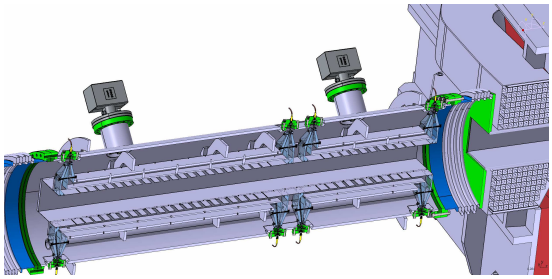

Figure 1: Cross sectional preliminary drawing of the full Palmer pickup tank(2 m installation length).

Simulations

Several unwanted modes which interfere with beam cooling were discovered and simulations with lossy ferrite material were conducted in order to damp these modes. Ferrite or some other lossy material will definitely be necessary within the pickup tank to maintain beam cooling performance. In 2014 a program was written which takes

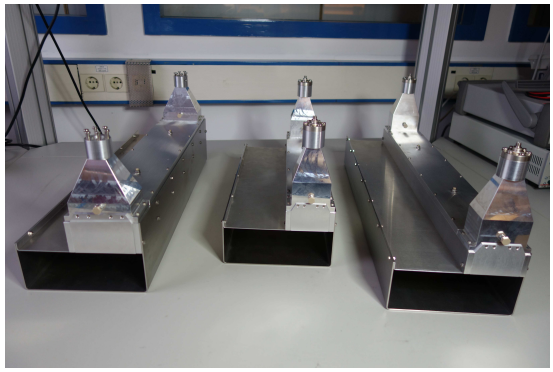

Figure 2: Three Faltin prototypes of one quarter of the pickup.

impedance and phase data of these waveguide pickups and adds signals from several of these pickups using delay lines of specific length to produce a flat impedance and linear phase over a desired band. This process was optimised using a genetic algorithm. This will be used for further optimisation of the pickup.

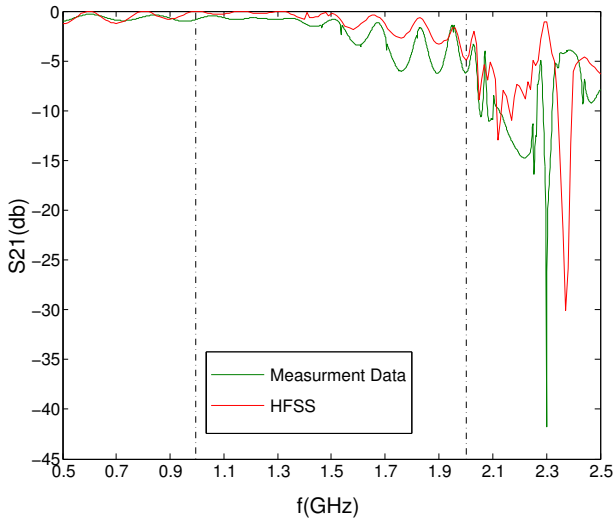

Figure 3: Comparison of measurements of S21 using a network analyser and S21 data from HFSS simulations.

References

[1] CR Technical Design Report 2014 and C.Dimopoulou et al., this report.

[2] D. Barker et al., JACoW Proc. COOL'13, WEPPO21.

DOI:10.15120/GR-2015-1-FG-GENERAL-35

Developments for the CR stochastic cooling system

C. Dimopoulou[1], *D. Barker*[1], *R. Böhm*[1], *M. Bräscher*[1], *M. Dolinska*[2], *R. Hettrich*[1], *M. Kelnhofer*[1], *J. Krieg*[1], *W. Maier*[1], *R. Menges*[1], *C. Peschke*[1], *J. Roßbach*[1], *A. Stuhl*[1], *L. Thorndahl*[3], *and S. Wunderlich*[1]

[1]GSI, Darmstadt, Germany; [2]Frankfurt University; [3]CERN, Geneva, Switzerland

The pertinent CR stochastic cooling system in the frequency bandwidth 1-2 GHz has been reviewed in [1] in the context of the FAIR project. Further progress was made in 2014 on in-house engineering and testing activities as well as procurements.

Metallised ceramic plates for slotline pick-up electrodes are under development in close interaction with a provider.

The water-cooled linear motor drive units, tested synchronously in the prototype pick-up tank (Fig. 1) at room temperature, fulfill the specifications: (i) their max. range of plunging is 70 mm and (ii) at the end, they move back out to their max. aperture within 200 ms, before a new beam is injected.

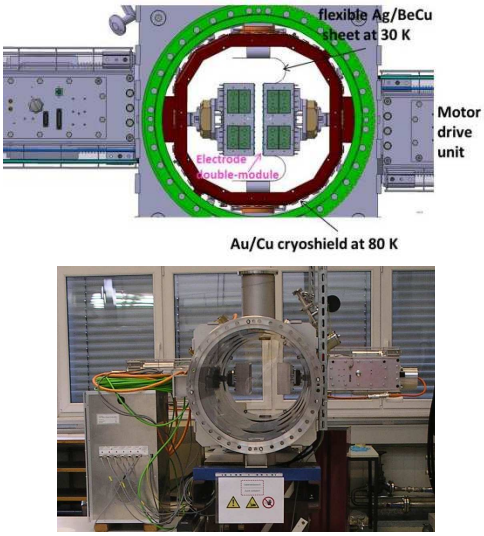

Figure 1: Section of the prototype pick-up tank. The motor units drive synchronously the slotline electrodes.

A special chamber for testing motor drive units under pre-vacuum conditions, at room temperature, was engineered, built and commissioned. It permits long-term tests and improvements of the mechanical concepts in horizontal or vertical orientation in view of the final pick-up tanks. It consists of 1/8 of pick-up tank with Cu-cryoshield dummy and an observation window (Fig. 2). One motor drive unit with electrode module can be mounted so as to slide along the flexible silver-plated copper beryllium sheets.

Simulations with the HFSS code converged to possible designs of the Faltin-type electrodes of the Palmer pick-up. Then, the Palmer cooling performance in the CR with such electrodes has been confirmed in a Fokker-Planck approach. Consequently, demanding prototype electrodes were manufactured, their measured RF poperties confirm the HFSS simulation (see [2] for details).

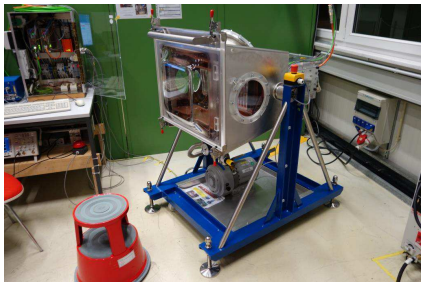

Figure 2: The testing chamber for motor drive units.

The procurement contract for the 1-2 GHz power amplifiers providing a total cw microwave power of 8 kW at the kickers has been awarded. The preseries unit is under development. The 2 optical notch filters (one for antiprotrons at v=0.97 c, one for RIBs at v=0.83 c) are finished (Fig. 3), their measured RF properties fulfill the specification i.e. notch depth below -30 dB within 1-2 GHz. In-house design of demanding RF components such as the pick-up module controller as well as the integrated powermeter has started.

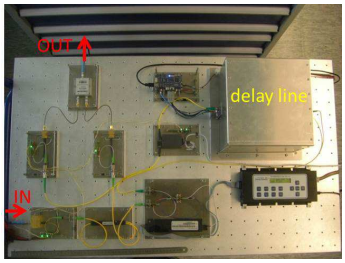

Figure 3: CR optical notch filter layout (0.6 m^2).

The new FAIR-compatible operation program covering the ESR stochastic cooling system has been successfully used with beam in 2014, particularly in demonstrating stochastic cooling of protons at v=0.71 c. This is a major step towards preparing such codes for the CR and gaining benchmarking experience for antiproton cooling in the CR.

A numerical model for simulating stochastic cooling of ions in the time domain is now available, benchmarked against ESR experimental data [3].

References

[1] CR Technical Design Report 2014 and C.Dimopoulou, ICFA Beam Dynamics Newsletter No. 64, p.108 (2014).

[2] D.Barker et al, this report.

[3] M. Dolinska et al., Proc. STORI'14, (in Physica Scripta).

DOI:10.15120/GR-2015-1-FG-GENERAL-36

Fabrication and characterization of Silicon-On-Diamond (SOD) sensors*

S. Sciortino[1,2,#], K. Kanxheri[3,4], S.Lagomarsino[1,2], A. Morozzi[3,4], G. Parrini[1], D. Passeri[3,4], L. Servoli[4], M. Citroni[5], S. Fanetti[5], E. Berdermann[6], C. J. Schmidt[6], M. Kis[6], M. Träger[6], R. Visinka[6]

[1]Department of Physics, Florence, Italy; [2]INFN, Florence, Italy; [3]University of Perugia, Italy; [4]INFN, Perugia, Italy; [5]LENS, Florence, Italy; 6GSI, Darmstadt, Germany;

We report on the preparation and characterization of integrated diamond detectors implementing the Silicon-On-Diamond (SOD) concept [1]. They have been fabricated by thinning (5×5 mm2) CMOS Monolithic Active Pixel Sensors (MAPS) down to 25 μm and bonding them to polycrystalline Chemical Vapour Deposited (pCVD) diamond plates (5×5×0.5 mm3), by a laser technique [2]. This class of devices exploits the capability of the charges generated in the diamond by ionizing radiation to cross the silicon-diamond interface and to be collected by the MAPS photodiodes. We have assessed that the charge induced in diamond by Minimum Ionizing Particles is collected by the MAPS electronics with an efficiency of about 20 %, depending on the quality of the SOD bonding process and on the silicon-diamond interface. The aim is to prepare low-noise, low material budget integrated radiation hard detectors with a new technique of bonding at the atomic level. Two SOD devices have been implemented (SOD-40 and SOD-43) in this study. The adhesion at the silicon-diamond interface turned out to be better for the SOD-43 device due to technical reasons discussed in [3]. First the CMOS MAPS have been calibrated with monochromatic X-rays, then the device have been tested with charged particles (electrons) either with and without biasing the diamond substrate, to compare the amount of signal collected, We analysed for both SOD prototypes a matrix of 32x32 small photodiode (2x2 μm^2) pixel. The two SOD devices response to X-rays fluorescence has been studied and the calibration relations are very similar. The two calibration factors for the 32x32 small photodiode pixel matrices are: 10.12 ± 0.31 ADC/keV for SOD-40 and 10.43 ± 0.30 ADC/keV for SOD-43. SOD-40 was tested with a ^{90}Sr/Y electron source while SOD-43 was exposed to an electron beam at Beam Test Facility of Frascati, Italy, with beam energy of 345 MeV. The signal collected by the MAPS will have always the component due to the ionization in the silicon layer, while the component due to the diamond should appear only when it is polarized. The carriers created into diamond drift along the applied field toward the silicon-diamond interface and diffuse in the silicon material to be collected by the MAPS. We found that the collected charge remains spatially localized, i.e., almost all the collected charge is inside the 5x5 matrix, centered around the pixel with the maximum signal. By increasing the cluster size we do not add other contributions to the total signal. To evaluate the maximum allowable diamond contribution to the signal we assume that there is no loss in crossing the interface. From a previous work [4] we derive that only a 37% of the charges located at the interface, i.e. at a 25 μm depth in the silicon, will be collected by the MAPS. Assuming a Most Probable Signal (MPS) in the range 7000-8000 e, at 500 V, for the diamond material used for our devices, the maximum signal to be expected from our MAPS is in the interval 2600-3000 e. Figure 1 shows a difference in ADC counts of about 20 for both devices when they are polarized. This amounts to about 540 e injected by diamond, i.e., an efficiency of about 20 % in crossing the silicon-diamond bonding interface. We note that the response due to diamond has an offset voltage of about 250 V which most likely depends on the defective interface. The signal of SOD-43 is higher at 400 V than that of SOD-40. This is tentatively ascribed to the better adhesion between silicon and diamond verified a posteriori in SOD-43, by optical microscopy. We could not verify this hypothesis at higher voltages, due to a high superficial current drawn by the silicon layer.

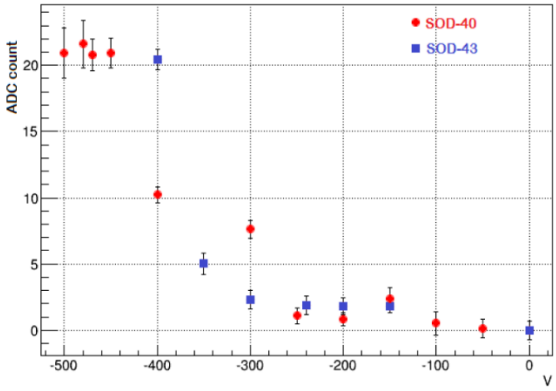

Figure 1: Bias scan for both fully polarized SOD-40 (circles) and not fully polarized SOD-43 in (squares).

References

[1] S. Lagomarsino et al., New perspectives for the Silicon-On-Diamond material, PoS(RD09)029

[2] S Lagomarsino et al., Silicon-on-diamond material by pulsed laser technique, Applied Phys. Lett. 96 (2010) 031901

[3] K. Kanxheri et al., First result on biased CMOS MAPs-on-diamond devices, Nucl. Instr. Meth. A, in press, corrected proofs, 10.1016/j.nima.2015.02.054

[4] S. Meroli, et al. Measurement of charge collection efficiency profiles of CMOS active pixel sensors. Journ. Of Instr. (2012) 07 P09011

* Work supported by EU (HadronPhysics3 project No. 283286) and GSI (Detector Technology and Systems Platform) and INFN Italy (experiment 3D_SOD)

#silvio.sciortino@unifi.it

DOI:10.15120/GR-2015-1-FG-GENERAL-37

Fabrication and characterization of efficiency and radiation tolerance of 3D diamond detectors*

S. Sciortino[1,2,#], S.Lagomarsino[1,2], M. Bellini[3], C. Corsi[1,4], V. Cindro[5], K. Kanxheri[6,7], A. Morozzi[6,7], D. Passeri[6,7], L. Servoli[7], E. Berdermann[8], C. J. Schmidt[8], M. Kis[8], M. Träger[8], R. Visinka[8], M. Schreck[9], S. Gsell[9], M. Fischer[9]

[1]Department of Physics, Florence, Italy; [2] INFN, Florence, Italy; [3]INO-CNR Florence, Italy; [4]LENS, Florence, Italy; [5]Jožef Stefan Institute, Ljubljana, Slovenia; [6]University of Perugia, Italy; [7]INFN, Perugia, Italy; [8]GSI, Darmstadt, Germany; [9]University of Augsburg, Germany;

3D diamond detectors combine the intrinsic properties of radiation tolerance of diamond with the advantages of the 3D architecture: a shorter inter-electrode distance and, consequently, lower trapping probability and operating voltage bias. 3D diamond electrodes can be fabricated by laser irradiation [1]. Femtosecond laser irradiation is required, because with longer laser widths, at least in the nanosecond range, a more defective modified material is obtained [2]. We have previously reported [1] on 3D monocrystalline Chemical Vapour Deposited (scCVD) diamond detectors, which exhibited a full collection to beta Minimum Ionizing Particles (MIP) at a voltage bias of a few volts, i.e., one order of magnitude lower than the bias level required for a two 2D sensor prepared with the same material. Since scCVD diamond are presently only obtained in very small areas, usually less than 1 cm^2, we decided to investigate the performances of 3D detectors fabricated on polycrystalline (pCVD) diamond, before and after neutron irradiation up to the highest fluence ever reported for diamond. From our results 3D diamond detectors seem the most radiation-hard detectors available at present. Heteroepitaxial growth of Diamond On Iridium (DOI) seems a very promising technique to obtain a high quality material, more homogeneous in its electronic properties than the pCVD one and not limited in surface area. A 3D sensor implemented on DOI material has also been tested and reported in this work.

Sample preparation ant tests

3D radiation sensors have been implemented on four pCVD samples (5×5×0.5 mm^3) by laser irradiation. Bulk electrodes were fabricated with an 800 nm Ti:Sa 30 fs laser with an energy density of 12 J/cm^2. The columns were started from one of the 5×5 mm2 faces and terminated about 80 μm away from the opposite one. They were connected by graphitic combs written on the surfaces with a Nd:YAG ns laser (schematics in Fig. 1). Two 3D sensors and a 2D reference sensor have been fabricated in each of the four sample as shown in Figure 1. The 3D electrodes are patterned by repeating two elementary cells of sizes 100×160 μm^2 (3D$_{100\times160}$ sensors) or 70×114 μm^2 (3D$_{70\times114}$ sensors). The CCE has been measured by means of a ^{90}Sr beta source, producing 18000 electron-hole pairs per MIP in the sample. The saturation collected charge was evaluated as 8700±300, 7200±300, and 7100±200 for the 3D$_{70x114}$, the 3D$_{100x160}$ and the 2D sensor, respectively.

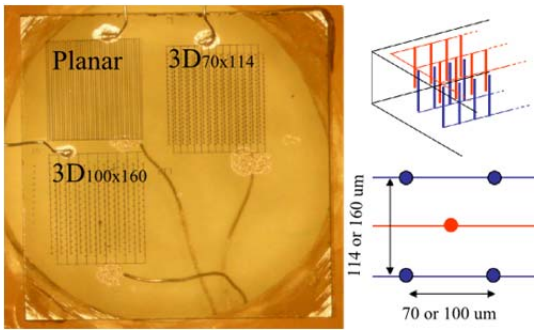

Figure 1: One pCVD sample with the 2D reference sensors and the two 3D sensors. On the right: the unit cell.

The 90% of these values were reached at 45 V, 60 V and 450 V, respectively. Hence, we assessed also for pCVD diamond, that the required bias voltage is an order of magnitude lower for the 3D than for the 2D sensors. The maximum signal for the 3D$_{100x160}$ and the 2D sensor have about the same value, but the 3D$_{70x114}$ sensors yield a collection efficiency about 20% higher. The CCE vs. voltage bias has been fitted by use of the following expression for the mean free path of the carriers:

$$\frac{1}{\lambda} = \frac{1}{\lambda_g} + \frac{1}{v\tau} \qquad (1)$$

where τ is the lifetime of the carriers, limited by the intra-grain defects, *v* is the drift velocity, which depends on the applied electric field (the bias voltage), λ_g is a mean path limited by the grain boundaries. The parameter values resulting from the fit of the 2D sensors data are τ = 4.3 ns and λ_g =160 μm. We assumed the same value of τ for the 3D sensors and evaluated numerical the CCE, by means of a three-dimensional finite element simulation of the electric field. The resulting values for λ_g were 29 and 25 μm for 3D$_{100x160}$ and 3D$_{70x114}$, respectively. The above values correlate well with the structure of the grains of the samples, which exhibit a truncated cone shape along the

* Work supported by EU (HadronPhysics3 project No. 283286) and GSI (Detector Technology and Systems Platform) and INFN Italy (experiment 3D_SOD)
#silvio.sciortino@unifi.it

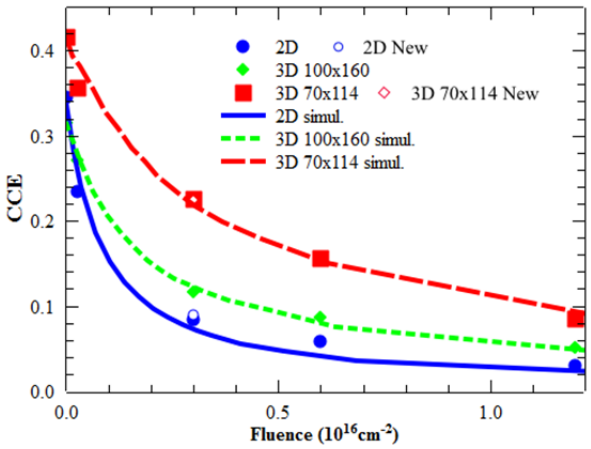

Figure 2: CCE vs, neutron irradiation fluence, 1 MeV equivalent.

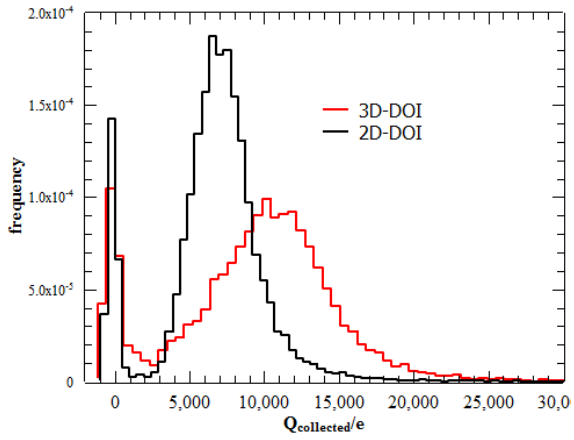

Figure 3: Pulse height spectrum of DOI 2D (at 600 V) and 3D (at 140 V) sensors.

diamond thickness, as evidenced by a morphological analysis carried out by optical profilometry. In the case of the 2D sensors the carriers drift almost parallel to the grain boundaries while in the case of 3D sensors they are strongly limited by the polycrystalline material in their path between the columnar electrodes.

Radiation Tolerance of the 3D sensors

We irradiated the four diamond samples at the experimental nuclear reactor of the Jožef Stefan Institute of Ljubljana, with fast neutron (neutrons of energy greater than 100 keV) at fluences ranging from 2.2×10^{14} cm^{-2} to 10^{16} cm^{-2}. Figure 2 shows the variation of the CCE with the equivalent fluence of 1 MeV neutrons, for the 2D and the 3D sensors. In order to prove that the all-carbon electrodes are not degraded by the neutron irradiation, we have also fabricated a new 2D sensor and new 3D $3D_{70x114}$ sensor, on the sample irradiated at 3×10^{15} cm^{-2} 1MeV-eq. neutrons. These new sensors exhibited the same response as the older ones after irradiation (see Fig. 2). The results from the planar sensors allow the immediate evaluation of the hardness factor *K* of the material, defined by the following relation:

$$\frac{1}{CCE} = \frac{1}{CCE_0} + KL\phi \qquad (2)$$

where ϕ is the fluence and L = 500 μm the thickness of the material. The result, K= (4.7±0.2) 10^{-18} μm^{-1} cm^2, is in good agreement with that previously reported in [3]. The data represented in Fig. 2 have been fitted by use of a modification of expression (1):

$$\frac{1}{\lambda} = \frac{1}{\lambda_g} + \frac{1}{v}\left(\frac{1}{\tau} + k\phi\right) \qquad (3)$$

A k value of about 1.5 10^{-6} cm^2 Hz can be used to fit consistently the three curves. The factor 3 in efficiency gained by the irradiated 3D detectors with the smaller pitch can be explained by the assumption that neutron damage results in the introduction of new intra-bandgap levels reducing the bulk mean lifetime of the charge carriers in the conduction and in the valence band, leaving unaffected the grain boundaries-limited mean free path λ_g.

Diamond On Iridium 3D sensors

A 3D sensor of the type $3D_{70\times114}$ has been implemented on a DOI plate together with a reference planar 2D sensor. The sample is about 500 μm thick, hence the overall generated charge from a MIP beta source is 18000 electrons. The collected charge was 7600 *e* corresponding to a CCE=42% for the 2D sensor at a bias voltage of 600 V. The 3D sensor yielded a mean value of 11000 *e*, corresponding to a CCE of 61%, at a bias voltage of 140 V. The relative gain from 2D to 3D is quite high. Figure 3 shows the pulse high spectrum for the two sensors at maximum collection. The DOI sample exhibits relevant pumping effect and polarization. The above results correspond to the pumped state (>100 Gy beta-irradiation). The 2D signal before pumping was 4000 *e* (21 % CCE). The study of the radiation tolerance of these sensors is under way.

References

[1] S. Lagomarsino et al., Diamond Relat. Mater. 43 (2014) 23.
[2] S. Lagomarsino et al., Appl. Phys. Lett. 103 (2013) 233507.
[3] G. Kramberger, Radiation damage in diamond detectors, September 2012, Vertex 2012, Jeju, Korea

DOI:10.15120/GR-2015-1-FG-GENERAL-38

Imaging of dislocation bundles by micro-Raman line width mapping to assess the structural quality of heteroepitaxial diamond for detector applications*

M. Mayr[1], M. Fischer[1], S. Gsell[1], C. Stehl[1], M. Schreck[1#], and E. Berdermann[2] for the ADAMAS collaboration

[1]Universität Augsburg, Augsburg, Germany; [2]GSI, Darmstadt, Germany

Within the ADAMAS collaboration, the role of the diamond group at the University of Augsburg is to develop and manufacture large-area high-quality single crystal diamond suitable for the construction of detectors for heavy ions and minimum ionising particles. In contrast to current samples grown by homoepitaxy on substrates with maximum lateral dimensions of ~10 mm, the heteroepitaxial deposition is done on the Ir/YSZ/Si(001) multilayer system that is available in 100 mm wafer size. As a consequence, these samples that are often known as "Diamond on Iridium" (DoI) offer a realistic chance for a scaling to large areas as required for tracking applications.

Major challenges, however, are the occurrence of polarization effects and an incomplete charge collection with charge collection efficiencies (CCE) varying from sample to sample. These effects are mainly attributed to properties of the bulk, namely lattice defects like dislocations and point defects, generating both deep and shallow charge carrier traps. Being able to control and further reduce the density of these defects is compulsory for future application of DoI material not only in particle physics.

Imaging and quantification of dislocations

A controlled optimization of material synthesis requires efficient concepts for a visualization and quantitative evaluation of threading dislocations. A standard technique for the assessment of dislocation densities uses preferential etching with subsequent counting of the etch-pits. Furthermore, inside the bulk dislocations create inhomogeneous strain fields which broaden XRD- and Raman line profiles. We recently revealed that the density of dislocations as derived from etching experiments shows a characteristic correlation with film thickness [1] and with the width of the diamond Raman line (see Fig. 1).

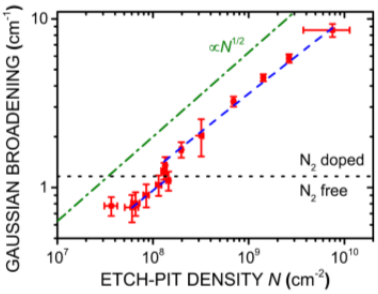

Figure 1: Broadening of the Raman peak vs. etch-pit density. The continuous variation of the dislocation density was achieved by growth of a thick film. The blue fit curve uses the relationship given by Eq. (1). The displaced green curve describes a simple $\sqrt{N}$ behaviour. [1]

* Work supported by EU (HadronPhysics3 project No. 283286) and GSI (Platform for Detectors and Systems).

#matthias.schreck@physik.uni-augsburg.de

The relationship between the mean square strain and the dislocation density N (in cm^{-2}) is described by (1):

$$\overline{\varepsilon_N^2} \propto N \cdot ln\frac{10^7}{2 \cdot \sqrt{N}} \qquad (1)$$

Using this approach, it is possible to image the spatial distribution of dislocations by mapping the Raman line width. The stripe pattern in the cross section map (see Fig. 2) is interpreted in terms of bundles of threading dislocations which are tilted away from the surface normal by several degrees. Tilting is attributed to lateral step flow during growth on off-axis substrates [2]. Understanding the interaction between dislocations and surface features is important for a further reduction of defect densities.

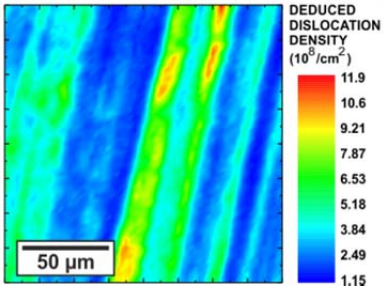

Figure 2: Cross-sectional dislocation density map of a DoI sample grown with 100 ppm N_2 on a (001) substrate with [100] off-axis direction, as derived from high-resolution Raman-line width measurements using the calibration curve in Fig. 1.

DoI: state of the art

In the meantime, continuous improvement in heteroepitaxial diamond growth and post-processing (lapping, polishing) has yielded DoI samples with lateral dimensions up to 2 x 2 cm^2 (see Fig. 3) and thin membranes down a thickness of 80 µm. For further thinning and also removing of polishing defects, reactive ion etching (RIE) was successfully applied.

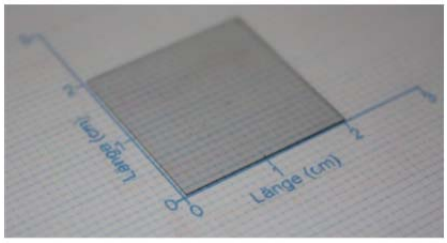

Figure 3: 2 x 2 cm^2 DoI sample supplied to GSI for measurements of the detector properties.

References

[1] C. Stehl et al., Appl. Phys. Lett. **103**, 2013.
[2] M. Mayr et al., Phys. Status Solidi A **211**, 2014 .

DOI:10.15120/GR-2015-1-FG-GENERAL-39

Project status of the new setting generation system for GSI and FAIR

D. Ondreka, I. Kraus, H. Liebermann, and B. R. Schlei
GSI, Darmstadt, Germany

The progress made on the new setting generation system for FAIR and GSI regarding machine modeling and application development is reported.

In 2014, the main activities were related to benchmarking tests of the SIS18 machine model and support for other technical groups during machine experiments. In this context, the new settings generation system proved extremely useful. In fact, it was essential for the realization of several machine development studies, which required operation schemes impossible to achieve with the present settings generation software SISMODI. In particular, the following machine experiments depended on the use of the new settings generation system: (i) Commissioning of the first module of the new MA cavity with beam and (ii) bunch merging studies using different merging times and amplitudes (both conducted by PBRF); (iii) multi-turn injection studies using a variable angle of the orbit bump at the electrostatic septum and (iv) resonance compensation studies employing a tune ramp with captured beam on the injection or extraction plateau (latter two conducted by PBBP). In all cases, the settings generation system excelled in providing control over the machine as requested by the respective experimentators. Below, a detailed report is given about the bunch merging and resonance compensation experiments.

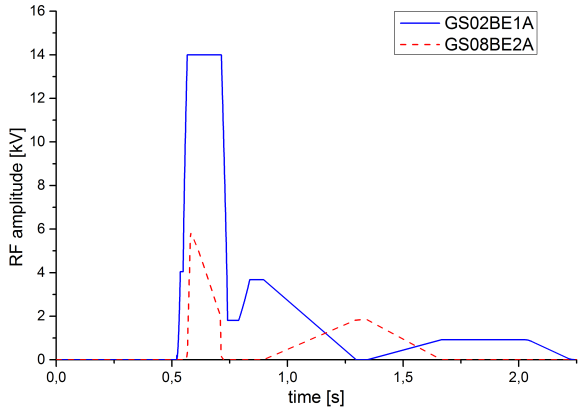

Figure 1: RF amplitudes of the two ferrite cavities in SIS18 for a cycle with two merging steps ($4 \rightarrow 2 \rightarrow 1$).

Because the cavities can be switched on and of sequentially with the new settings generation system, it is possible to combine ramping at full speed and bunch merging (see figure 1). Thus, at the end of the ramp one cavity is always available for the first bunch merging step. Also, the merging times are freely adjustable. This flexibility was extensively used to allow the RF department to test the performance of the bunch merging procedure as a function of the merging times.

The new system was also very helpful for resonance compensation measurements. Using the generic Java interface to the settings, it was possible to perform semi-automated parameter scans of tune and sextupole strengths. Up to 100 settings per hour were established. For each setting, the beam current was read out and saved for analysis. Figure 2 shows some of the recorded current readings, each curve corresponding to a different sextupole setting for a fixed tune. The current drop is a measure for the degree of compensation of the resonance.

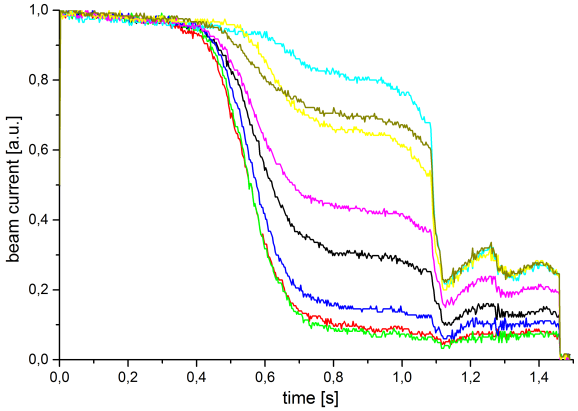

Figure 2: Beam current for different degrees of resonance compensation through variation of the sextupole strengths.

Besides the extensive support of the machine experiments, several development activities were pursued. Especially the work on the machine model for the CRYRING was continued with the main focus on the injector. Particular emphasis was put on modeling the RFQ structure, serving as a prototype for a generic cavity in linear accelerators.

Regarding applications, the development of the LSA version of the ion optics code MIRKO was continued. A satisfactory integration into the control system development environment was established. Concerning the steering and orbit correction program YASP, a collaboration with CERN was established to realize the integration into the FAIR control system.

References

[1] G. Franchetti et al., “Recent development in mitigation of long term beam loss”, HB2014.

DOI:10.15120/GR-2015-1-FG-GENERAL-40

Status of the CS framework and its successor CS++

H. Brand, D. Neidherr
GSI, Darmstadt, Germany

The *CS* framework is a LabVIEW based framework for developing event driven, multi-threaded control systems using an artificial object oriented approach. *CS* was upgraded to version 3.4 based on LabVIEW 2014. Upgrade experience is summarized.

CS++ **will become the successor of *CS* and is based on NI's Actor Framework which is using the native object oriented programming approach consequently following the data-flow paradigm.**

Motivation

The *CS* framework is in use since a couple of years at about 15 experiments at 10 institutes. A detailed description of *CS* is given in [1]. This text aims at describing the enhancements by the most recent version 3.4 and upgrade experience to LabVIEW 2014.

CS framework is using an artificial approach to object oriented programming in LabVIEW. Many features rely on convention and cannot be enforced since the support of the development environment is missing. Therefore we are working on its successor **CS++,** based on NI's Actor Framework [2], to be used for FAIR experiment control systems. The Actor Framework provides some simple base classes for active objects (threads) and well defined communication mechanism. The AF implements a much simpler design than the HGF Class Library [3], so it is much easier for newcomers to learn. In addition we can profit from NI support and community developments, so that for example the migration of the core components within the **CS++** is already done by NI.

Status of CS framework

Last year the *CS* framework had its 10 year anniversary. Since 2004 the core of the framework has been migrated to the most recent LabVIEW versions every three to four years. For the developers of experiment specific *CS* classes this normally means upgrading to the new LabVIEW version. They just have to copy the new core system and recompile their executables. The *CS* upgrade to 3.4 need more work.

For an unknown reason NI changed the way references are compared with each other. This leads not only to important changes in the core system of the *CS* but also to changes in the source code of each class. For this reason we wrote a tool using *VI-Scripting* methods to modify parts of the class specific source code automatically.

NI found a security issue which they closed in newer LabVIEW versions. For the *CS* this leads to several small changes for example in the way how an executable has to be built.

HITRAP @ GSI as well as ISOLTRAP @ CERN and LEBIT @ MSU migrated their systems to *CS* 3.3 (LV 2012). The PHELIX experiment @ GSI has already migrated to *CS* 3.4 (LV 2014). The step from *CS* 3.3 to 3.4 is marginal.

Status CS++

CS++ follows the recommendations of the Actor Framework. It provides base classes of common interest for objects to be used as entities, *CS++Base.lvclass*, and derived actor classes *CS++BaseActor.lvclass*.

- *CS++MessageLogger* client for DSC and Syslog
- *PVConnection* and *PVMonitor* for Shared Variables or DIM communication.
- *CS++DeviceActor* and *CS++DeviceGUI* e.g. CS++DCPwr, CS++DMM, CS++Fgen, CS++Osci, etc. Concrete implementation classes wrapping the IVI-Driver are already available.
- *CS++Factory* provides the methods to create initialized objects of such classes at runtime reading initialization data from configuration file.
- *CS++Reference* can be used to maintain object references respecting data-flow.
- More passive data classes are available providing new datatypes such as PV- or Alarm&Event data.
- *CS++DSCAlarmViewer* and *CS++DSCTrendViewer* connecting to the historical DSC database.

Status & outlook

The *CS* framework 3.4 is stable and in good shape. It will be maintained in future since many experiments rely on it and it cannot be easily replaced.

The **CS++** class libraries are still under development, but already available under the terms of the European Union Public Licence (EUPL) on Github [4]. Some simple demo applications to illustrate the usage and extension of the base classes are available. **CS++** will become the base for the serial test-stand sequencer for the SIS-100 dipole magnets. **CS++** applications can easily connect to *CS* Framework applications using DIM [5].

References

[1] D. Beck et al., Nucl. Instr. Meth. A 527 (2004) 567-579, http://wiki.gsi.de/cgi-bin/view/CSframework,
[2] https://decibel.ni.com/content/groups/actor-framework-2011?view=overview
[3] F.Berck "Prototyp für ein mobiles Agentensystem in NI LabVIEW", Hochschule Darmstadt University of Applied Science, FB EIT, 2010
[4] https://github.com/HB-GSI/CSPP
[5] http://www.cern.ch/dim

DOI:10.15120/GR-2015-1-FG-GENERAL-41

GPU Programming - Speeding Up the 3D Surface Generator VESTA

*B. R. Schlei**
GSI, Darmstadt, Germany

Abstract

The novel "Volume-Enclosing Surface exTraction Algorith" (VESTA) generates triangular isosurfaces from computed tomography volumetric images and/or three-dimensional (3D) simulation data. Here, we present various benchmarks for GPU-based code implementations of both VESTA and the current state-of-the-art Marching Cubes Algorithm (MCA). One major result of this study is that VESTA runs significantly faster than the MCA.

Introduction

NVIDIAs toolkits (*cf., e.g.,* Ref. [1]) for the development of CUDA®-based software contain, among many other things, example code for an extended version [2] of the original MCA [3]. Here, we compare the performance of this code with our CUDA®- and ANSI-C-based implementation of VESTA [4] on a Linux-based (*i.e.,* openSUSE 13.1) PC with a GeForce GTX 750 Ti graphics card.

In particular, the times that we have measured (*cf.,* Table 1) are averages over 1000 runs each. The measurements start after the data sets have been loaded into texture memory, and they stop after all point coordinates and triplets of point IDs (*i.e.,* triangles) have been computed on the GPU.

Technique	Extended MCA	Marching VESTA	
Mode	**DCED / L**	**DCED / L**	**Mixed / H**
(a) Points	19,218	12,814	15,292
Triangles	6406	6406	11,362
Time (ms)	**1.43(5)**	**1.28(5)**	1.37(4)
(b) Points	6,128,724	4,085,840	4,852,644
Triangles	2,042,908	2,042,908	3,576,516
Time (ms)	**98.5(1)**	**71.3(1)**	75.9(4)
(c) Points	5,566,998	3,699,086	4,346,120
Triangles	1,855,666	1,855,666	3,147,604
Time (ms)	**23.0(1)**	**18.7(1)**	22.4(1)
(d) Points	33,240	22,208	25,894
Triangles	11,080	11,080	18,350
Time (ms)	**0.82(4)**	**0.63(4)**	0.74(4)
(e) Points	13,859,304	9,267,824	11,178,649
Triangles	4,619,768	4,619,768	8,441,610
Time (ms)	**111.2(1)**	**84.4(1)**	94.6(6)

Table 1: Benchmarks for various processed tomographic data sets: for (a) – (c), *cf.,* Ref. [4] and Ref.s therein, (d) Bucky.raw data is a portion of [1], and (e) Happy Buddha VRI file [5]. For the selected isovalues, *cf.,* Fig. 1.

* b.schlei@gsi.de

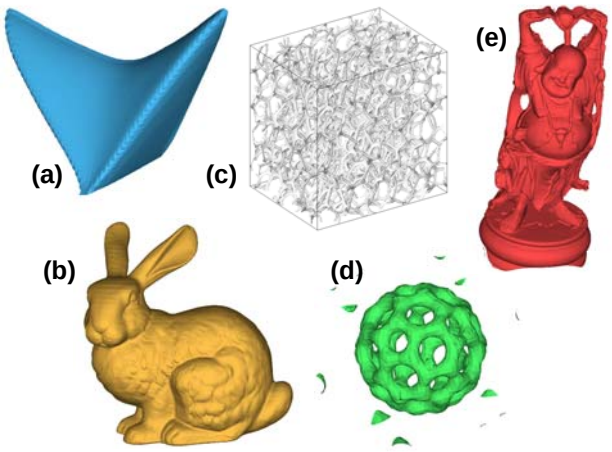

Figure 1: VESTA high resolution "mixed" mode (Mixed/H) isosurface renderings, where the isovalues are equal to (a) 139, (b) 150, (c) 135, (d) 128, and (e) 150, respectively.

Results

For the here considered data sets [1, 4, 5], the extended MCA is about (a) 12%, (b) 38%, (c) 23%, (d) 30%, and (e) 32%, *slower* than the marching variant of VESTA [4], when the latter is executed in its low resolution "disconnect" mode (DCED/L). Furthermore, VESTA is also faster even if higher resolution isosurfaces are computed (*cf.,* Fig. 1), which have about twice the number of triangles (*cf.,* Table 1).

Note that the current code implementation of VESTA does *not* yet use parallel streaming, *nor* it does call device kernels from within kernels. As a consequence, further GPU-based code optimisations may result in an even faster VESTA code.

References

[1] NVIDIA® CUDA® Toolkit 6.5; for more detail, *cf.,* https://developer.nvidia.com/cuda-toolkit/

[2] P. Bourke, "Polygonising a scalar field", May 1994; for more detail, *cf.,* http://paulbourke.net/geometry/polygonise/

[3] W. E. Lorenzen and H. E. Cline, "Marching Cubes: A High Resolution 3D Surface Construction Algorithm", Comput. Graph. 21 (1987), p. 163.

[4] B. R. Schlei, "Volume-Enclosing Surface Extraction", Computers & Graphics 36 (2012) p. 111, doi: 10.1016/j.cag.2011.12.008.

[5] http://graphics.stanford.edu/software/volfill/

DOI:10.15120/GR-2015-1-FG-GENERAL-42

CUPID: new system for scintillating screens based diagnostics

B. Walasek-Höhne[1], D. Acker[1], C. Andre[1], M. Bevcic[1], H. Bräuning[1], A. Bräuning-Demian[1], T. Brühne[1], E. Dierssen[1], C. Dorn[1], R. Fischer[1], H. Graf[1], F. Hagenbuck[1], M. Hartung[1], R. Haseitl[1], T. Hoffmann[1], K. Höhne[2], C. Kleffner[1], R. Lonsing[1], T. Milosic[1], I. Pschorn[1], A. Petit[1], A. Reiter[1], H. Rödl[1], U. Scheeler[3], C. Schmidt[1], M. Schwickert[1], K. Steiner[1], C. Wetzel[1], J. Wiessmann[1], J. Wohlers[1], D. Varentsov[1], and R. Vincelli[1]

[1]GSI, Darmstadt, Germany; [2]FAIR, Darmstadt, Germany; [3]MIT, Marburg, Germany

The Facility for Antiproton and Ion Research (FAIR) with its wide range of beam parameters poses new challenges for standard beam instrumentation like precise beam imaging. To cover a wide range of foreseen applications, a new technical solution was required for diagnostics upgrades for the PRIOR Experiment, CRYRING and between the Experimental Storage Ring (ESR) and Cave A as a precursor to the FAIR High Energy Beam Transport lines.

The new system (see Figure 1), including digital image acquisition, remote controllable optical system and mechanical design, was set up and commissioned during 2014 beam time. CUPID (Control Unit for Profile and Image Data) is based on the Front-End Software Architecture (FESA) to control beam diagnostic devices.

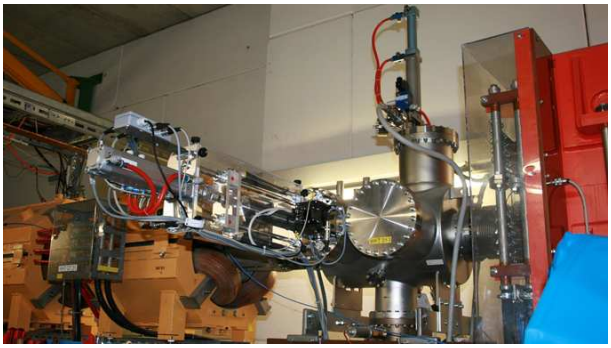

Figure 1: Scintillating Screen installation at High Energy Beam Transport Lines.

The FESA class for the digital GigE camera (IDS uEye UI-5240SE-M, CMOS type) acquires the images and preprocesses the optical data as required by the geometry of the setup (rotation, stretching). It calculates the projections and the intensity histogram and converts pixel number into a position in millimeters, which results in absolute beam position and width. The performance of the system reached more than 15 frames per second with one connected client.

Additionally, dedicated FESA classes access industrial Programmable Logic Controllers (PLCs) for a reliable slow control solution. A Siemens PLC (main unit and satellites) handles control of lens focus and iris motors (LINOS MeVis-Cm 16), read and set by a PID controller (FM355C). PLC digital outputs (SM322) switch the LED to illuminate the target for calibration issues. Camera control and timing, as well as, power supply and reset options for up to eight digital cameras are realized by the in-house developed Camera Power Supply controller CPS8 with network access.

For basic operation the camera controls are reduced to changing the opening of the iris and switching on or off the LED. An expert mode provides more detailed control like changing the exposure time or the binning of the image for low beam intensities. The CUPID system provides three acquisition modes. In the 'free run' mode suitable for slow beam extraction, the camera continuously acquires images with the specified exposure time and frame rate. The acquired images are displayed in the GUI as they arrive in real time. In the 'triggered' mode for fast extraction, the image acquisition is triggered by a machine event of the accelerator. At the time of the trigger, a single image is acquired by the FESA class and displayed by the GUI (see Figure 2). An extension of the 'triggered' mode is the 'sequence' mode, which acquires a predefined number of images with the specified frame rate after a trigger is received.

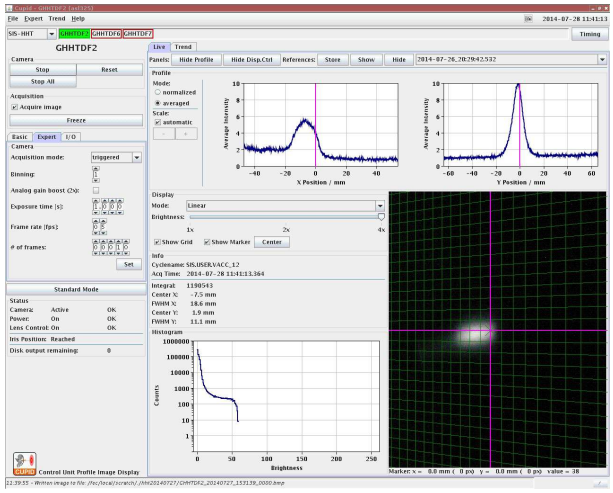

Figure 2: CUPID GUI with an image of 7×10^9 protons at 4 GeV on Chromox screen.

The CUPID system is currently running successfully at 16 different points in the GSI high energy beam transport lines. In daily operation it was used to image several beams from protons up to uranium with various beam energies and intensities. The generally positive feedback by the operating team highlights the simple usage of the GUI and the advanced features of the new system. The work experience gathered so far, confirms CUPID as a standard for scintillating screen based beam instrumentation at GSI and FAIR.

DOI:10.15120/GR-2015-1-FG-GENERAL-43

Optical spectra from Beam Induced Fluorescence (BIF) profile monitor*

Y. Shutko[1#], D.H.H. Hoffmann[1], P. Forck[2,3], P. Boutachkov[2], R. Haseitl[2], T. Sieber[2], B. Walasek-Höhne[2], V. Lavrik[3], S. Udrea[3], J. Wieser[4], A. Ulrich[4]

[1]TUD, Darmstadt, Germany, [2]GSI, Darmstadt, Germany; [3]Goethe-Universität, Frankfurt am Main, Germany,[4]TUM, München, Germany.

The development of non-interceptive beam diagnostics methods is of high relevance for the future FAIR accelerator facilities. One of these methods is based on Beam Induced Fluorescence (BIF), based on photons detection emitted by residual gas molecules, e.g. Nitrogen, excited and ionized by the ion beam. Such monitors are already in operation at GSI's LINAC since a few years [1]. However, further BIF-monitor developments are required for applying this method to high energy beams, as those to be delivered by FAIR's SIS100 synchrotron.

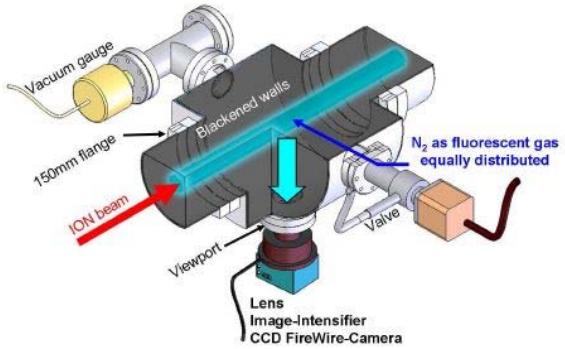

Figure 1: Typical set-up of a BIF profile monitor [2].

For this purpose beam profile and spectroscopic investigations have been performed with different gases in the pressure range from $1 \cdot 10^{-3}$ to 2 mbar. Heavy ion beams at energies between 100 and 900 MeV/u for slow and fast extraction mode could be used.

A typical experimental set-up is shown in Figure 1. The gas chamber is mounted on the beam line and has blackened inner walls to avoid light reflections. The chamber can be filled by different gases through a needle valve regulated by a vacuum gauge. Single photons emitted by the excited gas molecules are detected by image intensified cameras, either by an ICCD equipped with MCPs in Chevron geometry (Proxivison) or an emCCD (Princeton Instruments ProEM+:512B).

During the experiments performed in 2014 three different set-ups have been used: beam transverse profile set-up with the ICCD camera, beam transverse profile set-up with the emCCD camera and spectroscopy set-up with a CP140-202 spectrograph coupled to the ICCD camera. The grating of the spectrograph operates in the 190-800 nm wavelength range with 50 nm/mm dispersion. The ICCD camera has at least 40% of its peak sensitivity in the 200 to 600 nm wavelength range. To increase the light throughput of the system, the spectrometer's entrance slit has been set to 400 µm which resulted in a spectral resolution of about 12 nm.

As shown in Figure 2, in the case of nitrogen the measurements reveal no significant differences between the slow and fast extraction mode. Moreover, the spectra are consistent with previous results obtained at low ion energies [3].

The measured spectra obtained with Argon at pressures between 0.1 and 1 mbar showed different spectral compositions for the slow and fast extraction mode. This is shown in Figure 3 for measurements performed at 0.4±0.1 mbar N_2 equivalent. The additional, strong emission at 285 and 310 nm, significant only in the case of slow extraction, may be attributed to OH radicals excited by Ar* atoms [4].

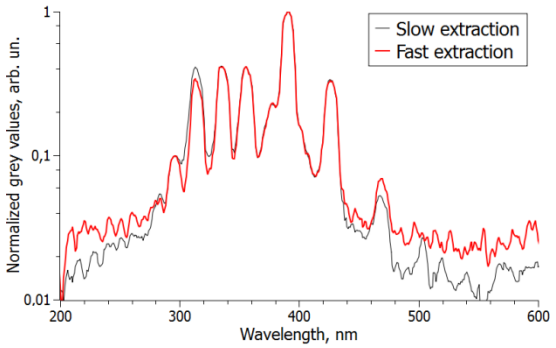

Figure 2: Nitrogen spectra for slow and fast extraction at 0.45±0.02 mbar, U^{73+} 300MeV/u beam.

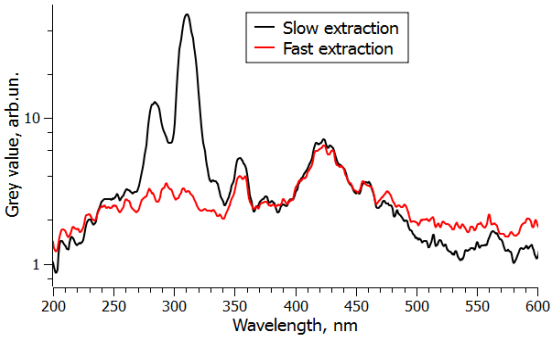

Figure 3: Argon spectra for slow and fast extraction at 0.4±0.1 mbar N_2 equivalent, U^{73+} 300MeV/u beam.

References

[1] C.A. Andre, et al, DIPAC2011 proc., p.185
[2] P. Forck et al, HB2010 proc., p. 497
[3] F. Becker, et al, IPAC2012 proc., p. 798
[4] A. Morozov, et al, Appl. Phys. Lett., **86**, 011502, (2005)

* Work supported by BMBF project No. 05P12RDRBN and Graduate School of Excellence ESE TU- Darmstadt.
#y.shutko@gsi.de

DOI:10.15120/GR-2015-1-FG-GENERAL-44

Beam induced fluorescence monitor development: Comparison of image intensified CCD and electron multiplying CCD cameras*

Y. Shutko[1#], D.H.H. Hoffmann[1], P. Forck[2,3] , T. Sieber[2], S. Udrea[3], V. Lavrik[3]
[1]TUD, Darmstadt, Germany, [2]GSI, Darmstadt, Germany; [3]Goethe-Universität, Frankfurt am Main, Germany.

Beam Induced Fluorescence (BIF) monitors offer the possibility for non-interceptive beam profile diagnostics and are therefore highly relevant for the future FAIR facility. Several BIF monitors are already in operation at the UNILAC accelerator [1] and are based on Image Intensified CCD (ICCD) cameras. However, recent technological developments of electron multiplying CCD (emCCD) cameras offer an alternative to the ICCD.

During the GSI beam time in 2014 profile measurements have been performed both with an ICCD (Proxivison/Basler) [2] and an emCCD (Princeton Instruments ProEM512B) camera [3]. These two cameras have different working principles: the ICCD camera uses electron multiplication within a microchannel plate (MCP) due to the high voltage applied between photocathode and phosphor screen. The emCCD camera achieves signal amplification by avalanche diode-like electronics in the extended portion of the serial readout register [3].

The goal of the experiments was to compare the performance of the two cameras under similar conditions. A typical experimental set-up is shown in Figure 1.

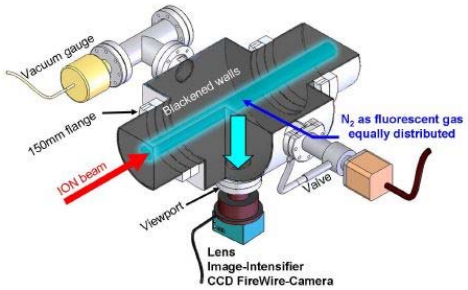

Figure 1: Typical set-up of a BIF profile monitor [2].

The measurements have been performed with 300 MeV/u ^{238}U ion beams in slow extraction mode, pulse duration 500 ms, beam widths 7.2 and 10.7 mm for ICCD and emCCD measurements, respectively. Nitrogen has been used as working gas at pressures of $5\cdot10^{-3}$, 10^{-2}, $2\cdot10^{-2}$ (ICCD) and $3.5\cdot10^{-2}$(emCCD) mbar. To increase the S/N ratio, averages over a few hundred acquisitions have been computed both for background and beam images. Figure 2 and Figure 3 show the transverse profiles obtained with the ICCD and emCCD cameras and also for comparison the profiles from a scintillating screen placed 1 m downstream of the BIF diagnostic chamber.

The magnitude of the ICCD profiles is basically proportional to the N_2 pressure (p). This is not the case for the emCCD. The profile taken at $3.5\cdot10^{-2}$ mbar shows a not expectable stronger increase in magnitude than at $5\cdot10^{-3}$ and 10^{-2} mbar. The proportionality of the intensity of the N_2 emission at 337 nm to p^2 may cause this behaviour.

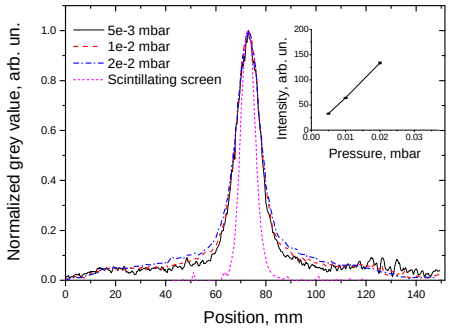

Figure 2: ICCD transverse profiles at different pressures.

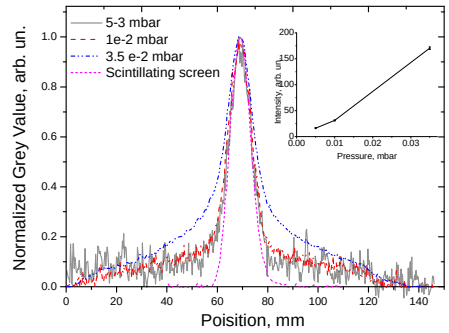

Figure 3: emCCD transverse profiles at different pressures.

The central part of the emCCD low pressure profiles is comparable to the one from the scintillating screen, while the ICCD profiles are systematically broadened. This behaviour can be explained by the fact that single photons produce wide spots in the ICCD acquired image. The effect can be mitigated by proper image processing. The tails of the BIF profiles and the strongly increased width at $3.5\cdot10^{-2}$ mbar are most probably due to the N_2 emission at 337 nm, known to give rise to wide profiles, which also are pressure dependent [4]. Filtering this line out should help to improve the profile width accuracy.

References

[1] C.A. Andre et al., DIPAC2011 proc., p.185
[2] P. Forck et al., HB2010 proc., p. 497
[3] David Dussault, Paul Hoess, Proceedings of SPIE Vol. 5563, pp.195-204 (2004)
[4] P. Forck et al., OPAC Workshop 2014

* Work supported by BMBF project No. 05P12RDRBN and Graduate School of Excellence ESE TU Darmstadt.
#y.shutko@gsi.de

In-beam tests of PMTs and voltage dividers for particle detectors at FAIR*

P. Boutachkov[1], *A. Reiter*[1], *C. Andre*[1], *H. Bräuning*[1], *C. Dorn*[1], *P. Forck*[1,2], *E-M. Glück*[1], *H. Graf*[1], *T. Hoffmann*[1], *V. S. Lavrik*[2], *A. Lieberwirth*[3], *Y. Shutko*[3], *and B. Walasek-Höhne*[1]

[1]GSI, Darmstadt, Germany; [2]Goethe University, Frankfurt, Germany; [3]IKP, Darmstadt, Germany

Scintillation counters are used for beam intensity, beam loss and spill structure measurements at GSI, they will be utilized at FAIR too, see [1] and the references therein. The presented study was started due to the phase out of the Photonis XP2972 photomultiplier, which is presently used in the beam diagnostic counters at GSI. Possible replacement photomultipliers (PMTs) and active voltage dividers (AVDs) were selected based on their characteristics and laboratory tests [1]. From the tested PMTs, Hamamatsu R6427 had the largest gain variation, while the ET Enterprises and the GSI in-house developed AVDs demonstrated stable operation at counting rates above 10 MHz. The response of the selected PMT and AVDs to the modulated spill structure of slowly extracted SIS beam was investigated.

Measurements and Results

The tested PMT and AVD was coupled to a 1 mm thick BC400 scintillator, in a configuration illustrated in Fig. 1 of Ref. [2]. Three scintillators were placed behind each other. The heavy ion beam penetrates the 3 mm plastic, depositing similar energy in the three detectors. The generated signals were recorded with a broad band oscilloscope, which was triggered at a programmable delay relative to the beginning of the spill extraction. A representative measurement is shown in Fig. 1, demonstrating the better performance at high counting rates of the GSI-AVD. Operating at these rates is advantageous for applications where an integrating detector, as an ionization chamber, is calibrated relatively to a scintillator counter.

The amplitude spectra shown in Fig. 2 illustrates two typical cases which can lead to inaccurate measurements: a radiation damaged scintillator and irregular spill structure. An amplitude measurement or a comparison of the counting rates above two different thresholds will provide a criteria of the measurement reliability, as shown in the inset of Fig. 2.

In conclusion, based on the tests described in this contribution and in Ref. [1], the optimum PMT-AVD combination for the future counters at FAIR and GSI is a Hamamatsu R6427 PMT powered by the GSI-AVD. In spite of the better PMT-AVD performance, a reliable measurement with the scintillation counters at instantaneous rates above 13 MHz would require amplitude information.

* It is pleasure to acknowledge the members of the GSI operating team for their support during the experiments.

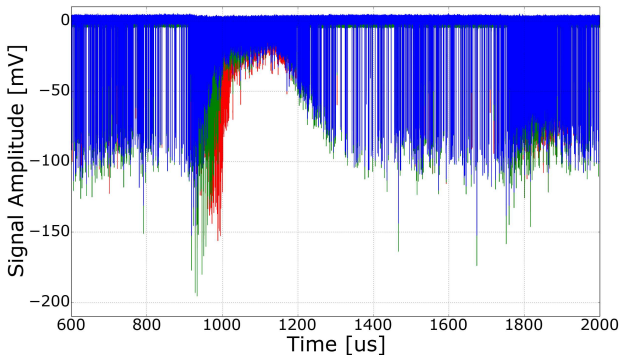

Figure 1: Pulses from ^{238}U ions at 300 MeV/u and average in spill intensity of 1 MHz. At Time$\sim$1 ms, the signal amplitude grows and falls down as the instantaneous beam intensity increases above 13 MHz. Signals from R6427 PMT powered by: GSI-AVD (in red), E220BFN2-01 (in green) and H7415MOD-AVD (in blue). The GSI-AVD withstand higher counting rates compared to the other AVDs.

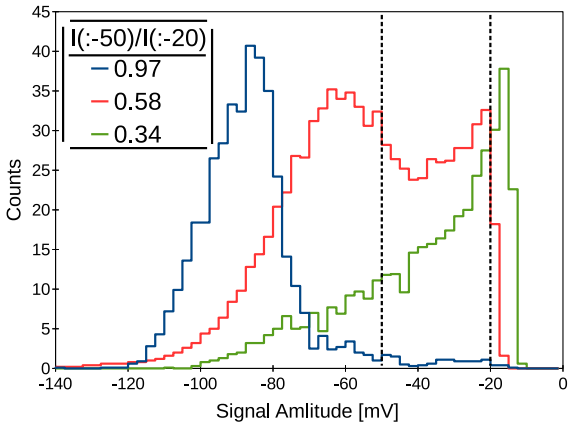

Figure 2: Signal amplitudes for normally operating PMT-AVD in blue, overloaded detector during parts of the spill in red and radiation damaged scintillator in green. The ratio of counts with amplitudes larger than 50 mV and 20 mV is shown in the inset.

References

[1] P. Boutachkov, *et al.*, "Bench Tests of PMTs and Voltage Dividers for Counting Applications at FAIR", GSI Scientific Rep. (2014)

[2] P. Forck, T. Hoffmann, DIPAC01, Grenoble, p. 129 (2001)

DOI:10.15120/GR-2015-1-FG-GENERAL-46

Bench tests of PMTs and voltage dividers for counting applications at FAIR

P. Boutachkov, C. Andre, A. Reiter, and T. Hoffmann
GSI, Darmstadt, Germany

This contribution presents selected results from tests of Photomultipliers (PMT) and active voltage dividers (AVD) with a laser diode.

At FAIR, plastic scintillator counters will be used for beam intensity and beam loss measurements [1]. Furthermore, the Photonis company phased out the production of the XP2972 PMT, which is presently used in the beam diagnostic counters at GSI [2,3]. Commercially available PMTs from Hamamatsu and ET Enterprises were selected, based on photo-cathode area, gain, signal rise time and transit time spread. The gain variation and the maximum counting rate were determined for combinations of the selected PMTs and AVDs at various luminances. These parameters determine the scintillator thickness necessary for detection of an ion accelerated by SIS18/100, and the instantaneous beam intensity which can be measured by the counters.

Measurements and Results

Measurements were performed with the Hamamatsu R6427, ET Enterprises 9442B and Photonis XP2972 PMTs. They were biased by a Hamamatsu-H7415MOD, ET Enterprises E220BFN2-01 and an in-house developed active voltage divider.

The PMTs and AVDs were tested with a fast switched laser diode by PicoQuant (FSL500 with a LDH-S-C-405 laser head). This light source emits at wavelength of 405 nm, matching the 420 nm wavelength of maximum emission for a BC400 plastic scintillator.

The full active area of the tested PMTs was illuminated by light pulses of a fixed duration, of approximately 3 ns. Their intensity was varied by changing the FSL500 power setting and by neutral glass filters. The laser was triggered by a white noise generator. The trigger frequency was measured by a rate meter, while the PMT minimum anode amplitude and average anode charge were determined by a 50 Ohm terminated broadband oscilloscope.

The tested PMTs were illuminated by the same light intensity at different repetition rates. For each series of measurements the AVDs high voltages were adjusted in order to observe signals with similar amplitude at 10-100 Hz trigger rate. Data from three measurements are shown in Fig. 1. Before reaching the maximum counting rate for a given PMT-AVD combination the signal amplitude increases, due to the higher voltage drop between the last dynodes.

In the GSI AVD the last 6 dynode voltages are stabilized. The stabilization is done by a voltage follower based on the BSS125 SIPMOS transistor. In comparison, the Hamamatsu divider has 3 stabilized dynodes, while in the ET Enterprises divider all dynodes are stabilized. The measurements showed that the ET Enterprises and the GSI AVDs can withstand counting rates above 10 MHz. Further in-beam tests [4] favored the GSI-AVD, due to better performance at higher counting rates.

Measurements with different neutral glass filters showed more than 10 times larger gain variation for the Hamamatsu R6427 PMT, compared to the ET 9442B and XP2972 PMTs. Based on the tests described in this contribution and in Ref. [4], one can conclude that the optimum PMT-AVD combination for the future counters at FAIR and GSI is a Hamamatsu R6427 PMT powered by the GSI AVD.

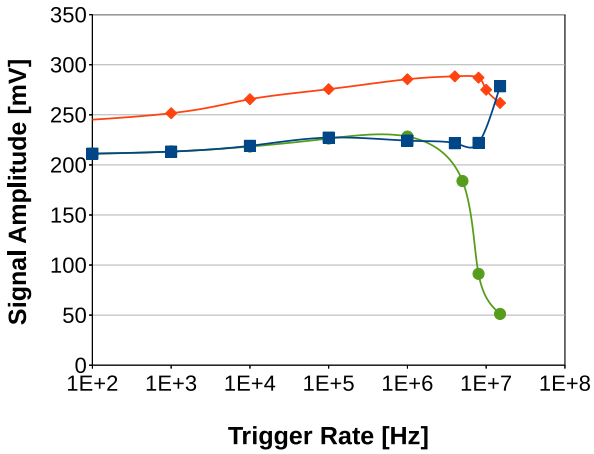

Figure 1: The solid curves follow the evolution of the signal amplitude of different PMT-AVD combinations as a function of the trigger rate. Blue-squares: Plots for the Hamamatsu R6427 PMT powered by GSI AVD. Orange-diamonds: ET 9442B PMT powered by E220BFN2-01. Green-circles: Hamamatsu R6427 PMT powered by Hamamatsu AVD.

References

[1] FAIR Technical Design Report (TDR) – High Energy Beam Transport, GSI, December 2008

[2] P. Forck, T. Hoffmann, DIPAC01, Grenoble, p. 129 (2001)

[3] T. Hoffmann, D. A. Liakin, P. Forck, Proc. 10th Beam Instrumentation Workshop, Upton, New York, p. 329 (2002)

[4] P. Boutachkov, *et al.*, "In-beam Tests of PMTs and Voltage Dividers for Particle Detectors at FAIR", GSI Scientific Rep. (2014)

DOI:10.15120/GR-2015-1-FG-GENERAL-47

Transverse beam shape measurements of intense Uranium beams using optical transition radiation

B. Walasek-Höhne[1], *C. Andre*[1], *H. Bräuning*[1], *C. Dorn*[1], *R. Fischer*[1], *P. Forck*[1], *H. Graf*[1], *F. Hagenbuck*[1], *R. Haseitl*[1], *K. Höhne*[2], *A. Lumpkin*[3], *R. Lonsing*[1], *A. Reiter*[1], *C. Schmidt*[1], *M. Schwickert*[1], *and R. Singh*[1]

[1]GSI, Darmstadt, Germany; [2]FAIR, Darmstadt, Germany; [3]FermiLab, Batavia, USA

Particle-beam diagnostic techniques based on Optical Transition Radiation (OTR) have been demonstrated at a number of facilities with relativistic electron and proton beams [1]. Optical transition radiation is generated when an ion of charge q and velocity β crosses the interface between two media with different dielectric constants. This radiation is emitted over the visible spectrum and standard optical imaging techniques can be used to acquire the OTR signal and then reconstruct beam size and position. Since OTR is a surface phenomenon, thin foils can be used as the converter to reduce beam scattering and minimize heat deposition. The OTR method can be used to measure beam properties as transverse profiles and 2-D shape, transverse position, divergence, emittance and intensity.

The OTR signal of a non-relativistic ion beam has been shown for the first time in 2011 with a pilot OTR experiment at the UNILAC [2]. During the 2014 beam time, usability of the OTR method to obtain profiles of high energetic ion beams was successfully demonstrated and first images were taken. Measurements were performed with 600 MeV/u Uranium beams from SIS18 of intensities up to around 2×10^8 particles per pulse (ppp) and 300 ms pulse length on a stainless steel target. In order to detect the low number of photons a standard CCD Camera (Prosilica GC650) with additional image intensifier (Lambert Instruments I187) was used.

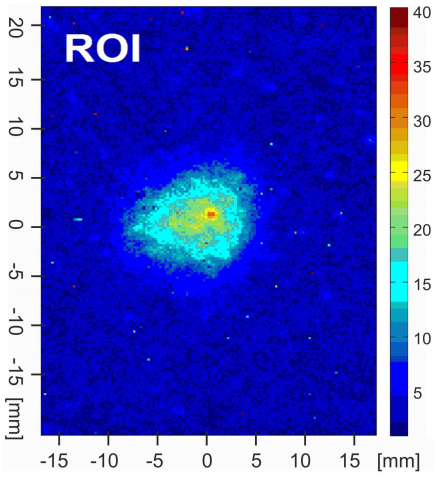

Figure 1: False colour OTR images of beam cross-section during irradiation with 1.5×10^8 U^{92+} ions. The beam energy was 600 MeV/u (pulse length 300 ms).

Various experiments have been performed to estimate the signal strength, to determine the imaging qualities and to evaluate the working regime of the OTR technique. Figure 1 shows a false colour OTR image from 1.5×10^8 U^{92+} ions impinging on the target.

For beam imaging OTR has the advantage that it is expected to show perfect linearity to the number of incident particles without the risk of saturation. In Figure 2 the integral OTR signal is displayed for different particle numbers per pulse. The beam current was measured with a Secondary Electron Monitor (SEM). In our studies the OTR signal shows a linear behaviour with respect to the incident particle number. For U^{92+} ions reasonable beam distributions were acquired down to 2×10^7 ppp.

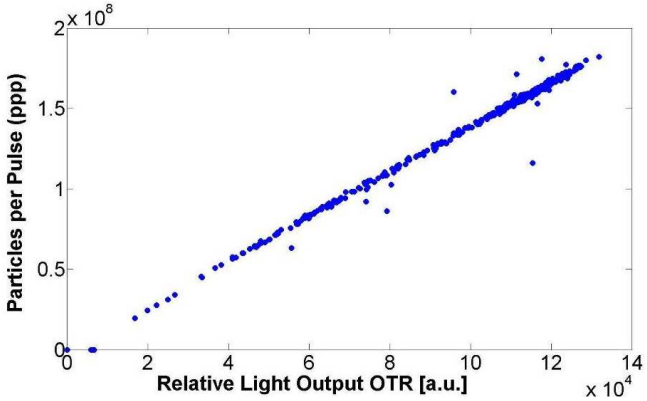

Figure 2: The OTR signal strength as a function of the particle number for the U^{92+} beam.

To determine the imaging qualities of the OTR method, additional profile measurements with a MWPC have been made. The beam profiles obtained with MWPC and OTR are in good agreement. OTR has an advantage of directly obtaining two dimensional beam shape.

The usage of OTR monitoring as a minimally intercepting method can be considered as an alternative to scintillators or BIF monitors.

References

[1] V. E. Scarpine et al., "OTR imaging of intense 120 GeV protons in the NuMI beamline at FNAL" PAC 2007 `http://www.JACoW.org/`

[2] B.Walasek–Höhne et al., "Optical Transition Radiation for non-relativistic ion beams" HB 2012 `http://www.JACoW.org/`

DOI:10.15120/GR-2015-1-FG-GENERAL-48

APD-photosensor serial characterization laboratory for FAIR experiments established

A.Wilms[1], the FAIR@GSI division RBDL[1,#]
[1]GSI, Darmstadt, Germany.

For the readout of the electromagnetic calorimeters of PANDA [1] and R3B [2] Avalanche Photodiodes (APDs) will be used. To this end the individual sensors need to be characterized before installation in the final detector systems. Therefore a screening laboratory has been established October 2014.

The new APD screening facility at GSI

The main part of the newly established APD laboratory inside the Heck hall is the mass screening room in which 100 devices can be characterized simultaneously inside fife climate cabinets. Each cabinet is humidity and temperature controlled and allows the temperature dependent full characterization of the sensors in nearly completely automatized procedures (see Figure 1).

Figure 1: Installation of 5 climate cabinets inside one room of the APD laboratory.

To reach the envisaged screening capacity of 2000 APDs per month, the APD laboratory of the RBDL division is operated in shift mode. For the PANDA EMC, all APDs need to be characterized twice, once before and once after gamma irradiation.

APD screening & results

In addition to the optical parameters measured at given wavelengths, the temperature dependence of the gain-bias characteristics may be measured. Further, the quantum efficiency at different temperatures, the electrical properties like capacitance and excess noise may be measured at the facility in the future, as soon as the ongoing validation of the respective apparatuses is done.

Approx. 4600 APDs have been characterized so far for the PANDA EMC with respect to their parameters at 20°C and at their nominal manufacturer-given gain of M = 100. The distributions for the voltage values to be applied to reach a gain of M = 100 as well as the breakdown voltages of approx. 3800 APDs are shown in Figure 2 and Figure 3 respectively.

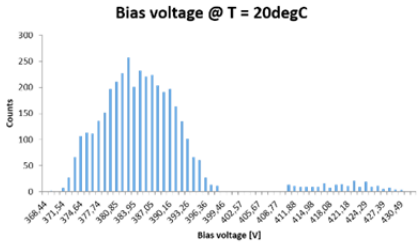

Figure 2: Bias voltage distribution for validated APDs at 20°C for M = 100.

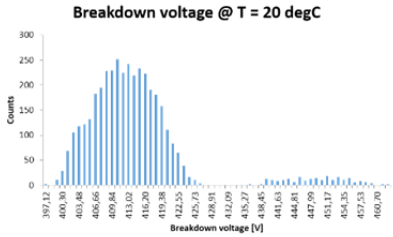

Figure 3: Distribution of breakdown voltage for the same APDs: Two groups of devices can clearly be identified. Both groups are still found within specifications.

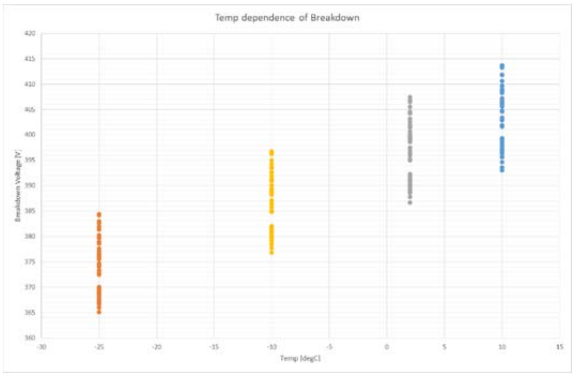

Figure 4 First preliminary data of a sample of 60 APDs showing the temperature dependence of the breakdown voltage. Each device shows a strictly linear behaviour.

Up to now only around 1‰ of the devices did not match the required technical specifications defined by the collaboration.

References

[1]: Technical Design Report for PANDA Electromagnetic calorimeter (2008) arXiv:0810.1216

[2]: Technical Report for the Design, Construction and Commissioning of the CALIFA Barrel (November 2011)

DOI:10.15120/GR-2015-1-FG-GENERAL-49

DOI:10.15120/GR-2015-1-FG-GENERAL-49

SIS100 status report 2014

P. Spiller, U. Blell, L. Bozyk, J. Ceballos Valesco, T. Eisel, E. Fischer, H.G. König, V. Kornilov, P. Kowina, J.P. Meier, A. Mierau, C. Mühle, C. Omet, D. Ondreka, H. Ramakers, N. Pyka, P. Rottländer, C. Roux, P. Schnizer, S. Wilfert, and D. Winters

GSI, Darmstadt, Germany

Introduction

SIS100 is the main accelerator of the FAIR project. It is a worldwide unique heavy ion synchrotron dedicated to accelerate highest intensities of intermediate charge state heavy ion and proton beams up to 100 Tm. From the technical point of view, most challenging issues are the fast ramped superconducting magnets and the acceleration of intense, intermediate charge state heavy ions beams. The latter required a unique lattice design (charge separator lattice) in combination with an ultra-high vacuum system based on distributed cryopumping with actively cooled magnet chambers, adsorption pumps and dedicated cryocatchers for local suppression of gas desorption.

Procurement status

The year 2014 was very much loaded with completing, reviewing and finishing specifications and drawings for all kind of components. Finally, shortly after end of 2014, all contracts for the major SIS100 components and the large series have been closed (i.e. Milestone ”M4” has been reached), which is a major step ahead. This corresponds to a bound value of 50% of the SIS100 costbook value. The last large in-kind contract regarding the quadrupole unit production has been successfully negotiated and closed with the Joint Institute for Nuclear Research (JINR, Dubna, Russia) and signed by JINR, GSI and FAIR management at an official ceremony at JINR at 2015/02/20, see fig. 1.

Besides the major series with long production times, many other components have been tendered or contracted, e.g. the injection kicker system, the resonance sextupole magnets (awarded to DANFYSIK, Denmark) and the cryocatcher system. The local cryogenics system will be delivered by the Wroclaw University of Technology (WrUT, Poland) and the manufacturing design review took place for the first bypass line segment. The contract for the production of the bypass line as been awarded to the company KRIOSYSTEM, Poland.

Building planning

Detailed planning for the accelerator tunnel and the supply area (K0923A/T110) complex, including 3D DMU models of the accelerator and its technical infrastructure, has matured and is transitioning to execution planning, which will take place in 2015, see fig. 2. This will allow the creation of the necessary building tendering documents in late 2015.

Figure 1: Signature of quadrupole unit production contract at JINR (l.t.r with the contract in their hands: B. Sharkov / FAIR and V. Matveev / JINR.

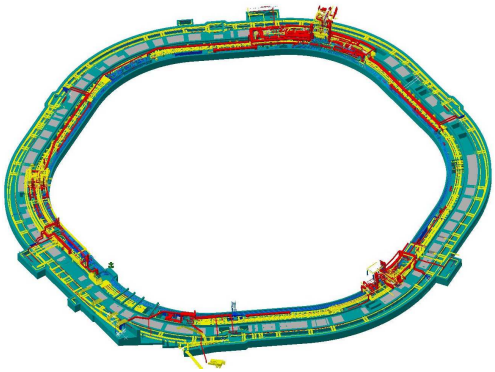

Figure 2: T110 design with cable trays (yellow), cooling water supply lines (blue) and venting (red).

Progress on component tendering and delivery

The first of the 109 s.c. 1.9 T dipole series magnets (FoS) has already been delivered in June 2013 and thoroughly tested under warm and cryogenic conditions. Although, the FOS dipole has a completely new coil design and is being operated at twice the electrical current as the prototype, the quench training showed excellent behavior. Nevertheless, the planned high current operation allows only minimum mechanical errors in the yoke production. Therefore, together with the manufacturer and external experts, the production and welding process has been review and optimized. A mechanically further improved FoS yoke will be produced and delivered until Q3/2015. After a short test period the series production will be released. The FoS thin wall, actively cooled dipole vacuum chamber has been

DOI:10.15120/GR-2015-1-FG-SIS100-01

delivered by the company PINK and tested at warm and cold conditions. The manufacturing has been done with excellent results and the specified UHV properties were achieved. However, the cryogenic pumping properties of the He cooling circuit has to be improved.

The s.c. quadrupole modules (83 pcs, see fig. 3) are very demanding due to their technical complexity and the international structure of the project. The quadrupole units (quadrupole magnet + corrector magnets) will be built at JINR, Dubna, whereas other components (vacuum chambers, cryocatcher, BPM's, local current leads, cryostats, ...) will be tendered by GSI. Currently, 80% of the specification work of the units and all manufacturing drawings for the quadrupole module type 2.5 FoS units are finished and are finally reviewed at JINR; the remaining 20% will be done when the external (industrialized) design work has been completed. The yoke steel (323 t in total) has been ordered at C.D. Wälzholz, Germany and the first lot will be delivered to JINR 04/2015. The cryocatcher tendering is nearly completed, bids do exist. Finally, smaller standardized components like voltage breakers and temperature sensors for the full quadrupole module series has been ordered by GSI in 2014, too.

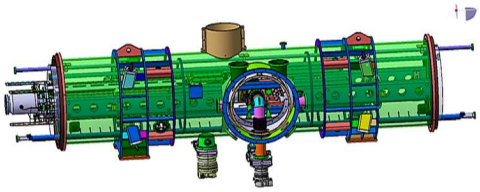

Figure 3: Design of the type 2.5 quadrupole module.

The RF acceleration system (14 pcs, 1.1...3.2 MHz, 20 kV_p, 30 kW beam power, see fig. 4) has been tendered by FAIR GmbH and awarded to a consortium of RI/AMPEGON in 11/2014. Preparation of the manufacturing concept is currently done by the consortium, the conceptual design review (CDR) will take place Q1/2015. Driver amplifier and LLRF procurement has been started, too.

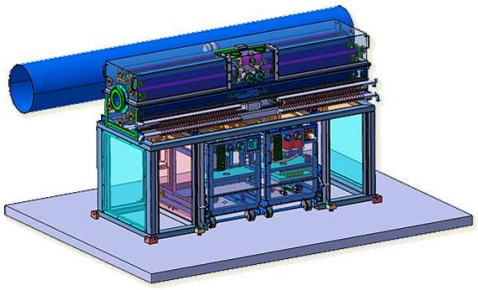

Figure 4: Design of the acceleration cavitiy.

The RF Bunch compression system (9 pcs) has been tendered by GSI and awarded to the company AURION (Germany) in 04/2014. The conceptual design review has been successfully concluded. As last step before the start of production a final design review (FDR) is foreseen, which will take place in 03/2015 - the 1st device will be delivered in 07/2015.

The design of the SIS100 injection straight section (sector 6) has been detailed; as a result, the injection kicker system (6 modules, 130 ns rise time, 7.5 mrad deflection angle) procurement has been started.

S.c. test facilities

The prototype test facility (PTF) has been equipped in 2014 with all missing infrastructure, 13 kA HTS current leads, power supplies, etc. to upgrade it for the testing of the dipole FoS tests. Fig. 5 shows the team after the first dipole cold test.

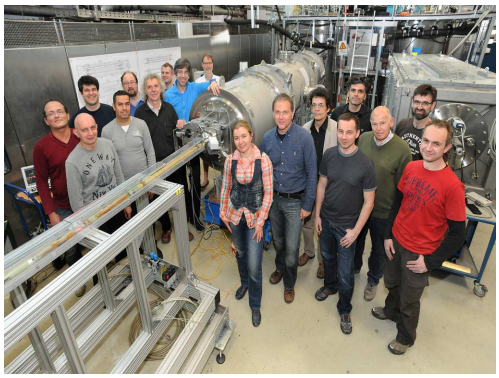

Figure 5: The test team at the PTF with the FoS dipole.

For the series dipole magnet test facility (STF), a dedicated building has been constructed at GSI (Bldg. SH5). The cryogenic system, including feed boxes and test benches is currently commissioned. The power converter for ramping the s.c. dipole magnets with 29 kA/s will be delivered in 04/2015. High precision magnetic field measurement equipment is currently built in a collaboration with CERN. This subproject runs smooth and is profiting a lot from the experience gained during the FoS dipole testing, where high precision mechanical measurement devices has been developed.

The quadrupole unit testing will be done at JINR, Dubna. Here, an R&D contract between GSI and JINR has been closed in 12/2013. The cryoplant at JINR has already been commissioned; measurement equipment will be designed by JINR in parallel to the construction of the first quadrupole units.

Finally, the SIS100 stringtest will comprise two dipoles, one quadrupole module, the cryogenic bypass line, feedbox and current lead box. The space is preserved at the STF and the layout has been completed. The contract for the bypass line has been closed (WrUT) and the FDR will take place in 02/2015. Specifications for the remaining items are 50% finished.

DOI:10.15120/GR-2015-1-FG-SIS100-01

Status of the superconducting magnets for FAIR*

E. Fischer†, V. Bezkorovaynyy, A. Bleile, J. Ceballos, E. J. Cho, W. Freisleben, N. Joshi, B. Körber, V. Maroussov, F. Marzouki, J. P. Meier, S. Meyer, A. Mierau, H. Müller, H. Raach, C. Roux, P. Schnizer, F. Seifert, A. Stafiniak, K. Sugita, P. Szwangruber, and H. Weiss

GSI, Darmstadt, Germany

Introduction

Within this paper we report shortly on all the many different activities of the group which now is mainly focused on procuring the magnets and associated systems for the FAIR project. While many activities were pursued the successful tests of the SIS100 dipole magnet stick clearly out.

Superconducting magnets

Rapidly cycling magnets for SIS100

Dipoles – production status and first tests The **F**irst **o**f **S**eries SIS100 main dipole was delivered last year and its testing campaign has been conducted since December 2013 with a successful cool down, measurement of the virgin field curve, required for field optimisation calculations, and finished with a successful training.

The coil structure was found to provide an insulation of 3 kV already at the factory test. During the first run the magnet quenched slightly below the nominal current with the second quench already above nominal field and reached up to now a maximum current of 15.7 kA and thus shows sufficient operation margin.

The AC losses produced by the SIS100 main dipole magnet are one of the main loads on the cyroplant. are well below the expected value of 70 W for a triangular cycle of 1 Hz. This is considered explainable by the choice of iron (M600-100A silicon steel), the superconducting low loss wire with a CuMn matrix and extra inserts at the magnet ends, foreseen for optimising the end field quality.

The magnetic field was measured using: a hall probe mounted on a mapper, a single stretched wire system, and rotating coil probes at different locations [1, 2]. The field measured with these different systems gave results which were matching each other with sufficient accuracy and second the soundness of the measurement system design.

So the overall tests of the magnets were successful: quench behaviour, magnetic field strength, AC losses. The magnetic field was however a bit deteriorated. The mechanical accuracy of the yoke assembly was investigated with appropriate gauges, which showed that the yoke mechanics was slightly out of specifications. Based on these measurements mitigation actions were discussed with the manufacturer and will be tested and incorporated in the production beginning next year.

Quadrupole modules Aside of the dipoles the main quadrupoles together with all corrector and steerer magnets are assembled into so called units consisting of a main quadrupole and up to two correctors. These quadrupole units will be produced and tested at cold temperature at **J**oint **I**nstitute for **N**uclear **R**esearch (JINR). The collaboration contract for production of quadrupole-, corrector- and steering magnets as well as the integration into units at JINR are finalised and will be signed in January 2015. The units are located within 83 quadrupole doublet modules split in 11 configurations and four basic classes with modules located in the arc, the end of the straight section of the SIS100 machine. All these modules are currently designed in interaction with Babcock Noell Gmbh Würzburg / Germany. The integration of the modules has to fulfill demanding stability criteria of $\pm$ 125 μm for the main quadrupoles, which makes the design challenging. The tendering process for the involved components and the integration of modules is in preparation and will be established also in 2015.

Rapidly cycling magnets for SIS300

After manufacturing of a first dipole magnet in collaboration with INFN, Italy, a second collared coil was built together with INFN and CERN in frame of the EU-CRISP project. Ongoing is also the design work on wide aperture quadrupoles for FAIRs HEDgeHOB experiment by IHEP in Protvino, who had already successfully built SIS300 quadrupole and corrector prototypes.

Magnets of the Super-FRS

The specifications of the SuperFRS magnets were released and the tender launched. The dipoles design has been finalised by CEA/Saclay. The multiplets have been thoroughly negotiated and the contract will be awarded soon.

Testing

Prototype test facility activities

While the magnet was produced in parallel the test facility was upgraded so that all parameters of the magnet could be derived including an upgrade of the power converter and procurement of HTS current leads.

* We acknowledge the support of the European Community-Research Infrastructure Activity under the FP7 program CRISP (Grant agreement no: 283745) Work Package 5. We acknowledge the support through the JINR–BMBF contract.

† e.fischer@gsi.de

CC BY
DOI:10.15120/GR-2015-1-FG-SIS100-02

The measurements of the field quality were made with the mole, i.e. a rotating coil probe system with a motor operating inside the magnetic field. For series measurements a measurement shaft will be used with cold coil probes as their cores. Together with CERN a system was adapted for measuring the magnetic field in cold conditions in vacuum and successfully tested. A shaft based on this principle will be tested beginning next year.

Series test facility activities

The seres test facility is being built up which is currently mainly dedicated for testing the SIS100 dipoles. The cryoinfrastructure including also the feed boxes have been procured supervised by our colleagues of the cryo group and are currently being tested. It will provide 4 test benches organised in 2 clusters and allow testing the SIS100 string.

At the beginning of the SIS100 series dipole testing all four benches will be used for the tests of the dipole magnets. When the first of series quadrupole doublet will be delivered to GSI one of the test benches will be used to operate the string test [3].

SIS100 quadrupole tests

The test facility at JINR for these magnets is currently being built up. The first power converter is being assembled and will be commissioned soon. Each test bench is equipped with a satellite refrigerator for cooling down and operating of the magnets. This concept simplifies the parallel operation of the test benches. Two satellite refrigerators have already been produced.

Testing Super-FRS magnets at CERN

The cold tests of Super-FRS will be done at CERN under a collaboration agreement between CERN and GSI. Three test benches, suitable for dipole magnets and multiplets respectively, will be available. This allows a continuous operation with one bench being cooled down, one cold and the measurements running, and the third being warmed up. Given that these choices have been made now the hardware can be procured. CERN is already refurbished the necessary cryogenic infrastructure and setting up the other necessary test equipment as, for example, power converters, quench detection systems, and systems for magnetic measurements.

Current leads

The successful test of the first pair of HTS current of last year gave the green light to produce the second pair which was delivered this year and successfully tested. So the series production of the current leads for the series test station and the SIS100 machine was launched. Along with this high current current low current leads have been designed. A prototype has been procured that will be tested beginning next year. For the γ_t-Jump-Quadrupole, a cold normal conducting magnet within a quadrupole doublet module, the design of current leads has been started. For the Hedgehob collaboration 4 pairs of 6 kA HTS current leads shall be procured. A specification is in preparation.

Electrical systems and magnet protection

The quench detection systems for the series test facility have been procured. While these systems could detect a quench reliably in the SIS100 machine, the required cables would create too large parasitic capacitance. Therefore an alternative based on transducers is currently under development.

Conclusion

After the procurement of the different superconducting magnets has been started in 2013, the first SIS100 dipole was tested thoroughly in 2014 and a new built chromaticity sextupole is ready now for testing as a first corrector type magnet. The dipole tests results proved that the magnet design is sound and the requested operation parameters are achievable. In-depth technologic investigations of the yoke production process, supporting the manufacturer, have shown that the remaining problems can be solved by improving the welding technology so that the specified tolerances of the yoke geometry can be achieved. Thus a second yoke will be produced and the corrected first dipole is expected to provide the required magnetic field accuracy. This will allow us launching the series production still in 2015. The production of the other magnets was also prepared in 2014. The telegraphic style of this paper reflects the many activities that are undertaken to realise the FAIR project within the given scope and schedule.

References

[1] P. Schnizer, E. Fischer, P. Akishin, J. P. Meier, A. Mierau, and A. Bleile. Advanced magnetic field description and measurements on curved accelerator magnets. In *Proceedings of IPAC2014, Dresden, Germany*, 2014.

[2] E. Fischer *et al.*, Fast ramped superconducting magnets for FAIR – production status and first test results. *IEEE T. Appl. Supercon.*, 2014. submitted for publication.

[3] K. Sugita *et al.*, String test preparation for the superconducting SIS100 accelerator of FAIR. *IEEE T. Appl. Supercon.*, 24(3):1–4, June 2014.

[4] A. Bleile *et al*. Thermodynamic properties of the superconducting dipole magnet of the SIS100 synchrotron. *Physics Periodica*, 2014. submitted for publication.

[5] E. Fischer *et al.* WEPRI083 IPAC2014, Dresden, Germany, 2014.

[6] H. Raach *et al.* 14 kA HTS current leads with one 4.8 K helium stream for the prototype test facility at GSI. *Physics Periodica*, 2014. submitted for publication.

[7] P. Schnizer *et al.* Low temperature test capabilities for the superconducting magnets of FAIR. *IEEE T. Appl. Supercon.*, 2014. submitted for publication.

DOI:10.15120/GR-2015-1-FG-SIS100-02

The SIS100 laser cooling facility*

D. Winters†[1], *T. Beck*[2], *G. Birkl*‡[2], *M. Bussmann*[3], *V. Hannen*[4], *Th. Kühl*[1,5], *X. Ma*§[6], *U. Schramm*‡[3,7], *M. Siebold*[3], *Th. Stöhlker*[1,5,8], *Th. Walther*‡[2], *W. Wen*§¶[3,6,7], *and P. Spiller*[1]

[1]GSI Helmholtzzentrum, Darmstadt, Germany; [2]Technical University Darmstadt, Germany; [3]Helmholtz-Zentrum Dresden-Rossendorf, Germany; [4]Münster University, Germany; [5]Helmholtz Institute Jena, Germany; [6]Institute of Modern Physics-CAS, Lanzhou, China; [7]Technical University Dresden, Germany; [8]Jena University, Germany

High-quality, stored ion beams can be obtained by means of electron cooling and/or stochastic cooling. At intermediate kinetic energies ($\gamma \approx 1$), these methods work very well. But at very high kinetic energies ($\gamma > 5$), they become less effective. For instance, to reach electron cooling at $\gamma = 12$, a very sophisticated (voltage up to 6 MV) and thus expensive electron cooling system is required. Therefore, another method was considered for the FAIR heavy-ion synchrotron SIS100: Laser cooling of bunched ion beams. Based on successful experiments with stored, relativistic heavy-ion beams at the ESR [1], it was (2013) decided to set up a laser cooling facility at the SIS100. Within the 3rd term of the Programme Oriented Funding (POFIII) of the Helmholtz Society, we wrote a proposal for this facility as part of accelerator research and development (ARD) within "Matter and Technologies" [2]. Early 2014, the proposal was approved and received the highest marks ('highlight').

Within FAIR@GSI primary beams, a special project group 'SIS100 laser cooling' (PSP-code 2.8.10) was formed, which tasks are to specify, design, order, construct, setup, and test the SIS100 laser cooling facility. (*Note*: The planned laser cooling facility can serve both the SIS100 and the future SIS300.) The project group consists of scientists from SPARC 'laser cooling' [3], which come from GSI and the collaborating partner universities and research centers in Dresden-Rossendorf, Darmstadt, Jena, Münster, and Lanzhou (China).

For laser cooling at the SIS100, the setup must be similar to that used at the ESR, and at least contain a laser system with a beamline (incl. optics and diagnostics), a set of scrapers, a buncher (exciter), and a dedicated fluorescence detection system. The facility will be located 20 m underground (see Fig.1). The laser light will be transported from the laser lab in the (inner) service tunnel to the (outer) accelerator tunnel, passing through concrete walls and a thick layer of soil between the two tunnels. This laser beamline (length 25 m, diameter 20 cm) should be made out of stainless steel vacuum tubes. Vacuum conditions are required to transport the laser light, which covers a very broad spectrum ranging from the IR ($\lambda \sim \mu$m) down to the XUV range ($\lambda \sim$nm). The laser lab (180 m^2) will contain a special cleanroom (50 m^2) to operate the laser systems. There will also be a detector cave (45 m^2) in which special detector systems for x-ray measurements can be installed (SIS300). Detectors for the IR- to the XUV-range are still compact enough to fit into the SIS100 tunnel. To couple the laser light in and out of the accelerator, special vacuum chambers with optics and diagnostics will be used. Spatial overlap (about 25 m) between laser and ion beam needs to be adjusted using scrapers and reference points.

First tests of the facility will use Li-like ions and laser systems provided by the groups in Darmstadt and Dresden. Once the facility has passed all the tests, and first laser cooling has been demonstrated, other ion species and/or laser systems could be used as well. We emphasize that also laser spectroscopy experiments can be performed! Once the cooling transition is found, it can also precisely be measured. Ultracold beams are also of great interest by themselves. Last, but not least, it will be attempted to extract the laser-cooled ions from the SIS100 and uniquely deliver very cold and very short ultra-relativistic ion bunches to experiments.

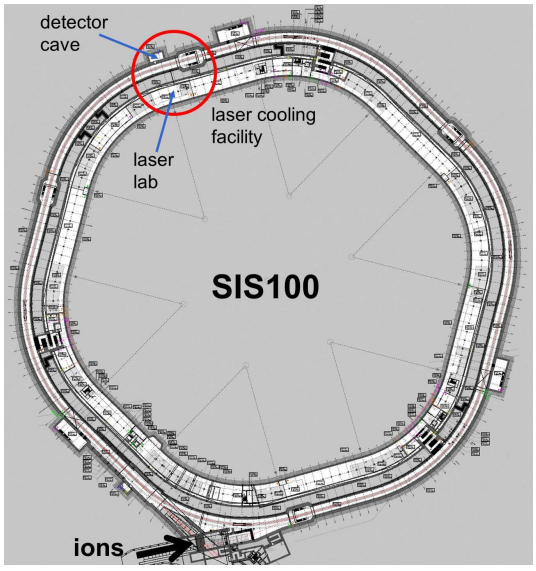

Figure 1: The FAIR heavy-ion synchrotron SIS100. The planned laser cooling facility is indicated by the red circle.

References

[1] U. Schramm *et al.*, Prog. Part. Nucl. Phys. **53** 583 (2004).

[2] https://www.helmholtz-ard.de/e25/

[3] https://www.gsi.de/sparc

* Work supported by HGF POFIII ARD-ST2.

† d.winters@gsi.de

‡ Work supported by BMBF.

§ Work supported by BMBF-WTZ.

¶ Work supported by DAAD.

Simulation of laser cooling of heavy ion beams at high intensities

L. Eidam[*†1,2] *and O. Boine-Frankenheim*[1,2]
[1]GSI, Darmstadt, Germany; [2]TEMF, TU Darmstadt, Germany

Abstract

In the past the principle of Doppler laser cooling was investigated and verified in low energy storage rings. In the SIS100 laser cooling will be applied to intense ion beams in the high energy regime for the first time. Laser cooling leads to an increase of the longitudinal phase space density and to non-Gaussian bunch distributions. In order to optimize the cooling process and ensure stable operation laser cooling has to studied numerically.

Principle of Laser Cooling

Laser cooling produces very cold beams by intersecting laser light anti parallel with the ion beam. The wavelength of the laser in the particle frame has to fit to an atomic transition with a short lifetime. The absorbed photons always give a kick in the same direction whereas the emitted photons kick the ions in any direction. This results in a net force pointing in the direction of the laser beam. The narrow force only interacts with particles with a momentum deviation of approximately $\Delta p/p \approx 10^{-7}$. The cooling of a hot ion beam is feasible by sweeping the laser frequency to interact with all particles in the bucket [1].

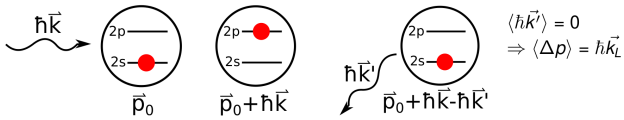

Figure 1: Schematic explanation of directional force for multiple scattering events during the laser cooling process.

Numerical Model

For the studies of the cooling process the simulation considers only the longitudinal phase space because the photon-particle interaction only affects the longitudinal motion. The tracking code contains different RF bucket configurations, intra beam scattering (IBS), space charge (SC) and the laser forces.

The laser forces are modelled statistically to take care of the so called 'random walk' [2]. This concept clarifies that the probability of absorbing the next photon changes after each scattering event. Therefore the assumption of an averaged force is not valid in general. For the simulation the laser interaction region is divided into slices. For each simulated particle in each slice the probability of a scattering event is calculated and statistically applied. The momentum change of a scattering event is given by:

$$\delta_j' = \hbar\vec{k}_{pf} \cdot (1 + \cos(\pi \cdot U_j)) \quad (1)$$

where $\hbar\vec{k}_{pf}$ is the momentum of the photon in the particle frame and U_j a random number. The therm $\cos(\pi \cdot U_j)$ describes the projection on the longitudinal axes of the randomly emitted photon. The probability of this momentum change is given by:

$$\rho(S, \Delta v) = \frac{L_{\text{intersec.}}}{n_{\text{slices}}\beta c_0 \gamma} \frac{\Gamma_L}{2} \frac{S}{1 + S + (2\Delta v/\Gamma_L)^2} \quad (2)$$

where the first factor describes the time interval of each slice and the rest is given by the well known probability of a spontaneous emission of a two level system with the saturation parameter S [2].

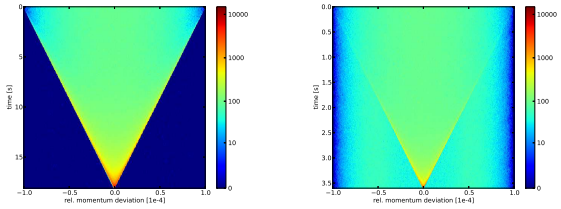

Figure 2: Momentum deviation over time during the cooling process for two different speeds of the laser sweep.

Figure 2 shows the simulated momentum deviation during the cooling process in a regular RF-bucket. In the second plot the sweep of the laser is too fast and some particles get lost behind the laser force and consequently for the cooling process.

Outlook

In the future the laser force and the IBS rates of possible transitions of different ion species will be analysed to find ions for a fast cooling process. Besides different cooling schemes with different RF configurations have to be analysed to optimize the cooling process.

References

[1] M. Bussmann et al, J. Phys.: Conf. Ser. 88, 012043 (2007)

[2] H.J. Metcalf, P. van der Straten, "Laser Cooling and Trapping of Atoms and Ions", Springer (1999)

* leidam@gsi.de

† Work supported by HGShire

DOI:10.15120/GR-2015-1-FG-SIS100-05

Investigation of thin-sheet approaches to simulate beam tube losses*

J. Trommler† [1] *and T. Weiland*[2]

[1, 2]Institut für Theorie Elektromagnetischer Felder, TU Darmstadt, Germany

Introduction

The beam tube in acceleration facilities is often made of very thin metal. During the switch-on or switch-off process of the dipole-magnets, the fast change in the magnetic field lead to eddy currents in the conductive beam tube. Applying a standard finite-element method (FEM) in order to simulate the parasitic effects results often in inappropriate meshes and high computational effort. Thin sheet approaches improve the mesh quality and speed up the calculations, like shown in Fig. 1. In our report of 2013, existing thin-sheet approaches were studied and compared, and the approach of [1] and [2] were selected to be most efficient for the calculation of beam tube losses. In this report our new algorithm, which was already introduced in the report of 2012 for simple 1D test scenarios, is applied to higher spacial dimensions to be able to compare its performance to the competitive methods.

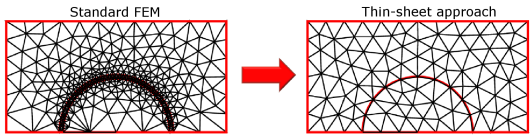

Figure 1: Mesh quality advantage of a thin-sheet approach.

Modified Bases in Higher Dimension

In taking the condition number of the system matrix into account, we developed in 2012 a new method [3] that outperforms the existing approaches according to this measure with respect to the accuracy. The basis functions of mesh elements that are directly connected to the interface are modified in order to account for the variation in thickness direction. But these modified bases are non-conform from one sheet adjacent element to the next. A penalization surface term has to be added to the weak formulation like also known from the discontinues Galerkin method or Raviart-Thomas elements.

A Two-dimensional Test Case

An electro-quasistationary test scenario was chosen to show the performance of our novel algorithm in higher spacial dimensions: A conductor excited by a harmonic voltage source of $U = 2\text{V}$ and $f = 50\text{Hz}$ and a small crack line with less conductivity in its center, see Fig. 2. The results

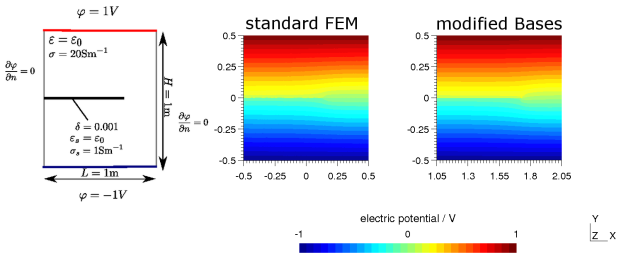

Figure 2: Geometry and result of test scenario.

of our thin-sheet approach are qualitatively comparable to standard FEM. Also the power loss is in good agreement with $P_{\text{el}} \approx 188.3\text{W}$. Fig. 3 shows the condition number of the final system matrix for different sheet thicknesses.

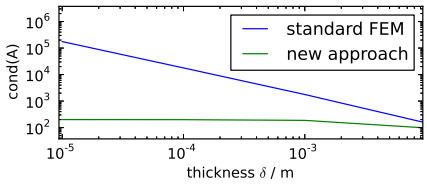

Figure 3: Conditioning with respect to sheet thickness.

Conclusion and Outlook

The promising approach of 2012 using modified bases is successfully applied to higher spacial dimensions, without loosing the advantageous properties. In a next step, the performance will be compared to the competitive methods of [1] and [2] in a beam tube simulation.

References

[1] Mayergoyz, I.D. and Bedrosian, G., “On calculation of 3-D eddy currents in conducting and magnetic shells”, IEEE Trans. Magn. 1995, vol. 31, no. 3, p. 1319–1324

[2] Schmidt, K. and Chernov, A., “A unified analysis of transmission conditions for thin conducting sheets in the time-harmonic eddy current model”, SIAM J. Appl. Math. 2013, vol. 73, no. 6, p. 1980–2003

[3] Trommler, J. and Koch, S. and Weiland, T., “A finite-element approach in order to avoid ill-conditioning in thin-sheet problems in frequency domain - Application to magneto-quasistatics”, JCAM 2012, vol. 236, no. 18, p. 4671–4680

* Work supported by GSI cooperation with university TU Darmstadt.

† trommler@temf.tu-darmstadt.de

Transverse BTF of bunched beams with Gaussian charge density at high energy

P. Görgen[1] *and O. Boine-Frankenheim*[1]

[1]TEMF, TU-Darmstadt, Germany

The transverse beam transfer function (BTF) is a widely-used diagnostic tool used in synchrotrons and storage rings. BTFs are commonly used for measurement of the machine tune and of stability diagrams. They can also be used to quantify transverse tune spread due to octupoles [1] or space charge [2] in coasting beams.

In this work the diagnostic power of beam transfer functions (BTF) with respect to bunched beams under the influence of a transverse nonlinearity was investigated in collaboration with Brookhaven National Laboratory (BNL). The work was motivated by the desire to recover the incoherent tune spread introduced by an electron lens such as the one recently installed at BNL for compensation of the incoherent beam-beam tune spread [3] directly via a BTF measurement. At GSI the tune spread caused by incoherent space charge in SIS 100 would be of interest. Building on the work by Berg and Ruggiero [1], transverse BTFs were investigated close to coasting beam conditions. In absence of coherent modes, it could be shown that while the exact distribution of incoherent tunes cannot be recovered from BTFs, the total width of the tune spread can be recovered [4]: In BTFs dominated by transverse tune spread such as BTFs of beams interacting with an electron lens in an otherwise very linear machine, the Landau damping arising from such a transverse nonlinearity dominates the beam transfer function and as a result the width of the peak in the imaginary part of the BTF allows determination of the incoherent tune spread. The recovery of tune spread from analytic BTF is shown in Figure 1.

To apply the analytic coasting beam results to bunched beams, it had to be shown that for the investigated working conditions, the effect of bunching is negligible. Beams in RHIC at high energy show nearly frozen synchrotron motion (synchrotron tunes of 10^{-3} and below). Synchrotron frequencies for SIS 100 proton operation are comparable. The transverse nonlinearity arising from the electron lens acts on particles in a bunch and a coasting beam alike. The assumption was validated in simulation for typical operating conditions. The simulations showed that the BTF did not change notably as a function chromaticity or synchrotron frequency. The recovery of the tune spread introduced by the electron lens works on bunches in simulation. The width of the peak in the imaginary part of the BTF still gives good estimate of the tune spread accurate to about 10-20% when applied to simulated BTF. The uncertainty is primarily caused by noise. The tune spread recovery method can be trivially automatized.

A validation measurement was carried out using the beam-beam effect to replicate the transverse fields of an electron lens while avoiding effects particular to the beam-beam effect. The tune spread recovered by the aforementioned method showed good agreement with the results obtained indirectly from the distance between coherent beam-beam modes in strong bunches and from emittance and beam current measurements.

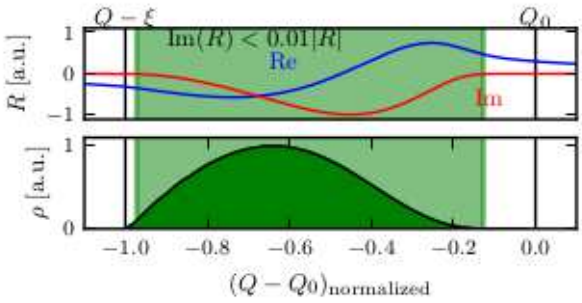

Figure 1: Analytic example BTF R with tune distribution ρ and the recovered tune spread (shaded green).

A generalized theory incorporating conditions for space charge in SIS 100 with protons at high energy is currently under development. The shape of the transverse fields giving rise to the tune spread is identical for a Gaussian electron lens and the self-fields of a transversely Gaussian proton beam. However, while an electron lens acts both on the center of charge of the beam and individual particles and thus also gives rise to a coherent tune shift, this is not the case with space charge: With space charge, the nonlinearity stays spatially aligned with the center of charge of the beam. As a result, space charge is not directly measurable in the BTFs of beams with space charge as the sole source of tune spread. In combination with chromaticity, a characteristic deformation of the BTF was observed for coasting beams [2]. In bunched beams with non-negligible synchrotron motion, a characteristinc pattern of head-tail modes is observed. We are validating the assumption that for near-frozen synchrotron motion, a middle regime exists, where the BTF of bunched beams resemble a superposition of BTF of coasting beams of different currents. In this case, the incoherent space charge tune shift could be obtained by means of a fit against measured BTF data.

References

[1] J. Berg, F. Ruggiero, CERN SL-AP-96-71

[2] S. Paret et al., doi:10.1103/PhysRevSTAB.13.022802

[3] W. Fischer et al., *Construction Progress of the RHIC Electron Lenses*, Proceedings of IPAC 2012

[4] P. Görgen et al., doi:10.1016/j.nima.2014.11.105

DOI:10.15120/GR-2015-1-FG-SIS100-07

Computation and bench measurements of beam coupling impedance

U. Niedermayer [*1], *L. Eidam*[1], *and O. Boine-Frankenheim*[1,2]

[1]Institut für Theorie Elektromagnetischer Felder, TU-Darmstadt, Schlossgartenstr. 8 64289 Darmstadt; [2]GSI Helmholtzzentrum für Schwerionenforschung

Introduction

Beam coupling impedance can cause excessive heat load and coherent beam instabilities in high intensity synchrotrons. Therefore, a quantification of the beam coupling impedance for the components in SIS100 is outlined. We describe the development of a 2D Finite Element (FEM) frequency domain solver for longitudinal and transverse beam coupling impedances for arbitrary relativistic beam velocity. This solver can compute space charge and resistive wall impedances on a triangular mesh. It is based on the open source FEM package FEniCS [1] and mesh generator GMSH [2] and it is available for download at [3].

The beam coupling impedance of different components was also measured by the wire method. The wire method is based on emulating the electromagnetic fields of a particle beam by a TEM mode, i.e. it corresponds only to an ultra-relativistic beam. In the following we show a comparison for a ferrite ring, which is also analytically accessible.

A Ferrite Ring as Example

A ferrite ring of outer diameter 3.05cm and length 2.54cm was chosen for the validation of both measurement technique and our simulation code. The measurement results, together with a 3D reference simulation in time domain by CST Particle Studio®[4] for relativistic velocity $\beta = 1$ can be seen in Fig. 1 (top). The discrepancy visible in the plot originates mostly from the error in the applied material data as given in the frequency domain by the manufacturer of the ring[5], and the fit of these data on a impulse response function, necessary to perform time domain computations. The measurement was performed with a Vector Network Analyzer, where the longitudinal impedance is obtained from the measured S_{21}-parameter by [6]

$$Z_{\parallel}(f) = 2Z_0 \ln \frac{S_{21}^{\mathrm{REF}}(f)}{S_{21}^{\mathrm{DUT}}(f)}, \qquad (1)$$

with Z_0 being the characteristic impedance and S_{21}^{REF} being the transmission in the empty measurement housing.

A 2D simulation with our code, compared to 2D analytic calculations is depicted in Fig. 1 (bottom). Such a simulation in frequency domain allows arbitrary relativistic velocity. The 2D calculations are valid for distributed impedances, i.e. above a certain length, see [7].

Details about our FEM frequency domain solver can be found in [8], and a detailed analysis of the wire measurement method is available in [7]. The wire measurement method was also applied to a SIS18 kicker magnet, see [9].

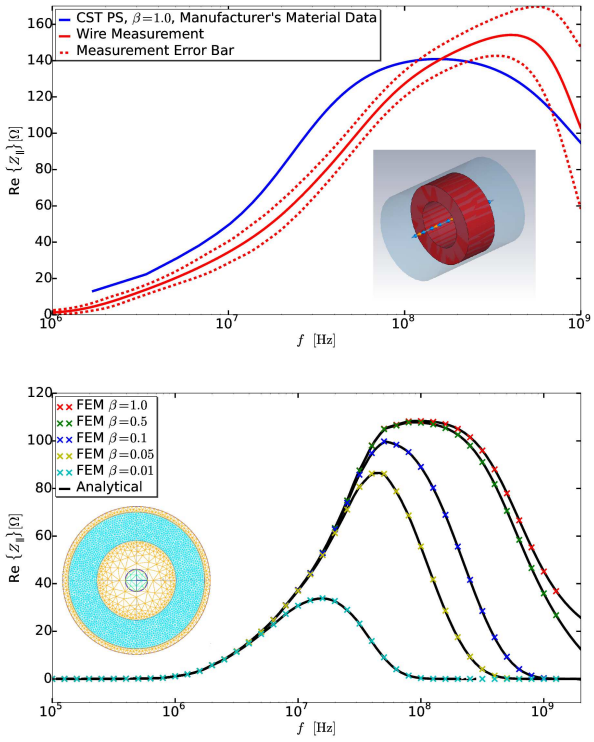

Figure 1: Top: impedance measurement using the wire method [7] vs. 3D numerical computation in the time domain. Bottom: 2D analytical and numerical calculation with the newly developed FEM code [8]. All computations rely on the manufacturer's material data [5], which is specified with 20% error range.

References

[1] FEniCS, www.fenicsproject.org, 2014

[2] C. Geuzaine and J.-F. Remacle, GMSH, www.geuz.org/gmsh, 2014

[3] https://bitbucket.org/uniederm/beamimpedance2d/src, 2015

[4] CST Studio Suite 2013, www.cst.com

[5] http://www.amidon.de/contents/de/d542.html, accessed 2013

[6] L. S. Walling et al., NIM-A 281, 433, 1989

[7] U.Niedermayer et al., NIM-A 776, 129-143, 2015

[8] U.Niedermayer et al., accepted for pub. in PR-STAB, 2015

[9] L. Eidam, Master Thesis, TU-Darmstadt, 2014

* u.niedermayer@gsi.de

DOI:10.15120/GR-2015-1-FG-SIS100-08

Emittance growth in bunches with space charge due to damping of transverse oscillations

I. Karpov[*1], *V. Kornilov*[2], *and O. Boine-Frankenheim*[1,2]
[1]TEMF TU Darmstadt, Germany; [2]GSI, Darmstadt, Germany

An emittance growth is an important issue in synchrotrons, which can reduce machine performance. One of the main sources of the transverse emittance blow-up is damping of coherent oscillations appearing after the bunch-to-bucket transfer between synchrotrons. The damping can be passive (decoherence due to chromaticity, octupoles and residual nonlinearities [1,2] and active (transverse feedback system). This process is strongly modified by space charge and rf nonlinearities, which is important for the SIS18, SIS100 synchrotrons of the FAIR project. Decoherence in long bunches due to chromaticity with space charge has been studied using measurements at the SIS18 heavy-ion synchrotron and particle tracking simulations in [3].

Recent measurements at the SIS18 were dedicated to study the influence of transverse nonlinearities and moderate space charge on the decoherence process. Bunches of Ni_{58}^{26+} ions were stored at the energy of 100 $\mathrm{MeV/u}$ and kicked transversally with a kick duration of one turn. The resulting transverse oscillations have been recorded with the help of beam position monitors. At the same time, the time evolution of the transverse emittance (using an ionization profile monitor) and the beam current has been stored. In order to model the effect of transverse nonlinearities (because of absence of octupoles magnets at the SIS18) the closed orbit was optimized or distorted for different measurements.

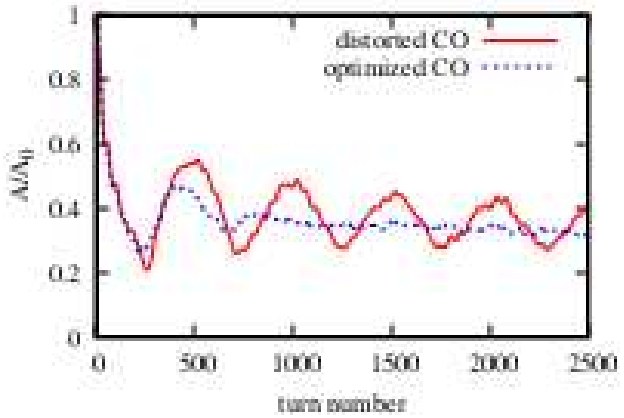

Figure 1: The time evolution of the bunch offset amplitude

As an example figure 1 shows the evolution of the bunch offset amplitude A normalized by the initial value A_0 extracted from the measured signals for two closed orbit settings. Figure 2 produced by plotting the bunch vertical traces and subtracting the total bunch offset, thus reducing the contribution of the head-tail $k = 0$ mode, shows a clear one-knot structure of the mode $k = 1$ which was not damped in the case of induced transverse nonlinearity. For this case the stronger emittance blow-up and beam losses were observed. The goal of theses studies is a detailed understanding of the interplay of the different effects.

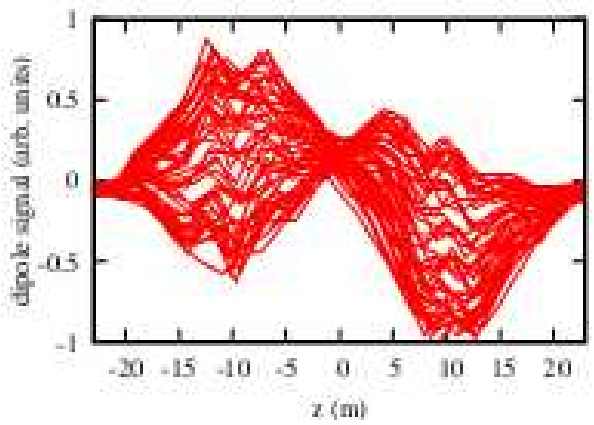

Figure 2: Traces of the transverse bunch signal for 50 consecutive turns. This result proves that the $k = 1$ remains during the process of bunch decoherence in the case of strong transverse nonlinearity.

For the SIS100 synchrotron the resulting bunch decoherence and beam blow-up is due to a combination of the lattice settings (like chromaticity), nonlinearities (residual or imposed by octupole magnets), strong space-charge, and the transverse feedback system. The next step is to study these effects for the SIS100 parameters using particle tracking simulations with the objective of correct combinations for a controlled beam blow-up. The results will be used for determination of requirements for the active and passive damping of coherent bunch oscillations at the SIS100.

References

[1] R.E. Miller, A.W. Chao, J.M. Peterson, S.G. Peggs, M. Furman, SSC Report SSC-N-360 (1987).

[2] M.G. Minty, A.W. Chao, W.L. Spence, Proceedings of PAC95, Dallas, Texas, USA, p. 3037 (1995).

[3] V. Kornilov, O. Boine-Frankenheim, Transverse decoherence and coherent spectra in long bunches with space charge Phys. Rev. ST Accel. Beams 15, 114201 (2012).

* karpov@temf.tu-darmstadt.de

DOI:10.15120/GR-2015-1-FG-SIS100-09

Verification of the longitudinal feedback topology in SIS18*

K. Groß†[1], *U. Hartel*[2], *H. Klingbeil*[1,2], *U. Laier*[2], *D. Lens*[2], *K.-P. Ningel*[2], *S. Schäfer*[2], *and B. Zipfel*[2]
[1]TEMF, TU Darmstadt, Germany; [2]GSI, Darmstadt, Germany

Introduction

To damp oscillations of bunched beams, SIS100 will be equipped with a bunch-by-bunch (BxB) longitudinal feedback system (LFB). This helps to stabilize the beam, to keep longitudinal emittance blow up low and to minimize beam losses. The proposed LLRF topology of the closed loop system is, in some aspects, similar to the beam phase control system [1]. The difference and challenge is mainly the BxB signal processing followed by the generation of a correction voltage in dedicated feedback cavities. The adapted topology was verified at SIS18 during a beam time in 2014 using LLRF prototype subsystems and the two ferrite acceleration cavities.

Experimental Setup

Instead of applying the frequency correction Δf to the group DDS, i.e. to *all accelerating cavities*, the phase correction $\Delta\varphi$ is converted into an additional, phase shifted RF signal Δu and fed into *dedicated feedback cavities* resulting in an I/Q modulation of the total voltage u_{total} seen by the beam (Fig. 1, bottom right). Copies of the setups shown in Fig. 1 are used to determine the excitation and the required correction voltage for each bunch (and mode). The gray-shaded paths were cut to length to reach all interaction points with the same time delay. During acceleration, the phase $\varphi(f)$ has to be set according to the frequency-dependent phase response of LLRF components and cavity system.

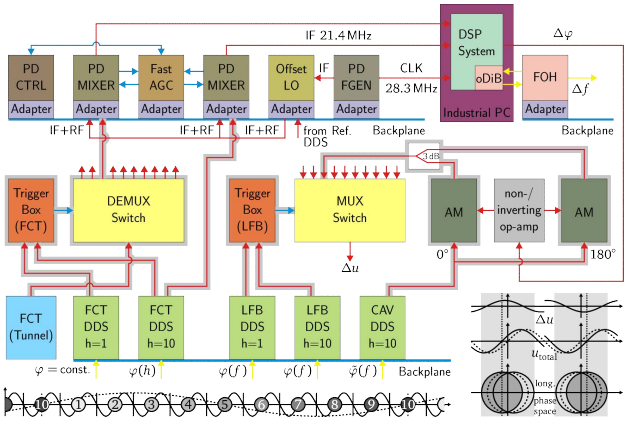

Figure 1: Sketch of LLRF of beam phase control system [2, 3] (top) with modifications for the LFB system (center) and principles of operation (bottom).

* Work supported by the German Federal Ministry of Education and Research (BMBF) under the project 05P12RDRBF.

† gross@temf.tu-darmstadt.de

Measurement Results

In 2014 individual bunches have been tracked several times over complete SIS cycles at harmonic number $h = 2$ and $h = 4$. In particular, coupled bunch oscillations (Fig. 2), as intentionally excited on Oct. 16th, can now be detected using the DDS-triggered demultiplexing of the beam signal (Fig. 1, bottom left).

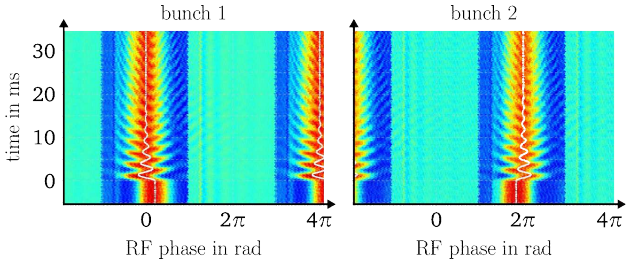

Figure 2: Waterfall plot of single bunches at $h = 2$ with BxB phase detection $\Delta\varphi$ (white lines) using one DSP system per bunch for an out-of-phase excitation.

A triggered LLRF signal (Fig. 3, left) providing the correction voltage for an individual bunch (cf. Fig. 2, left) at flattop was generated for the first time on Oct. 18th. The achieved damping of dipolar bunch oscillations shown in Fig. 3 (right) is a *proof of principle* for the proposed topology of the longitudinal feedback system.

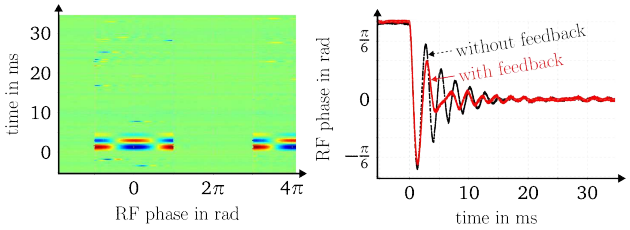

Figure 3: BxB LLRF correction signal Δu (left). Damping of dipole oscillations in SIS18 on Oct. 18th, 2014 (right).

The authors would like to thank D. Ondreka and H. Liebermann for the support and the customized machine setup which allowed to use one of the two main ferrite cavities as dedicated feedback cavity.

References

[1] Klingbeil et al., IEEE Trans. Nuc. Sci., Vol. 54, No. 6 (2007).

[2] Klingbeil, Laier, Regelsystemtopologie SIS18, internal note, revision 1.00, GSI (2009).

[3] Laier, SIS HF Phasen Synchronisationstopologie, internal note, revision 1.50, GSI (2011).

CC BY

A novel DC current transformer using magneto-resistance sensors for FAIR

E. Soliman[1, 2], H. Reeg[1], M. Schwickert[1], K. Hofmann[2]
[1]GSI, Darmstadt, Germany; [2]IES Institute, TU Darmstadt, Germany.

A Novel DC Current Transformer (N-DCCT) for FAIR SIS100 is under development at GSI Beam Diagnostic department in collaboration with IES Institute of TU Darmstadt. DCCTs are used as non-intercepting standard tools for online beam current measurement in synchrotrons and storage rings. The working principle of commonly used DCCTs is well known [1]. However, at certain bunch frequencies in ring accelerators inaccurate readings are observed due to inter-modulation distortion. The N-DCCT senses the magnetic field created by the ion beam current, using Tunneling Magneto-Resistance (TMR) sensors. Also a closed-loop N-DCCT is currently under development.

TMR Sensor for N-DCCT

Currently a N-DCCT based on TMR sensors is under development at GSI. The N-DCCT open-loop structure is shown in Figure 1 [2]. The main measurement principle is precise detection of the ion beam DC magnetic field by TMR sensors. In the present setup the TMR sensors from MultiDimension Company [3] are placed inside an air gap of a high permeability ferromagnetic ring core with 10 mm width (VITROVAC ‘6025F’). The value of the magnetic field inside the air gap is calculated according to the following formula:

$$B_{gap} = \frac{\mu_o}{d} I_P \qquad (1)$$

Where B_{gap} is the magnetic field inside the air gap in Tesla, µo is the permeability of vacuum in Tm/A, I_P is the beam current and d is the air gap width in m.

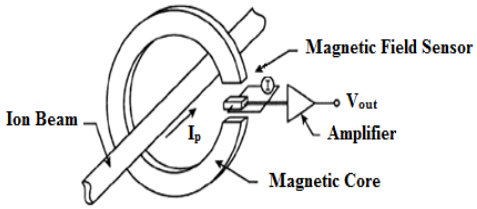

Figure 1: N-DCCT Open Loop Structure.

The TMR’s output voltage is directly proportional to the ion beam current. A voltage amplifier is added to enhance the N-DCCT resolution. Printed circuit boards were fabricated to compare the performance of different MR sensors. A test setup has been prepared for the N-DCCT as shown in Figure 2. A mechanical support was manufactured to hold the flux concentrator. In addition a µ-metal box for shielding covers the whole N-DCCT test setup.

* Work supported BMBF project ID: 05P12RDRBG.
#pt@desy.de

A DC current is generated in a conducting wire at the center of the core using a power amplifier and a signal generator. The value of the produced voltage from the power amplifier is ±32V. This will produce a ±0.32A in the wire. The value of the magnetic field intensity in the air gap of the core will be ±0.04mT. The output voltage of the TMR sensors is amplified with a voltage amplifier of gain 10.

Tests were carried out for two different TMR sensors, MMLH45F and MMLP57F. Figure 3 shows the output voltage of the N-DCCT versus input current for the MMLH45F. The slope of transfer characteristic is the sensitivity of the N-DCCT. The measured value from the experimental test is 0.566V/A, while the theoretical value is 0.75V/A. The sensitivity of the TMR sensor to the magnetic field is 0.453V/mT from the measurements and 0.6V/mT from the sensor’s datasheet. Measurements with the sensor type MMLP57F yielded a sensitivity of 0.275 V/A, compared to 0.31V/A (datasheet). The noise analysis for the system is currently under investigation.

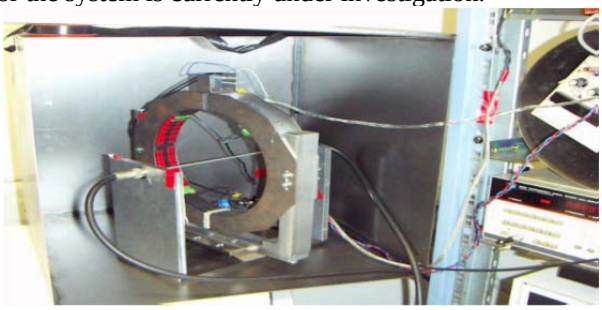

Figure 2: N-DCCT Test Setup.

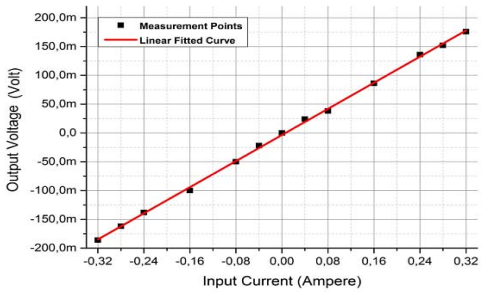

Figure 3: Output Voltage of the N-DCCT.

References

[1] K. Unser, “A Toroidal DC Beam Current Transformer with High Resolution”, IEEE Trans. Nuclear Science, NS-28 No. 3, June 1981
[2] M. Häpe et al., “High Dynamic Magnetic Beam Current Measurements ...”, DIPAC’05, May 2005, p. 102; http://www.JACoW.org
[3] MultiDimension Technology Co., Ltd., (CN)
[4] VACUUMSCHMELZE GmbH & Co. KG, (D).

DOI:10.15120/GR-2015-1-FG-SIS100-11

Heavy ion induced desorption measurements on cryogenic targets *

Ch. Maurer† [1,2], *L.H.J. Bozyk*[1], *P.J. Spiller*[1], *and D.H.H. Hoffmann*[2]
[1]GSI, Darmstadt, Germany; [2]TU Darmstadt, Institut für Kernphysik, Germany

Introduction

Heavy ion impact induced gas desorption is a key process that drives beam intensity limiting ionization losses in heavy ion synchrotrons. Minimizing this effect, by providing low desorption yield surfaces, is an important issue for maintaining a stable ultra high vacuum during accelerator operation with medium charge state heavy ions. At room temperature the desorption yield per incident ion η is known to scale with the electronic energy loss at the surface [1]. Nevertheless, measurements with the prototype cryocatcher for SIS100 showed a different scaling [2], which needs to be understood. An experiment to systematically examine this behaviour is presented. The cryogenic beam-induced desorption yields at different temperatures and for different beam parameters are investigated.

Experimental Setup

The experiment described in this article has been set up at the SIS18 at GSI. Its UHV system is connected to the accelerator's beamline via a differential pumping line, containing a conductance limiting pipe with small diameter. In the target area a pressure in the 10^{-10} mbar regime has to be reached in order to clearly resolve the desorption peaks. Therefore, the setup is partially baked. The cryogenic target has the geometry of the SIS100 cryocatcher's front part and is cooled by a coldhead. It gets hit by a fast extracted 1μs beam pulse. Gas desorbed by the beam impact spreads in the diagnostic volume which is well defined by the pipe mentioned above. The pressure evolution is measured an extractor gauge. A more detailed description of the setup is given in [3].

Methodology of the measurements

The extraction of the beam from the synchrotron triggers a fast pressure measurement of 10 s duration. It allows a fine resolution of pressure rise and relaxation, out of which the amplitude of the pressure peak is determined. By using the ideal gas law and the number of beam particles a desorption yield is obtained. The temperature of the target is varied by a heater and by activating and deactivating the coldhead. Measurements at intermediate temperature levels were taken with a thermally drifting target.

Results

The determined desorption yield η is plotted in figure 1 against the beam energy for different experimental parameters. At or close to room temperature the known scaling with the electronic energy loss at the surface could be observed. However, at cryogenic temperatures the scaling looks different than at room temperature, which is not yet understood. An accordance with earlier measurements with the cryocatcher protoype [2] could not yet be found.

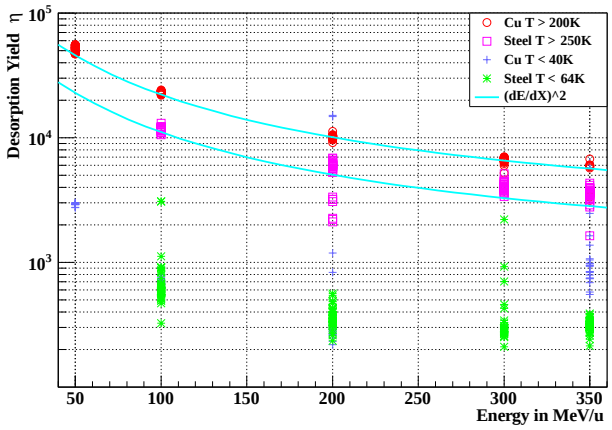

Figure 1: Comparison between the energy dependance of η for different experimental parameters.

Outlook

Data obtained from this experiment is still undergoing analysis, so no concluding statement can yet be made. A central part of this analysis will be a gas dynamic simulation to better understand the influence of de/adsorption on the setup's other cold/warm surfaces. Different experimental geometries are also bound to factor into the results, which will also be investigated by this method.

References

[1] H. Kollmus et al., "Measurements of Ion-beam Loss Induced Desorption at GSI", in AIP Conf. Proc. **773**, p. 207 (2005)

[2] L.H.J. Bozyk, H. Kollmus, P.J. Spiller, "Development of a Cryocatcher-System for SIS100", in Proc. of IPAC 2012, p. 3239

[3] Ch. Maurer et al., "Heavy Ion Induced Desorption Measurements on Cryogenic Targets," in Proc. of IPAC 2014, p. 867

* This project is funded by the german ministry for education and research (FKZ 06DA7031)

† C.Maurer@gsi.de

Systematic measurement of the pumping properties of a cryogenic surface

F. Chill[1,2], *L. Bozyk*[2], *O. Kester*[1,2], *and P. Spiller*[2]
[1]Goethe-Universität, Frankfurt, Germany; [2]GSI, Darmstadt, Germany

Introduction

The residual gas density in the beam vacuum system of a heavy ion synchrotron is a crucial factor for stable and reliable beam operation at highest intensities. The Interaction of the beam particles with the residual gas may cause severe beam loss. In combination with ion impact stimulated gas desorption from the beam pipe, this can lead to a reduced beam lifetime and transmission of the acceleration cycle. Therefore, beam induced pressure rise must be suppressed by the pumping system.

To achieve proper vacuum conditions, the vacuum chambers of SIS100 will act as cryogenic surface pumps. Cryogenic surfaces are able to pump gases according to their saturated vapor pressure (SVP) curves. This process is called *cryocondensation*. The reachable pressures for all heavy gases are sufficiently low for stable beam operation. The SVP of hydrogen is too high even at a temperature of 4.2 K. If the surface coverage is sufficiently low, hydrogen can be pumped to lower pressures by so called *cryosorption* [1]. This effect can be characterized by two parameters: The *sticking coefficient* which is the probability of a gas particle impacting on the surface to be bound. It is directly linked to the pumping speed provided by the cryogenic walls. The *mean sojourn time* describes how long a particle remains bound to a surface. Both parameters together determine the equilibrium pressure. This pressure as a function of the surface coverages at a specific temperature is called *isotherm*.

Measurements at cryogenic temperatures

An UHV experiment (see Figure 1) to determine these parameters has been set up. The cold surface is provided as a small stainless steel chamber which is cooled by a cryocooler. So far, measurements in the temperature range from 7.2 to 23 K have been conducted. The lower corner valve remains closed once the cryostat reaches its target temperature. It is adjusted by resistive counter heating of the inner chamber. Subsequently, hydrogen is let into the cryostat through the copper orifice. The gas flow is monitored by two extractor gauges. Its magnitude equals the pumping speed of the cold surface. Its value suggests, that all the particles entering the inner chamber are bound and do not reflect back through the Cold-Warm-Transition. In this case, the sticking coefficient is close to one and seems to be mostly independent of temperature and surface coverage within the examined range. The gas flow is stopped from time to time by closing the gate valve until an equilibrium pressure is reached. Integration of the gasflow over time yields the currently accumulated surface coverage. This value and its corresponding equilibrium pressure results in one point on the isotherm. The resulting isotherms for different temperatures are shown in Figure 2.

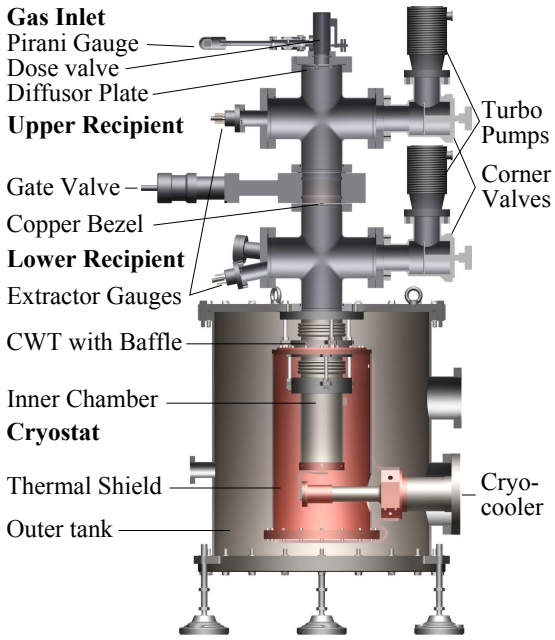

Figure 1: Measurement setup for cryosorption.

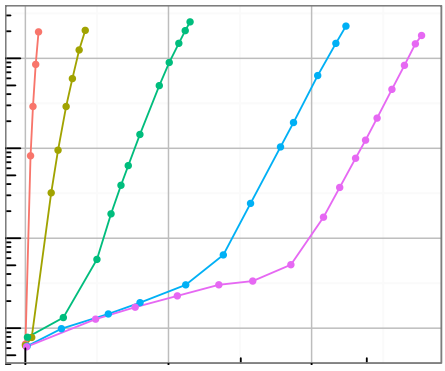

Figure 2: Preliminary isotherms for H_2 on stainless steel. A coverage of $\approx 2.2 \cdot 10^{15}$ cm^{-2} equals one monolayer [2].

References

[1] E. Wallén, J. Vac. Sci. Technol., A 14, 1996, p. 2916

DOI:10.15120/GR-2015-1-FG-SIS100-13

[2] K. Jousten, Wutz Vakuumtechnik, Springer 2013, p. 236

CC BY
DOI:10.15120/GR-2015-1-FG-SIS100-13

FLUKA study of beam loss monitors for SIS100: General diagnostics and quench prevention of superconducting magnets

S. Damjanovic[1]
[1]GSI, Darmstadt, Germany

In view of the planned coverage of the synchrotron SIS100 with beam loss monitors (BLMs), FLUKA studies were performed aiming at two goals: to evaluate the sensitivity of these detectors to the expected beam losses at SIS100, and to estimate the BLM quench prevention thresholds via the correlation between the energy deposition inside the superconducting coils and the BLM active volume. A large number of ion species and energies were considered. The results of these studies, described in detail elsewhere [1], very much support the use of the BLMs for quench prevention (protection of magnets) via an interlock generation, as used at the LHC.

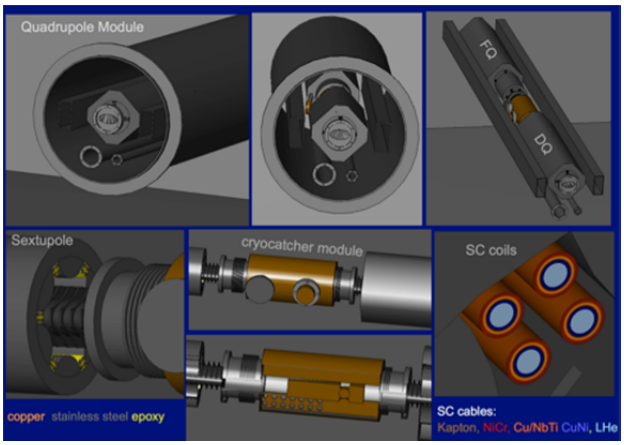

Figure 1: FLUKA geometry of a quadrupole module.

The goal as described required a precise modelling of the geometry of a SIS100 quadrupole module, the SIS100 extraction straight section and the SC coils including the cable details (Fig.1).The results on the response of the LHC-IC type BLMs to the beam losses within the warm quadrupole doublet of the SIS100 extraction straight section show a great sensitivity of these monitors. Instantaneous radiation caused by 0.1% beam loss at injection- and 0.0001% at extraction energy will be detected if BLMs are placed close to the source.

The different aspects of machine protection are usually based on a variety of systems. Quench prevention of SC magnets can only be ensured by a BLM system, the only active system in case of fast losses with time scales between 100 μs and 10 ms. While the total energy and therefore the overall damage potential is very much larger at the LHC, certain accidental scenarios can be equally severe at SIS100, due to the Z^2 dependence of the initial energy deposition. The responsible quantity for the quenching of SC coils is the local energy deposition, and as little as 1mJ/cm^3 quenches a magnet. Quenching would cause a downtime of more than hour, while real damage of a single magnet would cause much longer downtimes at very high costs. All this suggests that the protection of the SIS100 machine should also be strict.

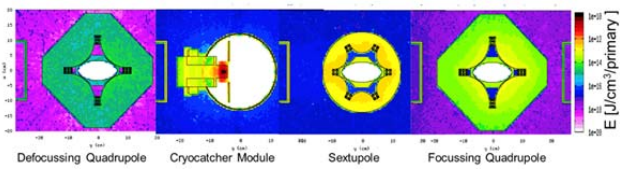

Figure 2: Energy deposition in the region of the SC coils.

The possibility of quench prevention of the SIS100 SC magnets by the planned BLM system has been studied with FLUKA simulations. As a representative example for a source of beam loss at SIS100, the losses due to charge exchange of U^{28+} beams were examined. The corresponding special distribution of the energy deposition within the individual components of a quadrupole module is shown in Fig.2. The LHC-IC type BLMs were found to be sensitive both to the quench prevention thresholds and to the loss rates expected due to these losses. In addition, a number of other ion species and energies including protons were considered to demonstrate a comparable sensitivity for all other beams to be accelerated with SIS100.

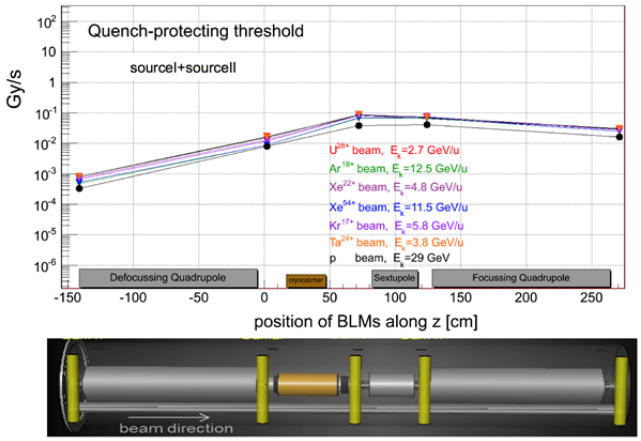

Figure 3: BLM quench prevention threshold along a quadrupole module for p and ions beams of different E.

An interesting finding of this study (Fig.3) was that, for the same beam loss location, the quench-prevention thresholds were almost identical for all ion species/energies including protons. In the future, a systematic investigation of all possible failures at SIS100 is required to optimally integrate the BLM system into the beam interlock system.

References

[1] S. Damjanovic, EDMS Note, Document FAIR-1SBDX-ER-0001, Id 1473055 (2015).

DOI:10.15120/GR-2015-1-FG-SIS100-14

FLUKA simulation of LHC BLMI response functions for different particles

V. S. Lavrik[1,2] *and A. Reiter*[1]

[1]GSI, Darmstadt, Germany; [2]Goethe University Frankfurt am Main, Frankfurt, Germany; GSI, Darmstadt, Germany

LHC-type beam loss monitors based on ionization chamber (LHC BLMI) are planned as beam loss detector for SIS 100 operation. This type of beam loss monitor has different response functions for various particle types. In this contribution FLUKA[1] simulations of the response functions for different types of particles are presented. In order to simulate a response function of the beam loss monitor, the model of BLMI was implemented in the Monte Carlo code FLUKA.

The BLMI consists of 60 parallel plate ionization chambers packed in a stainless steel cylindrical vessel with a 2 mm wall and covered on top and bottom by two stainless steel plates 5 mm and 4 mm thick respectively. The signal is created by collecting electron-ion pairs on a pile of 61 parallel aluminum electrodes with a thickness of 0.5 mm, diameter 75 mm and equally spaced by 5.75 mm. Electrodes are held by 6 stainless steel rods which are in turn fixed by insulating ceramic pieces. The volume of a detector is filled with nitrogen gas with overpressure of 100 mbar.

An ionizing particle deposits energy into the volume of BLMI and creates electron-ion pairs which are collected by electrodes. The minimum energy, which a particle needs in order to create an electron-ion pair, the so called W-factor, is 35 eV for nitrogen. The energy deposition was calculated by FLUKA in a sensitive volume between the electrodes and then converted into charge per primary simulated particle. The result is compared with simulations performed in Geant4 (version 8.0 patch-01) by CERN BLM group[2].

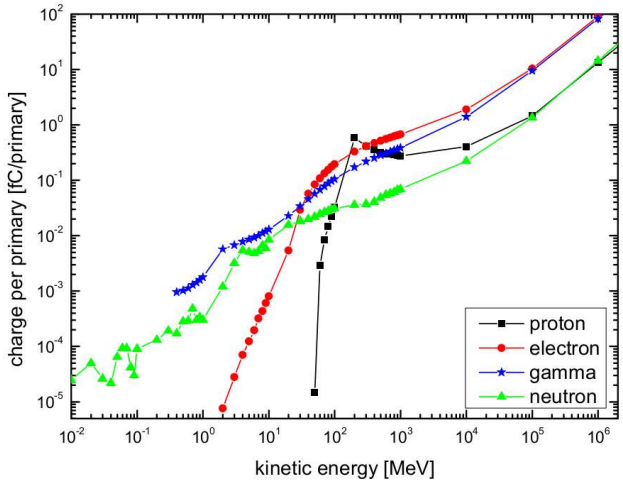

Figure 1: Response of the ionization chamber for particles impacting longitudinally to the detector axis.

Two series of simulations were performed depending on the impact direction of the beam: a longitudinal impact direction (the beam is uniformly distributed, parallel to the detector axis and has a circular cross section with a diameter of the detector) and transversal (the beam is uniformly distributed and has a rectangular cross section which is matched with a detector cross section). The response function was obtained for 4 types of particles: protons, electrons, gammas and neutrons in the range of 10KeV up to 1TeV.

The result of simulations is presented in Figures 1 and 2. The behavior of corresponding curves is similar for two different simulations. But the amplitude of the response functions in case of longitudinal irradiation is higher, because the large amount of material, traversed by the beam, generates a higher number of secondary particles. Both figures match the Geant 4 simulations which were cross checked with the experiment. These results are the base for further optimizations of the future SIS 100 Beam Loss Monitoring System.

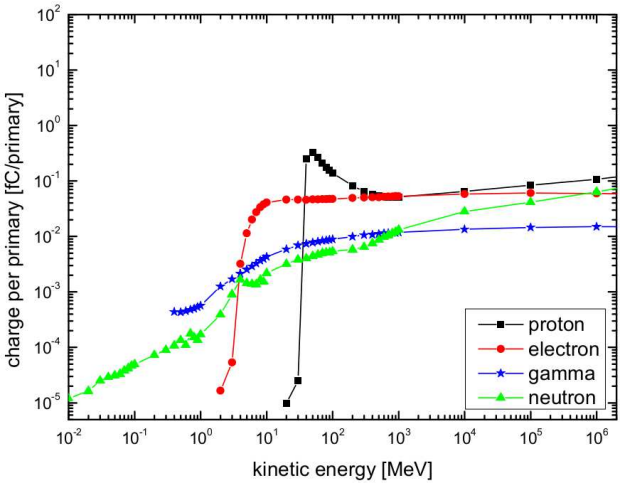

Figure 2: Response of the ionization chamber for particles impacting transversally to the detector axis.

References

[1] "The FLUKA Code: Developments and Challenges for High Energy and Medical Applications" T.T. Böhlen, F. Cerutti, M.P.W. Chin, A. Fassò, A. Ferrari, P.G. Ortega, A. Mairani, P.R. Sala, G. Smirnov and V. Vlachoudis, Nuclear Data Sheets 120, 211-214 (2014)

[2] M.Stockner et. all, CERN-AB-2006-086 BI

DOI:10.15120/GR-2015-1-FG-SIS100-15

Laboratory tests of beam loss monitor detectors for SIS 100*

V.S. Lavrik[1,2], *P. Boutachkov*[1], *S. Damjanovic*[1], *and B. Voss*[1]
[1]GSI, Darmstadt, Germany; [2]Goethe University Frankfurt am Main, Frankfurt, Germany

A main source of primary beams at FAIR will be the SIS 100 synchrotron. SIS 100 will deliver ion beams with more than two orders of magnitude higher intensity than SIS 18 and will be operated in a range of 18-100 Tm rigidity. During the machine operation beam losses are unavoidable. In order to achieve quantitative determination of beam losses LHC-type beam loss monitor (BLMI) are foreseen[1]. This detector is robust, easy to maintain and has a well understood response. This contribution describes the bench test and characterization of BLMI.

The CERN LHC beam loss monitor consists of parallel plate ionization chambers, packed in a cylindrical stainless steel vessel with a wall thickness of 2 mm. The volume of a detector is filled by nitrogen gas under overpressure of 100 mbar. The standard operation point for the detectors is 1.5 kV.

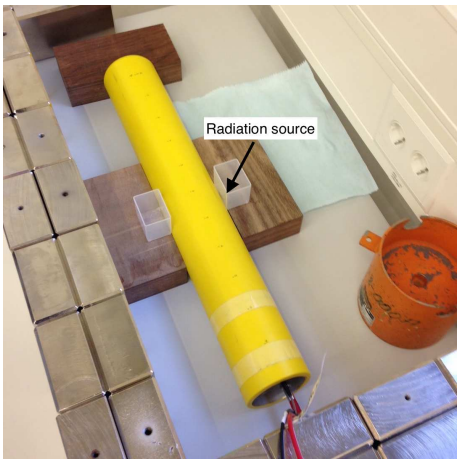

Figure 1: Testing bench of a BLMI characterization

Characterization of BLMI was performed in the detector laboratory of GSI. The test bench is shown in Figure 1. BLMI (yellow tube) was placed in a location which was surrounded by iron bricks in order to prevent unnecessary irradiation to the personnel. ^{60}Co γ source with activity of 2.3 MBq was placed on the detector surface as indicated in Figure 1. The ionization current was measured by a Keithley 6485 picoampermeter.

Two series of measurements were done: without a radiation source and with a radiation source. The results are shown in Figure 2. The black squares represent an ionization current with a subtracted leakage current for the corresponding detector. According to the experimental data all

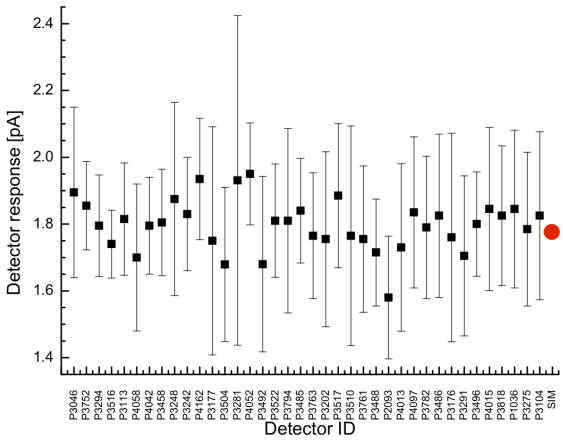

Figure 2: Black squares: ionization current in a ^{60}Co radiation field (leakage current is subtracted); red circle: FLUKA simulation

detectors have the same efficiency within the error bars.

The model of BLMI was implemented in FLUKA Monte-Carlo code[2]. The response function of a detector was calculated in an isotropic ^{60}Co radiation field and compared with a measured ionization current (Figure 2 red circle). Simulated response matches with measured ionization current within the error bar.

A testing bench for BLMI acceptance test was established and 38 BLMIs were characterized in the detector laboratory of GSI. The acceptance test shows that all the detectors have uniform response and can be integrated into the SIS 100 beam loss monitoring system. Also FLUKA simulations were done and match measured response within the error bars.

References

[1] Measurements and Simulations of Ionization Chamber Signals in Mixed Radiation Fields for the LHC BLM System M.Stockner et. all, CERN-AB-2006-086 BI

[2] "The FLUKA Code: Developments and Challenges for High Energy and Medical Applications" T.T. Böhlen, F. Cerutti, M.P.W. Chin, A. Fassò, A. Ferrari, P.G. Ortega, A. Mairani, P.R. Sala, G. Smirnov and V. Vlachoudis, Nuclear Data Sheets 120, 211-214 (2014)

* Work supported by BMBF-Projekt 05E12CD1

DOI:10.15120/GR-2015-1-FG-SIS100-16

Survey and alignment of the synchrotron SIS18

V. Velonas[1], I. Pschorn[1], T. Miertsch[1], K. Knappmeier[1]
GSI, Darmstadt, Germany

To fulfil the intensity requirement of the GSI Facility as well as projects and conceptions of the future facility of FAIR, a number of high precise geometrical 3D measurements as well as conceptual work have been carried out during the past year. Responsible for these activities was the survey and alignment (S&A) group of GSI, which is assigned to the project division *Engineering* within *FAIR@GSI*. The S&A team is involved in many projects like i.e. CryRing, EMTEX, SIS100 “first-of-series”(FOS) dipole and others for the different FAIR and GSI machines. This short report focusses on the realignment of the SIS18 synchrotron, which was carried out completely in one go, what was never done since the first installation.

A low grade of quality of the circling beam in the SIS18 made the commissioning in February 2014, after a 1 year lasting shutdown period, very difficult. This fact and the hypothesis that the construction activities for the future FAIR facilities, including piling and lowering the ground water level, will have an impact in the current position of the machine, lead to a total survey of the actual position of all SIS18 magnets, BPM and adjacent machine parts by 3D measurements.

Measuring the 3D point network, a Laser Tracker and a level instrument were used. The surveying of SIS18 was carried out within four days. All fiducials on the components just like the temporary points on the wall and pillars as well as the Laser Tracker stations were included in the network adjustment. Parts of the transfer line to the synchrotron (TK) as well as the HEBT area behind the SIS18 were surveyed in order to supervise these transit areas of the beam. The accuracy of the network points after the free adjustment, which was done to define the inner geometry of the network (minimal constraints), was between 0.02mm to 0.05mm in all three directions. For the geodetic datum only the fiducials on the dipoles were used. After the final adjustment calculation it turned out that the new coordinates had a huge variation regarding to the nominal coordinates. The relative deviation between the components in the lateral and in the vertical position was up to 4mm and 5mm respectively [1].

A major realignment of the whole area was needed from the analyses of the results.

All components of the SIS18 should be aligned, as well as four quadrupoles in TK9 area. The TASA-point system requires for alignment the use of a Laser Tracker to measure the two fiducial points on the magnets together with inclinometers that are needed to determine the precise lateral inclination of the components. In contrast to the magnets BPM chambers have up to now no fiducial points with a precise reference to the internals. Thus, the specified actual position of BPM internals and their alignment was based on assumptions.

The alignment tolerances for magnets and BPM in lateral and vertical direction were defined as better than 0.2mm; in a few cases up to 0.5mm was acceptable. The remaining lateral tilt after alignment should not exceed 0.1mrad.

Some problems appeared during the alignment which was relative with the number of the adjustment feet of the components. It was confirmed again that the alignment of a three-feet-component is much friendlier and faster compared to a component with four feet.

With few exceptions - caused by mechanical reasons - all magnets could be aligned within tolerance (fig. 1, 2). The complete alignment was carried out within four weeks.

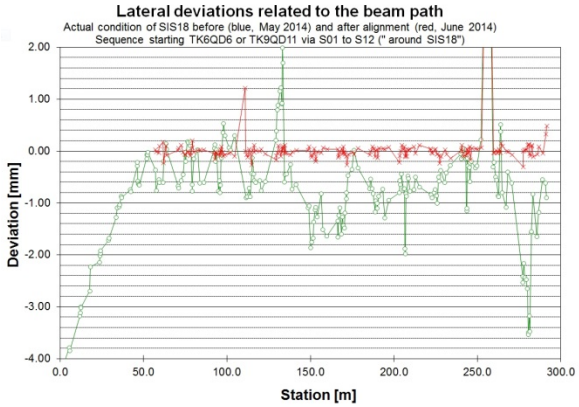

Figure 1: Beam plot for synchrotron SIS18. Lateral deviation before (green) and after (red) alignment

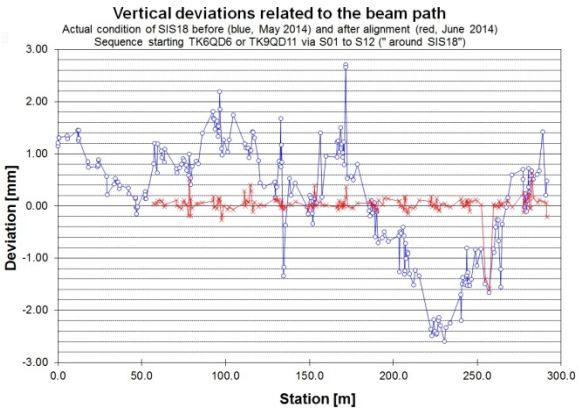

Figure 2: Beam plot for synchrotron SIS18. Vertical deviation before (blue) and after (red) alignment

References

[1] I. Pschorn, T. Miertsch, K. Knappmeier, V Velonas, „SIS18 Netz und Justage – interne Reports“

[1]alignment@gsi.de

DOI:10.15120/GR-2015-1-FG-SIS18-01

Observation of dynamic transverse emittance exchange in SIS-18

R. Singh, P. Forck, G. Franchetti, T. Giacomini, and P. Kowina
GSI, Darmstadt, Germany

The theory of linear coupling and the consequent dynamic emittance exchange is well known [1]. Transverse beam emittance exchange due to linear coupling was observed in SIS-18 during regular accelerator operation. Skew-quadrupoles are installed at GSI SIS-18 to control and utilize the linear coupling e.g. for optimization of the injection efficiency [2]. However, these skew-quadrupoles are not used during the normal operations, and any linear coupling due to misaligned magnets is usually neglected. Careful measurements were performed to verify the role of tune crossing on this exchange process. Preliminary attempts for compensation of linear coupling were made, using the emittance exchange as a diagnostic observable.

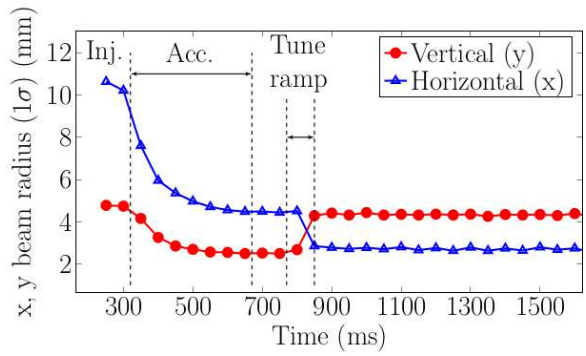

Figure 1: Evolution of the beam radii during the acceleration cycle during the high intensity operations at SIS-18.

Figure 1 shows the evolution of horizontal and vertical beam dimensions measured using an Ionization profile monitor (IPM) during the acceleration cycle for a high intensity (10^{10} stored particles) N^{7+} beam in the slow extraction mode. The high intensity working point at injection is $Q_x = 4.16$ and $Q_y = 3.29$. On the extraction flattop, the horizontal tune was ramped from $Q_x = 4.16$ to $Q_x = 4.33$ in $\approx$ 100 ms for the resonant slow extraction. Simultaneous transverse Schottky measurement established that the tune crossing and thus the linear coupling was the cause of this exchange. Figure 2 (top) shows the time evolution of the transverse beam profile before and after the exchange.

In follow-up measurements during summer 2014, emittance exchange was regularly observed due to tune crossing. This emittance exchange due to "residual" linear coupling is undesired since it led to beam losses when the vertical aperture could not accommodate the larger vertical beam due to emittance exchange. Therefore, first attempts for compensation of linear coupling were performed. The emittance exchange served as an online diagnostic for linear coupling. A scan of relative strengths of the two skew-quadrupoles was made such that, a compensation vector opposite to the natural skew error was constructed. Figure 2

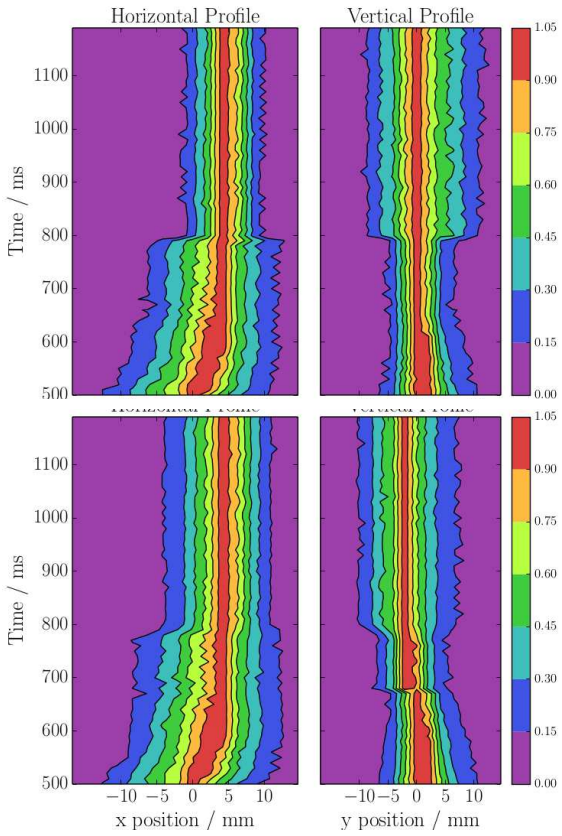

Figure 2: Horizontal and vertical beam profile evolution during the emittance exchange process for uncompensated (top) and compensated (bottom) linear coupling.

shows a comparison of transverse beam profile evolution with (bottom) and without (top) compensation. The plot shows the emittance exchange and a partial compensation of linear coupling. The reasons for partial compensation of linear coupling are unclear. Perhaps, the minimum strength of skew quadrupoles was too strong for construction of appropriate compensation vector. Linear coupling has been utilized beneficially at several synchrotrons and a better control of linear coupling is foreseen at SIS-18.

References

[1] A. Franchi et al., "Emittance sharing and exchange driven by linear betatron coupling in circular accelerator", PRST-AB 10, 064003 (2007)

[2] W. Daqa et al., "Linear Coupling With Space Charge in SIS18", Proceedings of IPAC10, Kyoto, Japan (2010)

DOI:10.15120/GR-2015-1-FG-SIS18-02

Space charge effects on quadrupolar oscillations in SIS-18

R. Singh, P. Forck, and P. Kowina
GSI, Darmstadt, Germany

Quadrupolar or beam envelope oscillations give valuable information about the injection matching and the incoherent space charge tune shift. The shift in quadrupolar mode oscillation frequency with respect to beam intensity gives a direct estimate of space charge tune shift. An asymmetric pick-up [1] is installed in SIS-18 to observe the quadrupolar moment oscillations.

Figure 1 shows the quadrupolar pick-up installed in SIS-18 along with an ion beam with horizontal and vertical displacement of $(\bar{x}, \bar{y})$ with respect to pick-up center and transverse dimensions of (σ_x, σ_y) . Let U_R, U_L, U_T and U_B be the voltages induced on right, left, top and bottom electrodes by the beam.

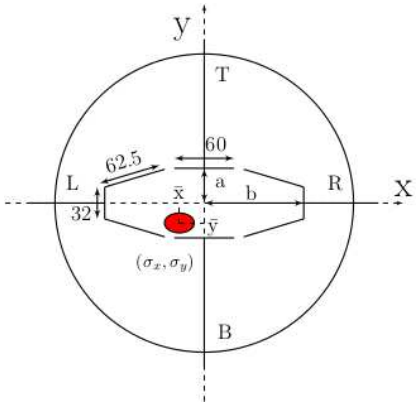

Figure 1: Front view of the pick-up design; a = 35.3 mm, b = 100.3 mm, length of the electrodes in longitudinal plane l = 216 mm. All the lengths are given in mm units.

The electrodes are connected in the "quadrupolar" configuration, i.e. $\Xi_q = (U_R + U_L) - (U_T + U_B)$ such that the quadrupolar moment of the beam $({\sigma_x}^2 - {\sigma_y}^2 + \bar{x}^2 - \bar{y}^2)$ is extracted as the first order signal component.

$$\Xi_q \propto Z \cdot I_{beam} \cdot m \cdot \left({\sigma_x}^2 - {\sigma_y}^2 + \bar{x}^2 - \bar{y}^2 \right) \quad (1)$$

where Ξ_q is the quadrupolar signal, Z is the transfer impedance of the pick-up and m is the quadrupolar sensitivity of the pick-up. Z and m are determined by electromagnetic simulations [1].

The frequency of quadrupolar oscillations is directly affected by the incoherent space charge tune shift as discussed in references [2, 3]. For an elliptic beam with a uniform transverse distribution, the space charge dependence of quadrupolar mode frequency is given by,

$$Q_{coh,1,2} = 2Q_{x,y} - (1.5 - 0.5\frac{\bar{\sigma}_{x,y}}{\bar{\sigma}_x + \bar{\sigma}_y})\Delta Q_{sc,x,y} \quad (2)$$

where ΔQ_{sc} is the incoherent tune shift, Q_x, Q_y are the horizontal and vertical tunes and $Q_{coh,1,2}$ represent the normalized quadrupolar mode frequencies. At low intensities, $Q_{coh,1,2}$ is twice the tune frequency $2 * (Q_x, Q_y)$.

Due to the absence of any suitable quadrupolar exciter in SIS-18, quadrupolar oscillations were excited using the injection beta mismatch from UNILAC to SIS-18. The beam conditions were kept similar except the injected beam current was varied from the UNILAC to increase the incoherent tune shift ΔQ_{sc}, while the quadrupolar signal Ξ_q, the mean transverse beam profile over several turns $(\bar{\sigma}_x, \bar{\sigma}_y)$ and the beam current I_{beam} was recorded.

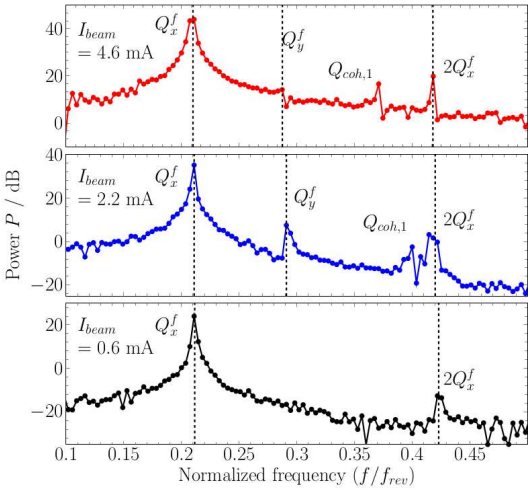

Figure 2: Shift of quadrupolar mode $Q_{coh,1}$ with respect to beam current. Q_x^f denotes the fractional part of Q_x.

Figure 2 shows the quadrupolar signal spectrum at three beam current levels. A strong mismatch was only induced in horizontal plane, and therefore only $Q_{coh,1}$ is visible in the spectrum. There was a clear dependence of $Q_{coh,1}$ on beam current in accordance to Eq. 2, as it moves away from $2Q_x^f$ as the beam current or ΔQ_{sc} is increased. Detailed report on these measurements can be found in [4].

References

[1] J. A. Tsemo Kamga et al., "Calculation of the quadrupole moment ${\sigma_x}^2 - {\sigma_y}^2$ for an asymmetrical Pick-up", GSI scientific report 2013.

[2] W. Hardt, "On the incoherent space charge limit for elliptic beams", CERN/ISR/Int. 300 GS/66.2.

[3] I. Hofmann, "Stability of anisotropic beams with space charge", Physical Review E 57 (4), 4713.

[4] R. Singh et al., "Observations of the quadrupolar oscillations at GSI SIS-18", Proc. of IBIC'14 (2014)

DOI:10.15120/GR-2015-1-FG-SIS18-03

Eigenmode computation for the GSI SIS 18 ferrite cavity*

K. Klopfer† [1], *W. Ackermann*[1], *and T. Weiland*[1]

[1]Technische Universität Darmstadt, Institut für Theorie Elektromagnetischer Felder (TEMF), Schlossgartenstraße 8, 64289 Darmstadt, Germany

Introduction

In the heavy-ion synchrotron SIS 18 two identical cavities are operated, which are loaded with the Ferroxcube 8C12m ferrite material. The permeability of the ferrites exhibits a characteristic dependence both on frequency and bias magnetic field strength. The latter is of particular importance for the tuning of the resonance frequency of the resonator system. Due to the extension of the existing facility to the FAIR, new interest in a better understanding of ferrite cavities of the SIS 18 type has aroused. As the aim of the presented study, a tool for the numerical simulation of the lowest eigenmodes of such resonators was developed. Clearly, its application to the SIS 18 cavity requires accurate material data. Hence, designated measurements were carried out at GSI.

Permeability measurement

The dependence of the permeability of the Ferroxcube 8C12m material on frequency and bias magnetic was determined using a reflection as well as a transmission measurement approach. The obtained values for low RF levels are fully compatible with each other within their estimated error margins up to moderate frequencies. A detailed discussion of the measurement results can be found in [1].

Computational approach

A dedicated solver was developed, implemented and successfully verified. It is able to efficiently handle nonlinear complex eigenvalue problems even on distributed memory machines, which arise in the context of the tensor material modeling. Furthermore, the distribution of the magnetic field excited by the bias current is precisely taken into account. For more details on the employed numerical methods we refer to [2, 3].

Analysis of the fundamental mode

The computational model used in the numerical simulation of the GSI SIS 18 cavity is depicted in Fig. 1. The simulation results for the resonance frequency of the fundamental mode are shown in Fig. 2. Also, additional results obtained with an alternative equivalent circuit model taking into account the radial dependence of the bias field are included. The simulation results are discussed in more detail in [3].

* Work supported by GSI.

† klopfer@temf.tu-darmstadt.de

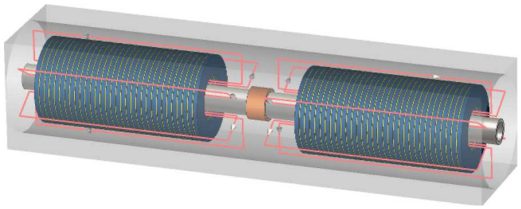

Figure 1: CAD model used for the numerical simulation of the GSI SIS 18 cavity. It consists of ferrite ring cores as well as copper discs. The coupling windings are represented by thin wires.

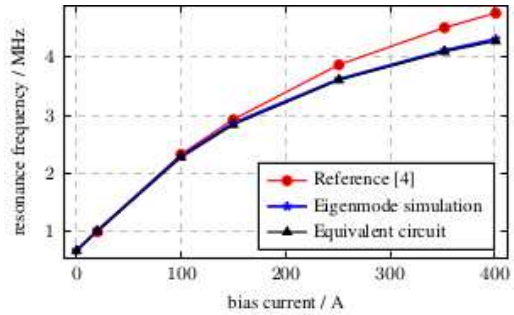

Figure 2: Resonance frequency as a function of the bias current for the prototype cavity with 29 cores on each side of the gap for small RF levels.

Summary

The computation of the fundamental mode of the GSI SIS 18 ferrite cavity has successfully been demonstrated.

References

[1] Klaus Klopfer, Uwe Niedermayer, Harald Klingbeil, Wolfgang Ackermann, Hans Günther König, and Thomas Weiland, “Measurement of the magnetic material properties and simulation and modeling of ferrite-loaded cavities”, Phys. Rev. ST Accel. Beams, vol. 18, issue 1, 2015.

[2] Klaus Klopfer, Wolfgang Ackermann, and Thomas Weiland, “Computation of Complex Eigenmodes for Resonators Filled With Gyrotropic Materials”, IEEE Trans. Magn., vol. 51, no. 1, 2015.

[3] Klaus Klopfer, “Computation of Complex Eigenmodes for Resonators Filled With Gyrotropic Materials”, PhD thesis, TU Darmstadt, tuprints: 4210, 2014.

[4] Uta Hartel, “Modellierung des Regelungs- und Steuerungssystems einer Beschleunigungseinheit für Synchrotrons”, Diploma thesis, TU Darmstadt, 2011.

DOI:10.15120/GR-2015-1-FG-SIS18-04

Simulations of a quadrupolar pick-up at GSI SIS-18*

Joel Alain Tsemo Kamga† [1], *Wolfgang F.O. Müller*[1], *and Thomas Weiland*[1]

[1]Technische Universität Darmstadt, Institut für Theorie Elektromagnetischer Felder (TEMF), Schlossgartenstrasse 8, 64289 Darmstadt, Germany

Introduction

This report presents the simulation results for an asymmetrical capacitive pick-up installed at GSI SIS-18. In the past, it was used as BPM (Beam Position Monitor) and is planned to be used for measuring the transverse beam size oscillations at SIS-18. The main goal of this project consists in estimating the properties of the pick-up and evaluating its usage as a quadrupole signal monitor. Due to the fact that the bunch for the SIS-18 operation is long compared to the pick-up electrode, first simulations have been performed with the electrostatic solver of the simulation software CST EM Studio to estimate the pick-up properties [1]. Now, to study the pick-up behavior in the frequency range of insterest for GSI, some simulations have been performed using the PIC solver of CST PS (Particle Studio) [2] and the results are presented in this report.

Simulations and Results

The pick-up design used for the simulations is shown below in Fig. 1

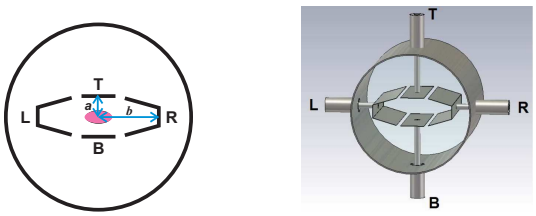

Figure 1: **Left**: front view of the pick-up design, b = 100.3 mm, a = 35.3 mm; **right**: perspective view of the pick-up from CST PS.

The quadrupolar signal Ξ for the traditional diff-over-sum method is given by $(U_R+U_L-U_T-U_B)/(U_R+U_L+U_T+U_B)$, where U_R, U_L, U_T and U_B are the amplitudes of the FFT signal voltages induced on the respective pick-up plates. Since the frequency range of interest for a typical SIS-18 opetration is between 10 kHz and 10 MHz, a high terminating resistor of 1 MΩ was connected at the output of each electrode to obtain a low 3 dB cutoff frequency of the plate. The simulation was carried out, as mentioned in the introduction, using CST PS, with a PIC solver in the frequency range of DC $\leq f \leq$ 200 MHz.

On the above diagram in Fig. 2, one can see that, the greater the horizontal beam size σ_x, the greater the

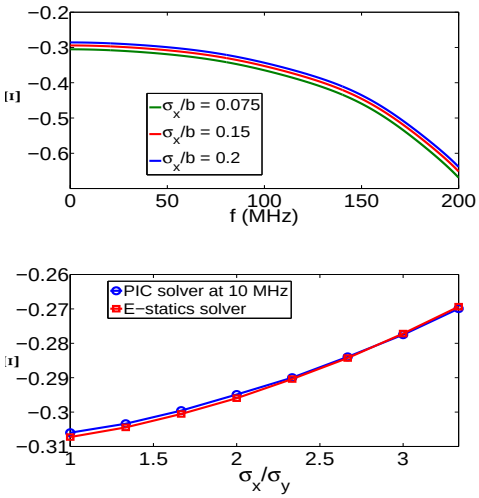

Figure 2: Quadrupolar signal Ξ for a centred beam; **above**: Ξ as a function of frequency; **below**: Ξ as a function of the horizontal beam size σ_x; σ_y/b = 0.075, b = 100.3 mm

quadrupolar signal in the whole frequency range, as expected. Furthermore, one can see that, in the frequency range of interest (10 kHz $\cdots$ 10 MHz) the quadrupolar signal is almost constant; the maximal deviation of $\Xi(f)$ (10 kHz $\leq f \leq$ 10 MHz) from the value of Ξ at 10 MHz is in the order of around 0.21%. The lower picture in the above figure shows the quadrupolar signal at 10 MHz for different values of σ_x/σ_y. One can state a good agreement between both solvers; the maximal relative deviation of the PIC solver results from the electrostatic ones is around 0.4%.

Conclusions

The simulations for an asymmetrical pick-up have been investigated in this project. One has seen that, in the frequency range of interest for GSI, the pick-up behaves capacitiv. Moreover, there was a good agreement between the PIC und electrostatic results. In conclusion, one can say that, for beams, whose longitudinal extent is much larger that the electrode length, the pick-up properties, like for instance the sensitivity, can be estimated very good electrostatically; this has the advantage that the simulation time is very low compared to that of the PIC solver.

References

[1] Joel A. Tsemo Kamga, et al., *GSI Scientific Report 2013.*

[2] CST AG, "CST Particle STUDIO", ww.cst.com

* Work supported by GSI

† tsemo@temf.tu-darmstadt.de

Streak camera as a new diagnostic tool for SIS18 ion beams*

L. Bozyk, M. Schwickert, R. Singh, P. Spiller, and B. Walasek-Höhne
GSI, Darmstadt, Germany

Streak cameras are typically used in electron accelerator facilities or plasma physics experiments to record processes with high time resolution. In 2014 a streak camera has been installed behind SIS18 at GSI. The streak camera will be used to study and optimize bunching and extraction of heavy ion beams from the synchrotron by measuring simultaneously in one spacial and in the time domain.

The extracted beam is observed with a BC400 plastic scintillator which is widely used in beam diagnostics. It has a rise time of 0.9 ns and decay time of 2.4 ns. It emits light with a maximal emission at 420 nm (violet/blue). Two scintillators are mounted in $45°$ with respect to the beam axis on a target ladder, which can be moved by a stepper motor. The scintillator is observed from below the beam axis. An optical system, consisting of four lenses and four mirrors, guides the emitted light to the streak camera. The optical system images 30 mm of the scintillator onto the 10 mm wide entrance slit of the streak camera, which observes the horizontal plane. Black moleton covering the setup enhances the contrast by excluding ambient light.

The installed streak camera is an "Universal Streak Camera", model C10910 by Hamamatsu. It allows streak times between 1 ns and 120 ms and has a motorized slit to be fully remote operable. Sensitive components, as the control PC, are placed in a measurement room, USB and firewire connections are extended via optical fibre. The whole system can be operated from the main control room of GSI via remote desktop access. In the fast extraction mode, the streak camera is triggered by the same signal, as the kicker modules of SIS18. It is generated in the electronics room by the Rf-system and has a jitter of 10 ns to 20 ns. By means of a delay generator one can account for trigger delays and time-of-flight of the beam. The long streak time of 120 ms is used to observe slow extracted beams. In this mode, the setup is triggered by timing events.

In autumn 2014 the streak camera system has been commissioned with different heavy ion beams from SIS18. Figure 1 shows the time-evolution of the horizontal profile of four bunches U^{28+} hitting the scintillator. The bunches hit at the same position, but obviously have different intensities. In Figure 2 the projection of streak data of an U^{29+}-beam onto the time axis is compared with the signal of the fast beam current transformer in the extraction line. In figure 3 the flattop voltage was chosen to low. The streak camera system also allows to resolve the spill structure and movements of the extracted beam during slow extraction .

First test with the streak camera in the SIS18 extraction line look very promising and show good capabilities to observe dynamics within the bunches.

* Work supported by BMBF, projectt 05E12CD1

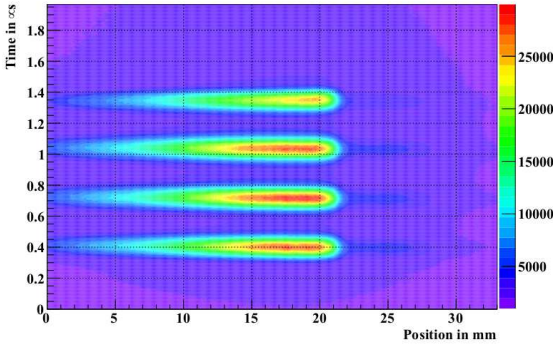

Figure 1: Streak picture of fast extracted U^{28+} beams at 200 MeV with four bunch operation (1H4). 30 pictures have been averaged.

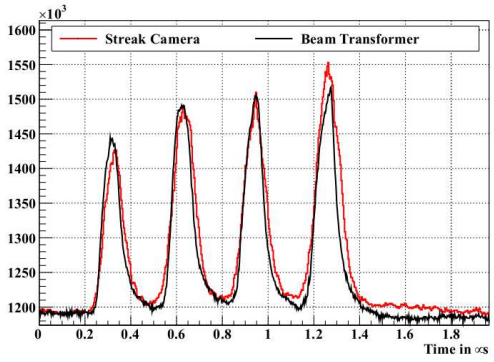

Figure 2: Comparison between the signal recorded with the beam transformer in the extraction beam line and the projection of a single streak picture onto the time axis for a U^{29+}-beam in arbitrary units.

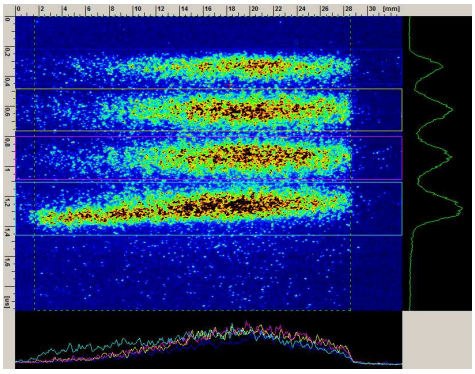

Figure 3: Screenshot from the online-display with U^{29+}-beam at 210 MeV: The flattop voltage (1 kV) is chosen slightly to low. The deformed bunch can not be recognized on the beam transformer.

DOI:10.15120/GR-2015-1-FG-SIS18-06

Recent improvements in TOPOS

R. Singh, K. Lang, and P. Kowina
GSI, Darmstadt, Germany

TOPOS is the digital Tune, Orbit and POSition measurement system which is currently under operation at GSI SIS-18 [1]. TOPOS provides bunch-by-bunch position from all 12 beam position monitors (BPMs) during the full acceleration cycle. It can also provide digitized raw BPM signal from all 48 pick-up electrodes (4 per BPM) at 125 MSa/s for ≈ 300 ms. TOPOS is designed to operate under a high dynamic range (90 dB) of beam currents in SIS-18.

TOPOS has been extensively utilized for SIS-18 optimisation and operation as well as for studying beam dynamics [2, 3, 4] in the past years. The widespread usage of TOPOS brought out the following technical issues:

1. An amplifier gain dependent closed orbit position variation of up-to 2 mm was observed as shown in Fig. 1 for 20 and 30 dB gains.
2. Erroneous position data for periods much longer than the set acquisition time was acquired by TOPOS system. This occured randomly for several BPMs.
3. Beam-based bunch detection for short bunches (with $< 7 - 8$ ADC samples) failed during the high energy proton beam operation.

Several beam-based tests were performed with TOPOS in response to the recurring operational issues mentioned above. The conclusions as well as the resulting upgrades to the TOPOS are reported in the next section.

Tests and Conclusion

Amplification dependent position variation was suspected to be an error in the present position calculation algorithm (i.e. weighted mean) due to its reliance on a complicated baseline restoration procedure described in [5]. Therefore, an alternate and simpler method for position calculation based on regression fitting was implemented. Figure 1 shows the comparison of the calculated horizontal position along the acceleration ramp between both algorithms. The amplifier gain dependence of beam position remains the same irrespective of the algorithms used. A small systematic bias (≤ 0.1 mm) between the positions calculated by both algorithms is due to the difference in their noise suppression characteristics. On further investigation it was found, that the calibration of the distinct amplifier chains connected to the 4 BPM electrodes were performed by a fixed amplitude signal generator. This calibration configuration allowed calibration only in a small range of amplification (i.e 10 to 20 dB). A new front-end electronics will be installed in SIS-18 where a calibration method based on varying input amplitude will be used to correct this error.

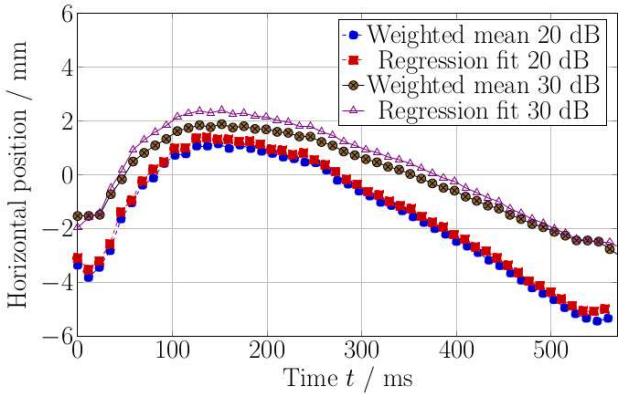

Figure 1: Comparison of measured horizontal beam position during the acceleration at two separate gain settings with both algorithms.

The problem with the erroneous acquisition length was related to the storage of the RF synchronous time-stamp generated for each bunch in the Libera FPGA. The error occurred when the time-stamp was not reset after the measurement cycle was finished. This happened in special conditions such as, when the end of measurement cycle coincided with the read strobe signal responsible for reading and clearing the time-stamp. This issue is resolved.

The issue of short bunch detection was studied by applying FPGA simulations. It was found that the bunch detection worked well for Gaussian shaped bunches with a sufficiently high amplitude even for a bunch length down to three samples. Offline simulations with recorded beam data with short bunches (upto 6 samples) also worked fine. Thus, the problem could not be reproduced during the investigations and is probably linked to the erroneous acquisition length issue.

References

[1] K. Lang, “TOPOS: A new tool for beam position measurements at SIS-18”, GSI scientific report 2010 (2010)

[2] V. Kornilov et al., “Transverse decoherence and coherent spectra in long bunches with space charge”, Phys. Rev. ST Accel. Beams 15, 114201 (2012)

[3] R. Singh et al., “Interpretation of transverse tune spectra in a heavy-ion synchrotron at high intensities”, Phys. Rev. ST Accel. Beams 16, 034201 (2013)

[4] G. Franchetti et al., “Recent development in the mitigation of long term high intensity beam loss at FAIR”, Proc. of HB 2014 (2014)

[5] R. Singh, “Tune measurements at SIS-18: Methods and Applications”, TU Darmstadt (2013)

DOI:10.15120/GR-2015-1-FG-SIS18-07

Commissioning of a sensitive tune monitoring system in SIS-18

R. Singh, T. Hoffmann, and P. Forck
GSI, Darmstadt, Germany

The front-end hardware of the baseband tune measurement system (BBQ) [1] has been routinely used for sensitive tune measurements at SIS-18 with real time spectrum analyser as the acquisition component [2]. The new TUne MEasurement system (TUME) integrates the BBQ front-end hardware with a FESA [3] based data acquisition and control element, and a Java based graphical user interface. The first operational results of the new TUME system at SIS-18 are presented.

The TUME system is designed to fulfil the following requirements :

- Monitor the tunes during the whole acceleration cycle or the time specified by the user. It should be possible to use different time-scales for calculating tunes.
- Provide facilities to filter and store the measurement data via a simple user interface.

Figure 1 shows the various components of the tune monitoring system. The pick-up signal is connected to the BBQ front-end hardware which consists of peak detectors and an amplifier chain. The output of BBQ front-end is connected to a VME based front end controller (FEC) which consists of the 8 channel, 16-bit, 100 MSa/s SIS-3302 ADC module. Two channels are used for the digitization of the output of the BBQ front-end for horizontal (x) and vertical (y) planes. The ADC module is clocked by the SIS-RF signal

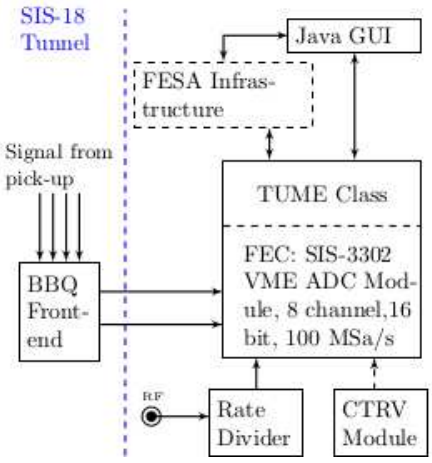

Figure 1: The data acquisition scheme for the tune measurement system.

followed by a rate divider to control the clock rate. This is required to support the various harmonic operational modes of SIS-18. The GSI machine timing events are converted to CERN timing events which are fed to the TUME FESA class via the CERN timing receiver VME (CTRV) module.

A TUME FESA class performs an FFT on the acquired samples based on user preferences to obtain the tune spectrum. A peak search routine extracts the tune value from the spectrum. Clients can subscribe to the properties of this FESA class to obtain the tune spectrum and tune values throughout the acceleration cycle. A Java based GUI (shown in Fig. 2) was developed to display the evolution of tune spectrum during the whole cycle. It provides further options for FEC settings, filtering the data, storage of data and advanced techniques for frequency spectra estimation.

The first beam based tests were performed in Autumn 2014 with 10^9 U^{28+} particles accelerated from 11.4 to 300 MeV/u. The BBQ front-end was connected to a pick-up in the quadrupolar configuration. Therefore, both x and y tunes are visible in channel 1 as shown in Fig. 2.

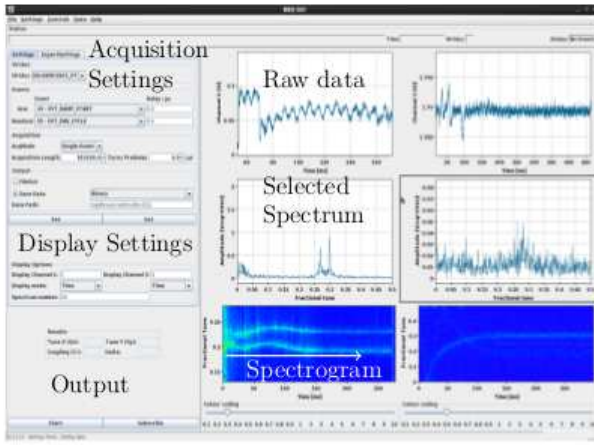

Figure 2: The TUME GUI shows the evolution of tune spectrum and tune over time.

The top plot shows the raw time domain data from the BBQ front-end. The middle plot shows the spectrum for a selected time window (from display settings). The lowest plot shows the tune spectra over time for the specified duration in acquisition settings. The FESA class and GUI are still under development, and will be brought into regular operation at the beginning of next SIS-18 run.

References

[1] M. Gasior, "High sensitivity tune measurement using direct diode detection", Proc. of BIW'12 (2012)

[2] R. Singh, "Tune measurements at GSI SIS-18: Methods and applications", PhD Thesis, TU Darmstadt (2012)

[3] T. Hoffmann, "FESA - The front end software architecture at FAIR", Proc. of PCaPAC08, Ljubljana, Slovenia (2008)

DOI:10.15120/GR-2015-1-FG-SIS18-08

Spill time-structure and main dipole power converter ripple in SIS-18

M. Kirk, D. Ondreka, H. Welker, C. Kleffner, P. Kowina, R. Singh and P. J. Spiller
GSI, Darmstadt, Germany

Tracking studies were carried out with an in-house code in order to estimate the severity of the power converter induced ripple in the dipoles as concerns its influence on the roughness of the spill when undergoing transverse RF "Knock-Out" (KO) excitation. The excitation comes from a strip-line exciter. In addition, a lattice resonance at Q_x=13/3 is created by sextupole magnets which were powered to provide an amplitude of K_2L=0.03 m^{-2}. The working point's tunes were Q_x=4.3296 and Q_y=3.27. With the longitudinal RF off, the reference $^{12}C^{6+}$ DC beam had a Half-Width in its relative momentum spread of $\delta_{p,2\sigma}$=0.04%. A Hardt condition was imposed on the optics to minimize ions lost to the first extraction septum by adding the offset K_2L=0.206 m^{-2} to each of the 1C-sextupoles and setting K_2L=-0.369 m^{-2} to each 3C-sextupole, producing losses at the septum's wires ≈3.5% of the initially stored ions, with ripple in the dipoles taken from Fig. 1. This loss is close to the simulated loss of 3.3% in the absence of the dipole magnet B-field ripple. It is therefore assumed that the ripple in the spill in Fig. 2, is not caused by septum collisions to a large extent.

A single power converter is connected in series to the dipoles. Fig. 1 taken from [1] shows the dipole circuit ripple at the nominal direct current of I_n=1190 A which was (partially) reconstructed from the discrete Fourier transform of an 8-bit oscilloscope trace of the difference between the set-point and actual current. With identifiable components in the range 100 to 1100 Hz (including the anticipated 300 and 600 Hz) added together to give Fig. 1 and implemented in the simulation, Fig. 2 was produced.

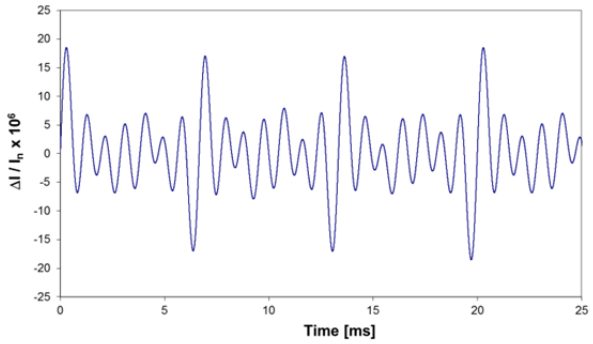

Figure 1: Partially reconstructed dipole current ripple. Maximum relative deviation in current is ca. 1.8x10^{-5}.

Each of the stored ions received, per transit through the exciter, a perturbation in its horizontal trajectory angle made with the design orbit, the magnitude of which was sampled randomly (per ion) from a Gaussian distribution cut at ±3σ, thereby allowing the contribution to the spill from just the dipole current to be determined. In Fig. 2 which shows the induced spill-ripple, the regularly spaced strong peaks occurring at 150 Hz are suspected to be directly correlated to the power converter ripple's signal envelope.

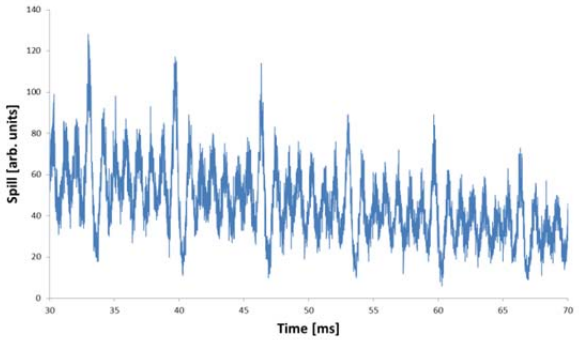

Figure 2: Simulated spill with dipole ripple.

In Fig. 3, which shows the distribution of the spill's Maximum-to-Average current from a 100-bin window (10 μs bins) moving over the spill of Fig. 2, one sees a clear degradation in spill smoothness. However, with nominal operation (K_2 offsets zero) for which the amplitude was raised to K_2L=0.064 m^{-2}, to permit a potential closed orbit bump of ~20 mm, no spill-ripple was observed.

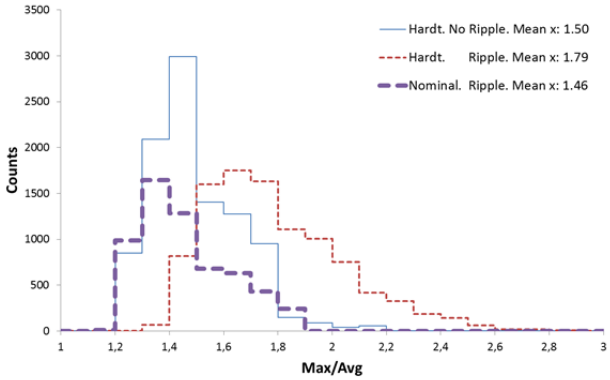

Figure 3: Simulated spill "roughness" distribution.

Measured spill-ripple, due to magnets, is considered excessive. Ions crossing the separatrix faster should reduce it. To this end, a recent prototype modification to the KO system, capable of delivering a new KO voltage form and higher maximum voltage, may achieve this.

References

[1] M. Kirk et al., "SIS-18 RF Knock-Out Optimisation Studies", IPAC'13, Shanghai, May 2013, MOPFI007, http://www.jacow.org .

DOI:10.15120/GR-2015-1-FG-SIS18-09

Super-FRS design status report*

M. Winkler[†1], *S. Althoff*[1], *F. Amjad*[1], *K.-H. Behr*[1], *A. Bergmann*[1], *T. Blatz*[1], *A. Brünle*[1], *E.J. Cho*[1], *W. Freisleben*[1], *H. Geissel*[1,2], *M. Gleim*[1], *C. Karagiannis*[1], *B. Kindler*[1], *H. Kollmus*[1], *E. Kozlova*[1], *A. Krämer*[1], *A. Kratz*[1], *J. Kurdal*[1], *H. Leibrock*[1], *H. Müller*[1], *G. Münzenberg*[1], *C. Mühle*[1], *I. Mukha*[1], *C. Nociforo*[1], *L. Orona*[1], *S. Pietri*[1], *A. Prochazka*[1], *S. Purushotaman*[1], *M.V. Ricciardi*[1], *C. Scheidenberger*[1,2], *F. Schirru*[1], *C. Schlör*[1], *P. Schnizer*[1], *H. Simon*[1], *C. Schlör*[1], *P. Szwangruber*[1,3], *F. Wamers*[1], *H. Weick*[1], *A. Wiest*[1], *C. Will*[1], *J.S. Winfield*[1], *Y. Xiang*[1], *and FAIR@GSI division*[1]

[1]GSI, Darmstadt, Germany; [2]JLU Giessen, Germany

System design

The revised layout of the Energy Buncher Spectrometer [1] has been finalized. It consists of two dipole stages deflecting the beam in opposite direction, forming a S-shape system. The new layout allows for a much simplified rectangular geometry of the required LEB cave. The ion-optical design includes an intermediate focus between the two dipole stages keeping the overall dispersion in limits. Details of the ion-optics are given at [2].

Magnets

CEA Saclay took over the design revision of the superconducting dipole magnets for Super-FRS. Although the existing prototype dipole fulfilled the magnetic parameters it required a revision of the cryostat including the cold mass. The FDR on the revised design (see Fig.1) was already held. CEA is now finalizing the design and preparing the tendering documents including the necessary specification. The magnets will then be tendered by FAIR.

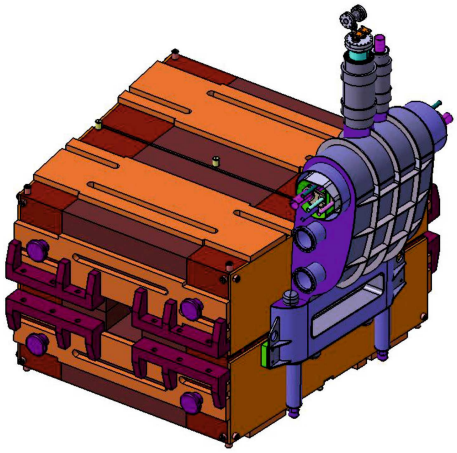

Figure 1: Revised design of SC the dipole magnet.

Unfortunately the tendering of the superconducting multiplets needed to be paused in September2014 due to formal reasons. The already qualified companies were asked to submit new offers. Contract negotiations are ongoing at the moment of writing this report and awarding is expected now for Q2/2015.

A handling test was performed for the existing radiation resistant dipole magnet. Later this 95 ton device must be installed in several parts in the highly shielded target area by means of the overhead crane in the target building of Super-FRS. The installation procedure was simulated with the help of a truck-mounted crane.

Moreover we needed to revise the adjustment support. The alignment of the magnet as well as other components in the target area can only be done remotely without any interivisibility. It turned out that the existing support unit does not satisfy the very high demand on reliability which requires the design of a new adjustment unit.

Figure 2: Simulation of the NC dipole installation.

Local cryogenics

For the planning of the Super-FRS magnet testing at CERN, several important topics related to the cryogenic safety have been investigated by CSCY together with the colleagues at CERN. Those include the final settle-down of the set pressure for the safety devices of the Super-FRS magnets according to the Pressure Equipment Directive (PED), the non-symmetrical forces on the multiplet cryostat in case of sudden loss of insulation vacuum to air, and the vacuum tank protection in case of a possible break-down of the cryogenic piping in the multiplet cryostat. In addition, the dynamic forces on the magnet support struc-

*Work supported by EU, CRISP contract No. 283745/CEA-IRFU/KVI-CART/FAIR@GSI PSP code: 2.4

† m.winkler@gsi.de

DOI:10.15120/GR-2015-1-FG-SFRS-01

tures for the test facility in the testing hall 180 have been checked for the case of helium gas release during worst-case quench. The results coming out of the investigations have been evaluated by the Safety Department at CERN and the submitted documents provide the basis to get the approval for the design and the operation of the test facility at CERN. Furthermore, the physical interfaces have been finalized between the cryogenic infrastructures, i.e., the jumper-connection, and the magnet cryostats, which is one of the most important interfaces through the magnet design and fabrication, the magnet testing at CERN and the final installation and operation at FAIR/GSI. Based on the cryogenic parameters including the heat loads of the magnet cryostat, the pressure drops, the flow rates and the cooldown time estimation provided by the CSCY, a preliminary cryogenic design of the test facility has been done at CERN in summer 2014.

Beam instrumentation

The development and production of the slit systems for Super-FRS was contracted as the first project within the framework of the Collaboration Agreement between GSI and KVI-CART. Altogether 18 slit pairs (horizontal as well as vertical) will be installed in the Super-FRS. Most of the slit-jaws will consist of Densimet blocks having dimensions of up to 200x180x250 mm^3. The overall weight of the heaviest slit-systems will be close to 1 ton. The preliminary design could already be finished including aspects like remote handling capability (in the Pre-Separator). Special care was taken on thermal effects which could arise in the Pre-Separator due to high beam/fragment intensities [3].

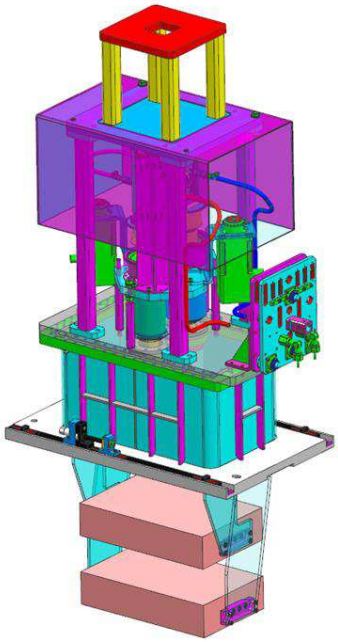

Figure 3: Daesign proposal of the y-slit system including remote controlled media pannel.

Target area / handling system

A Hot-Cell mock-up was installed on the ESR roof (see Fig.4). It consists of a metallic frame and two master-slave manipulators. The frame simulates the front area/shielding window of the future Super-FRS Hot Cell [4] and serves as the support for the manipulators. The manipulators are double telescopic systems with a load capacity of 20 kg and a maximum slave extended length of 3270 mm. The arms are completely equilibrating in all operational positions (with no load). It is foreseen to transfer and install these manipulators to the future Hot-Cell.

Figure 4: Hot-Cell mock-up mounted on the ESR roof

The main purpose of the mock-up is to validate the concepts of the equipment which is under development now and must be designed for remote-handling (target, beam catcher, etc., but also equipment used at the pbar separator). Another important aspect is the training of personnel in advance of 'hot' operation. Partially we collaborate here with SPIRAL2 in the framework of the EU CRISP project and remote handling tests with our French colleagues could be performed.

References

[1] H. Geissel et al., "Dispersion-matched spectrometer in the low-energy branch of Super-FRS", NIM B 317 (2013) 227

[2] J. Winfield et al., "Status of Ion-Optics for the Super-FRS", this report

[3] J. Gellanki et al., "Super-FRS Slit System and Possible Passive Cooling Techniques", this report

[4] M. Winkler et al., "Super-FRS Design Status Report", GSI Scientific Report 2010 (2011) 133

Super-FRS slit system and possible passive cooling techniques

J. Gellanki[1], C. Douma[1], N. Kalantar-Nayestanaki[1], O. J. Kuiken[1], M. F. Lindemulder[1], H. Moeini[1], C. Nociforo[2], C. Rigollet[1], H. A. J. Smit[1], H.J. Timersma[1], K. H. Behr[2], C. Karagiannis[2], M. Gleim[2], C. Schlör[2], H. Simon[2], and M. Winkler[2]

[1a]KVI-CART, University of Groningen, NL-9747 AA, Groningen, The Netherlands; [2b]GSI, D-64291 Darmstadt, Germany

X− and Y− position slit systems will be used to stop the unwanted charge states of the primary beam and fragments produced at the reaction target of the Super-FRS at the FAIR facility, GSI. In the case of the most frequently used fission reaction of ^{238}U beam at 1.5 GeV/u on ^{12}C target (2.5 g/cm^2), one of the lowest charge states of ^{238}U fragments produced at the target may reach one of the X-slits with an energy of about 1.3 GeV/u with a maximum power of 500 W. The basis of the Super-FRS X− and Y− slit systems are two DENSIMET®185 (97% Tungsten, 2% Nickel and 1% Iron) metal blocks, which have to move in a vacuum chamber in horizontal direction $(0 - 400\ \mathrm{mm})$ and in vertical direction $(0 - 200\ \mathrm{mm})$, respectively. Due to the highly radioactive environment,

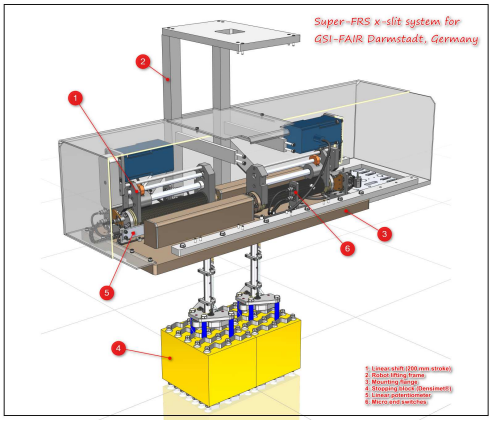

Figure 1: Schematics of the Super-FRS slit system which is under construction at KVI-CART, is shown.

some of the slits are designed to allow for robot handling. Overview of Super-FRS slit system is shown in the Fig. 1. NX advanced thermal simulations Ref. [1] are carried out to estimate the maximum and minimum temperature values on the slits and on the apparatus in the neighborhood of the slits. Several cooling methods have been simulated on a block of DENSIMET with a proposed dimensions of $200 \times 180 \times 250\ \mathrm{mm}^3$, and which will be used in the pre-separator of the Super-FRS beam line. The present results from the thermal simulations suggest two new possible passive cooling techniques to lower the temperature of the block by substantial amounts without any water cooling during experiments.

Simulations and the new passive cooling techniques have been tested by a test run at the AGOR beam line at KVI-CART. In this run, three different densimet blocks: 1) pure densimet (emissivity $\sim$ 0.07; as per literature), 2) densimet block with welded stainless steel (SS) strips as radiators (SS emissivity $\sim$ 0.65) and 3) densimet block with cerablack coating Ref. [2] of thickness 0.15 mm (cerablack emissivity $\sim$ 0.9) have been used. The pure block and the block with SS strips having the same dimensions of $30 \times 30 \times 50\ \mathrm{mm}^3$ and the coated block is of $25 \times 25 \times 50\ \mathrm{mm}^3$. Each block has been exposed with ^{20}Ne beam of power Q = 21 W for about four hours. Preliminary results of this test run are shown in the Fig. 2. As seen from the figure, the densimet block with the cerablack coating radiates out the heat much faster than the other two blocks. Further details can be found in Ref. [3].

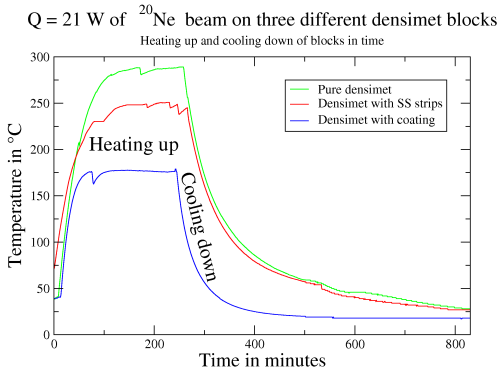

Figure 2: Preliminary results of test run with ^{20}Ne beam are shown. Heating and cooling responses of the pure densimet block are shown in green. The same is shown for the block with stainless steel welded strips and cerablack coating by the red and the blue solid lines, respectively. As seen in the picture, each densimet block was exposed to a beam (heating up) for about four hours. The decrease in temperature of each curve represents the cooling down of the corresponding block. For more details see text.

References

[1] Siemens NX (NX Thermal and Flow) software.

[2] http://atfinet.com/index.php/applications/thermal-management/high-emissivity-coatings.

[3] J. Gellanki et al., *To be submitted to Nucl. Instr. Meth. Phys. Res. A.*

DOI:10.15120/GR-2015-1-FG-SFRS-02

Profile monitors for the Super-FRS*

C. Nociforo[1], J. Adamczewski-Musch[1], K.H. Behr[1], A. Brünle[1], J. Frühauf[1], N. Kurz[1], S. Löchner[1], A. Reiter[1], K. Rytkönen[2] and M. Witthaus[1] and the FAIR@GSI division
[1]GSI, Darmstadt, Germany; [2]University of Jyväskylä, Department of Physics, 40014 Jyväskylä, Finland

Profile monitors providing precision measurement of horizontal and vertical beam profiles are essential for transport and targeting of Super-FRS beams.

Introduction

At GSI the beam monitoring technique based on Secondary Electron EMission (SEM) is routinely used for the high power UNILAC beams. When charged particles hit a metallic surface, secondary electrons are liberated, escaping from it forming a measurable signal. Wire SEM grids are widely used as device to measure the profile of the ion beams. While the yield probability of secondary electron emission is low, these devices can produce signal up to 10nC/wire in case of SIS beam. At FAIR beam intensities, e.g. $4.5x10^{11}$ ^{238}U/spill, beam passing through the wire, undergoes to a significant energy loss (few GeV) even if the particle are not stopped, and wires can be damaged by the temperature rise. Presently, SEM-grids of different material and geometry satisfying the Super-FRS beam parameters are under investigation.

Beam test

A standard GSI monitor DG1010 [1] designed with wire spacing and diameter of 1.5 mm and 0.1 mm, respectively, was installed in vacuum at the first focal plane F1 of the FRS and irradiated with U beam. The number of horizontal and vertical W wires was 16. To simulate an experimental condition similar to that of the Super-FRS, the wire signals were transported over a long cable (length >50 m). A current-to-frequency converter QFW POLAND [2] was used to measure the profile of the beam. The electronics was triggered by the start of extraction TTL pulse delivered by the accelerator timing system.

The response of the detector was studied with slow-extracted $^{238}U^{73+}$ beam at 300 MeV/u and fast-extracted $^{238}U^{29+}$ beam at 125 MeV/u. At higher energy the beam intensity did not exceed $2.8x10^{8}$ ions/s. At lower energy the maximum intensity delivered by the SIS18 was equal to 10^{10} ions/spill. Due to the small area of the detector one single charge state distribution per time could be measured by the grids. The intensities of the different charge states of the beam were simulated and compared with the measured ones. The horizontal profile of $^{238}U^{90+}$ beam reaching F1 with a magnetic rigidity of 8.085 Tm corresponded to a measured charge of 0.19 nC. The U charge state distribution produced in 40 μm of Ti material inserted at the FRS target position was estimated by using the GLOBAL code [3]. The emission of secondary electrons from the W surface was calculated by the Sternglass formula [4]. Under the assumption that 7% of the beam crossed the wires, the estimated charge was 1.46 times the measured one.

The response of the detector to fast-extracted beam was tested after adding a capacitance of 4.7 nF to stretch the pulse.

The 3D measurement of a time-resolved beam profile of $^{238}U^{88+}$ at about 125 MeV/u, reaching F1 after impinging a 10 μm Ti foil, is shown in Figure 1. The ratio between measured and simulated charges decreased up to 0.36 for the maximum intensity (assuming no losses up to the FRS target).

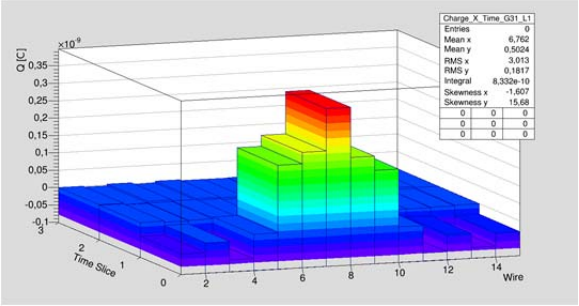

Figure 1: $^{238}U^{88+}$ profile at 125 MeV/u (fast extraction).

Further analysis of the test results will add constraints to the mechanical design of the Super-FRS SEM-grids. Effects of off-axis charge states hitting the frame and return wires were noted. Although a larger geometric coverage is required at the Super-FRS, present results ensure a standard operation along the separator.

Outlook

Further optimization, not only for the emission yield but also to increase precision of measured position and width of the beam, are foreseen. At the Super-FRS target, because of the high power absorption, different SEM material will be tested.

References

[1] P. Strehl, “Beam Instrumentation and Diagnostics”, Springer (2006), p.105.
[2] http://wiki.gsi.de/cgi-bin/view/EE/POLAND.
[3] C. Scheidenberger et al., Nucl. Instr. Meth. B142 (1998) 441.
[4] E. J. Sternglass, Phys. Rev. 108 (1957) 1.

* PSP code: 2.4.6.1.4

DOI:10.15120/GR-2015-1-FG-SFRS-03

In-Beam Test of the TwinTPC at FRS*

A. Prochazka[1], *M. Pikna*[2], *B. Sitar*[2], *P.Strmen*[2], *I.Szarka*[2], *C. Nociforo*[1], *S. Pietri*[1], *and FAIR@GSI Division*[1]

[1]GSI, Darmstadt, Germany; [2]Comenius University, Bratislava, Slovakia

One of the crucial requirement for the future tracking detector at the Super-FRS [1] is a high efficiency tracking at particle intensities around 1 MHz. To improve the efficiency at high rates of the standard TPC [2] and future GEMTPC detector [3] so called Twin design is proposed.

The main idea of the Twin design is to use two independent drift volumes with electric fields of opposite direction. This allows to calculate a Control Sum which is in principle sum of the drift times from the drift volumes. As the sum should be a constant it can be used for for pile-up and noise rejection and for multi-hit track reconstruction.

The TwinTPC prototype was built at Comenius University Bratislava. The TwinTPC drift volumes were filled with P10 gas at normal temperature and pressure and were operated at electric field of $400V/cm$. Each drift space was read by two anode wires and a delay line. The anode wires were used to calculate drift time (y-coordinate) and delay line was used to measure x-coordinate. For the future the single-strip readout with multi-hit digital electronics is foreseen for x-coordinate measurement. The signals were processed by conventional electronics (pre-amplifiers, shaping amplifier, discriminator) and time was measured by multi-hit TDC (Caen V1290) with $25ps$ time resolution. All times were measured relative to reference times derived from the hits of a plastic scintillator. The Control Sum was calculated as $t_{CS} = t_1 + t_2 - 2 \cdot t_t$, where t_1 and t_2 are drift timed from the two drift spaces and t_t is the reference time coming from scintillator. All times are measured in multi-hit mode.

The test was done using Au beam at $700MeV/u$ at the FRS. The particle rate was estimated from the number of hits registered by the plastic scintillator which were sent to scaler unit and the mutli-hit TDC. The efficiency was measured at different beam intensities and was estimated from the number of events for which we can unambiguously assign drift times fulfilling the control sum condition. The typical distribution of the control sum is shown in Fig 1. The width of the control sum is partially determined from the time resolution of the drift time measurement. The achieved time resolution (RMS) of the single drift volume was around $1ns$ for rates below 100kHz, corresponding to about $50\mu m$ position resolution for P10 gas. At higher rate (700kHz) the time resolution dropped to $3ns$.

The measured efficiency of the drift time reconstruction using the Twin design at different rates is shown in Fig. 2. The obtained results are compared with the efficiency of the single-volume TPC with single-hit readout and with simulation as described in [4]. The results conclude the Twin design works and show possible areas for improvement.

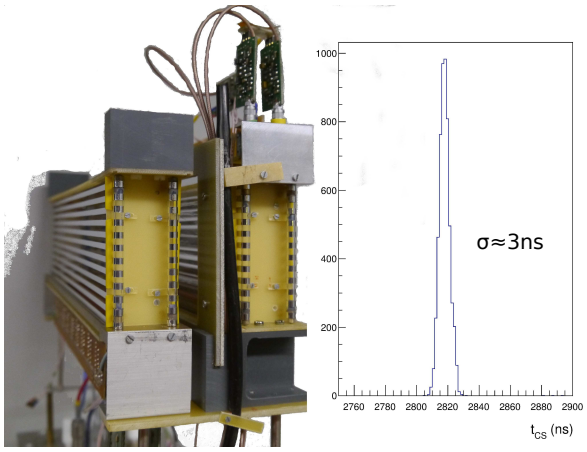

Figure 1: Left: TwinTPC prototype photo showing two drift volumes. Right the distribution of the Control Sum

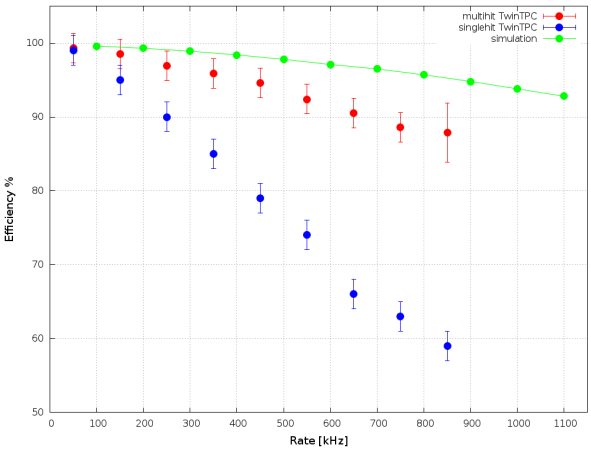

Figure 2: The TwinTPC drift time reconstruction efficiency (red points) as a function of rate. The blue points are efficiency of the single drift volume with single-hit electronics, the green points are simulation.

References

[1] H. Geissel et al.,Nucl. Instr. and Meth. B204(2003)71-85

[2] R. Janik et al.,Nucl. Instr. and Meth. A640(2011)54-57

[3] F. Garcia et al.,GSI Scientific Report 2012(2013)173

[4] A. Prochazka et al., GSI Scientific Report 2012(2013)174

* PSP code: 2.4.6.1.3

DOI:10.15120/GR-2015-1-FG-SFRS-04

On the Crystal Structure of Intrinsic CVD Diamond-on-Iridium Sensors*

E. Berdermann[1#], M. Kiš[1], C. J. Schmidt[1], M. Träger[1], R. Visinka[1], K. O. Voss[1], M. Fischer[2], S. Gsell[2], M. Mayr[2], M. Schreck[2], K. Afanaciev[3], and M. Ciobanu[4]

[1]GSI, Darmstadt, Germany; [2]Universität Augsburg, Germany; [3]NC PHEP, Minsk, Belarus; [4]ISS, Bucharest, Romania

Ion Beam Induced Current (IBIC) experiments were performed with high-quality Diamond-on-Iridium (DOI) sensors aiming to visualize shape and spatial distribution of crystal dislocations in this new detector-grade diamond type. For the first time, DOI samples were irradiated with ^{12}C microbeams of 3.6 and 11.4 AMeV kinetic energy in two crystallographic directions, the [001] (i.e. along the surface normal) and the [110] (lateral) direction. Different ion energies enable the imaging of the Collected Charge (CC) in diverse crystal planes lying in depths corresponding to the Bragg maxima (here: 25µm and 170µm, respectively). Stopped, mono-energetic ions generate the same amount of electron - hole (e-h) pairs in intrinsic single crystal sensors - independent of the point or angle of the ion incidence. Ideal detectors have a CC efficiency (CCE) equal unity showing uniform maps, whereas real sensors reveal reduced CC and maps modified by crystal defects.

Sample Preparation and Mounting

A sensor of 265µm thickness and (5x5) mm² area [1] was re-metallized with six edgeless stripe electrodes connected in parallel to an SMA connector used for biasing and readout (Fig. 1, left). Edgeless contacts are difficult but indispensable in lateral IBIC tests. They produce occasionally abnormal leakage currents disturbing bias stability and energy resolution. Figure 1 (right) shows two sensors mounted for lateral experiments.

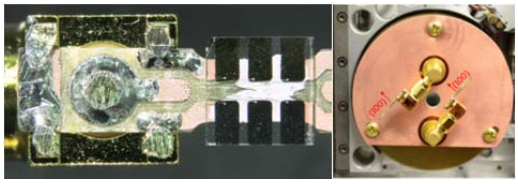

Figure 1:(left) Edgeless DOI sensor mounted on an SMA. (right) Two sensors aligned for lateral IBIC tests.

First IBIC Results

In Figures 2 and 3, examples of top-view (001) and lateral (110) maps are presented, obtained from layers in 25µm (at 3.6 AMeV) and 170µm depth (at 11.4AMeV) behind the corresponding diamond surface. In each case, areas of (288 x 232) µm² have been irradiated.

The selected pulse-height conditions used are indicated in the right spectra. The X-axes of the CC distributions are calibrated in energy values, assuming 13.4 eV per ion-induced charge carrier in diamond. The 3.6 AMeV data are presented in the range 0 - 45 MeV in 1keV/ch and the 11.4 AMeV in the range 0 - 290 MeV in 100 keV/ch, respectively. Note that, the colour values (i.e. the CC plot

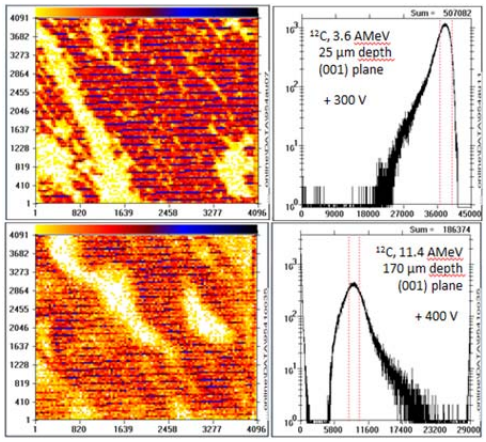

Figure 2: (001) IBIC maps (left) obtained with the conditions shown in the spectra (right). The data correspond to layers below the contact in a depth of 25µm (top) and 170µm (bottom), respectively.

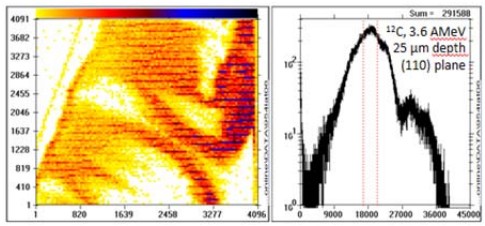

Figure 3: (110) Lateral IBIC maps and spectra (s. text).

ted on the Z-axis of the 3D maps) do not represent pure signal amplitudes, since these are generated by weighting each pulse height with the number of events at that place. However, considering the strict homogeneous irradiation performed with the micro-beam facility, the maps confirm predominantly areas of high, rather homogeneous CCE.

Preliminary Conclusions

Top-view and cross-section maps differ significantly in the CC pattern. In top view, granular structures are visible with a characteristic length of 50 -100 µm. In contrast, the cross-section maps are dominated by stripes along the growth direction of a slightly tilted angle. Both observations show intriguing similarities to the shape and alignment of threading dislocations bundles observed by mapping the Raman-line widths [2]. Further studies are required to establish the preliminary results and to elucidate the influence of the contacts on the CCE patterns.

References

[1] E. Berdermann et al., GSI Scientific Report (2011)
[2] M. Mayr et al., Phys. Status Solidi A **211** (2014)

* Work supported by EU, HadronPhysics3, contract No. 283286
#e.berdermann@gsi.de

Development of large area diamond detectors for time-of-flight measurements of heavy ions

F. Schirru[1], C. Nociforo[1], M. Kiš[1], M. Ciobanu[1,2], J. Fruehauf[1], M. Träger[1], R. Visinka[1], K. Behr[1], A. Brünle[1], I. Dillmann[1,3], C. Karagiannis[1], A. Kratz[1], N. Kurz[1], M. Marta[1], A. Prochazka[1], S. Pietri[1], S. Perushothaman[1], B. Szczepanczyk[1], H. Weick[1], M. Winkler[1]

[1]GSI, Darmstadt, Germany, [2]ISS, Bucharest, Romania, [3]TRIUMF, Vancouver, Canada

A few experiments have been carried out in order to assess the Time-of-Flight (ToF) performances of radiation detectors based on diamond material.

In early 2014, two diamond devices of 0.3 and 0.6 mm thickness, respectively were irradiated at JINR (Dubna, Russia) using an ^{40}Ar beam at 40.5 MeV/u. Amplification of the induced signal was performed by broadband preamplifiers (DBA-IV) [1]. In this case, the sensors, mounted a couple of cm away from each other, showed a resolution of σ_{tof} ~ 80 ps per detector pair.

In August 2014, another experiment was performed with the FRS at GSI. This time, large-area radiation detectors based on two 20x20x0.3 mm^3 polycrystalline CVD diamonds have been developed. Electrodes were fabricated in house in a 16-strips geometry by depositing on both sides of the diamond samples Cr/Au layers of 50/100 nm thickness, respectively. Each device was then mounted on a board (Fig. 1) which has an integrated amplification stage [2] and is able to provide LVDS signals as output. The novelties of this experiment were: the use of integrated electronics, a distance between the diamond detectors of more than 30 m, and experimental conditions similar to those expected at the Super-FRS [3].

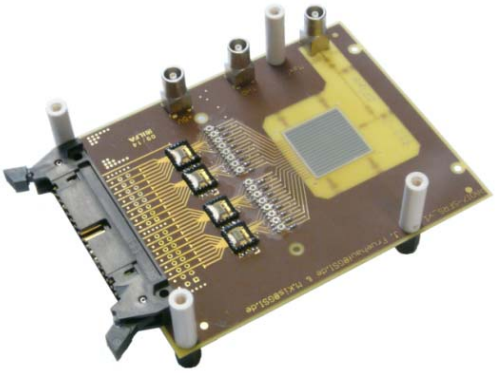

Figure 1: Diamond detector and its integrated electronics.

In this experiment at GSI, the diamond detectors have been irradiated with a ^{197}Au beam at 1 GeV/u. ToF measurements were performed in two ways: i) placing the detectors only 2 cm apart (S4 case) and ii) placing them more than 30 m apart (S2-S4 case).

As for the S4 case, first the effect of the threshold and bias voltage on the ToF resolution of the sensors was studied. It was observed that the best performances could be achieved with a voltage of -200 V. In this case, σ_{tof} =39.8 ps has been found between two strips of the front and back diamond detector. This value has shown also no dependence on the beam rate in the range of 1 – 10 kHz. For the S2-S4 case with 30 m flight path, the diamond sensors showed a resolution of σ_{tof} =52.7 ps. Taking advantage of the Time Projections Chambers (TPCs) [4] mounted along the beam line, a position correction was applied which led to an excellent resolution of σ_{tof} =45.7 ps (Fig. 2). No dependence on the beam rate over the range 10 – 80 kHz was found.

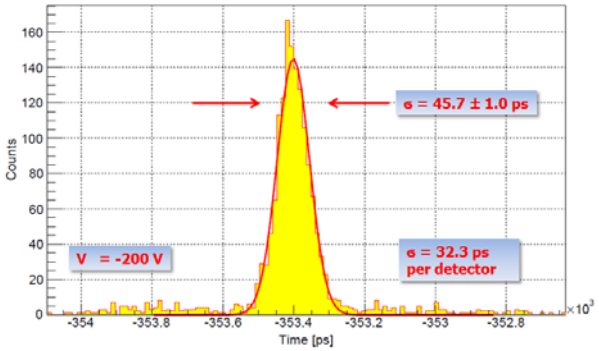

Figure 2: Diamond ToF resolution (S2-S4 case).

The new developed diamond detectors have shown excellent timing properties making this material an attractive solution for the next generation of experiments foreseen at the FRS and Super-FRS. It has to be mentioned that the ToF resolution of the diamond detectors can be further improved once a correction for the deposited energy will be done.

References

[1] P. Moritz et al., Diam. Relat. Mater. 10, p. 1765, (2001).
[2] M. Ciobanu et al., IEEE Transactions on Nuclear Science, vol. 58, n. 4, 2073, (2011).
[3] M. Winkler et al., Nucl. Instr and Meth. B 266, 4183, (2008).
[4] R. Janik et al., Nucl. Instr and Meth. B 640, 54, (2011).

* This work has been supported by the German Helmholtz Association via the Young Investigators Grant "LISA - Lifetime Spectroscopy for Astrophysics" (VH-NG627).

DOI:10.15120/GR-2015-1-FG-SFRS-06

Proposal of an RF-only double-funnel system for ions extraction from a cryogenic stopping cell for the Super-FRS at FAIR

Victor Varentsov[1, 2,*]

[1]Facility for Antiproton and Ion Research in Europe (FAIR GmbH), Darmstadt, Germany; [2]Institute for Theoretical and Experimental Physics, Moscow, Russia

In 2001 we proposed [1] an idea to replace a radio-frequency quadrupole (RFQ) or sextupole (SPIG) rod structure, which are conventionally used for an ion beam extraction from stopping gas cells into vacuum, by an RF-only ion funnel. Later we suggested [2] the using this technique for production of focused ion beams. Recently this RF-only ion funnel concept has been successfully checked [3] at Stanford University, USA in measurements of ions extraction into vacuum from a high-pressure (10 bar) noble-gas environment.

Here we propose the RF-only double-funnel system for ions extraction from a cryogenic stopping cell for the Super-FRS at FAIR, which prototype device is described in details in [4]. A schematic representation of this double-funnel system is shown in Fig. 1.

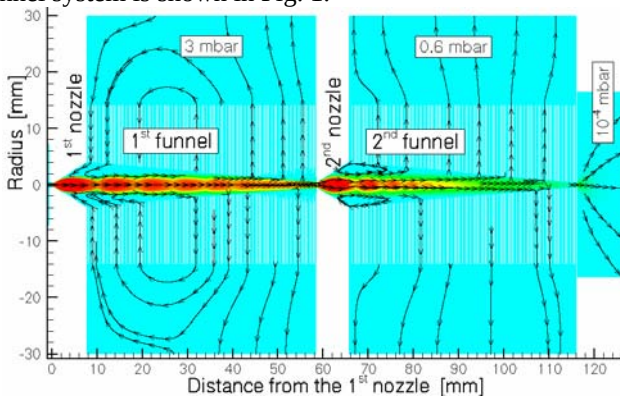

Figure 1: (color online) Schematic design of the RF-only double-funnel system for ions extraction from a cryogenic stopping cell for the Super-FRS at FAIR. The simulated velocity field for helium buffer gas at the stagnation pressure of 2 bar and temperature of 75 K in the gas cell is shown in addition. See text for explanation.

The ions are extracted from gas cell (not shown in the Fig.1) via supersonic He buffer gas flow through the 1st converging-diverging nozzle that has the following dimensions: the subsonic converging cone has the entrance diameter of 1.3 mm, the length of 1 mm; nozzle throat diameter is 0.3 mm; the supersonic diverging cone has the length of 7.7 mm and the exit diameter of 8.0 mm. The funnels are connected through the 2nd diverging nozzle having the throat diameter of 0.8 mm, the length of 7.2 mm and the exit diameter of 8.0 mm. The both funnels have the same following geometry: the number of ring electrodes is 144, they have the same outer diameter of 28 mm and the inner diameter decreasing from 8.0 mm at the funnel entrance to 0.8 mm at the funnel exit; ring electrodes made from 0.1 mm thick stainless steel sheets; the gap between electrodes is 0.25 mm. It should be notice, that the design of these funnels is identical (except of the length and the number of ring electrodes) to funnel that has been used in the Stanford's apparatus [3].

RF-voltages applied to the funnels (in such a way that phase shift between adjacent ring electrodes is 180°) confine the ions inside the funnels while the most part of the buffer gas flow out through the gaps between funnel rings and pumped. No any DC field is applied to the funnel electrodes and the ions are transported through this double funnel system only under a combined action of RF field and the buffer gas flow. The both nozzles have a ground potential.

The operation of this double-funnel system we have explored by means of detailed computer simulations. First, we made gas dynamic simulations for the buffer gas flow. Then the results of these simulations (flow fields of gas density, temperature and velocity) we used as input for ion-trajectory Monte-Carlo simulations. A detailed description of the similar computer simulations one can find elsewhere ([2, 3] and references inside). Notice that the measurements in [3] are in a good agreement with these computer simulations.

The results of gas dynamic simulation for the helium buffer gas velocity field at the stagnation pressure of 2 bar and temperature of 75 K in the gas cell is shown in the Fig. 1 for illustration. A complex gas flow barrel shock-wave structures inside the funnels are clear visible. The gas flow rate through the 1st nozzle is 123.7 mbar l/s (at the room temperature of the vacuum pumps). At the background gas pressures in the 1st and the 2nd vacuum chamber, which are maintained by pumping, of 3.0 mbar and 0.6 mbar, the gas flow rates through these chamber are 99.5 mbar l/s and 24 mbar l/s, correspondingly. The gas flow rate into the next vacuum chamber (downstream the 2nd funnel exit) is only 0.19 mbar l/s that allows extracting ions into the high-vacuum conditions ($2 \cdot 10^{-4}$ mbar) with the use of 1000 l/s turbo molecular pump.

Some results of the ion-trajectory simulations are shown in next figures. Fig. 2 shows the ion transmission as function of ion mass at fixed RF frequency and funnel RF voltages. The influence of the 1st funnel RF voltage on the ion transmission for ion masses m = 20 and m = 100 at fixed RF frequency and the 2nd funnel RF voltage is shown in the Fig. 3. The effect of the 2nd funnel RF voltage on the ion transmission for ion masses m = 20 and m = 100 at fixed RF frequency and the 1st funnel RF voltage is shown in the Fig. 4. The influence of the RF frequency on the ion transmission for ion masses m = 20 and m = 100 at fixed 1st funnel RF voltage 20 V_{pp} and 2nd funnel RF voltage 10 V_{pp} is shown in the Fig. 5.

DOI:10.15120/GR-2015-1-FG-SFRS-07

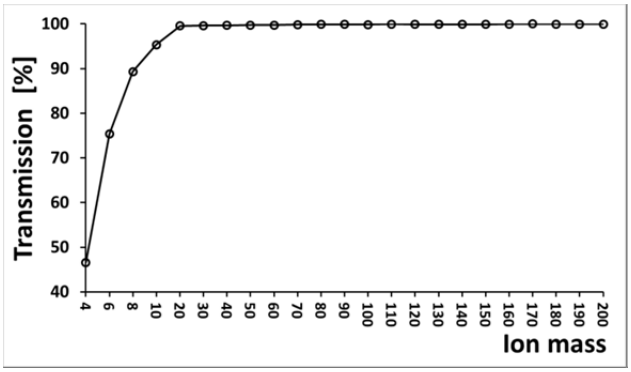

Figure 2: Ion transmission as function of ion mass at fixed 1st funnel RF voltage 20 V_{pp} and 2nd funnel RF voltage 10 V_{pp} and RF frequency 5 MHz.

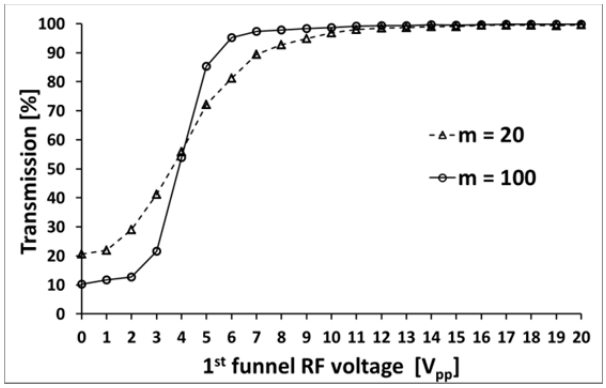

Figure 3: Ion transmission for ion masses m = 20 and m = 100 as function of the 1st funnel RF voltage at fixed 2nd funnel RF voltage 10 V_{pp} and RF frequency 5 MHz.

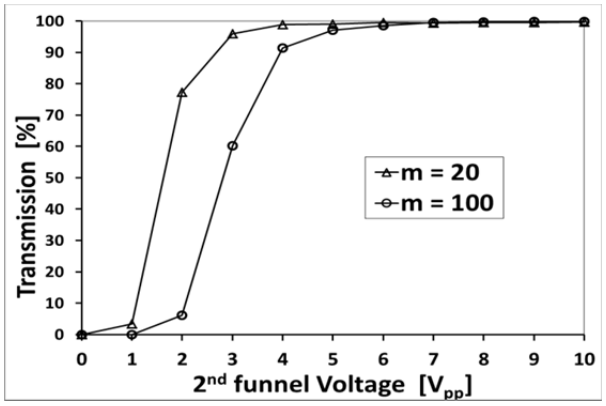

Figure 4: Ion transmission for ion masses m = 20 and m = 100 as function of the 2nd funnel RF voltage at fixed 1st funnel RF voltage 20 V_{pp} and RF frequency 5 MHz.

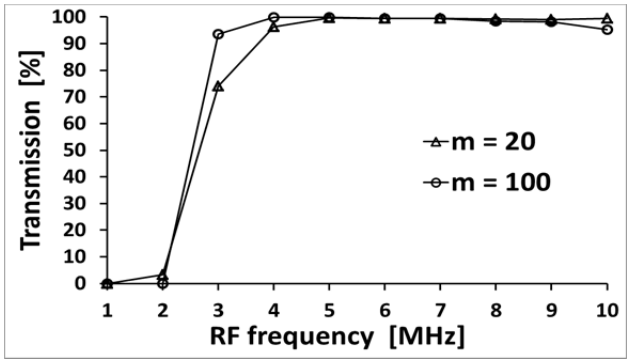

Figure 5: Ion transmission for ion masses m = 20 and m = 100 as function of RF frequency at fixed 1st funnel RF voltage 20 V_{pp} and 2nd funnel RF voltage 10 V_{pp}

The presented results make it apparent that our proposal of the RF-only double-funnel system looks very promising and can be used for ions extraction from a cryogenic stopping cell for the Super-FRS at FAIR. It has the extraction efficiencies of more than 99% for ions in a wide range of masses, it is compact, has relatively simple design and do not require big vacuum pumps for the buffer gas evacuation. Moreover, it has big advantage over the present prototype device [4] because it allows the gas cell operation at much higher stagnation pressure (2 bar). The design pressure in [4] is only 0.3 bar that corresponds to a stopping cell length of 100 cm for the required gas thickness of 20 mg/cm^2. It means that the gas cell can be made much shorter (15 cm) and will allow, in addition, for a smaller time of ions transportation through the stopping gas cell by applying a higher longitudinal DC potential gradient.

References

[1] V.L. Varentsov, “A new approach to the extraction system design”, SHIPTRAP Collaboration Workshop, Mainz, Germany, March 19-20, 2001, unpublished.

[2] V.L. Varentsov, Proc. SPIE 7025 (2008) 702509-12. doi:10.1117/12.802356.

[3] T. Brunner, et al., Int. J. Mass Spectrom. 379 (2015) 110. doi: 10.1016/j.ijms.2015.01.003.

[4] M. Ranjan, et al., Nucl. Instr. and Meth. A 770 (2015) 87.

DOI:10.15120/GR-2015-1-FG-SFRS-07

Eddy current effect of quadrupole and CR dipole magnet beam chambers

S. Y. Shim, K. Dermati, S. Wilfert, A. Dolinskii, O. Gorda, and R. Fuchs
GSI, Darmstadt, Germany

In order to keep the stable particle operation, beam chamber needs to have the high-quality vacuum state and thermal stability from external influence. The time-dependent magnetic field produces the secondary effects of heating and stray magnetic field, which can disturb the quality of the inside vacuum and the magnetic field. We present here the numerical simulation results for the recent issues related to the vacuum beam chambers of SIS100 quadrupole magnets and the current ripple effect of CR dipole magnet for the field stability optimization.

QP Star shaped beam chamber

The rib distance of the star-shaped beam chamber for quadrupole (QP) magnet has been changed from 17 mm to 7 mm. More number of ribs increase mechanical stability and the heat conduction between cooling pipe and beam chamber surface. The opposite effect is that it reduces electric resistance on the beam chamber which can be a cause of increasing eddy current. Therefore, we need to confirm the results of this design modification. The eddy loss depends on magnetic field operation scenario and we consider the 2c and triangular cycle which have higher operation load compared to other scenarios. Considering the planned boundary and initial conditions, we could find the effect of changing rib distance. Compared to previous design, the 7 mm rib distance shows small increasement of heat loss and temperature. The magnitude of increments are ΔT = 0.17 K, ΔW = 0.3 W/m at 2c and ΔT = 0.23 K, ΔW = 0.7 W/m at triangular cycle. These opposite effects are compensated and not considerably high.

Jump QP beam chamber

Jump QP has an operation scenario with ramping rate of 1600 T/s. It is the ramping rate of the integral field of the field gradient in QP magnet. After considering the real magnet dimensions, we found the ratio of 13.333 between the effective length and reference radius. With this dimensional ratio, we can interpret 1600 T/s to the value of 120 T/s at the reference radius and the corresponding maximum field is 300 G. Even though it is not extreme operation condition, this high ramping rate initiates us to confirm the effect of this operation. The simulation result shows that the time delay is $\sim$ 22.4μs between driving current and magnetic field. Figure 1 shows the maximum temperature on the beam chamber as a function of time. Each cycle corresponds to the ramping cycles. Due to the short duty cycle with high field ramping rate, it has dynamic temperature variation. The conversed maximum temperature is estimated $\sim$ 7.5 K after infinite operation. The influence of Jump QP magnet operation on beam chamber is less than SIS100 main QP magnet.

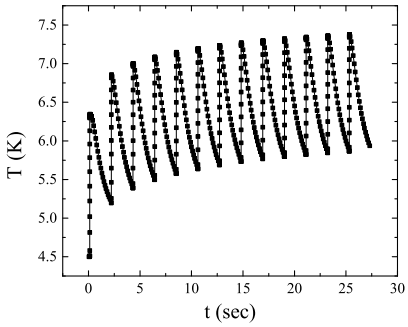

Figure 1: Maximum temperature on the beam chamber with respect to operation time.

CR dipole beam chamber

The magnet for the Collector Ring (CR) is designed to keep constantly accurate magnetic field. Therefore, the stability of the applied electric current is an important parameter for the field stability. The maximum tolerance of field variation is $\Delta B_{max}/B_0 \cong 10^{-6}$. The reported maximum current ripple is $\Delta I_{max}/I_0 \cong 10^{-4}$ considering all magnet circuits. Based on these parameters, we simulate the frequency dependence of the magnetic field from 10 Hz to 10 kHz. The maximum normalized field variation is found to be $\sim 6.3 \times 10^{-5}$ at 10 Hz. This value shows exponential decay with increasing the ripple frequency. Through the simulation procedure, we found that the reason of this field shielding effect was the secondary magnetic field by eddy current in the beam chamber. The field tolerance less than 10^{-6} have been found around 2 kHz and 5.5 kHz in the middle of magnet and the beam space inside the beam chamber, respectively.

References

[1] A. Dolinskii, et.al. Proceedings of IPAC'11 Conference, San-Sebastian, 2011, WEPC054

[2] S. Y. Shim, The Influence of Driving Current Ripple on CR Dipole Magnet, 6th BINP-FAIR-GSI workshop, 2014

DOI:10.15120/GR-2015-1-FG-CS-01

Status of the SIS100 local cryogenics*

B. Streicher[1], *T. Eisel*[1], *J. C. Velasco*[1], *M. Chorowski*[2], *A. Iluk*[2], *P. Duda*[2], *M. Kauschke*[1], *J. Polinski*[2], *A. Täschner*[1], *F. Wamers*[1], *and H. Kollmus*[1]

[1]GSI, Common Systems: Cryogenics, Darmstadt, Germany; [2]Wroclaw University of Technology, Poland

Introduction

The cryogenic system for the FAIR (Facility for Antiproton and Ion Research) superconducting (SC) SIS100 synchrotron and its first specified components were described in [1]. The design progress, project evolution as well as newly specified components are described in the following sections.

By-Pass Line

By-pass Lines (BPLs) pass each of the six straight warm sections of SIS100 to supply liquid helium and cold electrical connections to the SC quadrupole doublets within these sections. Detailed technical specification [2] concerning the BPL system was prepared and approved at GSI in 2013. Based on this, the in-kind contract was signed between FAIR and the Wroclaw University of Technology (WrUT). In conjunction with the cryogenic group CSCY, the WrUT has worked out a detailed technical design of the first BPL part connecting the cryogenic feed-in point at SIS100 directly to the cold arc magnet (see Fig. 1). The design details and interfaces were settled during the Final Design Review held at GSI in February 2015. It includes the design of process pipes, bus-bars, vacuum vessel, supports and instrumentation. The production of this first component will start during first quarter of 2015 and is supposed to be finished and delivered to GSI before the end of 2015. This component will be a part of the SIS100 String Test set-up tested at Serial Test Facility connecting first dipole and quadrupole. Moreover, a new clamping system to fix the bus-bar pairs was developed at WrUT and is currently being tested at GSI. This clamping system shall be used in the SIS100 BPLs.

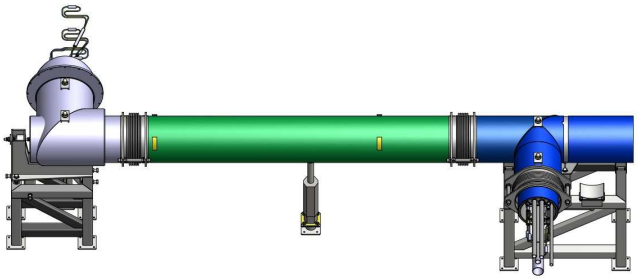

Figure 1: 3D model representation of the final design for BPLP50 (see [2]) made by WrUT.

* FAIR@GSI PSP code: 2.8.12 and 2.14.8.1.6

Current Lead Box (CLB)

In order to supply the electrical connections for 4 types of SC magnets, in total 8 electrical circuits have to be cooled from normal conducting state to the SC state entering the SIS 100 accelerator ring. Devices called Current Lead Boxes perform this duty. The detailed specification of this particular component for the local cryogenic system of SIS100 was finished and submitted to the EDMS system in October 2014 (see [3]). An elaborated 3D model (see Fig. 2) was already prepared at GSI as well as flow scheme and control and instrumentation including basic P&ID. Based on this document, WrUT together with GSI shall prepare this component's design till the end of 2015. The in-kind contract concerning this component is currently being prepared at GSI.

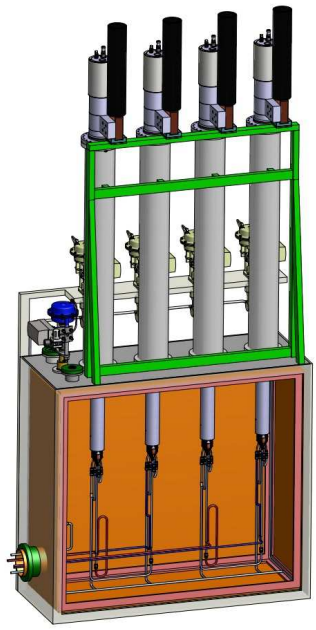

Figure 2: Schematic representation of a SIS100 current lead box specified at GSI (see [3]).

References

[1] B. Streicher et.al., Cryogenics for SIS100 Accelerator, GSI Preprint (http://repository.gsi.de/record/68024)

[2] Detailed Specification of the Local Cryogenic By-Pass System for SIS100 (https://edms.cern.ch/document/1261140/8)

[3] Current Lead Boxes for SIS100 (https://edms.cern.ch/document/1174196/1)

DOI:10.15120/GR-2015-1-FG-CS-02

Status and commissioning of the Helium Supply Plant (HeSu) and the Series Test Facility (STF)

A. Breidert[1], C. Schroeder[1], A. Beusch[1], M. Kauschke[1], B. Streicher[1], F. Walter[1], and H. Kollmus[1]
[1]GSI, Common Systems: Cryogenics, Darmstadt, Germany

The Helium Supply Plant (HeSu)

For the FAIR Project a standard helium liquefier with a capacity of approx. 20 l/h has been installed at GSI. The liquefied helium is stored in 3000 l stationary Dewar vessel and transferred to mobile vessels using a decant station. A recovery line has been installed connecting the testing hall via the UHV lab to a 20 m^3 storage balloon. The HeSu will be used for LHe consumers on laboratory scale. At a later stage of the FAIR project the whole liquefier plant will be used for experiments with no direct connection to the campus distribution system.

The contract with Air Liquide was signed in 2013. The installation on site was performed in summer 2014 and the commissioning started in September and was successfully completed in November 2014. The first users appeared already in the same year. Main customers in the next years are supposed to be the CW-Linac, beam diagnostics, and the UHV group.

Figure 1: The HeSu plant. From right to left: purifier cold box and LHe storage

The Series Test Facility (STF)

In order to test the 108 fast-ramped superconducting dipole magnets of the SIS100, a cryogenic test facility has been specified by GSI and manufactured and installed by Linde KT. It is currently under commissioning at GSI with a site acceptance test (SAT) in late spring of 2015.

The overall cooling capacity of the cryo plant is about 1.5 kW (4.5 K equivalent) and can be distributed to four test benches individually. The capacity of the cryogenic system is designed to simultaneously cool down one magnet while another one is being operated at cold state for the cryogenic and magnetic measurements. The other two test benches serve for warming up and for magnet exchange, respectively. Beyond the SIS 100 dipoles, the high flexibility of the setup allows also the testing of other FAIR magnets, like the SIS100 quadrupole modules, the operation of a string configuration or even SuperFRS magnets. The plant is designed for subcooling to 4.4 K at 1.8 bar. The overall capacity is divided into 690 W cooling power at 4.4 K, a liquefaction rate of 6 g/s, and 2 kW cooling power at 50 K to 80 K for shield cooling.

The magnet is placed between feed and end box. The magnet and the end box are moveable on a rail system. The magnet extends into the feed and end box. By using large flanges on both sides of the boxes easy access to the interface area is guaranteed. This design saves space and avoids bellows for the insulation vacuum cryostats.

The magnet is fixed in space on the rail system, while feed and end box have to be flexible to compensate the mechanical tolerances. This is realized by rubber compensators, such as normally used for compressors. Also the jumper line to the feed box is flexible.

The planning started already in early 2012, after the tendering process the kick-off with the contractor took place mid of 2013. After finishing the new annex building SH5 all components were delivered during spring to summer 2014. The first component was the helium cycle compressor with an electrical power consumption of 465 kW, followed by the oil removal system, the gas management panel and the main cold box together with a 3000 l liquid helium Dewar. All this components were placed in the annex building. In front of SH2/SH5 3 buffer tanks were installed, one 100 m³ gaseous helium storage tank for the helium inventory, one 50 m³ gaseous helium storage tank for quench gas and one 40 m³ liquid nitrogen tank for the precooling of the helium in the cold box. In SH2 the cold end of the cryo plant was installed. On a 2nd floor two distribution boxes and the so called string box were placed, left and right hand side two test benches on a rail system with feed and end boxes, see figure 2. In December 2014 all installation work was finished and the point of mechanical readiness was reached and the commissioning phase was started. In spring 2015 the commissioning will be complete and it will end with the side acceptance tests (SAT).

Figure 2: Ground floor: The two right-hand test benches. First floor: The two distribution boxes and the multipurpose terminal.

DOI:10.15120/GR-2015-1-FG-CS-03

THttpServer and JavaScript in ROOT*

J. Adamczewski-Musch[1], B. Bellenot[2], S. Linev[1], and the FAIR@GSI project[1]
[1]GSI, Darmstadt, Germany, [2]CERN, Geneva, Switzerland

Introduction

The ROOT [1] software framework is widely used in most HEP experiments. ROOT is also often applied for monitoring and control at different stages of data taking and online analysis. Many such online tasks could be solved with web technologies – http protocols for data exchange, and powerful JavaScript/HTML graphics to implement user interfaces.

JavaScript ROOT

The prominent functionality of JavaScript ROOT (JSROOT) library is the ability to read binary ROOT files and provide interactive ROOT-like graphics in web browsers (Figure 1). Many significant changes and improvements have been implemented in 2014 compared to original JSRootIO [2] code.

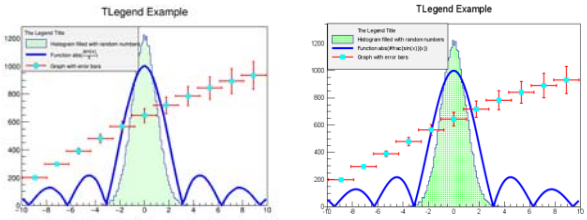

Figure 1: Same canvas, displayed with native ROOT graphics (left) and JSROOT (right)

The I/O part of JSROOT has been organized modular and structurally similar to native ROOT I/O functionality. Most objects stored in binary ROOT files now can be read from the web-browser, using meta-information provided within ROOT files (so-called “streamer-infos”). Several special cases of custom streamers (like TCanvas or TList) are treated in a central place, making it much easier to maintain and extend functionality in the future. It is possible to display and overlay data from different ROOT files in the same browser window.

The graphical part of JSROOT code has been fully rewritten and decoupled from I/O part of the JSROOT library. The main focus was put on flexibility – now JSROOT graphics can be inserted in any webpage, and one can update graphics interactively. Many new features have been implemented, e.g. context menu, statbox update, comfort zooming.

JSROOT code, documentation and examples are available online [3] and with ROOT distribution.

THttpServer class

The new THttpServer class of ROOT implements http protocol by means of embeddable Civetweb [4] server. With simple http requests syntax one could obtain object data from application in different form. (binary, xml, json, png). The TBufferJSON class has been developed to convert ROOT objects into JSON (JavaScript Object Notation), which can be directly evaluated in web browsers.

The user interface for THttpServer has been implemented with JSROOT (Figure 2). One could browse, display, and monitor objects registered to the server. In addition one could execute registered commands (like start/stop analysis or clear histograms) in the server application. There is also the possibility to perform TTree::Draw() on the server and display results in the browser.

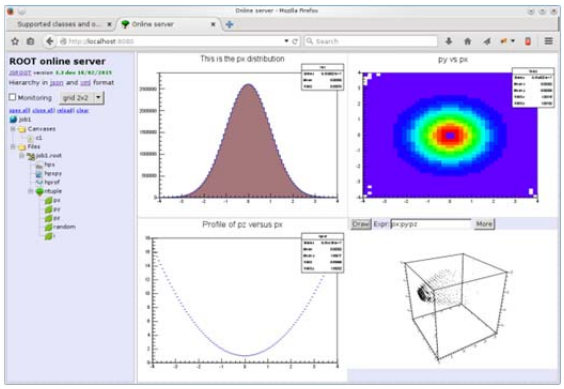

Figure 2. Browser with objects available from httpserver.C macro. The objects hierarchy is on the left side, several displayed objects are on the right. Also tree draw functionality is shown.

Source code, documentation, and several examples for THttpServer are included into the ROOT distribution.

Conclusions and outlook

THttpServer together with JSROOT provide a powerful tool set to create ROOT-based online applications. JSROOT functionality is also used to implement web interface for DABC, MBS and Go4 frameworks [5].

References

[1] ROOT project homepage http://root.cern.ch
[2] B.Bellenot, S.Linev, “ROOT I/O in JavaScript”, Journal of .Physics: Conference Series, vol 513, Proceedings of CHEP 2013, http://iopscience.iop.org/1742-6596/513
[3] JSROOT homepage https://root.cern.ch/js/jsroot.html
[4] Civetweb embeddable webserver, project homepage https://github.com/bel2125/civetweb
[5] S. Linev, “Web interface in DABC”, GSI scientific report 2013, doi:10.15120/GR-2014-1-FG-CS-12

* PSP codes: SFRS 2.4, ILIMA 1.2.2.4, R3B 1.2.5.1.4, 1.2.6.6, 1.2.5.1.2, HADES 1.1.2.4

DOI:10.15120/GR-2015-1-FG-CS-04

Status and developments for DAQ system MBS v6.3*

J. Adamczewski-Musch[1], N. Kurz[1], S. Linev[1], and the FAIR@GSI project[1]
[1]GSI, Darmstadt, Germany

Introduction

The software framework MBS (Multi Branch System) has been established as common DAQ system at GSI for more than 20 years [1]. Various experiments apply MBS for data taking. Besides supporting the users when setting up the experiment, the MBS framework is continuously being improved and developed due to changed requirements. This article reports the most recent experiences and ongoing developments of MBS.

MBS installation update

In 2014 19 new MBS systems (12 VME based, 7 PC/PCI Express based) have been installed and came into operation at GSI and worldwide. In addition 9 MBS systems have been upgraded to the MBS production version or to new operating system versions. Furthermore three travel MBS systems for experiments outside of GSI have been set up.

Developments

Improved PCI Express (PCIe) readout

The MBS driver software for PEXOR/KINPEX PCIe optical receiver boards has been improved for x86 Linux platforms [2]. This consists in a new kernel module *mbspex* with corresponding C library. Additionally, a command line tool *gosipcmd* allows front-end configuration and controls concurrently to running MBS DAQ. If the MBS user readout function calls *mbspex* library functions only, a safe read-out will be possible simultaneous with external control system access. However, backward compatibility to existing readout code is provided by the new driver.

White rabbit timing system

In the GSI test beam campaign 2014 synchronisation with White Rabbit timing receivers (WTR) [3] has been introduced successfully at the experiment Land/R3B for the first time. With the help of the VETAR (VME) and PEXARIA (PCI Express) WTRs several independent MBS systems running with global triggers systems have been synchronised.

In addition a prototype of the R3B silicon tracker (SITR) could be included in the White Rabbit time stamp scheme. The SITR is designed to run without global, but with individual detector input signal triggers (local triggers). It provides for each signal over threshold a charge (energy) and a White Rabbit time stamp.

To accomplish synchronisation with the MBS systems running with global triggers, two LVDS signal lines have been sent from a VETAR WTR into the SITR: 1) White Rabbit controlled 200 MHz for time counting; 2) A 100 KHz pulse train, phase stable with the 200 MHz clock. The 64 bit White Rabbit time reference is sent serially encoded in each ten microsecond interval of consecutive pulses.

MBS systems running with global triggers and a system running with local triggers could be successfully synchronised. This serves as blueprint for FAIR data acquisition setups, where these conditions will be standard.

Controls with DABCs

Control and monitoring MBS nodes via tcp/ip socket from remote is since long time possible: a status server would deliver run state and rate information to monitoring clients like Go4, and multiple MBS nodes would receive commands via prompter socket. Additionally, for DABC controls two new channels have been introduced for MBS v6.3: a remote log server (“logrem”) sending log output to the control client; and a remote command channel (“cmdrem”) in the MBS dispatcher process that inserts client commands beside the local MBS console input. These new channels may be started from the beginning by command line argument (“*mbs -dabc*”), or started from running dispatcher session by new commands (“*start logrem*”, “*start cmdrem*”). DABC library offers modules to connect these channels. The DABC executable *mbscmd* can either control the MBS dispatcher process via *cmdrem* socket, or the MBS prompter process via the already existing multi-node control socket.

Webserver GUI

The MBS control sockets may be accessed by a separate DABC process running an http web server [4]. The DABC web server will forward http command requests via the *cmdrem* channel to MBS dispatcher. It will retrieve log messages from MBS *logrem* channel and DAQ status from MBS status socket, and may export this information to the web. This allows remote control of each single node dispatcher from web browser. In addition to the default DABC tree display of these web objects, a dedicated MBS control GUI has been developed for this DABC web server using JavaScript with the *jQuery UI* environment.

* PSP codes: SFRS 2.4, ILIMA 1.2.2.4, R3B 1.2.5.1.4, 1.2.6.6, 1.2.5.1.2.5, SPARC 1.3.1.3.11,, SD-SEM 2.3.6.5.1.6.30

DOI:10.15120/GR-2015-1-FG-CS-05

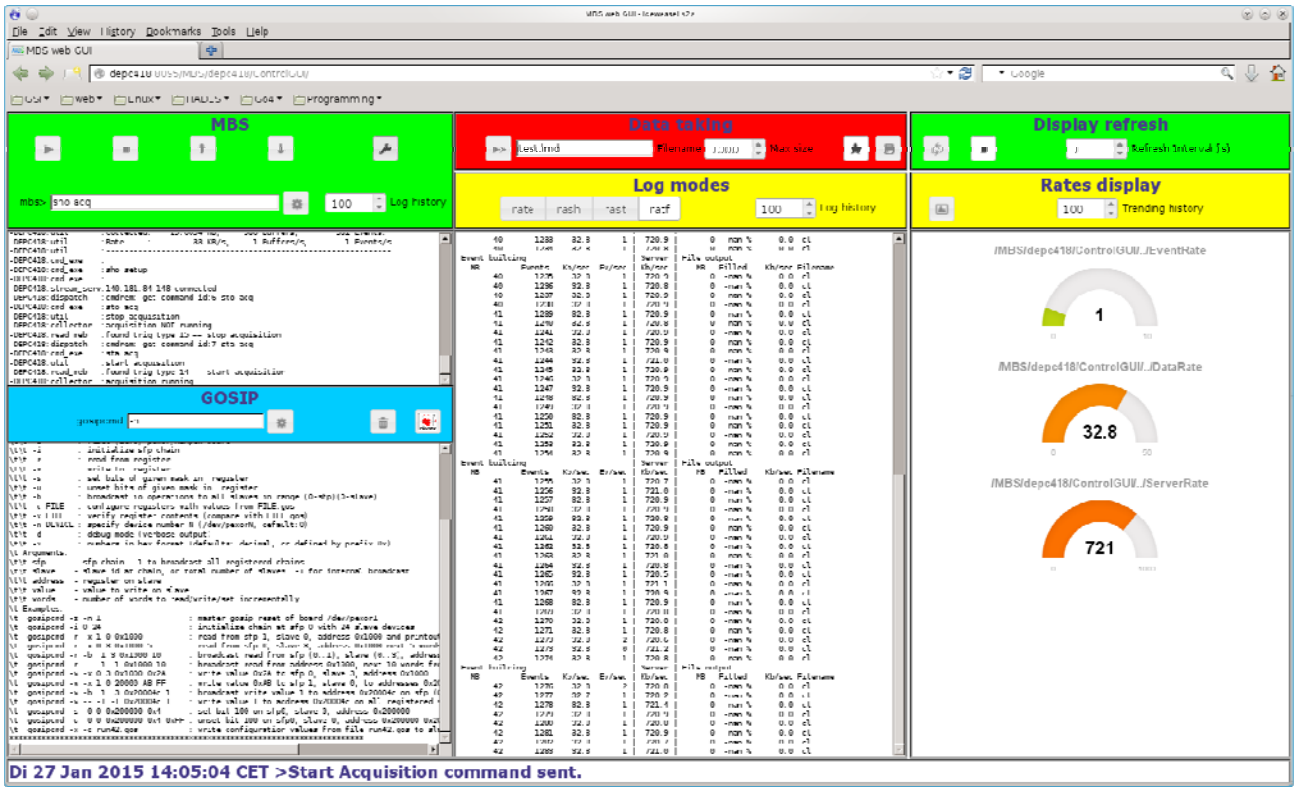

Figure 1: The MBS web browser control GUI

Figure 1 shows a screenshot of such a GUI. The dispatcher interactive command line appears in the browser and offers additional shortcut buttons for mostly used commands, like start/stop acquisition, *@startup*, *@shutdown*. Data taking commands and status is shown in a separate tile with control buttons for open/close file, file mode and RFIO/local disk set up. The run or file status of the acquisition is visualized by red or green background colours of the control tiles. Data rates are displayed both as graphical gauge or trending rate meters, and as text terminal output of the previously known *rate*, *rash*, *rast*, or *ratf* shell commands of MBS. Automatic refresh frequency of the browser display can be set in a dedicated box. Moreover, when running on MBS Linux PC, the DABC web server also offers to call the frontend configuration tool *gosipcmd* [2], so a command line and output box for this tool can optionally be shown in the browser. Additionally, a dedicated frontend configuration GUI, like POLAND setup [2], may be started by a button in a different browser window.

Outlook

The new features described above are partially already installed at GSI as development version 6.x ("mbslogin deve") and can be tested. They will be part of the future production version MBS 6.3 to be released in 2015. Moreover, adjustments to new PC hardware and 64bit Linux are currently under work and will be available with this release.

References

[1] Multi Branch System home page: *http://www.gsi.de/mbs*

[2] J. Adamczewski-Musch, N. Kurz, S. Linev, "mbspex driver software for PEXOR/KINPEX readout boards", this report

[3] D. Beck et al., "Paving the Way for the FAIR General Machine Timing System", GSI scientific report 2013, doi:0.15120/GR-2014-1-FG-CS-08

[4] S. Linev, "Web interface in DABC", GSI scientific report 2013, doi:10.15120/GR-2014-1-FG-CS-12

DOI:10.15120/GR-2015-1-FG-CS-05

mbspex driver software for PEXOR/KINPEX readout boards*

J. Adamczewski-Musch[1], N. Kurz[1], S. Linev[1], and the FAIR@GSI project[1]
[1]GSI, Darmstadt, Germany

Introduction

The GSI PEXOR/KINPEX ("PEX family") PCIe boards were designed for data read out from various detector front-ends via optical SFP connections to an X86 PC host [1]. Communication between PEX and front-end hardware is handled via the *gosip* protocol [2]. For triggered data acquisition, the trigger module TRIXOR can be connected to PEX. The PEX boards have been applied for many years with the data acquisition framework MBS [3]. An improved Linux kernel module driver *mbspex.ko* has been implemented such that concurrent access from MBS and separate control processes is now possible. The new application library *libmbspex* provides higher level functionality to user space. Moreover, a command line tool *gosipcmd* allows inspection and configuration of any front-end register from an interactive shell, GUI, or remote web server. Fig. 1 shows these *mbspex* software components in a typical Linux host PC with MBS DAQ and several control applications.

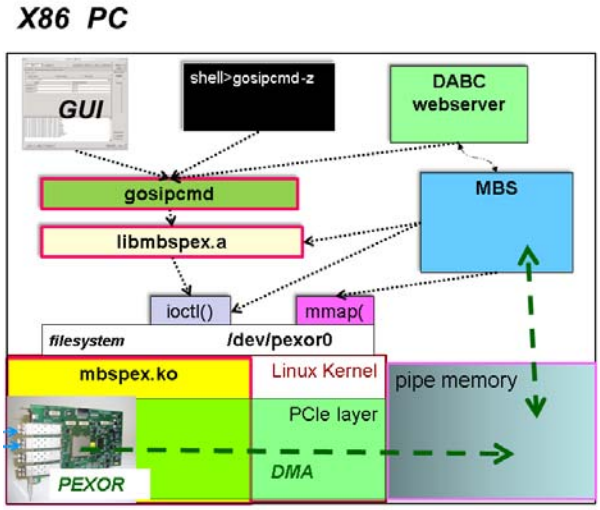

Figure 1: Overview of *mbspex* software components on an X86 Linux node

Linux device driver

Access of any user program to PEX and the connected front-end hardware requires device driver software, usually consisting of a kernel module and optionally a corresponding user space library.

Kernel module

The *mbspex* kernel module merges the previous simple driver *pexormbs* for MBS data acquisition with the larger *pexor* driver for DABC and FESA frameworks [4]. It implements all basic *gosip* protocol functionalities, like initialization of chains, front-end field bus access, and "token" data request, as *ioctl()* functions. Additionally, there are DMA operations to send data to any destination pointer in physical memory (MBS "pipe", see Fig.1). All these *ioctl()* calls are protected by a kernel mutual exclusive semaphore. This allows concurrent access to the PEX device without crashing the system.

Since the kernel module keeps track of all initialized devices at the sfp chains, a "broadcast" i/o is possible: with one *ioctl()* the same value can be written to the same address on all devices of a chain, or of all chains. Furthermore, several registers of each frontend can be configured at once from a single *ioctl()* data bundle. This can be combined with broadcast mode and allows in principle to safely reconfigure all frontends at once while data acquisition read out is running.

On the other hand, all *ioctl()* calls of *pexormbs* driver are remained in *mbspex* driver with the same key values. So any legacy MBS code may ignore the "locked" *ioctl()* features and still work directly on the PEX board control registers. For this purpose file operation *mmap()* is still implemented to map the PEX board memory to virtual addresses of the MBS process. Alternatively, *mmap()* can map any physical PC memory to user space. MBS is using this to access the reserved "pipe" memory for subevent buffering.

Finally, *mbspex.ko* exports some PEX and TRIXOR registers via the kernel sysfs feature. The properties can be inspected by reading corresponding file handles under directory */sys/class/mbspex/*.

User library

The *libmbspex* user space library is written in C language and uses the file system handle */dev/pexor0* with *ioctl()* calls as interface to the kernel module (see Fig.1). It provides high level functions for register i/o with the PEXOR board, with any single front-end, or with all configured front-end boards in a "broadcast" mode. Additionally, *gosip* "token mode" data transfer from the front-end buffers and DMA transfer to PC host memory can be initiated by simple function calls. All these functions are protected against concurrent access already in the kernel module. So different control applications like *gosipcmd* may link and use *libmbspex* simultaneously. Moreover, MBS user readout code can be based on *libmbspex* function calls only.

Application for MBS DAQ

The MBS DAQ framework does not operate the front-end hardware directly, but just ensures that user read-out functions are called whenever module TRIXOR receives a trigger signal. It does not require *libmbspex* functionali-

* PSP code: SD-SEM 2.3.6.5.1.6.30.

DOI:10.15120/GR-2015-1-FG-CS-06

ty, but interacts with *mbspex.ko* by means of *ioctl()* and *mmap()* file operations. They are merely applied to wait for next trigger, and to map the pipe buffer physical memory (Fig. 1). These calls have been kept compatible with the previous kernel module *pexormbs.ko*, so no modifications to MBS framework have been needed. Also any legacy user readout code will work with *mbspex.ko*, since memory mapped access to PEX control registers is still supported.

However, to provide safe concurrent frontend access between MBS and external control tools, adjustments in MBS user readout code are necessary. Here any token data request must use primitive function calls of *libmbspex*. An example of such readout code has been provided for POLAND/QFW front-ends of FAIR beam diagnostic projects [5].

Command line tool gosipcmd

The command line tool *gosipcmd* works as shell application on top of *libmspex* (Fig.1). It provides interactive command access to PEX board and the SFP-connected frontend registers via gosip protocol. The resulting values are printed to terminal. The main functionalities cover:

- reset PEX board, initialize SFP chains
- read/write any address on frontend slave
- incremental read/write from start address
- register bit manipulation
- broadcast mode: read/write same register at all connected frontends
- configure / verify with script files *.gos
- plain or verbose, hex or decimal output mode

A more complete list of available options can be printed using “gosipcmd -h”. At GSI *gosipcmd* is already provided at X86 Linux installations (hosts “X86L-nn”) for MBS v6.2.

Frontend control GUI

Since *gosipcmd* uses *stdin*/*stdout* as plain text data interface, it can serve as base for any special front-end configuration script, or graphical user interface (GUI) application.

POLAND GUI

An example of such frontend GUI has been developed for configuration of POLAND charge to frequency converters of beam diagnostics [5]. It is designed with Qt4 graphics library and shown as screenshot in Fig.2. Since it uses *gosipcmd* calls only, it is decoupled from the actual *mbspex* library version and may work both with *mbspex* and *pexor* driver installations, i.e. with MBS or FESA read out. The *stdout* of *gosipcmd* is redericted to an embedded text window which allows verbose register inspection, and dumping of event data buffers. PEX board and SFP chains may be initialized on click. Each POLAND frontend device can be selected and the meaningful registers displayed and manipulated. Moreover, it is possible to broadcast same register settings to all devices, as this is already supported at kernel module level. Also configuration scripts of *gosipcmd* (*.gos) may be selected and applied from the GUI.

The POLAND GUI is installed at GSI for MBS v6.2 on X86 Linux and available via alias “poland”.

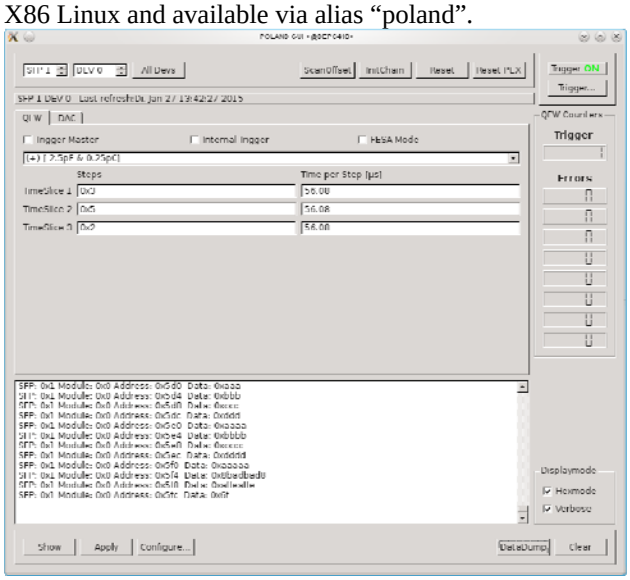

Figure 2: POLAND Qt4 GUI using *gosipcmd* interface

DABC webserver GUI

Besides such local control GUI, a remote control of *gosipcmd* has been implemented as gosip plug-in for the webserver of software framework DABC [6]. This webserver runs as independent DABC process on the MBS Linux node (Fig.1) and provides a full interface to the local *gosipcmd* via HTTP request and response. A web browser version of the POLAND GUI has been implemented for this mechanism, using JavaScript with *jQuery UI* plug-ins (Fig.3).

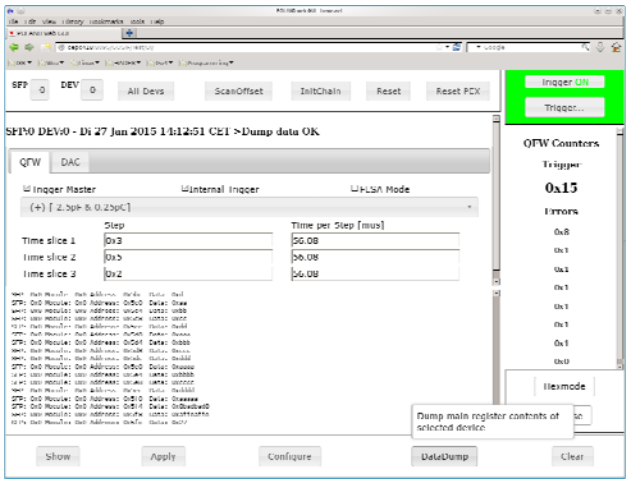

Figure 3: POLAND web GUI at DABC web server

Additionally, a generic *gosipcmd* browser command line GUI will be available as part of the DABC webserver controls for MBS v6.3 [7].

DOI:10.15120/GR-2015-1-FG-CS-06

References

[1] J. Hoffmann, N. Kurz, S. Minami, W. Ott, and S. Voltz, “PCI-express Optical Receiver”, GSI scientific report 2008, p 258.

[2] S. Minami, J. Hoffmann, N. Kurz, and W. Ott, “Design and Implementation of a Data Transfer Protocol via Optical Fibre“, presented at the 17th IEEE Real-Time Conference, Lisboa 2010, Paper PDAQ-31

[3] Multi Branch System (MBS) home page: http://www.gsi.de/mbs

[4] J. Adamczewski-Musch, H.G.Essel, S. Linev, “The DABC Framework Interface to Readout Hardware”, IEEE TNS Vol.58, No.4, August 2011, pp. 1728-1732

[5] S. Löchner, J. Adamczewski-Musch, H. Bräuning, J. Frühauf, N. Kurz, S. Linev, S. Minami, M. Witthaus, “POLAND - Low Current Profile Measurement Readout System”, GSI Scientific Report 2013, doi:10.15120/GR-2014-1-FG-CS-13

[6] Data Acquisition Backbone Core (DABC) home page: http://dabc.gsi.de

[7] J. Adamczewski-Musch, N. Kurz, S. Linev, “Status and developments for DAQ system MBS v6.3”, this report

Applications of the TRB3 and Associated Front End Electronics in Recent Beam Times*

Michael Traxler[1], *Joern Adamczewski-Musch*[1], *Matthias Hoek*[2], *Marcin Kajetanowicz*[3], *Grzegorz Korcyl*[3], *Sergey Linev*[1], *Ludwig Maier*[4], *Jan Michel*[5], *Andreas Neiser*[2], *Marek Palka*[3], *Manuel Penschuck*[5], *Pawel Strzempek*[3], *Cahit Ugur*[1], *and FAIR@GSI Division*[1]

[1]GSI, Darmstadt, Germany; [2]Institute for Nuclear Physics, Johannes Gutenberg-Universität Mainz, Germany; [3]Institute of Physics, Jagiellonian University, Poland; [4]Physik Department E12, Techn. Univ. München, Germany; [5]Institut für Kernphysik, Goethe-Universität Frankfurt, Germany

The TRB3 platform [1] with its associated Front-End-Electronics has been proven in the recent years to be very useful for many applications and has been successfully used by several experiments/groups in 2014.

The HADES collaboration performed a pion test beam experiment in May 2014 and two production pion beam runs in July and August/September 2014, where the TRB3 was used by several detector systems. The HADES pion tracker (see [2]) located in the NE5 area in front of the HADES experiment was used to determine the momentum of each pion. The FEE, based on the n-XYTER ASIC, was read out by the TRB3 and seamlessly integrated in the HADES DAQ, where the TRB3 had a pure digital task.

The pion hodoscope used the Padiwa-AMPS FEE board together with the TRB3 (see [3]) for precise TDC and QDC measurements. The diamond start detector employed the TRB3 for the precise T0 time determination.

The CBM-TOF collaboration used a large setup of 7 TRB3 boards together with 14 TOF-FEE (detector specific strip-down of the TRB3) modules to perform RPC-detector test beam times in April and October 2014. The PADI-FEE delivered the LVDS signals to the TRB3 based system for digitisation. The desired time precision as well as the required DAQ-event rates have been reached during the second beam time.

The PANDA-Barrel-DIRC group set up a system of 20 MCP-PMTs (each 64-channel) with PADIWAs as FEE and 24 TRB3s for test beams in April and July/September 2014 to test the DIRC optics in beam together with the readout electronics.

The CBM-RICH group set up a RICH-detector prototype at CERN with 16 64-channel MA-PMTs with a Padiwa + TRB3 (18 were used) based readout. An online display of the RICH rings is shown in fig. 1. Preliminary analysis results show good efficiency for RICH rings.

Additional to these experiments and test beams the TRB3 has been used in other production experiments like the DIRC-Detector in the WASA experiment in Jülich.

Furthermore, a larger number of test setups of various groups exists, who used the TRB3 platform in 2014 to read out their detectors and plan to use the TRB3 in their final setups. Just to have some of these groups mentioned: PANDA STT, CBM-MVD, HADES-ECAL, MUSE collaboration, A1 Neutron detector, Coimbra-PET, Cracow-PET, etc.

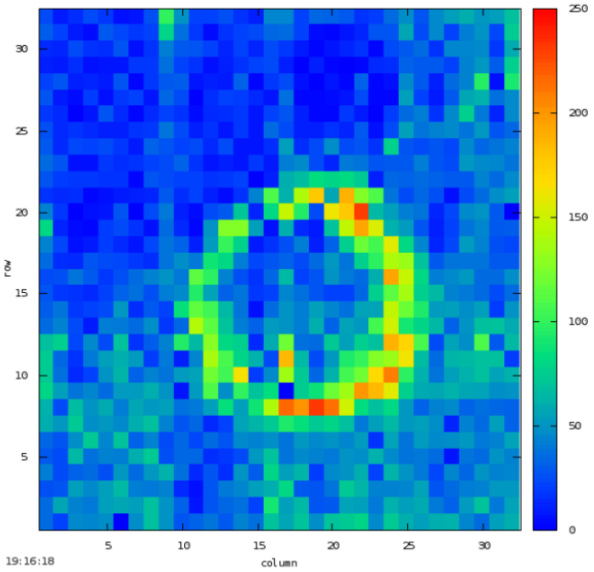

Figure 1: Online heat map of hits measured in the the array of 1024 MA-PMT channels of the CBM-RICH detector. The ring is visible during spills from the SPS beam.

All these experiences, together with the users, improved the platform substantially. The lessons learned jointly with new developments on the TDC side (see [4] will also lead to developments like a crate based TRB3 system "TRB3SC" and the joint effort for an optimized FEE+TDC+DAQ electronics "DIRICH" for PANDA-DIRC, CBM-RICH and HADES-RICH.

References

[1] All information about the TRB3 can be found here: http://trb.gsi.de

[2] L. Fabbietti et al., "Integration of the Pion-Beam Tracker into the HADES DAQ", GSI-SR2013-NQM-HADES-10, GSI Scientific Report 2013

[3] M. Traxler et al., "A Precise Multi-Channel QDC FEE utilizing FPGAs as Discriminators and Delay Elements Based on the TRB3 as TDC and Readout Platform", GSI-SR2013-NQM-HADES-13, GSI Scientific Report 2013

[4] C. Ugur et al., "FPGA Based Multi-Channel TDC Development", GSI Scientific Report 2014

* Work supported by FAIR@GSI PSP codes: 1.4.1.5, 1.1.2.4

DOI:10.15120/GR-2015-1-FG-CS-07

Numerical simulations of a field emitter-based extractor gauge for pressure measurements in cryogenic vacuum systems

M. Lotz[1,2], St. Wilfert[1], A. Krämer[1], and O. Kester[1,2]
[1]GSI, Darmstadt, Germany, [2]Goethe University of Frankfurt, Germany

Pressure measurement in the UHV and XHV range in cryogenic vacuum environments has always been considered a metrological problem. However, especially for the cryogenic beam vacuum sections of the SIS100 a pressure measurement would be useful since local pressure rises caused by dynamic vacuum can lead to self-amplifying beam loss effects.

In general, conventional hot-filament ionization gauges can be used in cryogenic vacuum systems. However, during operation they generate a huge heat load causing numerous disadvantages in low temperature systems. Therefore, an ionization gauge was developed where the heat-generating filament was replaced by a non-thermal cathode. The electron release mechanism of this cathode type is based on field emission. It has been shown in a previous study [1] that it is possible to read pressures under cryogenic vacuum conditions using this type of gauge. Unfortunately, the lower pressure measuring limit of the used gauge is too high to measure the low pressures expected in the future SIS100. This was caused inter alia by the low electron current relative to the current used in a commercial extractor gauge with thermionic filament. To increase the current, the carbon nanotube-type (CNT) field emitter will be replaced by a field emitter array (FEA), which is developed at the Paul Scherer Institute (PSI) in Switzerland.

The FEA consists of an array of micro-structured molybdenum tips and has an integrated micro grid for electron extraction at a very short distance. Therefore, even small extraction voltages between 100-150 V are sufficient to generate an emission current in the range of mA. These emitters were repeatedly tested at PSI and showed promising emission properties [2].

Numerical simulations on the previously studied CNT-based gauge have been carried out using the program suite *AMaze*. The results showed that in this gauge configuration many electrons directly hit the anode grid end closure without the typical oscillation within the ionization volume, i.e. the volume inside the anode grid (Figure 1).

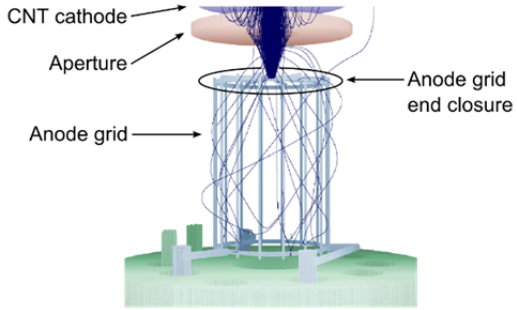

Figure 1: Electron trajectories in the CNT-based extractor gauge.

Since ions generated outside the ionization volume do not reach the ion collector electrode, the detectable pressure dependent ion current is very low. In order to increase the ion current signal the electrons must run on elongated paths through the ionization volume. This can be facilitated by a change of the cathode position. Therefore, an improved gauge design is developed in which three individual field emitter spots are arranged as a ring around the anode grid. This geometry is similar to that of conventional extractor gauges with ring-shaped thermionic cathodes. Numerical simulations on this improved gauge design have confirmed the considerations on the electron trajectories within the gauge (Figure 2). As a result, the gauge sensitivity should be substantially increased relative to the CNT-based extractor gauge previously investigated.

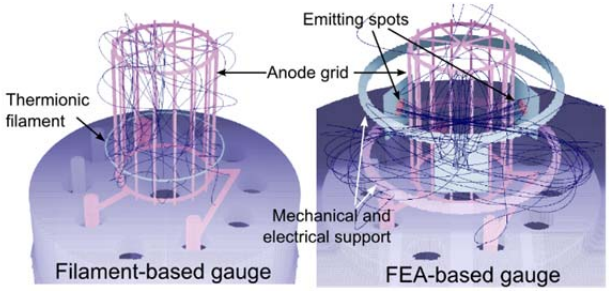

Figure 2: Comparison of electron trajectories in a FEA-based and a filament-based extractor gauge.

The improved gauge design, as shown in Figure 3, will be realized and studied extensively in terms of its operating performance in both room temperature and cryogenic vacuum environments. The experimental investigations will provide information on whether the lower pressure measuring limit is shifted to significantly lower pressures by the modifications made.

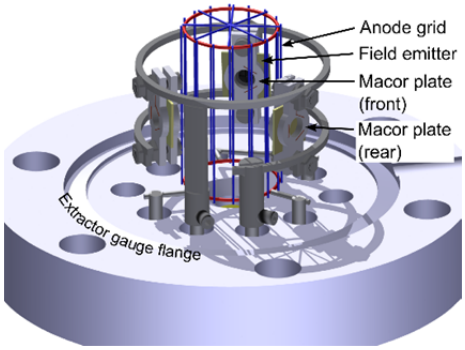

Figure 3: The improved FEA-based extractor gauge.

References

[1] Lotz, M. *et al.*, GSI Report 2013-1, 263 p. (2013)
[2] Kirk, E. *et al.*, J. Vac. Sci. Technol. B 27, 1813 (2009)

DOI:10.15120/GR-2015-1-FG-CS-08

New tests of large area Continuous Position Sensitive Diamond Detector

M. Ciobanu[1], M. Pomorski[2], E. Berdermann[3], C. Bunescu[1], H. Comisel[1], V. Constantinescu[1], M. Kiš[3], O. Marghitu[1], M. Träger3, K-O.Voss[3]and P.Wieczorek[3]

[1]ISS, Bucharest, Romania; [2]CEA, Saclay, France; [3]GSI, Darmstadt, Germany

The first Continuous Position Sensitive Diamond Detector (CPSDD) was made on a single crystal (sc) based material [1]. The high efficiency of sc provides a high enough Signal to Noise ratio (S/N) to fully test the CPSDD with alpha particles.

The first Large Area CPSDD (LACPSDD) was made on a 30 x 30 mm^2 polycrystalline (pc) diamond plate [2], obtained by chemical vapor deposition. In beam tests with ^{54}Ni 1.7AGeV particles it shows an ion rate limitation due to the detector time constant.

We made two new pc LACPSDD, one having 10 x 10 mm^2 (x 110 µm) and the second one (Fig. 1) having 20 x 20 mm^2 (x 180 µm). On each detector side a DLC layer is deposited, equipped with two metallic charge collection electrodes. The relative impact position can be obtained by charge division measurement. Each detector is connected to four charge sensitive amplifiers (CSA).

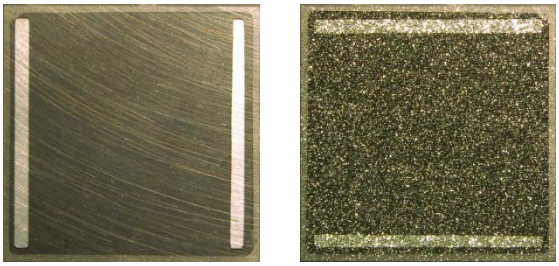

Figure 1: The 20 x 20 mm^2 LACPSDD. Left: view of the substrate side. Right: view of the growth side. On each side there are visible the DLC layer (dark) and the metallic electrodes for charge collection (light). The two pairs of metallic electrodes are oriented at 90°. The DLC layer has R_D ~ 30 KΩ/□, and capacitance between layers C_D ~100 pF.

Tests with alpha particles highlighted that the induced signal delay depends on particle impact position: it is maximal in the centre of the detector and minimal near the electrode. Since the peaking time of the CSA must be greater than the maximal delay, we have modified all the used CSAs [3] to have a 1.5 µs peaking time thus minimizing the ballistic deficit. We obtained a very good correlation between the total collected charges by the two layers and found that the main limitation is due to the small value of the S/N i.e. maximum of 16 in case of alpha particles (the energy lost by an alpha particle is 5.486 MeV, equivalent to an induced signal charge of approx. 67 fC). In addition, the pc material has a broad dispersion of the detection efficiency.

Detector was also tested in ^{12}C micro-beam at 11.4 MeV/A beam energy [4], which provides approx. 25 times larger S/N ratio for stopped particles. We have manually positioned the beam into 62 discrete positions and used the automatic beam micro-sweeps in small rectangles of 280 x 230 $µm^2$. Subsequently, the data were processed as follows:

1. Electrical calibration by using a pulse and 4 ways distributor; offsets and different gains were corrected.
2. For each position, the median centre (x.y) and standard deviation $\sigma_{x,y}$ were obtained. Data outside the centre $\pm 4\sigma_{x,y}$ and outside collecting strips were ignored.
3. The remaining points were fitted to 2D Gaussian distributions, providing higher accuracy for estimates of the measured centres.
4. For each of the 62 micro-beam positions, an error vector is derived, based on the known micro-beam focus and on the fitted actual position of the centre.
5. The x and y components of the error vectors are fitted by series expansions of 2D Legendre polynomials of 5th degree, which provides a continuous 2D coverage.
6. All data points that were not filtered out at step 2 were corrected by continuous 2D error vector (Fig. 2).

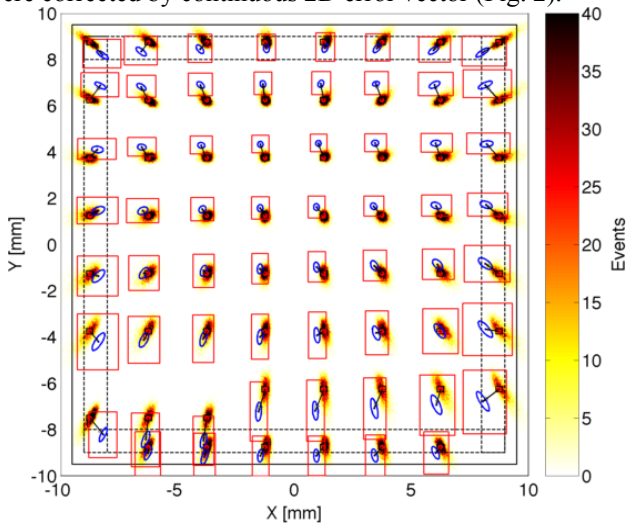

Figure 2: The original (blue contours), micro-beam injection frames (red) and reconstructed spots, after electrical calibration, data filtering (red rectangle contours) and geometrical calibration.

After correction, the 62 measured distributions agree very well with the micro-beam injection frames.

References

[1] M. Pomorski et al., Phys. Stat. Sol. A, 206, pp. 2109-2114, (2009).
[2] M. Ciobanu et al., GSI-Sci. Rep. 2012, pp. 213.
[3] M. Ciobanu et al., IEEE NSS Conf. Rec., N30-20, pp. 2028-2032, (2008).
[4] M. Ciobanu, Large Area Continuous Position Sensitive Diamond Detector Tests (2014), http://www-adamas.gsi.de/index.php?mgid=6#ADAMAS03

DOI:10.15120/GR-2015-1-FG-CS-09

Femtosecond laser enhanced transient current technique*

S. Sciortino[1,2,#], S.Lagomarsino[1,2], C. Corsi[1,3], M. Bellini[4], T. Apostolova[5], E. Berdermann[6], C. J. Schmidt[6], M. Kis[6], M. Träger[6], R. Visinka[6]

[1]Department of Physics, Florence, Italy; [2] INFN, Florence, Italy; [3]LENS, Florence, Italy; [4]INO-CNR Florence, Italy; [5]INRNE, Sofia, Bulgaria; [6]GSI, Darmstadt, Germany

The aim of this work is to understand the processes involved in laser irradiation of diamond below and close to the graphitization threshold. The study is performed under the same conditions of the experimental procedure used to produce 3D diamond detectors [1], in order to improve the technique of preparation of 3D diamond sensors with optimal performances.

To this purpose a Transient Currents Technique (TCT) has been used to measure laser-induced current signals in a diamond detector, in a wide range of laser intensities, from low fields up to the diamond graphitization threshold, at different bias voltages.

The current transients vs. time and the overall charge collected have been recorded to be compared with theoretical simulations.

Transient currents were produced by laser irradiation in a 500 μm thick monocrystalline diamond detector, biased at different voltage values, from 0 to 600 V.

A Ti:Sa mode-locked laser source has been used for excitation, with central wavelength 800 nm, pulse width 30 fs, repetition rate 1000 Hz. The energy densities at a focus of 8 μm diameter are in the range of 0-8 J/cm^2, i.e., the maximum energy per pulse was 4 μJ.

The current vs. time was acquired by a broadband (6 GHz) oscilloscope.

At low laser fields a 2.5 GHz, 40 dB amplifier was used. In this way it was possible to span on four order of magnitude of current intensity. The lower current signal detectable was 0.4 μA and the highest current 3 mA.

The current transients are observed in a time window increassing from 25 ns to 1.2 μs as the energy per pulse goes from 0.1 μJ to 4 μJ. This increase is due to the high density of the plasma generated by the field and the mutual attraction of holes and electrons.

A semi-quantitative model which accounts for these two processes has been developed to fit the current lineshapes.

Figure 1 shows the plot of the collected charge vs. the energy per pulse I at a 500 V bias voltage. This has been determined from the collected charge by integrating the current transients. The slope of the curve up to 1 μJ is fitted with a power trend $Q \propto I^m$, with an exponent m = 4.4, pointing out that the excitation is a mixed non-linear effect involving four and five photon ionizations.

This is consistent with the fact that the frequency emission of the laser corresponds to a broad photon energy range centered at 1.55 eV and the direct bandgap of diamond is about 7 eV, so that at least four photons are required to excite free carriers. We also observe a flattening of the curve at higher laser intensity. This is probably due to the electron-hole recombination occurring during the very long transients, typical of the high energy irradiation pulses.

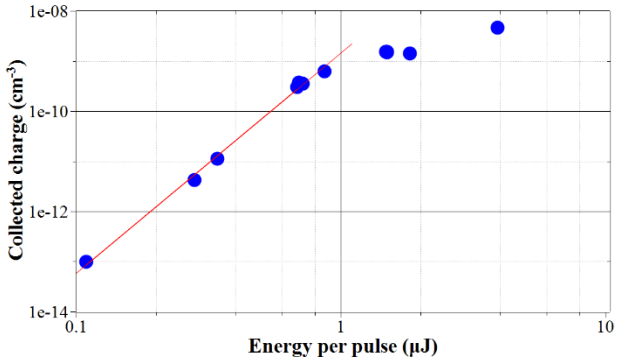

Figure 1: Collected charge vs. energy per pulse

Further measurement aimed to reach the graphitization threshold are under way.

Theoretical modeling aimed to simulate the experimental conditions of excitation and graphitization is also in progress.

References

[1] S. Lagomarsino, M. Bellini , C. Corsi , F. Gorelli , G. Parrini, M. Santoro, and S. Sciortino, Appl. Phys. Lett. 103 (2013) 233507.

* Work supported by EU (HadronPhysics3 project No. 283286) and GSI (Detector Technology and Systems Platform) and INFN Italy (experiment 3D_SOD)

#silvio.sciortino@unifi.it

CC BY
DOI:10.15120/GR-2015-1-FG-CS-10